

Nuclear positioning and functional regulation of endogenous genes and transgenes in the fruit fly *Drosophila melanogaster* and in mammalian cells

Dissertation

an der Fakultät für Biologie
der Ludwig-Maximilians-Universität München

vorgelegt von
Elena Rybakina
aus St.Petersburg
November 2006

Ehrenwörtliche Versicherung

Hiermit versichere ich, dass ich die vorliegende Arbeit selbständig und ohne unerlaubte Hilfsmittel angefertigt habe.

Elena Rybakina
München, November 2006

Nuclear positioning and functional regulation of endogenous genes and transgenes in the fruit fly *Drosophila melanogaster* and in mammalian cells

Dissertation an der Fakultät für Biologie
der Ludwig-Maximilians-Universität München (LMU)

vorgelegt von
M.Sc. Elena Rybakina
aus St.Petersburg

Dissertation eingereicht am: 21.11.2006
Tag der mündlichen Prüfung: 15.12.2006

Erstgutachter: PD Dr. Daniele Zink
Zweitgutachter: Prof. Dr. Peter Becker

Table of Content

1. Introduction	6
1.1. Histone modifications specific for euchromatin and heterochromatin	6
1.2. PcG-mediated regulation of transcriptional activity	10
1.3. Interactions between PREs in <i>Drosophila</i>	14
1.4. Nuclear architecture and gene regulation	17
1.5. Goals	21
2. Materials and methods	22
2.1. Materials	22
2.1.1. Chemicals, culture media and additives	22
2.1.2. Enzymes	24
2.1.3. Nucleotides, nucleic acids and vectors	24
2.1.4. Antibodies and conjugates	26
2.1.5. Dyes and markers	29
2.1.6. Kits	29
2.1.7. Buffers and solutions	29
2.1.8. Microscopes	32
2.1.9. Image processing software	33
2.1.10. <i>Drosophila melanogaster</i> lines	34
2.1.10.1. Wild type flies	34
2.1.10.2. Transgenic flies	34
2.1.10.2.1. Transgenic constructs 5F3, 5F24 and 24F6	34
2.1.10.2.2. Transgenic lines	35
2.1.11. Cell lines	36
2.1.11.1. <i>Drosophila</i> cells	36
2.1.11.2. Human cells	36
2.1.11.3. Porcine cells	37
2.1.11.3.1. Wild type (WT)	37
2.1.11.3.2. Cells from transgenic pigs, carrying lentiviral construct LV-PGK	37
2.1.11.3.3. Transgenic cell lines	38
2.2. Methods	40
2.2.1. Mammalian cells	40
2.2.1.1. <i>In vitro</i> culture of mammalian cells	40
2.2.1.2. Seeding cells on coverslips	40
2.2.1.3. Methanol-acetic acid fixation	40
2.2.1.4. Formaldehyde fixation of cells	41
2.2.1.5. Immunostaining of formaldehyde-fixed cells	41
2.2.1.6. Fluorescent in situ hybridization (FISH)	42
2.2.1.6.1. Labelling the probes	42
2.2.1.6.2. Enzymatic digestion of PCR-labelled probes	45
2.2.1.6.3. Precipitation of DNA probes	45
2.2.1.6.4. Denaturation, hybridization and detection	46
2.2.1.6.5. Detection	46
2.2.1.7. RNA interference	46
2.2.1.8. CFTR expression in HeLa cells	47
2.2.2. <i>Drosophila melanogaster</i> cells and tissues	47
2.2.2.1. <i>Drosophila</i> cell culture	47
2.2.2.2. <i>Drosophila</i> fly stock maintenance	48

2.2.2.3. The preparation of <i>Drosophila</i> polytene chromosomes from salivary glands	48
2.2.2.4. Dissection of other <i>Drosophila</i> larval tissues	48
2.2.2.5. Formaldehyde fixation of cells	48
2.2.2.6. Immunostaining of formaldehyde fixed Kc cells	49
2.2.2.7. Immunostaining of <i>Drosophila</i> tissues	49
2.2.2.8. Fluorescence in situ hybridization (FISH)	51
2.2.2.8.1. Probe preparation	51
2.2.2.8.2. Probe labelling	51
2.2.2.8.3. Labelling efficiency and specificity of the probes	53
2.2.2.8.5. Precipitation of the probes	55
2.2.2.8.6. FISH on polytene chromosomes	55
2.2.2.8.7. FISH on tissue samples	57
2.2.2.8.8. ImmunoFISH on tissue samples	58
2.2.2.8.8.1. Protocol A	58
2.2.2.8.8.2. Protocol B	59
2.2.3. Image analysis	60
2.2.3.1. Image analysis of methanol / acetic acid fixed nuclei	60
2.2.3.1.1. 2D erosion analysis	60
2.2.3.1.2. Distance measurements between the signal and a chromocenter	60
2.2.3.2. Image analysis of formaldehyde fixed nuclei	60
2.2.3.2.1. Measuring the distance between two gene loci	61
2.2.3.2.2. Measuring the distance between a gene locus and the nuclear lamina / heterochromatin	62
2.2.3.2.3. Distance corrections	63
2.2.3.3. Analysis of 3D organization of PcG bodies	64
3. Results	67
3.1 Nuclear positioning of endogenous genes and transgenes in nuclei of larval tissues of <i>Drosophila melanogaster</i>	67
3.1.1. Spatial organization of chromatin in <i>Drosophila</i> nuclei	67
3.1.2. Nuclear positioning of endogenous genes and transgenic constructs	72
3.1.2.1. Nuclear positioning of inactive endogenous loci in <i>Drosophila</i> tissues	73
3.1.2.1.1. <i>Abdominal-B (Abd-B)</i>	73
3.1.2.1.2. <i>Scalloped (sd)</i>	75
3.1.2.1.3. <i>Ultrabithorax (Ubx)</i>	77
3.1.2.2. Nuclear localization of Fab-7 containing transgenes at different states of activity	80
3.1.2.2.1. Nuclear positioning of the 5F24 transgene in FLW-1 larvae	81
3.1.2.2.2. Nuclear positioning of the 5F3 construct in FLW-1 larvae	85
3.1.2.2.3. Nuclear localization of the 24F6 construct in FLW-1 larvae	89
3.1.2.3. Nuclear positioning of other PREs in their active and inactive states	91
3.1.3. Do homologous PREs interact physically?	92
3.1.3.1. Relative positioning of transgenic and endogenous Fab-7 elements in FLW-1 larvae	93
3.1.3.2. Endogenous and transgenic copies of Fab-7 in 5F24 25,2 larvae: do temperature and the chromosomal background influence presumable interactions?	96
3.1.3.3. Is the chromosomal localization of the transgenic copy of Fab-7 important? Distance measurements between transgenic and endogenous Fab-7	

elements in FLFW-1 larvae	98
3.1.4. The spatial distribution of the Polycomb protein in larval interphase nuclei	101
3.1.4.1. Endogenous Pc-GFP binding sites associate with the active form of RNA pol II at the boundary of the heterochromatic domain	110
3.2. Nuclear localization of active versus inactive LV-PGK transgenes in porcine fibroblasts obtained from transgenic animals (<i>Sus scrofa scrofa</i>)	113
3.2.1. Immortalized cells	113
3.2.2. Primary cells	116
3.2.3. Activation of the LV-PGK transgene with 5-azacytidine	120
3.2.4. Localization of the active LV-PGK construct in infected WT cells	122
3.3. The role of the Tpr protein in the nuclear positioning of the CFTR locus in HeLa cells	124
3.3.1. The effect of the knock-down of Tpr on the nuclear localization of CFTR in HeLa cells	124
3.3.2. The knock-down of Tpr induced a positional shift of CFTR without changing its transcriptional activity	127
4. Discussion	130
4.1. Positioning of the PRE Fab-7 in nuclei of <i>Drosophila melanogaster</i>	130
4.1.1. The spatial organisation of different chromatin fractions in nuclei of <i>Drosophila melanogaster</i>	130
4.1.2. The spatial organization of factors associated with euchromatin	132
4.1.3. The association of active sites with the boundary of heterochromatin	133
4.1.4. Factors that contribute to the subnuclear localization of chromatin in <i>Drosophila</i>	137
4.1.4.1. The nuclear envelope and the localization of inactive endogenous loci in <i>Drosophila</i>	137
4.1.4.2. The positioning of <i>Abd-B</i> and <i>Ubx</i> in transgenic flies	140
4.1.5. The nuclear localization of active and inactive Fab-7-containing transgenes in larval tissues of <i>Drosophila</i>	141
4.1.6. Associations between homologous PREs in larval tissues of <i>Drosophila</i>	144
4.1.6.1. Diploid and polytene tissues and the question of tissue-specific interactions	145
4.1.6.2. The impact of the chromosomal background and temperature on PRE associations	147
4.1.7. The 3D nuclear organization of Pc-binding sites in <i>Drosophila</i> nuclei: challenges of interpretation	149
4.2. Integration site and transcriptional activity determine the nuclear localization of LV-PGK transgenic constructs in porcine cells	153
4.3. The Tpr protein, associated with the nuclear pore complex (NPC), contributes to the peripheral positioning of inactive gene loci in human cells	155
5. Summary	158
6. Acknowledgements	160
7. References	162
Supplementary material	174
Curriculum Vitae	175
Publications	176

1. Introduction

The cell nucleus is the characteristic organelle of eukaryotic cells and contains the genetic information. The DNA strands harboring the genetic information have a length of about 2 m in human cell nuclei, which display diameters in the range of only 10-20 μm . In the nucleus the DNA is tightly packaged and complexed with histone and non-histone proteins, and this DNA / protein complex is called chromatin. Many years before Watson and Crick discovered in 1953 the structure of DNA, two types of chromatin were described. In 1928 Heitz found that in nuclei from different species chromatin is unevenly stained by carmine acetic acid (Heitz, 1928). There were densely stained domains which appeared to remain highly compact throughout the cell cycle, which he termed heterochromatin, in contrast to euchromatin, which was weakly stained and seemed to be decondensed. Nowadays, the general agreement is that heterochromatin is the fraction of chromatin that remains highly condensed throughout the cell cycle, contains relatively few genes, replicates late during S phase, contains hypermethylated DNA and hypoacetylated histones, and can suppress the transcriptional activity of genes translocated into its neighborhood (Elgin, 1996; Elgin and Grewal, 2003; Weiler and Wakimoto, 1995). Euchromatin, on the other hand, typically replicates early, is decondensed in the nucleus, contains the vast majority of genes, contains hyperacetylated histones, and is sensitive to nuclease digestion (Dillon and Festenstein, 2002; Gaszner and Felsenfeld, 2006; Grewal and Elgin, 2002). The following paragraphs describe in more detail structural and functional features of eu- and heterochromatin, its nuclear organization and its influence on gene expression.

1.1. Histone modifications specific for euchromatin and heterochromatin

The fundamental subunit of chromatin is the nucleosome. A nucleosome consists of an octamer of core histones (two of each H2A, H2B, H3 and H4) and approximately ~146 base pairs (bp) of DNA wrapped around the core histone octamer. Nucleosome packaging results in a 5-10 fold compaction of DNA (Kornberg, 1974). Nucleosomes are connected by so-called linker DNA. It is thought that histone H1 proteins bind to the entry and exit sites of DNA at the nucleosome and stabilize the nucleosomal structure in this way (Fletcher and Hansen, 1995). The core histones and especially their amino-terminal ends, or „tails“, can be modified in many different ways and these modifications include methylation, acetylation, phosphorylation, ADP-ribosylation or ubiquitinylation at specific lysine, serine or arginine residues (Davie, 1998; Jenuwein and Allis, 2001; Lachner et al., 2003; Luger and Richmond, 1998; van Holde, 1989; Wu et al., 1986). It has been proposed that these modifications and

their combinations constitute a „histone code“, which provides a functional signature of chromatin domains and is essential for the regulation of chromatin-templated processes (Jenuwein and Allis, 2001; Strahl and Allis, 2000; Turner, 2000). This hypothesis is based on a large body of results, which showed that distinct modifications of histone „tails“ are characteristic for transcriptionally active or transcriptionally silent chromatin states. Especially acetylation and methylation are well studied in this regard.

A relationship between histone acetylation and transcriptional activity was proposed already in 1964 (Allfrey et al., 1964). Also subsequently obtained results indicated a direct link between core histone acetylation and transcriptionally active chromatin (Hebbes et al., 1988). A breakthrough was the development of antibodies specific for histone H4 isoforms acetylated at specific lysine residues (Turner et al., 1992). In this classical study, Turner et al. (1992) showed that histone H4 acetylated at lysines 5 or 8 is distributed in similar patterns throughout the euchromatic arms of polytene salivary gland chromosomes of *Drosophila melanogaster*. In contrast, acetylation at lysine 16 was found exclusively at the transcriptionally hyperactive male X chromosome. All these isoforms were absent in centromeric heterochromatin, which showed enrichment in histone H4 acetylated at lysine 12 (Turner et al., 1992). Acetylation at lysine 12 of histone H4 was also found in heterochromatin of yeast and was associated here with transcriptional silencing (Braunstein et al., 1996).

At histone H3 acetylation occurs mainly at lysines 9, 14, 18 and 23 in most species (Grant et al., 1999; Kuo et al., 1996; Thorne et al., 1990). Clear evidence for a link between histone acetylation and transcriptional activity was obtained in 1996 after cloning of the transcription-associated histone acetyltransferase type A (HAT A) of *Tetrahymena* (Brownell et al., 1996). It was shown that subunit p55 of HAT A is a homolog of the Gcn5p (general control nonrepressed) yeast adaptor protein, which is required for the full activity of a subset of transcriptional activators (Brownell et al., 1996). Later, in experiments using chromatin immunoprecipitation (ChIP) it was shown that increased acetylation of histones H3 and H4 at promoters is associated with the initiation of transcription of inducible genes in different species (Kuo et al., 1998; Parekh and Maniatis, 1999). Furthermore, a close connection between hyperacetylation of histones H3 and H4 and transcriptional activity / competence has been found in many studies, which took advantage of ChIP to investigate single loci, larger chromosomal domains, or whole genomes of different model organisms (Myers et al., 2001; Schubeler et al., 2000; Schubeler et al., 2004).

Histone acetylation is controlled by a variety of histone acetyltransferases and histone deacetylases (HATs and HDACs, respectively), which display distinct substrate specificities. For example, yGcn5 preferentially acetylates lysine14 of histone H3 and lysines 8 and 16 of histone H4 (Kuo et al., 1996), whereas HDA1/RPD3 preferentially deacetylates lysines 5 and 12 of histone H4 (Rundlett et al., 1996). In *Drosophila*, the HAT MOF has a strong preference for lysine 16 of histone 4 (Akhtar and Becker,

2000). Acetylation of histone 4 at lysine 16 is a specific mark of the hyperactive male X chromosome (Turner et al., 1992) and is necessary for dosage compensation, which in *Drosophila* is achieved by two-fold increased transcriptional activity of the male X chromosome (Lucchesi, 1996). MOF appears to be targeted to the male X-chromosome by binding to roX RNAs, which are components of the dosage compensation complex (Akhtar et al., 2000).

In addition to acetylation also methylation at specific lysine or arginine residues is associated with active or inactive chromatin. Methylation of histone H3 at lysine 4 generally marks active or potentially active euchromatic genes. This modification was found in the transcriptionally active macronucleus of *Tetrahymena* (Strahl et al., 1999) and in euchromatin of yeast (Noma et al., 2001). Later it was shown that in fission yeast dimethylation of lysine (K) 4 occurs at both active and inactive euchromatic sites, while trimethylation of K4 exclusively marks transcriptionally active sites (Santos-Rosa et al., 2002). Results obtained during a genome-wide analysis of chromatin in *Drosophila* Kc cells, however, indicated that histone H3 dimethylated at lysine 4 was concentrated in transcribed regions and that active genes were both hypermethylated at lysine 4 of histone H3 and hyperacetylated at histones H3 and H4. Moreover, di- and trimethylation of H3K4 (dimH3K4 and trimH3K4, respectively) showed a similar distribution and both were preferentially associated with active loci (Schubeler et al., 2004). Similar results regarding di- and trimethylated isoforms of H3K4 were obtained recently during an analysis of active and inactive genes in chicken erythrocytes (Schneider et al., 2004). These findings suggest that the association of di- and trimethylated isoforms of H3K4 with active genes might be different in yeast compared to animals. In addition to methylation at K4, methylation of H3 at lysines 37 and 79 also correlates with transcriptional activity (Lachner et al., 2003; Schubeler et al., 2004).

In contrast to the modifications described above, methylation of H3 at lysines 9 and 27 and of H4 at lysine 20 marks heterochromatin and transcriptionally repressed euchromatin (see Lachner et al (2003) for review). In *Drosophila*, constitutive heterochromatin is enriched in H3 dimethylated at lysine 9 (dimH3K9) (Schotta et al., 2002). In contrast, in mammals trimethylation of H3 at lysine 9 and of H4 at lysine 20 was found in constitutive heterochromatin (Schotta et al., 2004) and H3 tetramethylation at lysine 9 in facultative heterochromatin (Peters et al., 2002). Selective methylation of H3 at lysine 9 is carried out by specific histone methyltransferases (HMTs). One of the best characterized HMTs is Su(var)3-9 of *Drosophila melanogaster*. The gene Su(var)3-9 belongs to the class of modifiers of PEV (position effect variegation). PEV occurs when a euchromatic gene is translocated into the vicinity of heterochromatin, which results in a random silencing pattern and mosaic expression of this gene. It is thought that silencing is due to spreading of heterochromatin into such euchromatic genes (Boivin and Dura, 1998; Wallrath and Elgin, 1995). The probability of silencing can be influenced by mutations in unrelated gene loci and the group of genes, in which

loss-of-function mutations lead to suppression of PEV, is referred to as Su(var)-group of genes (Platero et al., 1995; Rea et al., 2000; Reuter and Spierer, 1992; Wallrath and Elgin, 1995). Mutations in *clr4*, the *S. pombe* homolog of Su(var)3-9 (Ivanova et al., 1998), result in disruption of heterochromatin formation and in chromosome segregation defects (Ekwall et al., 1996). More recently it was discovered that Su(var)3-9 is a HMT specific for H3K9. Also the Su(var)3-9 homologues from human (SUV39H1) and mice (Suv39h1) and their yeast homolog *clr4* were shown to encode histone H3K9-specific methyltransferases (Lachner et al., 2001; Peters et al., 2001; Rea et al., 2000).

It was shown that the SU(VAR)3-9 class HMTases have two highly conserved domains: the SET domain and the chromatin organization modifier (chromo) domain. The SET domain was initially identified as common motif in *Drosophila* SU(VAR)3-9, the Polycomb-group protein E(Z) and the trithorax-group (*trxG*) protein TRX (see (Jenuwein et al., 1998; Kouzarides, 2002) for review). The SET domain of SU(VAR)3-9-related HMTases catalyses the methylation of H3 at lysine 9, while the SET domain of the *trxG* protein ASH1 specifically methylates H3 at lysine 4 (Byrd and Shearn, 2003; Jenuwein et al., 1998). The SET domain requires adjacent cysteine-rich domains (Rea et al., 2000). Many SET-domain proteins are known in different species (Briggs et al., 2001; Jenuwein et al., 1998; Kouzarides, 2002). The exact mechanism of SET domain activity, however, is still unclear.

The chromo domain was originally identified as a 30-50 amino acid domain common for the Polycomb (Pc) protein and the heterochromatin protein 1 (HP1) of *Drosophila melanogaster* (Koonin et al., 1995; Paro and Hogness, 1991). The chromo domain of HP1 binds with high affinity to histone H3 methylated at lysine 9 (Bannister et al., 2001; Lachner et al., 2001). HP1 forms complexes with *Drosophila* SU(VAR)3-9 (Schotta et al., 2002), and M31 (a mammalian homologue of HP1) binds to SUV39H1 and Suv39h1 (the human and mouse homologues of SU(VAR)3-9, respectively) (Aagaard et al., 1999). Similar data were obtained with fission yeast: the correct localization of Swi6 (homolog of HP1) depends on Clr4 (a homologue of the mammalian SUV39H1) (Ekwall et al., 1996). Thus, HP1 and its homologs form complexes with the HMTase which creates the specific binding site for HP1. This „loop“ was suggested to be a key regulatory mechanism for induction and propagation of heterochromatin (Jenuwein, 2001; Lachner et al., 2001).

While the chromodomain protein HP1 binds to constitutive heterochromatin of *Drosophila melanogaster*, the chromodomain protein Pc does not bind to this fraction of chromatin but binds specifically to about 120 euchromatic sites, as has been shown on polytene chromosomes from salivary glands and in embryonic nuclei (Buchenau et al., 1998; Rastelli et al., 1993; Zink and Paro, 1989). It was shown that histone H3 methylated at lysine 27 is a mark recognized specifically by chromo domain of Pc (Fischle et al., 2003), which is more than 60% identical to the chromo domain of HP1 (Paro and Hogness, 1991). Pc and other Polycomb-group (PcG) proteins are essential

for transcriptional silencing of euchromatic genes, and in the next chapter the possible mechanisms of PcG-mediated repression will be addressed more closely.

1.2. PcG-mediated regulation of transcriptional activity

During early embryogenesis of *Drosophila*, the spatially restricted expression patterns of homeotic (Hox) genes are established by different regulatory cascades (Ingham and Martinez Arias, 1992). During subsequent stages of development, active or repressed states of Hox genes are maintained by two antagonistic groups of proteins: trithorax group (TrxG) proteins, which are essential for maintaining active states, and PcG proteins, which are essential for maintaining repressed states (Francis and Kingston, 2001; Pirrotta, 1998; Ringrose and Paro, 2004).

In *Drosophila*, PcG proteins act in three separate multiprotein complexes. (1) The **PRC1** (Polycomb repressive complex 1), which contains Pc, Polyhomeotic (Ph), Posterior sexcombs (Psc), Sexcombs extra (Sce, also known as dRING1), and components of basal transcriptional machinery (Franke et al., 1992; Saurin et al., 2001; Shao et al., 1999). PRC1 is able to inhibit the nucleosome remodelling ability of the SWI/SNF complex *in vitro* (Francis et al., 2001; Levine et al., 2002; Shao et al., 1999). (2) The **ESC-E(Z)** (extra sex combs-Enhancer-of-zeste) complex (also known as PRC2), which contains Esc, E(z), the suppressor of PEV Su(var)12, histone deacetylases Rpd3 and the histone-binding protein p55 (also a component of the chromatin remodelling complex NURF) (Czermin et al., 2002; Muller et al., 2002; Ng et al., 2000; Tie et al., 2001). The ESC-E(Z) complex functions as a HMT that specifically methylates histone H3 at lysine 27 *in vitro* (Czermin et al., 2002; Muller et al., 2002; Muller and Kassis, 2006; Orlando, 2003). Thus, the PRC2 complex creates binding sites for the chromodomain of the Pc protein associated with the PRC1 complex. Both PRC1 and ESC-E(Z) complexes are conserved between flies and mammals, although mammalian PRC1 appears to lack most of non-PcG components (Levine et al., 2002; Ringrose and Paro, 2004). (3) The **PhoRC** (Pho repressive complex) which was purified from *Drosophila* embryos and characterised very recently (Klymenko et al., 2006). PhoRC contains Pho (Pleiohomeotic) and dSfmbt, a novel PcG protein which is crucial for Hox gene silencing. Pho is the fly homolog of the mammalian transcriptional regulator YY1 (Brown et al., 1998). dSfmbt selectively binds to mono- or dimethylated lysine 9 of histone H3 or lysine 20 of histone H4 (Klymenko et al., 2006). Since PhoRC targeting to PREs (Polycomb response elements, see below) depends on the Pho DNA-binding ability, it is thought that binding of dSfmbt to methylated histones is not required for PhoRC targeting but is needed for repression (Klymenko et al., 2006; Muller and Kassis, 2006). To date, most components of PRC1, ESC-E(Z) and PhoRC have been shown to specifically bind at PREs of Hox and other target genes (Klymenko

et al., 2006; Orlando et al., 1998; Papp and Muller, 2006; Strutt et al., 1997; Strutt and Paro, 1997).

There exist several models of how PcG-mediated repression could be achieved. (a) Since Pc and HP1 have a homologous chromo domain, it was suggested that PcG proteins package the DNA into a heterochromatin-like structure (Breiling et al., 1999; Busturia et al., 1997; Messmer et al., 1992; Paro and Hogness, 1991). (b) Another model proposes that PcG complexes assembled on PREs might interact with each other, bringing PREs together and thus forming loops or nuclear subcompartments where the target genes are isolated from transcription factors and RNA polymerase (Breiling et al., 1999; Felsenfeld, 1996; Orlando, 2003; Pirrotta, 1995; Pirrotta, 1998). (c) Some data suggest that PRE DNA-looping interactions might change from promoter-enhancer to promoter-PcG interactions (Bienz and Muller, 1995; Pirrotta, 1998). (d) Another suggestion is that PcG-mediated repression might involve inhibiting the assembly or function of the transcription machinery (Francis and Kingston, 2001; Simon and Tamkun, 2002). Experimental evidence exists in support of each of these models, although the exact mechanism of the Pc-mediated repression remains to be unveiled.

TrxG proteins also function in multiprotein complexes, four of which were purified from *Drosophila* embryos so far: the 2 MDa BRM complex, the 2 MDa ASH1 complex, the 0,5 MDa ASH2 complex and the 1 MDa TRX complex (TAC1) (see (Ringrose and Paro, 2004; Simon and Tamkun, 2002) for review). The **2 MDa BRM** complex consists of the trxG proteins Brahma (Brm), Osa, Moira (Mor) and Snr1. This complex is closely related to the SWI/SNF nucleosome remodelling complex (Kal et al., 2000; Papoulas et al., 1998; Petruk et al., 2001). Other trxG proteins can interact with the BRM chromatin remodelling complex. For example, the BRM complex is an essential co-activator for Zeste, a trxG protein with DNA-binding activity (Kal et al., 2000). Many BRM-related chromatin remodelling factors were also found in vertebrates (see (Papoulas et al., 1998) for overview). The **2 MDa ASH1** and **0.5 MDa ASH2** complexes contain the Ash1 and Ash2 TrxG proteins, respectively. They do not stably interact with the BRM complex (Papoulas et al., 1998). Ash1 (absent, small, or homeotic discs 1) is a HMTase reported to methylate H3 at lysines 4 and 9 and H4 at lysine 20 (Beisel et al., 2002; Byrd and Shearn, 2003). The **1 MDa TAC1** complex contains the trxG protein Trx, the histone acetyltransferase Cbp (CREB binding protein), and the antiphosphatase Sbf1. TAC1 acetylates core histone tails, suggesting a possible role in the epigenetic maintenance of gene activity (Petruk et al., 2001).

PcG and trxG complexes bind to *cis*-regulatory elements of their target genes and maintain the status of transcriptional activity of these genes over many cell generations. These *cis*-regulatory DNA elements are so-called Polycomb- or trithorax response elements (PREs and TREs, respectively) (Fauvarque and Dura, 1993; Simon et al., 1993). Several PREs like the Fab-7 and Mcp elements have been identified in

Drosophila and over 100 PREs are expected to be present in the *Drosophila* genome since there are over 100 Pc binding sites in embryonic nuclei (Buchenau et al., 1998) and on polytene chromosomes from larval salivary glands (Rastelli et al., 1993; Zink and Paro, 1989). This is in accordance with their predicted numbers (Ringrose et al., 2003). Surprisingly, it was found that PcG and trxG proteins bind simultaneously to PREs (Orlando et al., 1998; Strutt et al., 1997). It was shown that the trxG proteins Trx and Ash1 bind to many PREs on polytene chromosomes, which are also simultaneously bound by the PcG, and additionally to a number of other sites (Chinwalla et al., 1995; Rozovskaia et al., 1999). Therefore, these elements are also called PRE/TREs (Polycomb/Trithorax response elements) (Ringrose et al., 2003) or just PREs. Several short motifs which occur at least once in all known PRE/TREs have been identified (Ringrose et al., 2003). Using these motifs and a newly invented sequence-based search tool, a genome-wide PRE/TRE prediction was made which identified 167 candidate PRE/TREs (Ringrose et al., 2003). Since these regulatory elements are essential for maintaining a defined state of gene activity during subsequent cell generations, they were also termed „cellular memory modules“, or CMMs (Cavalli and Paro, 1998; Paro and Harte, 1996). Despite the fact that many homologs of *Drosophila* PcG and trxG proteins are known in mammals, which also act antagonistically on Hox genes (Hanson et al., 1999), regulatory elements like PREs were not yet discovered in mammals (Ringrose and Paro, 2004).

One of the best studied *Drosophila* CMMs is the Fab-7 element from the Bithorax complex (BX-C), which is involved in the regulation of parasegment-specific transcription patterns of the Abdominal-B gene (Busturia and Bienz, 1993). In order to address the question whether heterochromatic structures inaccessible to transcription factors assemble at this element, several transgenic fly lines were created containing constructs where Fab-7 elements were adjacent to a GAL4-driven lacZ reporter and a marker mini-*white* gene (Zink and Paro, 1995). Number and orientation of Fab-7 elements were specific for each transgenic construct. Results obtained with corresponding transgenic flies showed that the transgenic Fab-7 element induced mosaic expression of the lacZ reporter gene as well as of the distantly located mini-*white* gene, which resulted in variegated eye colour. This effect was reminiscent of heterochromatin-induced PEV; however, none of the transgenes mapped to heterochromatic regions, suggesting the PRE as the cause of variegation. Similar results were obtained in other studies investigating the effects of PREs on reporter gene expression (Chan et al., 1994; Fauvarque and Dura, 1993). FISH experiments and experiments with Pc-null mutants confirmed that the transgenic Fab-7 element bound Pc, and that the silencing of reporter genes flanking the Fab-7 element was dependent on the dose of Pc (Zink and Paro, 1995). A pulse of GAL4, however, could relieve Pc binding to Fab-7 and Pc-induced silencing and resulted in activation of reporter genes. The degree of repression and activation depended on the ratio between Pc

and GAL4. In the experiments performed by Zink and Paro (1995), GAL4 expression was induced at larval stages of development, which resulted in transient activation. Analyses of expression of the mini-*white* reporter gene also revealed that repression was pairing sensitive and temperature dependent. Furthermore, it was demonstrated that the repression mediated by Fab-7 depended on the orientation of the element in the construct: the proximal-dorsal orientation resulted in increased repression (Zink and Paro, 1995).

These findings led way to subsequent experiments further exploring the effects of GAL4 upon Pc-mediated silencing in the transgenic flies, produced by Zink and Paro (1995). Introduction of a heat-shock activatable GAL4 driver provided the opportunity to induce GAL4 pulses at defined stages of development. Using several transgenic fly lines with Fab-7-containing transgenes it was shown that an embryonic pulse of GAL4 led to stable activation while larval pulses resulted in transient activation (Figure 1) (Cavalli and Paro, 1998; Zink and Paro, 1995). These effects were not

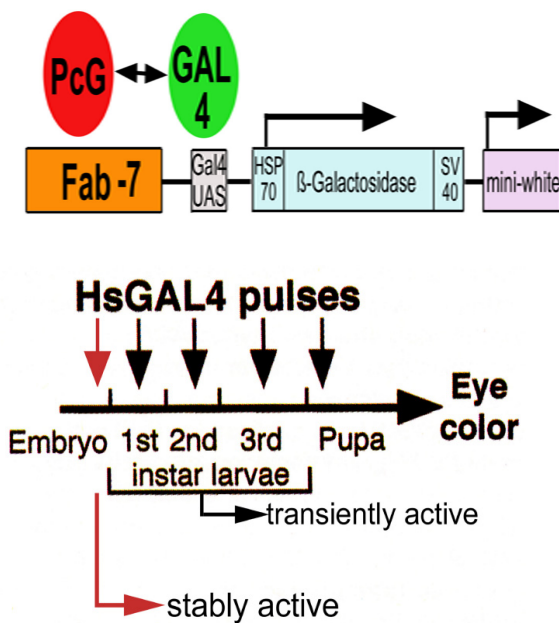


Figure 1. Stable and transient activation of transgenes (from Cavalli and Paro (1998) and Zink and Paro (1995) with minor changes). The upper scheme shows an example of a transgenic construct. The reporter genes are under the control of Fab-7 bound by PcG and the Gal4UAS bound by GAL4. A single 1h heat-shock induces GAL4 expression and activates transgenes under UAS_G control (see also Figure 2). A heat-shock applied during embryonic development led to stable activation of transgenes, while a GAL4 pulse at later stages of development resulted in transient activation of the constructs.

dependent on the orientation of Fab-7 in the transgenic construct. Similarly, since Pc-mediated repression was enhanced at higher temperatures (Zink and Paro, 1995), a hyperrepressed state could be induced if embryos developed at 28°C instead of 18°C. Both stably active and hyperrepressed states of Fab-7 were mitotically inheritable throughout development and could be transmitted through female meiosis in a GAL4-

independent manner to subsequent generations (Cavalli and Paro, 1998). Interestingly, immunostaining of polytene chromosomes of 3rd instar larvae without GAL4 inductions as well as after an embryonic pulse of GAL4 showed that PcG proteins were bound to the Fab-7-containing transgene at its inactive as well as stably active state (Cavalli and Paro, 1999). These data were in agreement with other results which indicated that PcG proteins can be associated with active genes (Strutt and Paro, 1997). Further experiments showed that histone H4 hyperacetylation was not present at the inactive Fab-7 element but associated with the stably active state, suggesting that H4 hyperacetylation might be a heritable epigenetic tag of the activated element (Cavalli and Paro, 1999).

Experiments with the transgenic flies, described above, and other transgenic lines also showed that the *white* repression was more pronounced when the transgene was in the homozygous state (Fauvarque and Dura, 1993; Zink and Paro, 1995). This phenomenon is known as pairing-sensitive repression (see (Kassis, 2002; Pirrotta, 1999) for review). This phenomenon will be addressed in more detail in the next chapter.

1.3. Interactions between PREs in *Drosophila*

In the beginning of the last century, examinations of cytological preparations from *Drosophila* and other Dipteran insects revealed that in non-meiotic nuclei homologous chromosomes were commonly associated with each other. This phenomenon of pairing of homologous chromosomes in somatic nuclei is called somatic pairing (Csink, 2001; Henikoff, 1997). The function of somatic pairing is unclear. It was suggested that such pairing might allow one allele of a gene to contribute to the regulation of the expression of the second allele of this gene, and the term transvection was invented to refer to this type of interaction between alleles (Lewis, 1954). Phenomena of transvection or trans-sensing have been reported for several loci in *Drosophila* (see (Pirrotta, 1999) for review). There are two basic models to explain such phenomena: (a) transmission of soluble macromolecules such as a short-lived RNA transcript from one homologue to another, and (b) physical interaction between the homologous elements ((Gemkow et al., 1998) and references therein). Since these models are not mutually exclusive, it is also possible that both mechanisms contribute to the interaction.

Apart from classical transvection, other trans-interactions between homologous sequences have also been observed. In particular, it was shown that Pc-mediated silencing is enhanced by trans-interactions between homologous PREs (Chan et al., 1994; Fauvarque and Dura, 1993; Muller et al., 1999; Vazquez et al., 2006; Zink and Paro, 1995). This phenomenon is termed pairing-sensitive silencing. In one more recent study, this effect was further investigated using transgenic flies which harbored

Fab-7-containing transgenic constructs (Bantignies et al., 2003). One of the transgenic lines, used in most of experiments of Bantignies et al. (2003), was of particular interest since it was also used in the experimental work performed here. This line was named Fab-X by Bantignies et al. (2003) but its original name was 5F24 25,2 (Zink and Paro, 1995). The line harbors the 5F24 transgenic construct, which contains the Fab-7 element in dorsal-proximal orientation and two reporter genes, *lacZ* and *mini-white*, under the control of the GAL4-binding site, and is inserted into the *scalloped* (*sd*) locus (the *sd* gene is essential for wing blade formation) on the X chromosome (Zink and Paro, 1995). Both *mini-white* and *sd* genes showed pairing-sensitive repression as females homozygous for the insertion showed stronger repression than heterozygous females or males with a single X chromosome (Zink and Paro, 1995). Interestingly, repression of both of these genes was dependent on the presence of the endogenous Fab-7 element (Bantignies et al., 2003). These data suggested interactions between the endogenous and transgenic copies of Fab-7. To test whether direct interactions took place, analyses of the relative nuclear positions of the *sd* locus (X chromosome) and *Abd-B* (chromosome 3) were performed by Bantignies et al. (2003) in whole-mount embryos using fluorescent in situ hybridization (FISH). Embryos were imaged using epifluorescence microscopy with deconvolution, and subsequent image analyses showed pairing (colocalization) between the *sd* locus and *Abd-B* in 7% of cells from WT embryos and in 23% of cells from transgenic embryos. When the endogenous copy of Fab-7 was removed, the pairing frequency in transgenic embryos was the same as in the WT embryos. Enhanced pairing was observed in wing imaginal discs from 3rd instar larvae: transgenic Fab-X larvae showed pairing of the *sd* and *Abd-B* loci in 43% of cells while in wing imaginal discs from WT larvae only 5% of cells displayed colocalization. Removal of the endogenous copy of Fab-7 in transgenic larvae reduced the percentage of colocalization to 14%. These results were confirmed by using other transgenic lines with a different chromosomal localization of the transgenic copy of the Fab-7 element. Other larval tissues were not examined. In agreement with previously obtained data (Cavalli and Paro, 1998; Zink and Paro, 1995), it was shown that Pc-mediated repression depended on the temperature, and that derepression of the *sd* locus could be transmitted through meiosis (Bantignies et al., 2003).

Similar long-distance interactions were observed between homologous copies of another PRE from the BX-C, the Mcp element (Vazquez et al., 2006). In these experiments, an *in vivo* microscopy assay based on green fluorescent protein (GFP)-Lac repressor/operator recognition was used, which ensured that the nuclear architecture was not disturbed by fixation or hybridization procedures. A P-element construct, carrying the Mcp element, the *mini-white* gene, the *white* enhancer, and a ~2.5-kb array of *lac* operator (*lacO*) sequences, was used to transform a *white* mutant *Drosophila* strain, while a heat-shock inducible system used for expression of GFP-Lac repressor protein allowed visualization of the transgene in live tissues. From 10

lines obtained, 8 showed pairing-sensitive repression of mini-*white*, indicating that the lacO array did not interfere with the induction of pairing-sensitive silencing by the Mcp element. The ability of Mcp to mediate long-distance interactions was tested in crosses with lines which carried transgenes on chromosomes 2, 3 or X. In eye imaginal discs from different lines, pairing between the transgenes was observed in more than 90% of nuclei. Association was observed when the inserts were located on the same chromosome or on different chromosomes. In other larval tissues, such as brain and wing imaginal discs, pairing was also observed but with a markedly lower frequency (20-60%). In several polytene tissues, which were tested, no pairing was found. These observations strongly suggest that pairing is tissue-specific and also depends on the level of polyteny. This would be in agreement with the data obtained with Fab-7: pairing between endogenous and transgenic copies of Fab-7 was found in 43% of nuclei from wing imaginal discs (Bantignies et al., 2003), but in polyploid nuclei from the peripodial membrane of these discs the frequency of colocalization was close to 0% (F. Bantignies, personal communication). Interestingly, Mcp-mediated interactions were not limited by the copy number: in a transgenic line, which carried 4 copies of the construct, the majority of nuclei from eye imaginal discs showed pairing of all four inserts (Vazquez et al., 2006). Time-lapse series, performed with eye imaginal discs from several transgenic lines, suggested that pairing between constructs was stable. In rare cases when the inserts were not paired, they did not associate *de novo* during a time lapse series. Together, the data obtained with Fab-7 and Mcp elements suggested that long-distance interactions between PREs are sequence- and tissue-specific, and seem to be stable once established. It was also shown that several components of the RNAi machinery, such as *AGO1*, *piwi* and *aub*, are required for the maintenance of such long-distance Fab-7 mediated chromosomal interactions (Grimaud et al., 2006).

Since it was shown that PREs can interact physically, one would expect to observe aggregations of PcG proteins in the interphase nucleus, indicating those sites where PREs associate. In fact, the existence of such compartments was proposed already in 1993 (Orlando and Paro, 1993): „PcG multimeric complexes might not be simply involved in a condensation of chromatin into a regular higher order superstructure, but rather be responsible for trapping inactive genes into particular subdomains of the nucleus“ (Orlando and Paro, 1993). However, it is unclear whether this is the case. More than 100 Pc-binding sites were observed on polytene salivary gland chromosomes (Franke et al., 1992; Rastelli et al., 1993; Zink and Paro, 1989). Data, obtained with tissue culture *Drosophila* SL2 cells, also indicated that nuclear enrichments of Pc represent individual chromosomal binding sites (Messmer et al., 1992). Using high-resolution confocal laser scanning microscopy and careful image processing, Buchenau et al. (1998) showed that in *Drosophila* embryos Pc, Ph and Psc are distributed throughout most of the nuclear volume as 100 and more discrete spots (Buchenau et al., 1998). A similar distribution of Pc in interphase embryonic nuclei

and imaginal discs of 3rd instar larvae was also shown using a Pc-eGFP transgenic fly line, although no quantitative analysis was made (Dietzel et al., 1999). These data suggested that at least the majority of Pc-binding sites are not assembled into higher order compartments in *Drosophila* nuclei.

Other research groups, however, obtained different data. Ficz et al. (2005) investigated the dynamics of PcG complexes in living *Drosophila* embryos and larval tissues obtained from Pc-GFP and Ph-GFP transgenic fly lines (Ficz et al., 2005). Using high-resolution confocal microscopy and thorough image analysis, they showed that while more than 100 Pc-GFP or Ph-GFP foci can be detected in embryos, both of these proteins were found in only 30-40 foci in larval wing imaginal discs (Ficz et al., 2005). Recently, Grimaud et al (2006), using different microscopic and image processing techniques, detected 45-50 Pc and Ph aggregations in *Drosophila* embryonic nuclei, while in larval imaginal discs there were only about 30 such aggregations found, for which they used the term „Polycomb bodies“ (Grimaud et al., 2006). Taken together, the whole body of the data demonstrates that it is currently unclear whether PcG proteins form Pc bodies in *Drosophila*. The discrepancies between results obtained by different groups are likely due to the different imaging and image analysis techniques used and the difficulty to count correctly hundreds of small foci in tissues containing nuclei of only a few μm in diameter.

In mammals the nuclear distribution and binding properties of PcG proteins appear to be different. Although no PREs have been identified in mammals up to date, it was shown that in human and mouse cells PcG proteins form specific aggregations (Alkema et al., 1997; Gunster et al., 1997; Saurin et al., 1998). In several cell lines, transformed as well as primary, human PcG proteins formed discrete foci unrelated to other known nuclear domains. These aggregations were termed „Pc bodies“, which were found to be stably associated with heterochromatin in interphase nuclei, including pericentromeric heterochromatin of several chromosomes (Saurin et al., 1998). In *Drosophila*, PcG proteins were not shown to associate with pericentromeric heterochromatin.

The probable association of PREs indicates a presumable role of nuclear architecture in the regulation of gene expression. Many findings suggest that also other forms of nuclear architecture might be involved in transcriptional regulation. The next chapter gives a more detailed overview.

1.4. Nuclear architecture and gene regulation

During the last decades it became more and more clear that not only the linear arrangement of genes, but also their spatial positioning in the nucleus is important for their functional regulation. A growing body of evidence accumulates which suggests

that different nuclear compartments might create environments favorable for active or inactive states, and that changes of the nuclear location are associated with changes in the state of activity. For example, insertion of a heterochromatic block into the *bw* sequence (the *bw^D* allele) does not only inactivate this allele but also results in inactivation of the *bw⁺* allele on the homologous chromosome, in larval tissues but not in embryonic nuclei (Csink et al., 2002; Dernburg et al., 1996). The *bw⁺* allele is associated with the *bw^D* allele in larval nuclei due to somatic pairing of homologs, and this obviously leads to inactivation. Somatic pairing is well known for *Drosophila* (Csink and Henikoff, 1998) but is generally not observed in mammals (Lamond and Earnshaw, 1998). However, association of inactive genes with heterochromatin has been observed in mammals, too. It was shown in murine cells that inactive genes preferentially associated with centromeric heterochromatin assembled into chromocenters, while active loci did not associate with these domains (Brown et al., 2001; Brown et al., 1997; Schubeler et al., 2000). Thus, pericentric heterochromatin and chromocenters appear to be nuclear compartments, which are involved in gene silencing.

The nuclear periphery was also shown to be important for transcriptional regulation. This compartment is commonly considered as a zone of transcriptional repression, both in yeast and higher organisms. In budding yeast telomeres form clusters at the nuclear periphery, resulting in enrichment of the silent information regulators (Sir) proteins, which are involved in gene silencing (Cockell and Gasser, 1999). Silencing of the mating-type loci in *S. cerevisiae* is facilitated at the nuclear periphery but also requires here at least a weak silencer (Andrulis et al., 1998; Feuerbach et al., 2002). This shows that in this case silencing does not take place in the absence of silencers, and suggests that high concentrations of repressors at the nuclear periphery can compensate for partially impaired silencer functions. In *Drosophila* Kc cells many genes were identified recently, which directly interact with B-type lamin. Generally, these genes are transcriptionally silent and are localized very close to the nuclear periphery (Pickersgill et al., 2006). In human lymphocytes and fibroblasts, even whole gene-poor chromosomes were shown to be positioned at the nuclear periphery, while gene-rich chromosomes with a higher transcriptional activity had a more central location in the nucleus (Boyle et al., 2001; Cremer et al., 2001; Croft et al., 1999). During lymphocyte development in mice the immunoglobulin (Ig) loci were preferentially positioned at the nuclear periphery, but not at centromeric heterochromatin, in cells where they were inactive (hematopoietic cells and pro-T cells) but were located in the nuclear interior in pro-B cells where they will be expressed (Kosak et al., 2002). The human CFTR locus was found to be preferentially associated with the nuclear periphery in various human primary cell types and cell lines where it is not expressed, while in Calu-3 cells where it is transcriptionally active CFTR was embedded into euchromatin in the nuclear interior (Zink et al., 2004). In mammals, not only endogenous gene loci but also transgenes showed association with the nuclear periphery in their inactive states while they were

occupying more internal positions after transcriptional activation (Dietzel et al., 2004; Tumber and Belmont, 2001).

Recent data suggest that the nuclear periphery is not only a repressing compartment but has a more complex role in gene regulation. In yeast, boundary activities (which separate regulatory domains) link active chromatin to the nuclear pore complex (Ishii et al., 2002). Another study (Casolari et al., 2004) on *S. cerevisiae* demonstrated that many genes are associated with the NPC, including the silent mating-type loci, subtelomeric genes and many transcriptionally active genes as well. NPC-associated genes were enriched for binding sites of Rap1, a transcriptional regulator. ChIP experiments as well as microscopy showed that when the yeast substrate was switched from glucose to galactose, key genes of the galactose metabolism pathway relocated from the nuclear interior to the NPC (Casolari et al., 2004). In *Drosophila*, the gypsy insulator and its binding proteins preferentially localize at the nuclear periphery, forming large „insulator bodies“, pulling with them the sequences where gypsy is integrated (Gerasimova et al., 2000). Thus, the nuclear periphery can provide a suitable environment for gene repression as well as gene activation. It is thought that the most likely mechanism which can ensure simultaneous negative and positive regulation at the nuclear periphery is looping of chromatin regions or differential association due to flexibility of chromatin (Gerasimova et al., 2000; Misteli, 2004).

An important question is what the functional relationships are between nuclear positioning, transcriptional activity, histone modifications, and replication timing. The relationships between histone acetylation, transcription activity and nuclear localization were addressed using the human CFTR locus as a model (Zink et al., 2004). In cell lines where CFTR was not expressed it was associated with the nuclear periphery and hypoacetylated chromatin, while in the expressing cell line it occupied more interior nuclear positions within chromatin, which was hyperacetylated at histone H4 (Zink et al., 2004). When the expressing cells were treated with the transcriptional inhibitor 5,6-dichlorobenzimidazole riboside (DRB), the transcriptional activity of CFTR was reduced to ~50% and it occupied significantly more peripheral positions in comparison to control cells. Analysis of the β -globin locus in Calu-3 cells with and without DRB treatment showed that DRB did not induce general changes in chromatin structure. Thus, repositioning of the CFTR locus to the nuclear periphery was related to its reduced transcriptional activity. To test whether the level of histone acetylation also provides positional information, different cell lines were treated with the drug trichostatin A (TSA), which induces hyperacetylation of histones. This treatment led in non-expressing cells to repositioning of CFTR from the perinuclear to the interior compartment without inducing transcription (Zink et al., 2004). These results suggested that the level of histone acetylation at the CFTR locus might provide positional information. Together, the results of DRB and TSA treatments indicated that the nuclear positioning of CFTR was dependent on its transcriptional activity and not

vice versa.

Previous data demonstrated that a large region on human chromosome 7, which includes the CFTR gene, switched its replication timing from late to early when CFTR became transcriptionally active (Selig et al., 1992). The relationships between replication timing, transcriptional activity, nuclear positioning, and histone acetylation were studied using CFTR and its two neighboring genes, GASZ (ASZ1) and CORTBP2 (CTTNBP2). Individual analyses of the nuclear localization of these loci showed that interior positioning and association with hyperacetylated and early replicating euchromatin correlates with early replication timing of genes (Englmann et al., 2005; Zink et al., 2004). TSA treatment induced repositioning of the CFTR locus from the nuclear periphery into more interior compartments (Zink et al., 2004) and switching to an earlier replication timing (Englmann et al., 2005), but not its transcriptional activation (Zink et al., 2004), indicating that the switch to an earlier replication timing is not dependent on changes in transcriptional activity. All together, these results suggest that although CFTR replicates early when it is transcriptionally active, these two processes are not directly connected. Both replication timing and transcriptional activity appear to be linked via the localization of CFTR within different chromatin fractions.

These results, together with data from other studies (see (Zink, 2006) and references therein) resulted in a model concerning the relationships between histone modifications, transcriptional activity, replication timing and association of genes with different fractions of chromatin (Englmann et al., 2005; Zink, 2006). The model suggests the following course of events: the patterns of histone modifications (particularly histone acetylation) define the nuclear positions of gene loci, which in turn determine their replication timing. This is not dependent on transcriptional activation (Schubeler et al., 2000; Zink et al., 2004). However, active transcription might induce further changes in histone modifications (see (Schubeler et al., 2004) for review) and nuclear positioning, which, in turn, could also affect replication timing. Switches in replication timing associated with changes in nuclear positioning and histone modifications might lead to the establishment of stable feedback loops (Englmann et al., 2005). This is suggested by the observation that the replication timing of a locus can impact on its histone acetylation patterns (Zhang et al., 2002). It is further proposed that these feedback loops are involved in the maintenance of established gene expression patterns. Thus, nuclear positioning would be mainly involved in maintaining established states of activity (Englmann et al., 2005; Zink, 2006). However, the exact role of nuclear positioning must be further clarified.

1.5. Goals

The goal of this study was to find out whether higher order nuclear compartmentalization is involved in the regulation of PREs. To address this problem, different lines of transgenic flies should be used. These lines harbor constructs which contain the Fab-7 element, the GAL4-binding site and two reporter genes (Cavalli and Paro, 1998; Zink and Paro, 1995). The constructs can be stably or transiently activated by a pulse of GAL4 at embryonic or larval stages of development, respectively. It was planned to investigate the nuclear localization of the constructs at different states of activity. Of particular interest were presumable associations with nuclear domains shown before to be involved in gene regulation, namely the heterochromatic chromocenter and the nuclear periphery. Furthermore it was planned to address the question whether pairing of PREs and the formation of „Polycomb bodies“ is a general mechanism involved in the regulation of PREs. Also the nuclear localization of several endogenous genes should be analyzed for comparison.

In addition, the results obtained with *Drosophila* should be compared to results obtained with mammalian cells. In mammals the positioning of transgenic constructs should be addressed using cell lines obtained from transgenic pigs (Hofmann et al., 2003). These cell lines carry a LV-PGK retrovirus (Follenzi et al., 2000), which has a defined level of activity in each cell line. It was planned to analyze the nuclear positioning of the construct in different cell lines with regard to the nuclear periphery and chromocenters. The effect of transcriptional activation of inactive constructs on their nuclear localization should also be addressed.

Furthermore, it was planned to address the involvement of Tpr in the peripheral positioning of inactive genes in human cells. Tpr is associated with the nuclear basket of the nuclear pore complexes. It was planned to use the CFTR locus as a model, and the effect of down-regulation of Tpr on its nuclear localization should be analyzed.

2. Materials and methods

2.1. Materials

2.1.1. Chemicals, culture media and additives

Chemical	Manufacturer
Acetic Acid 100%	Merck, Darmstadt
Agar	Fluka, Buchs
Agarose	Cambrex, USA
Aqua Ultra Pure	Invitrogen, Karlsruhe
Bovine Serum Albumine (BSA) (fraction V)	Sigma-Aldrich, Schnelldorf
CHAPS (3-[3-(Cholamidopropyl)dimethylammonio]-1-proanesulfonate)	Roche Diagnostics, Mannheim
Colcemid (10 μ g/ml)	Seromed Biochrom, Berlin
Dextrane sulfate	Pharmacia, Braunschweig
Diethylether	Merck, Darmstadt
DMSO (Dimethyl Sulfoxide)	Sigma-Aldrich, Schnelldorf
Disodium hydrogenphosphate	Merck, Darmstadt
EDTA (Ethylenediaminetetraacetic Acid)	Sigma-Aldrich, Schnelldorf
EGS (Ethylene Glycol-bis(succinic acid N-hydroxysuccinimide Ester)	Sigma-Aldrich, Schnelldorf
EGTA (Ethylene Glycol-bis(2-aminoethylether)-N,N,N',N'-tetraacetic Acid)	Sigma-Aldrich, Schnelldorf
Ethanol absolute p.a.	Merck, Darmstadt
Ethidium bromide	Sigma-Aldrich, Schnelldorf
Formaldehyde, stabilized	Merck, Darmstadt
Formamide	Merck, Darmstadt
Formamide, deionized	Sigma-Aldrich, Schnelldorf
Glucose	Sigma-Aldrich, Schnelldorf
Glutaraldehyde (electron microscopy grade, 70% in aqueous solution)	Sigma-Aldrich, Schnelldorf
Glycerol	Sigma-Aldrich, Schnelldorf
HEPES (4-(2-hydroxyethyl)-1-piperazineethanesulfonic acid)	Sigma-Aldrich, Schnelldorf
n-Heptane	Sigma-Aldrich, Schnelldorf
Hydrochloric acid	Merck, Darmstadt
IPTG (Isopropyl- β -D-Thiogalactopyranoside)	Sigma-Aldrich, Schnelldorf
Isopropanol	Sigma-Aldrich, Schnelldorf

Kanamycine	Sigma-Aldrich, Schnelldorf
Magnesium chloride	Merck, Darmstadt
Methanol	Merck, Darmstadt
Peptone	Fluka, Buchs
PIPES (Piperazine-1,4-bis(2-ethane-sulphonic acid))	Sigma-Aldrich, Schnelldorf
Pluronic F-68	Sigma-Aldrich, Schnelldorf
Potassium chloride	Merck, Darmstadt
Potassium dihydrogenphosphate	Merck, Darmstadt
Potassium hydroxide	Sigma-Aldrich, Schnelldorf
Saponin	Sigma-Aldrich, Schnelldorf
Sigmacote	Sigma-Aldrich, Schnelldorf
Sodium acetate	Merck, Darmstadt
Sodium chloride	Merck, Darmstadt
Sodium citrate dihydrate	Sigma-Aldrich, Schnelldorf
Sodium dihydrogenphosphate	Carl Roth, Karlsruhe
Sodium hydroxide	Sigma-Aldrich, Schnelldorf
Sodium hypochlorite	Carl Roth, Karlsruhe
Sodium tetrahydridoborate	Aldrich Chemical Company, USA
Sodium thiocyanate	Sigma-Aldrich, Schnelldorf
Spermidine	Sigma-Aldrich, Schnelldorf
Spermine	Sigma-Aldrich, Schnelldorf
Trizma hydrochloride	Sigma-Aldrich, Schnelldorf
Trizma base	Sigma-Aldrich, Schnelldorf
Triton X-100	Merck, Darmstadt
Trypton	Fluka, Buchs
Tween 20	Merck, Darmstadt
Vectashield	Vector, Burlingame, USA
Yeast extract	Sigma-Aldrich, Schnelldorf

Culture media and additives	Manufacturer
Dulbecco's high glucose medium (DMEM)	Invitrogen, Karlsruhe
Fetal calf serum (FCS), inactivated	Invitrogen, Karlsruhe
Natural goat serum	Sigma-Aldrich, Schnelldorf
Penicillin/Streptomycin, 100x	Invitrogen, Karlsruhe
Schneider's Drosophila medium	Invitrogen, Karlsruhe
Trypsine-EDTA solution with HEPES, 1x	Invitrogen, Karlsruhe

2.1.2. Enzymes

Enzyme*	Manufacturer
Alu I (10 U/ μ l)	Fermentas, St. Leon-Rot
DNAse I (1 U/ μ l)	Invitrogen, Karlsruhe
Klenow enzyme (2 U/ μ l)	Roche, Mannheim
RNAse A, powder	Roche, Mannheim
Pdm I (10 U/ μ l)	Fermentas, St.Leon-Rot
Taq DNA Polymerase (5 U/ μ l)	Roche, Mannheim
Taq DNA Polymerase (5 U/ μ l)	Amersham Biosciences, Freiburg
Taq DNA Polymerase	New England Biolabs, Frankfurt

*all enzymes require corresponding reaction buffers (usually delivered together with the enzyme)

2.1.3. Nucleotides, nucleic acids and vectors

Nucleotide	Manufacturer
Biotin-16-dUTP (1mM)	Roche, Mannheim
Cy3-dUTP, Cy5-dUTP (1mM)	Amersham Biosciences, Freiburg
dATP, dCTP, dGTP, dTTP Mix (each 10mM)	Roche, Mannheim
dATP, dCTP, dGTP, dTTP (5mM)	Roche, Mannheim
Digoxigenin-11-dUTP (1mM)	Roche, Mannheim
Fluorescein-12-dUTP (1mM)	Roche, Mannheim
Hexanucleotide mix, 10x	Roche, Mannheim

Nucleic acid	Manufacturer/Supplier
CF1 probe for 5' region of CFTR locus (Zink et al., 2004)	Kindly provided by Dr. Andreas Englmann, LMU Munich
Human Cot-1 DNA (1 mg/ml)	Invitrogen, Karlsruhe
Herring Sperm DNA (10 mg/ml)	Invitrogen, Karlsruhe
Porcine Hyblock DNA (1 mg/ml)	Applied Genetics Laboratories, Melbourne, Australia
Painting probes for pig chromosomes	Kindly provided by Dr. Roscoe Stanyon, University of Florence, Italy
LV-PGK probe	Kindly provided by Prof. Alexander Pfeifer, LMU Munich
Probes for ppt-PGK, GFP and W-3'LTP fragments	Kindly provided by Prof. Alexander Pfeifer, LMU Munich
yeast tRNA, lyophilized	Roche, Mannheim

Oligonucleotide	Manufacturer/Supplier
PCR PRIMERS	
Specific primers for <i>Drosophila</i> PREs	Kindly provided by Dr. Leonie Ringrose, ZMBH, Heidelberg
Primers for CF1 probe <i>forward</i> (B3F): 5'-AATGTAACAGCCTTCTGGGAG-3' <i>reverse</i> (C16D): 5'-GTTGGCATGCTTTGATGACGCTTC-3'	Kindly provided by Dr. Andreas Englmann, LMU Munich
Primers for LV-PGK full length <i>forward</i> : 5'-CTCGACGCAGGACTCGGCTT-3' <i>reverse</i> : 5'-GCAGATCTTGTCTTCGTTGGGAGT-3'	Kindly provided by Prof. Alexander Pfeifer, LMU Munich
Primers for ppt-PGK fragment of LV-PGK <i>forward</i> : 5'-AGAATAGTAGACATAATAGC-3' <i>reverse</i> : 5'-GTCGGTGATTCGGTCAACGA-3'	Kindly provided by Prof. Alexander Pfeifer, LMU Munich
Primers for GFP fragment of LV-PGK <i>forward</i> : 5'-ATGGTGAGCAAGGGCGAGGA-3' <i>reverse</i> : 5'-TTGTACAGCTCGTCCATGC-3'	Kindly provided by Prof. Alexander Pfeifer, LMU Munich
Primers for W-3'LTR fragment of LV-PGK <i>forward</i> : 5'-ACGAGAAGCGCGATCACATGGTC-3' <i>reverse</i> : 5'-CTGCTAGAGATTTTCCCACTGAC-3'	Kindly provided by Prof. Alexander Pfeifer, LMU Munich
DOP-PCR: 6MW (5'-CCG ATC CGA GNN NNN NAT GTG G-3') (Telenius et al., 1992)	Metabion, Martinsried
Alu-PCR: CL1 (5'-TCC CAA AGT GCT GGG ATT ACA G-3') (Lengauer et al., 1992)	Metabion, Martinsried

siRNAs	
TPR, var. A: (5'-UAG AGC UUC AAC AUC AGC AGC AUG C-3')	Invitrogen, Karlsruhe
TPR, var. C: (5'-GCU UAA ACA AAG GAA UGG AGC CUU A-3')	Invitrogen, Karlsruhe

Negative control: Alexa-488 (5'-UUC UCC GAA CGU GUC ACG U)dTdT-3'	Quiagen, Hilden
OTHER OLIGOS	
Drosophila satellite DNA: (5'-AAG AGA AGA GAA GAG AAG AGA AGA GAA GAG AAG GAG AGA G-3')	Metabion, Martinsried

Vector	Gene locus	Source
PBluescript derived plasmids	PREs: Distalless (Dll), engrailed (en), homothorax (hth) and vestigial (vg) (each ~3 kb)	Kindly provided by Dr. Leonie Ringrose, ZMBH, Heidelberg
P1 DS07696 (Busturia and Bienz, 1993)	Abdominal-B (<i>Abd-B</i>) (~80 kb)	Kindly provided by Dr. Donna Arndt-Jovin, MPI for Biophysical Chemistry, Goettingen
λ 8053 (Hagstrom et al., 1997)	Frontoabdominal-7 (Fab-7) (~3,8 kb)	Kindly provided by Prof. Renato Paro, ZMBH, Heidelberg
sd λ 2-4a, sd λ 1-40a (Zink and Paro, 1995)	scalloped (<i>sd</i>) (~13,5 kb)	Kindly provided by Prof. Renato Paro, ZMBH, Heidelberg
P1 DS03126 (Hartl et al., 1994)	Ultrabithorax (<i>Ubx</i>) (~78 kb)	Kindly provided by Dr. Donna Arndt-Jovin, MPI for Biophysical Chemistry, Goettingen

2.1.4. Antibodies and conjugates

Primary antibodies	Manufacturer/Supplier
Anti-acetyl-Histone H4 (rabbit antiserum) Used at 1:50 in 5% BSA / PBT	Biomol, Hamburg.
Anti- β -Galactosidase (rabbit IgG) Used at 1:75 in 5% BSA / PBT	Molecular Probes, USA
Anti-dimethyl-Histone H3 (Lys4) (rabbit antiserum) Used at 1:30 in 5% BSA / PBT	Biomol, Hamburg
Anti-dimethyl-Histone H3 (Lys9), biotin conjugated (rabbit IgG) Used at 1:30 in 5% BSA / PBT	Biomol, Hamburg

Anti- <i>Drosophila</i> lamin (T40 mouse monoclonal) Used at 1:100 in 5% BSA / PBT	Kindly provided by Prof. H. Saumweber, University of Berlin
Anti-Fibrillarin (mouse monoclonal) Used at 1:200 in 5% BSA / PBT	Abcam, Cambridge
Anti-Heterochromatin Protein 1 (HP1) of <i>Drosophila</i> (rabbit polyclonal) Used at 1:50 in 5% BSA / PBT	Kindly provided by Dr. S. Elgin, University of Washington
Anti-human HP1 (goat polyclonal) Used at 1:50 in 5% BSA / PBT	Santa Cruz, Heidelberg
Anti-HP1 beta, 80% homology with <i>Drosophila</i> HP1 (rabbit polyclonal) Used at 1:30 in 5% BSA / PBT	Abcam, Cambridge
Anti-Polycomb (rabbit polyclonal) Used at 1:50 in 5% BSA / PBT	Kindly provided by Dr. Leonie Ringrose, ZMBH, Heidelberg
Anti-Polyhomeotic (rabbit polyclonal) Used at 1:50 in 5% BSA / PBT	Kindly provided by Dr. Leonie Ringrose, ZMBH, Heidelberg
Anti-Posterior Sex Combs (Psc) (rabbit polyclonal) Used at 1:50 in 5% BSA / PBT	Kindly provided by Dr. Leonie Ringrose, ZMBH, Heidelberg
Anti-RNA polymerase II, active form (CTD7 phosphorylated at Ser 2) (rat) Used at 1:2 in 5% BSA / PBT	Kindly provided by Prof. Dirk Eick, Prof. Elisabeth Kremmer, GSF, Munich
Anti-Translocated Promoter Region (Tpr) (mouse monoclonal) Used at 1:1000 in 4% BSA / 4xSSCT	Kindly provided by Dr. Volker Cordes, ZMBH, Heidelberg
Anti-trimethyl-Histone H3 (Lys4) (mouse monoclonal) Used at 1:50 in 5% BSA / PBT (immunostaining) 1:30 in 5% BSA / PBT (immunoFISH)	Abcam, Cambridge
Anti-TPR (guinea pig polyclonal) Used at 1:300 in 4% BSA / 4xSSCT	Kindly provided by Dr. Volker Cordes, ZMBH, Heidelberg
Anti-Trithorax (Trx) (rabbit polyclonal) Used at 1:50 in 5% BSA / PBT	Kindly provided by Dr. Leonie Ringrose, ZMBH, Heidelberg

Secondary antibodies / conjugates	Manufacturer
Anti-Digoxigenin-Alkaline Phosphatase (AP) (1:1000 for Dot Blot)	Roche, Mannheim
Anti-Digoxigenin-Fluorescein, -Rhodamin (sheep) Used at 1:50 in 5% BSA / PBT (<i>Drosophila</i> tissues) 1:75 in 3% BSA / PBT (<i>Drosophila</i> polytene chromosomes) 1:100 in 4% BSA / 4xSSCT (mammalian cells)	Roche, Mannheim
Anti-Digoxigenin-Cy3 (sheep)* Used at 1:50 in 5% BSA / PBT (<i>Drosophila</i> tissues) 1:150 in 3% BSA / PBT (<i>Drosophila</i> polytene chromosomes) 1:100 in 4% BSA / 4xSSCT (mammalian cells)	Boehringer, Mannheim
Anti-Green Fluorescent Protein (GFP)-Alexa-488®, -Alexa 555® (rabbit) Used at 1:50 in 5% BSA / PBT	Molecular Probes, USA
Anti-Goat-Cy5 (donkey) Used at 1:100 in 5% BSA / PBT	Dianova, Hamburg
Anti-Guinea Pig-Cy3 (donkey) Used at 1:100 in 4% BSA / 4xSSCT	Dianova, Hamburg
Anti-Mouse-Cy5, -FITC, -TRITC (goat) Used at 1:100 in 4% BSA / 4xSSCT	Dianova, Hamburg
Anti-Rabbit-Cy3, -FITC (goat) Used at 1:30 - 1:50 in 5% BSA / PBT	Dianova, Hamburg
Anti-Rabbit-TRITC (goat) Used at 1:50 in 5% BSA / PBT	Zymed Laboratories, San-Francisco, USA
Anti-Rat-Cy3 (goat) Used at 1:50 in 5% BSA / PBT	Dianova, Hamburg
Avidin-Cy3, -Cy5, -FITC conjugates Used at 1:30 in 5% BSA / PBT (<i>Drosophila</i> tissues) 1:75 in 3% BSA / PBT (<i>Drosophila</i> polytene chromosomes) 1:100 in 4% BSA / 4xSSCT (pig)	Dianova, Hamburg

* Anti-digoxigenin Fab fragments (sheep) (Boehringer, Mannheim, Germany) were labelled with Cy3 hydroxysuccinimide (Amersham, Buckinghamshire, UK) according to the manufacturer's instructions.

2.1.5. Dyes and markers

Dye	Manufacturer
DAPI (4'-6-Diamidino-2-Phenylindole) (2mg/ml)	Sigma-Aldrich, Schnelldorf
Loading Dye, 6x	Fermentas, St. Leon-Rot
NBT / BCIP (Nitro Blue Tetrazolium Chloride / 5-Bromo-4-chloro-3-indolyl phosphate, toluidine salt) stock solution	Roche, Mannheim

Marker	Manufacturer
Mass Ruler DNA Ladder Mix	New England Biolabs, Frankfurt

2.1.6. Kits

Kit	Manufacturer
Cy3 Ab Labelling Kit	Amersham Biosciences, Freiburg
Dig DNA Labelling Kit	Roche, Mannheim
DNA 3'-End Labelling Kit	Roche, Mannheim
Expand High Fidelity Kit	Roche, Mannheim
First Strand cDNA Synthesis Kit for RT-PCR (AMV)	Roche, Mannheim
Large Construct Kit	Qiagen, Hilden
QIAEx II Gel Extraction Kit	Qiagen, Hilden
QIAquick Nucleotide Removal Kit	Qiagen, Hilden
RNeasy Mini Kit	Qiagen, Hilden
Nick Translation System	Invitrogen, Karlsruhe
RNAiFect Transfection Kit	Qiagen, Hilden
Tyramide Signal Amplification Kit	Molecular Probes, USA

2.1.7. Buffers and solutions

Buffer / solution	Recipe
Agarose Gel (standard)	Add 0,5 g of agarose to 50 ml of 1xTAE buffer, boil shortly. After cooling to ~50°C add 5 µl of ethidium bromide (10 mg/ml).
AP buffer	0,1 M Tris HCl pH 9.5 0,1 M NaCl 2mM MgCl ₂ 0,05% Triton X-100

Buffer A, pH 7.4	60 mM KCl 15 mM NaCl 0,5 mM spermidine 0,15 mM spermine 2 mM EDTA 0,5 mM EGTA 15 mM PIPES
Buffer B, pH 7.4	20 mM KH_2PO_4 130 mM NaCl 20 mM KCl 10 mM EGTA 2mM MgCl_2 0,1% Triton X-100 0,5% glutaraldehyde
DAPI working solution	DAPI stock 1:4000 in 1xPBS
DAPI stock solution	2 mg/ml in dH_2O
EGS working solution	50 mM in PBS, dilute just prior to use.
EGS stock solution	EGS dissolved in liquid DMSO
Hybridization mixture (<i>Drosophila</i> tissues)	50 ml formamide 20 ml 2xSSC 30 ml 0,167 M Na-PO_4 mixture (see below) 100 μl Tween 20
Hypotonic solution	0,06 M KCl (0,9 g KCl in 200 ml H_2O)
LB medium, pH 7.0	10 g Trypton 5 g yeast extract 10 g NaCl ad 1000 ml dH_2O
Mastermix	20% Dextran sulfate in 2xSSC
NaBH_4 working solution (1 mg/ml)	167 μl 3M stock solution ad 20 ml dH_2O
*0,5 M Na-PO_4 mixture pH 7.0	0,5 M NaH_2PO_4 pH ~4.1 0,5 M Na_2HPO_4 pH ~8.6 mix them so that pH comes to 7.0
NBT / BCIP working solution	200 μl stock solution 10 ml AP buffer
PBS 10x, pH 7.0	80 g NaCl 2 g KCl 14,4 g Na_2HPO_4 2,4 g KH_2PO_4 ad 1000 ml dH_2O

PBT buffer	0,1% Tween 20 in 1xPBS
PBTT buffer	1xPBS 0,2% Triton X-100 0,2% Tween 20
RNAse A working solution (50 mg / ml)	dissolve 100 mg RNAse powder in 2 ml dH ₂ O, boil for 5-7 min to inactivate proteinases, then aliquote and store at -20°C.
SSC 20x, pH 7.0	175 g NaCl 88 g tri-sodium citrate <i>ad</i> 1000 ml dH ₂ O
SSCT, pH 7.0	200 ml 20x SSC 0,2% Tween 20 (2 ml) <i>ad</i> 1000 ml dH ₂ O
TAE 50x, pH 8.0	242 g Tris base 57,1 ml acetic acid 100 ml 0,5 M EDTA <i>ad</i> 1000 ml dH ₂ O
Tyrode's buffer, pH 7.2	135 mM NaCl 10 mM KCl 0.4 mM MgCl ₂ 1 mM CaCl ₂ 5.6 mM glucose 10 mM HEPES

2.1.8. Microscopes

Microscope	Description	Manufacturer																				
Epifluorescence microscope	<p>Axiovert 135 TV</p> <p>Objective: Plan-Apochromat 63x, NA 1.4, oil immersion</p> <p>Filter set (wavelengths in nm):</p> <table border="1"> <thead> <tr> <th>detection</th> <th>excitation</th> <th>emission</th> <th>beam splitter</th> </tr> </thead> <tbody> <tr> <td>DAPI</td> <td>BP 356</td> <td>LP 420</td> <td>FT 395</td> </tr> <tr> <td>FITC</td> <td>BP 450-490</td> <td>LP 515-565</td> <td>FT 510</td> </tr> <tr> <td>TRITC</td> <td>BP 546</td> <td>LP 575-640</td> <td>FT 560</td> </tr> <tr> <td>Cy5</td> <td>BP 575-625</td> <td>LP 660-710</td> <td>FT 645</td> </tr> </tbody> </table> <p>CCD camera: MicroMAX pixel size: 6,8 μm x 6,8 μm</p>	detection	excitation	emission	beam splitter	DAPI	BP 356	LP 420	FT 395	FITC	BP 450-490	LP 515-565	FT 510	TRITC	BP 546	LP 575-640	FT 560	Cy5	BP 575-625	LP 660-710	FT 645	<p>Carl Zeiss, Jena</p> <p>Princeton Instruments Monmouth, USA</p>
detection	excitation	emission	beam splitter																			
DAPI	BP 356	LP 420	FT 395																			
FITC	BP 450-490	LP 515-565	FT 510																			
TRITC	BP 546	LP 575-640	FT 560																			
Cy5	BP 575-625	LP 660-710	FT 645																			

Microscope	Description	Manufacturer																
Confocal Laser-Scanning Microscope	<p>LSM 410</p> <p>Objective: Plan-Apochromat 63x, NA 1.4, oil immersion</p> <p>Epi-fluorescence slider:</p> <table border="1"> <thead> <tr> <th>detection</th> <th>excitation</th> <th>emission</th> <th>beam splitter</th> </tr> </thead> <tbody> <tr> <td>DAPI</td> <td>BP 356</td> <td>LP 420</td> <td>FT 395</td> </tr> <tr> <td>FITC</td> <td>BP 450-490</td> <td>LP 515-565</td> <td>FT 510</td> </tr> <tr> <td>TRITC</td> <td>BP 546</td> <td>LP 575-640</td> <td>FT 560</td> </tr> </tbody> </table> <p>mirror for laser scanning microscopy</p> <p>Ar Laser emission filters: BP 502-542 for 488 (blue) excitation He-Ne laser emission filters: BP 575-640 for 543 (green) excitation RG 665 for 633 (red) excitation</p>	detection	excitation	emission	beam splitter	DAPI	BP 356	LP 420	FT 395	FITC	BP 450-490	LP 515-565	FT 510	TRITC	BP 546	LP 575-640	FT 560	<p>Carl Zeiss, Jena</p>
detection	excitation	emission	beam splitter															
DAPI	BP 356	LP 420	FT 395															
FITC	BP 450-490	LP 515-565	FT 510															
TRITC	BP 546	LP 575-640	FT 560															

Microscope	Description	Manufacturer
Confocal Laser-Scanning Microscope	Leica SP2 AOBS Objective: HCX PL APO 63x 1,4 oil immersion Diode Laser: 405 nm ~20mW Argon-Laser: 488nm ~20mW DPSS-Laser: 561nm ~10mW HeNe-Laser: 594 nm ~2,5mW HeNe-Laser: 633nm ~10mW	Leica Microsystems, Heidelberg
Confocal Laser-Scanning Microscope	Leica SP The objective and lasers used were the same as for Leica SP2, with exception for the diode laser which was not present in this model	Leica Microsystems, Heidelberg
Binocular microscope	Stemi 2000-C	Carl Zeiss, Jena
Phase Contrast Microscope	Dialux Objectives : 10x, 25x, 40x Phaco	Leitz, Munich

Selective plane illumination microscope (SPIM)	Objective : 63x, water dipping, NA 0,95 Used laser : 488 nm For details see (Huisken et al., 2004; Keller et al., 2006)	EMBL, Heidelberg
--	---	------------------

2.1.9. Image processing software

Software	Manufacturer
Amira 3.0	TGS, Paris
ImageJ 1.34	Rasband, W.S., ImageJ, U. S. National Institutes of Health, Bethesda, Maryland, USA, http://rsb.info.nih.gov/ij/ , 1997-2006
LCS Lite 2.5	Leica Microsystems, Heidelberg
MatLab 7.0 (custom routine written by Jim Swoger was used for the analysis)	MathWorks Inc, Massachusetts, USA
Metamorph 4.0/4.6	Visitron, Munich
Photoshop 6.0, 7.0	Adobe, Munich

2.1.10. *Drosophila melanogaster* lines

2.1.10.1. Wild type flies

Wild type (WT)

Name	WT
Transgene (s)	-
Cytology	-
Phenotype	WT
Source	kindly provided by Dr. David de Lorenzo, LMU Munich
Reference	-

2.1.10.2. Transgenic flies

2.1.10.2.1. Transgenic constructs 5F3, 5F24 and 24F6

For detailed information about the constructs 5F3 and 5F24 see Zink and Paro (1995); the correct orientation of the Fab-7 element is shown in Cavalli and Paro (1998). For information about 24F6 see Cavalli and Paro (1998); Zink and Paro (1995).

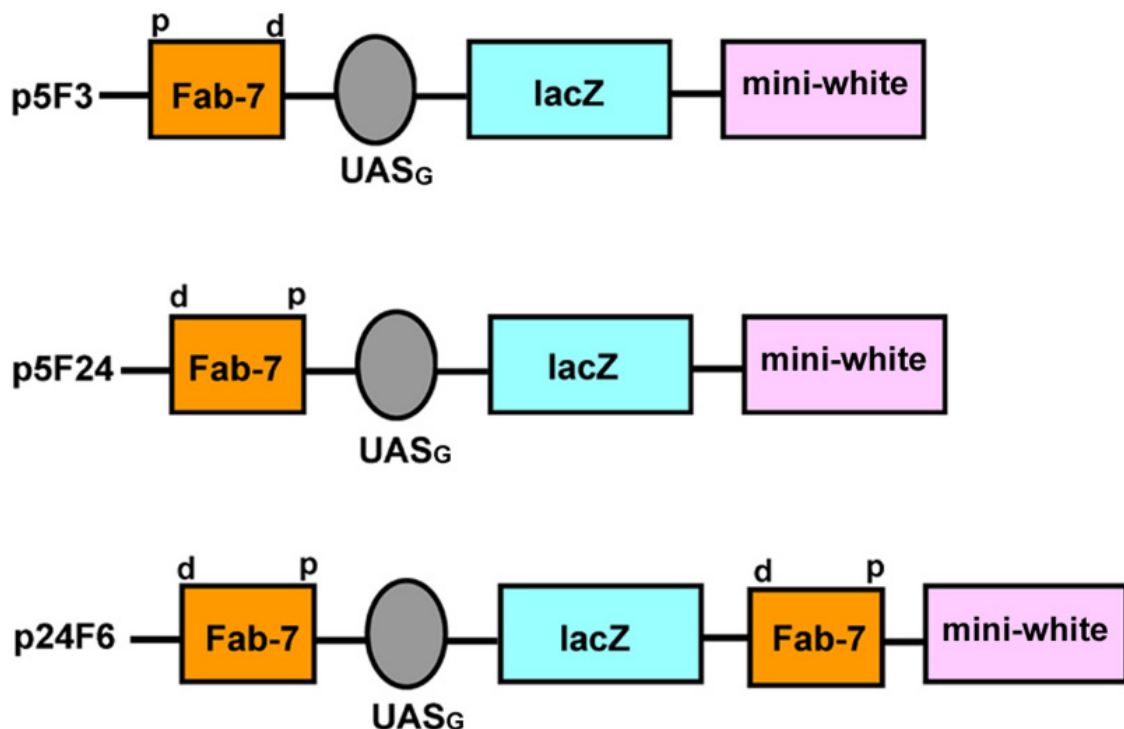


Figure 2. Transgenic constructs 5F3, 5F24 and 24F6 (from Zink and Paro (1995) with minor changes). The proximal-distal (d, p) orientation of the Fab-7 element is shown. The constructs contain lacZ and mini-white reporter genes. GAL4 binding sites (UAS_G) are located upstream of the lacZ reporter gene.

2.1.10.2.2. Transgenic lines

FLW-1 line

Name	FLW-1
Transgene (s)	5F24 (Fab-7 in d-p orientation, lacZ , mini- <i>white</i>); hsGAL4
Cytology	5F24 is inserted into the <i>sd</i> locus (13F), hsGAL4 is located on Chr. 2
Phenotype	see Cavalli and Paro (1998); Zink and Paro (1995)
Source	kindly provided by Prof. Renato Paro, ZMBH, Heidelberg
Reference	(Zink and Paro, 1995)

fLW-1 line

Name	fLW-1
Transgene (s)	5F3 (Fab-7 in p-d orientation, lacZ , mini- <i>white</i>); hsGAL4
Cytology	5F3 is inserted into the <i>sd</i> locus (13F), hsGAL4 is located on Chr. 2
Phenotype	see Cavalli and Paro (1998); Zink and Paro (1995)
Source	kindly provided by Prof. Renato Paro, ZMBH, Heidelberg
Reference	(Zink and Paro, 1995)

FLFW-1 line

Name	FLFW-1
Transgene (s)	24F6 (Fab-7 in d-p orientation, lacZ , Fab-7 in d-p orientation, mini- <i>white</i>); hsGAL4
Cytology	24F6 is inserted into the 61C9 locus, hsGAL4 is located on Chr. 2.
Phenotype	see Cavalli and Paro (1998); Zink and Paro (1995)
Source	kindly provided by Prof. Renato Paro, ZMBH, Heidelberg
Reference	(Zink and Paro, 1995)

5F24 25,2 line*

Name	5F24 25,2
Transgene (s)	5F24
Cytology	Insertion into the <i>sd</i> locus (13F)
Phenotype	(Zink and Paro, 1995)
Source	kindly provided by Prof. Renato Paro, ZMBH, Heidelberg
Reference	(Cavalli and Paro, 1998; Zink and Paro, 1995)

*this line is also known as *Fab-X* (Bantignies et al., 2003)

Pc-EGFP line

Name	Pc-EGFP
Transgene (s)	Polycomb protein is fused to EGFP (for details see Dietzel et al (1999))
Cytology	Insertion into the 45F locus
Transgenic derived from	white 1118
Source	kindly provided by Prof. Renato Paro, ZMBH, Heidelberg
Reference	(Dietzel et al., 1999)

2.1.11. Cell lines

2.1.11.1. *Drosophila* cells

Name	Kc
Organism	<i>Drosophila melanogaster</i>
Description	Embryonic cells
Medium	Schneider's <i>Drosophila</i> medium with 10% FCS. Antibiotics are not necessary if the technique is sterile
Notes	Semi-adherent cells, grow best at 25°C. A CO ₂ incubator is not required. Cells have variable morphology and are tetraploid
Source	Kindly provided by Prof. Peter Becker, LMU Munich
Reference	(Echalier and Ohanessian, 1970)

2.1.11.2. Human cells

HeLa

Name	HeLa
Organism	Human
Description	Cervix epitheloid carcinoma cells, a substrain of CCL-2. Hypotriploid
Medium	DMEM, 10% FCS, 1x Penicilline/Streptomycine (P/S)
Source	Kindly provided by Dr. Volker Cordes, ZMBH, Heidelberg
Reference	(Scherer and Hoogasian, 1954)

SH-EP N14

Name	SH-EP N14
Organism	Human
Description	Epithelial neuroblastoma cells, a derivate of SK-N-SH, stably transfected with N-Myc expression vector (Wenzel et al., 1991)
Medium	DMEM, 10% FCS, 1x P/S
Source	Kindly provided by Prof. Manfred Schwab, DKFZ, Heidelberg
Reference	(Ross et al., 1983; Wenzel et al., 1991)

2.1.11.3. Porcine cells

2.1.11.3.1. Wild type (WT)

Name	SFF WT
Organism	Sus scrofa
Description	Primary skin fibroblasts
Medium	DMEM, 15% FCS, 1x P/S
Source	Kindly provided by Prof. Alexander Pfeifer, LMU Munich
Reference	(Hofmann et al., 2003)

Name	SFF WT TA _g
Organism	Sus scrofa
Description	Immortalized with T-large Antigen skin fibroblasts
Medium	DMEM, 15% FCS, 1x P/S
Source	Kindly provided by Prof. Alexander Pfeifer, LMU Munich
Reference	(Hofmann et al., 2003)

Name	SFF WT pgk-GFP
Organism	Sus scrofa
Description	Primary skin fibroblasts, infected <i>in vitro</i> with LV-PGK construct
Medium	DMEM, 15% FCS, 1x P/S
Source	Kindly provided by Prof. Alexander Pfeifer, LMU Munich
Reference	(Hofmann et al., 2003)

2.1.11.3.2. Cells from transgenic pigs, carrying the lentiviral construct LV-PGK

For the detailed information about the vector's generation and functional relationships of its components see (Follenzi et al., 2000) and <http://www.unifr.ch/biochem/DREYER/LENTIVIRU1.htm> .



Figure 3. The LV-PGK lentiviral construct (modified from Follenzi et al. (2000)). The construct contains the following elements:

LTR - Long Terminal Repeats

5'SD - splice donor site

gag – gene for a structural viral protein

RRE – Rev Responsive Element

3'SA - splice acceptor site

cPPT – central Polypurine Tract

PGK – Phosphoglycerate Kinase (promoter)

eGFP – gene for enhanced Green Fluorescent Protein

WPRE – Woodchuck hepatitis virus Posttranscriptional Regulatory Element

2.1.11.3.3. Transgenic cell lines

SFF 9338

Name	SFF 9338
Organism	Sus scrofa
Transgenic construct	LV-PGK vector
Description	Primary skin fibroblasts. High level of GFP expression
Medium	DMEM, 15% FCS, 1x P/S
Source	Kindly provided by Prof. Alexander Pfeifer, LMU Munich
Reference	(Hofmann et al., 2006)

SFF 8777

Name	SFF 8777
Organism	Sus scrofa
Transgenic construct	LV-PGK vector
Description	Immortalized skin fibroblasts. High level of GFP expression
Medium	DMEM, 15% FCS, 1x P/S
Source	Kindly provided by Prof. Alexander Pfeifer, LMU Munich
Reference	(Hofmann et al., 2006)

SFF 9206

Name	SFF 9206
Organism	Sus scrofa
Transgenic construct	LV-PGK vector
Description	Primary skin fibroblasts. Variegated GFP expression: ~20% of cells are highly expressing, the rest does not express
Medium	DMEM, 15% FCS, 1x P/S
Source	Kindly provided by Prof. Alexander Pfeifer, LMU Munich
Reference	(Hofmann et al., 2006)

SFF 9192

Name	SFF 9192
Organism	Sus scrofa
Transgenic construct	LV-PGK vector
Description	Primary skin fibroblasts. No expression of GFP
Medium	DMEM, 15% FCS, 1x P/S
Source	Kindly provided by Prof. Alexander Pfeifer, LMU Munich
Reference	(Hofmann et al., 2006)

SFF 9193

Name	SFF 9193
Organism	Sus scrofa
Transgenic construct	LV-PGK vector
Description	Primary skin fibroblasts. Weak or no expression of GFP
Medium	DMEM, 15% FCS, 1x P/S
Source	Kindly provided by Prof. Alexander Pfeifer, LMU Munich
Reference	(Hofmann et al., 2006)

SFF 9196

Name	SFF 9196
Organism	Sus scrofa
Transgenic construct	LV-PGK vector
Description	Primary skin fibroblasts. No expression of GFP
Medium	DMEM, 15% FCS, 1x P/S
Source	Kindly provided by Prof. Alexander Pfeifer, LMU Munich
Reference	(Hofmann et al., 2006)

SFF 8779

Name	SFF 8779
Organism	Sus scrofa
Transgenic construct	LV-PGK vector
Description	Immortalized skin fibroblasts. Low level of GFP expression in all cells
Medium	DMEM, 15% FCS, 1x P/S
Source	Kindly provided by Prof. Alexander Pfeifer, LMU Munich
Reference	(Hofmann et al., 2006)

2.2. Methods

2.2.1. Mammalian cells

2.2.1.1. *In vitro* culture of mammalian cells

Cells were grown at 37°C in presence of 5% CO₂. **HeLa** cells were kept in 25cm² and 75 cm² flasks with filter caps (Nunc, Wiesbaden). **Porcine** cells were grown in 100x20 mm tissue culture dishes (Sarstedt, Newton, NC, USA). Cells were split once in 5-8 days, depending on the cell line. When the cells were ~70% confluent, they were washed briefly with 1xPBS, and then left for 2-5 min with 2-3 ml of trypsin-EDTA at 37°C. When the cells detached, about 5 ml of fresh medium was added to inhibit trypsin. Cells were carefully pipeted up and down 1-2 times to homogenize the suspension, which then was diluted 1:10 with fresh medium.

For detailed descriptions of freezing and thawing procedures see Englmann (2005). Cell were regularly checked for the presence of mycoplasmas using DAPI staining according to standard procedures (Chen, 1977). No contamination was observed.

2.2.1.2. Seeding cells on coverslips

1. Break off one corner of 21x26 mm coverslips with fine forceps or a diamond pen to mark the upper side, wash coverslips in dH₂O and then in 80% EtOH, and let them air-dry under the hood. Then place them in 6-well or quadriperm dishes.
2. Trypsinise and resuspend cells with 10 ml of fresh medium. Then place ~300 µl of suspension on each coverslip and let the cells attach (20 min - 1 h, depending on the cell line).
3. When the cells have attached, add ~ 5 ml of medium and put the cells in the incubator.

2.2.1.3. Methanol-acetic acid fixation

To increase the number of metaphase cells, add colcemide (100 µl for 25 cm² flask) 2-3 h prior to fixation and then return cells to the incubator.

1. Wash the cells with 1xPBS, trypsinise them and resuspend with 15 ml of fresh medium (37°C). Transfer to a 50 ml tube.
2. Centrifuge cells 5 min at 1000 RPM.

3. Remove the supernatant except 5 ml. Carefully resuspend cells by gently tapping the tube and whirling its contents.
4. Add 10 ml of hypotonic solution (0,06 M KCl , 37°C) dropwise, constantly shaking the tube. Add KCl up to 30 ml and put the tube in a water bath at 37°C for 15-18 min (optimal time must be determined experimentally for each cell line).
5. Add 5 ml of cold fixative (methanol / acetic acid 3:1, freshly made, -20°C) dropwise, carefully shaking the tube.
6. Centrifuge 7 min at 1100 RPM.
7. Remove all but 5 ml of supernatant, resuspend the pellet by shaking the tube (slow vortexing may be used but it will increase the debris), slowly add 25 ml of fixative while shaking the tube.
8. Repeat 3 times steps 6 and 7.
9. To check the quality of the preparation, drop 50 µl of the suspension on a slide (the slide has to be cleaned with EtOH / ether 1:1 v/v and cooled in ice cold water) and examine with the phase contrast microscope.

2.2.1.4. Formaldehyde fixation of cells

When the cells on a coverslip reach ~70% confluence:

1. Remove medium and wash the cells with 1xPBS.
2. Incubate in ca. 5 ml of fixative (3,7% formaldehyde in 1xPBS) for 10 min at RT.
3. Remove fixative, wash cells 3 times with 1xPBS.

Coverslips can be stored in 1xPBS at 4°C for some months.

For cells fixed with formaldehyde on coverslips all hybridization and immunostaining procedures were performed in the following way: hybridization mixture (20 µl per slide) or antibodies (50 µl per slide) were placed on a slide, and the coverslip was put on it cell-side down.

2.2.1.5. Immunostaining of formaldehyde-fixed cells

1. Fix cells with formaldehyde.
2. Permeabilize with PBTT for 10 min at RT.
3. Block with 4% BSA / 4xSSCT for 1h at 37°C in a humid chamber, then rinse shortly with 4xSSCT.
4. Incubate with primary antibodies in a humid chamber at 37°C for 1 h.

5. Wash with 4xSSCT (42°C) 3x 5 min.
6. Incubate with fluorescently labelled secondary antibodies in a humid chamber at 37°C for 1 h.
7. Wash with 4xSSCT (42°C) 3x 5 min.
8. Optionally: stain with a DNA dye for 5 min in a dark humid chamber, then wash with dH₂O. Do not let the slide dry.
9. Mount with Vectashield (~20 µl), carefully mop with a tissue paper to remove excessive liquid, and seal with transparent nail polish. Wait till the nail polish dries out before the examination.

Slides should be stored in the dark at 4°C.

2.2.1.6. Fluorescent in situ hybridization (FISH)

2.2.1.6.1. Labelling the probes

The CF1 probe for the CFTR locus was kindly provided by Dr. Andreas Englmann, LMU Munich. Labelling, enzymatic degradation and precipitation of the probe were performed exactly as described in Englmann (2005).

Pig chromosome paints were labelled with FITC using PCR protocols kindly provided by Dr. Roscoe Stanyon, University of Florence, Italy, who also provided the paint probes.

PCR mixture (50 µl):

- 4 µl DNA (painting probe)
- 5 µl 10xNEB (New England Biolabs) buffer
- 5 µl dNTPs (see below)
- 2 µl 1 mM FITC-dUTP
- 2 µl 50 mM 6MW primer
- 0,5 µl NEB Taq-polymerase
- 1 µl 25 mM MgCl₂
- 30,5 µl dH₂O

dNTPs mixture: 2 dATP : 2 dCTP : 2GTP : 1 dTTP. Stock solutions of the nucleotides were at 100mM.

„PIGPAINT“ PRC program

Cycle	Temperature	Time	Number of repeats
1	94°C	3 min	1
2	94 °C 58°C 72°C	1 min 1 min 1,5 min	30
3	72°C	10 min	1

Probe for LV-PGK was labelled by PCR (DOP-PCR) or by nick-translation.

PCR mixture (50 µl):

- 2 µl DNA (~70 ng/µl)
- 4 µl 5 mM AGC mix (see below)
- 2 µl 5 mM dTTP
- 2 µl 1 mM dig- / Cy3-dUTP
- 2,5 µl forward primer (100 pM/µl)
- 2,5 µl reverse primer (100 pM/µl)
- 5 µl 10x buffer
- 0,5 µl Taq-polymerase (Roche)
- 29,5 µl dH₂O

5 mM AGC mixture: 12,5 µl each of dATP, dCTP, dGTP plus 212,5 µl dH₂O. Stock solutions of the nucleotides were at 100 mM.

„L-DOP“ PCR program

Cycle	Temperature	Time	Number of repeats
1	95°C	5 min	1
2	95°C 32°C 72°C	1 min 1 min 3 min	5
3	95°C 62°C 72°C	1 min 1 min 3 min	35
4	72°C	5 min	1

Nick-translation mixture (50 µl):

- 25 µl DNA (~1,25 µg)
- 5 µl 1 mM AGC mix (provided with the kit)
- 2,5 µl 1 mM dTTP
- 2,5 µl 1 mM bio- / dig-dUTP
- 5 µl enzyme mix (Invitrogen BIONICK kit)
- 10 µl dH₂O

Incubate for 2 h at 15°C in PCR machine, stop the reaction by heating to 60°C for 10 min.

Probes for ppt-PGK, GFP and W-3'LTR fragments of LV-PGK virus were labelled by PCR or nick-translation, using the pipeting schemes described above for the labelling of the LV-PGK probe.

PCR program for ppt-PGK and W-3'LTR fragments:

„PIG3AND5“ PCR program

Cycle	Temperature	Time	Number of repeats
1	95°C	5 min	1
2	95°C 49°C 72°C	35 sec 30 sec 30 sec	39
3	72°C	5 min	1

PCR program for GFP fragment:

„PIG4“ PCR program

Cycle	Temperature	Time	Number of repeats
1	95°C	5 min	1
2	95°C 57°C 72°C	35 sec 30 sec 30 sec	39
3	72°C	5 min	1

All PCR and nick-translation reactions were performed using Hybias Omni Gene PCR-machine (MWG-Biotech, Munich).

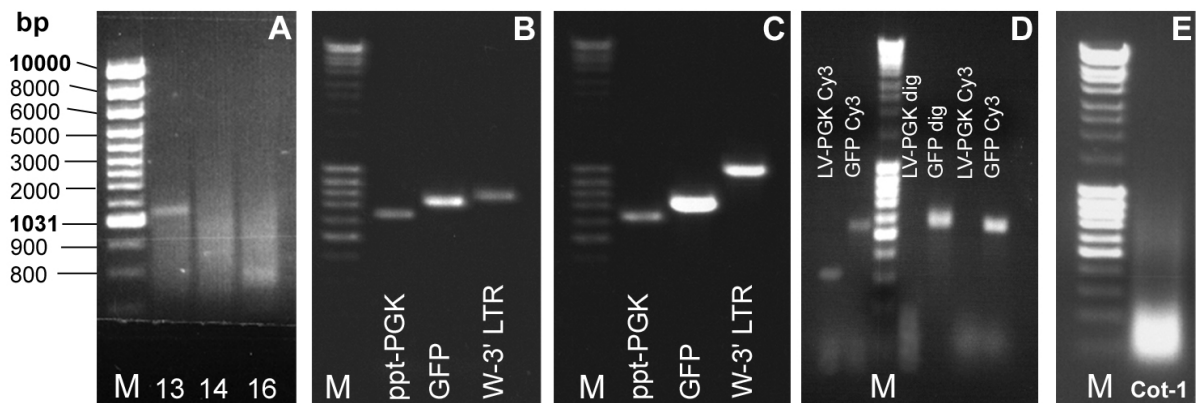


Figure 4. Agarose gel electrophoresis of labelled pig chromosomal paints, amplified or labelled fragments of the LV-PGK vector and enzymatically digested human Cot-1 DNA. 5 µl of PCR- /nick-translation product was mixed with 5 µl of 6x OLD and loaded onto 1% agarose gels together with the marker (M; Mass Ruler, Fermentas). The gels run for ~ 50 min at 100 V. (A) Paints for pig chromosomes 13, 14 and 16 were FITC-labelled by PCR with the PIGPAINT program. (B) PCR amplified ppt-PGK, eGFP and W-3' LTR fragments of the LV-PGK vector. (C) ppt-PGK, eGFP and W-3' LTR fragments after labelling with Cy3 using corresponding PCR programs. (D) LV-PGK and eGFP fragments were labelled with Cy3 or digoxigenin (as indicated on the picture) using PCR (on the left from the marker) or nick-translation (on the right from the marker). (E) DNase digested Cot-1 DNA.

2.2.1.6.2. Enzymatic digestion of PCR-labelled probes

To reduce the length of the probe fragments to optimize for FISH (400-500 bp):

mixture I:

- 50 µl PCR product
- 1,5 µl Alu I
- 1,5 µl Pdm I
- 5 µl Tango buffer
- 2 µl dH₂O

Incubate for 1,5 – 2 h at RT, stop by heating to 60°C for 5 min. If necessary, perform a further **digestion with DNase I** (*DNase I has to be diluted 1:75 in dH₂O just prior to use*):

- 60 µl mixture I
- 20 µl dH₂O
- 10 µl 10x buffer for DNase I
- 10 µl DNase I (diluted)

Incubate 3-5 min at RT, stop by heating to 80°C for 1-2 min and then immediately transfer to ice.

2.2.1.6.3. Precipitation of DNA probes

Precipitation of the CF1 probe was made exactly as described in Englmann (2005).

For precipitation of the LV-PGK probe and its fragments **enzymatically digested human Cot-1 DNA** was used (can be sonicated optionally). *DNase I has to be diluted 1:75 in dH₂O just prior to use*. The reaction was performed in the following way:

- 40 µl Cot-1 DNA (1 mg/ml)
- 40 µl dH₂O
- 15 µl 10x buffer for DNase I
- 15 µl DNase I (diluted)

Incubate for 5 min at RT and stop by heating to 80°C for 1-2 min. Immediately transfer to ice. Fragment length should be 100-300 bp (Figure 4).

Precipitation of the LV-PGK probe and its fragments:

- 15 μ l DNA (labelled probe)
 - 15 μ l Herring Sperm DNA (10 mg/ml)
 - 20 μ l human Cot-1 DNA (digested)
 - 5 μ l 3M Sodium acetate (10% of Σ A)
 - 140 μ l EtOH (2,5 x Σ B)
- } Σ A } Σ B

For pig paints porcine Hybloc DNA was used instead of human Cot-1 DNA.

All precipitations described below were performed overnight at -20°C or for 2 h at -80°C .

2.2.1.6.4. Denaturation, hybridization and detection

These steps of the FISH procedure for methanol-acetic acid and formaldehyde fixed cells were done as described in Englmann (2005).

2.2.1.6.5. Detection

The detection of the biotin-labelled GFP fragment of the LV-PGK vector using the Tyramide Signal Amplification kit was performed according to the manufacturer's instructions with some modifications according to the following protocol. After the FISH procedure, which was carried out as described in Englmann (2005), the washing and detecting steps were:

1. 3x5 min 4xSSCT (42°C).
2. 3x5 min 1xSSC (60°C).
3. Rinse shortly in 4xSSCT.
4. Incubate with 5% BSA / 1xPBS for 1 h in a humid chamber at 37°C .
5. Incubate with SA-HPR (1:50) for 1h at 37°C .
6. 3x5 min 4xSSCT (42°C).
7. Incubate with Tyramide (1:50) for 7 min at 37°C .
8. 3x5 min 4xSSCT (42°C).
9. DAPI staining (1:4000) for 5 min in a dark humid chamber.

2.2.1.7. RNA interference

This method was used to knock-down the Tpr protein in HeLa cells. All procedures were performed using the RNAiFect Transfection Kit (Quiagen, Hilden) according to the manufacturer's instructions. 15 μ l of each siRNA (20 μM) were used for 1 experiment.

Cells were grown on coverslips in 6-well dishes (see 2.2.1.2). When they

reached ~30% confluence the siRNA transfection complex was added and cells were incubated for 4 days. The efficiency of the knock-down was checked by immunostaining and by Western Blot, the latter was kindly performed by Dr. Andreas Englmann, LMU Munich.

2.2.1.8. CFTR expression in HeLa cells

To find out whether knock-down of the Tpr protein with RNAi affects transcription of the CFTR locus, semi-quantitative PCR was used. Total cellular RNA was isolated using the RNeasy kit (Quiagen, Hilden) according to the enclosed protocol. For synthesis of cDNA the First Strand cDNA Synthesis Kit for RT-PCR (AMV) with the RT_NICO_ program (see below) were applied. The following primers were used for RT-PCR: forward B3R and reverse C16D (Ramalho et al., 2002), see online supplemented material in Zink et al. (2004). These experimental procedures were kindly performed by Dr. Nicolas Sadoni, LMU Munich.

«RT_NICO_» program

Cycle	Temperature	Time	Number of repeats
1	95°C	3 min	1
2	95 °C 57°C 72°C	1 min 1 min 2 min	30
3	72°C	10 min	1

2.2.2. *Drosophila melanogaster* cells and tissues

2.2.2.1. *Drosophila* cell culture

Kc cells were grown at 25°C in normal atmosphere in 25cm² or 75 cm² flasks with filter caps (Nunc, Wiesbaden). As the cells adhere very loosely to the substrate it is sufficient to blow medium at them from a serological pipette to obtain a suspension which then should be split 1:10.

Although usually antibiotics are not required, the medium is very rich and a contamination may easily occur. Therefore, all procedures have to be performed under sterile conditions. Otherwise, P/S may be used at the same concentration as for mammalian cells. Standard protocols for freezing and thawing of *Drosophila* cells are provided at: <http://dgrc.cgb.indiana.edu/cells/protocols.html>

2.2.2.2. *Drosophila* fly stock maintenance

Flies were raised and kept according to standard procedures (for details see Zink (1994)) when not indicated otherwise.

For both embryonic and larval heat-shocks tubes with corresponding animals were immersed in a water bath (37°C) for 45 min. Embryos were kept under standard conditions for further development. Larvae were allowed to recover after the heat-shock for 2 hours before dissection.

2.2.2.3. The preparation of *Drosophila* polytene chromosomes from salivary glands

was performed as described in Kenninson (2000).

2.2.2.4. Dissection of other *Drosophila* larval tissues

Several tissues from 3rd instar larvae were used in this study: eye-antennal, leg and wing imaginal discs, brain, anterior epidermis, fat body cells, salivary glands, malpighian tubules, and anterior midgut. They were taken from actively moving, healthy-looking 3rd instar larvae under microscopic control.

Larvae were dissected in 0,1% pluronic / PBS within 30 min. Tissue samples were transferred using forceps or a Pasteur pipette in an Eppendorf tube filled with the same solution.

For imaging with the SPIM microscope tissues from Pc-GFP larvae were dissected in Tyrode's buffer and then immediately embedded into agarose and mounted for microscopy (for details see Huisken et al. 2004, Keller et al. 2006).

2.2.2.5. Formaldehyde fixation of cells

For cells fixed on coverslips all hybridization and immunostaining procedures were performed in the following way: hybridization mixture (20 µl per slide) or antibodies (50 µl per slide) were placed on a slide and the coverslip was put on it cell-side down.

Kc cells are semi-adherent. Therefore it is recommendable to use poly-L-lysine to attach them to coverslips.

Cells were fixed in the following way:

1. A suspension of Kc cells (well diluted) was placed on a coverslip and cells were allowed to attach for ~40 min. Cells should be well spaced.

2. For FISH: cells were briefly rinsed in 1xPBS (careful as not to dislodge them) and then fixed and permeabilized for 40 min in buffer B (37°C) at RT. The fixed cells should then be used immediately.
3. For immunostaining: cells were briefly rinsed in 1xPBS and then fixed with 2%FA / PBS for 7,5 min on ice. Cells should then be used for immunostaining as it is not recommendable to store them.

2.2.2.6. Immunostaining of formaldehyde fixed Kc cells

1. Permeabilize fixed cells in 1%PFA / 0.25% Triton X-100 / PBS for 7.5 min on ice.
2. Wash briefly 2x in 1xPBS.
3. Block with 2%BSA, 5% goat serum in 1xPBS in a humid chamber for 1 h at RT. All subsequent steps are performed at RT.
4. Incubate with primary antibodies for 1 h in a humid chamber.
5. Wash 3x 5 min in 1xPBS.
6. Incubate with fluorescently labelled secondary antibodies for 1 h in a humid chamber.
7. Wash 3x 5 min in 1xPBS.
8. Optionally: stain with a DNA dye for 5 min in a dark humid chamber, then wash with dH₂O. Do not let the slide dry.
9. Mount with Vectashield (~20 µl), carefully mop with a tissue paper to remove excessive liquid, and seal with transparent nail polish. Wait till the nail polish dries out before the examination.

Slides should be stored in the dark at 4°C.

2.2.2.7. Immunostaining of *Drosophila* tissues

All steps were performed in a transparent 1.5 ml Eppendorf tube. 1 ml of the corresponding solution was used for fixation, blocking and washing steps. All these steps were performed on a rotating wheel. Therefore 1-2 min before the next step the Eppendorf tube should be taken off to allow the tissues to sink to the bottom. When a solution is being removed leave ~15 µl of it above the tissues to ensure that the tissues are not sucked off.

All hybridization and immunostaining steps should be performed in 100-150 µl buffer volume. When antibody dilutions are made, one has to take into account the volume of tissues in the Eppendorf tube (40-50 µl). For example, when antibodies should be used at a 1:50 dilution, one dilutes them 2:50 and adds this solution to the tissues, which results in a final dilution of 1:50.

Immunostaining protocol

1. Fix dissected tissues with 4% FA / 0.2% pluronic / Buffer A for 20 min on a rotating wheel. Triton X-100 may be used instead of pluronic.
2. Incubate with 5% BSA / PBT for 5 min to stop the fixation.
3. Wash 2x 5 min with PBT. If the tissues are not used immediately they should be prepared for storage (see below).
4. Block with 5% BSA / PBT for 30 min.
5. Incubate with primary antibodies for 1.5 h at 37°C with gentle shaking or overnight at 4°C.
6. Wash 3x 5 min with PBT.
7. Incubate with fluorescently labelled secondary antibodies for 1 h at 37°C.
8. Wash 3x 5 min with PBT.
9. Stain with DAPI (1:4000) or another DNA dye for 5 min in a dark humid chamber.
10. Shortly rinse with PBT.
11. Carefully suck out tissue samples with some PBT using a 1000 µl pipette. Place them on a slide and remove excessive liquid using a 20 µl pipette or tissue paper. Put a drop of Vectashield on the slide so that tissue samples are embedded. If necessary, separate the tissue samples from each other using 2 fine syringe needles under the control of phase contrast microscopy (the minimal possible light should be used to avoid bleaching). Cover with a coverslip and wait until Vectashield spreads evenly. Using tissue paper remove all liquid that comes out. Seal the slide with transparent nail polish (see below).

Slides should be stored in the dark at 4°C.

If the tissues are not used immediately transfer them stepwise to methanol (5 min each step):

1. 70% 1xPBS / 30% EtOH.
2. 50% 1xPBS / 50% EtOH.
3. 30% 1xPBS / 70% EtOH.
4. 100% EtOH.
5. 50% EtOH / 50% methanol.
6. 100% methanol

Store the tissues at -20°C and rehydrate in 1xPBS for 10 min when continuing.

Some components of the nail polish diminish the GFP fluorescence. Therefore, when

working with tissues from the Pc-GFP line one has to use the slides either immediately for microscopy or use other materials to seal the slide, as candle wax, for example.

2.2.2.8. Fluorescence in situ hybridization (FISH)

2.2.2.8.1. Probe preparation

Plasmids containing DNA sequences of ***Abd-B*** and ***Ubx*** genes and the λ -clone with the ***Fab-7*** sequence were isolated from corresponding bacterial cultures and purified with the Large Construct Kit (Quiagen, Hilden) according to the manufacturer's instructions. The bacterial stock cultures were handled in the following way: cultures were inoculated by picking a single colony from a selective plate. Bacteria were grown in 5 ml of LB medium with kanamycin and incubated overnight at 37°C with vigorous shaking. 3 ml of this culture were centrifuged for 15 min (4000 RPM at 4°C). The pellet was dissolved in 1 ml of 30% glycerol. Aliquots were put into cryovials, frozen with liquid nitrogen and stored at -80°C.

Isolated DNA of λ -clones containing the ***sd*** sequence was kindly provided by Prof. Renato Paro, ZMBH Heidelberg. To remove traces of circular or fragmented DNA I performed purification using gel-electrophoresis in a 0.8% agarose gel (100 V, 1h 20 min). Subsequently, the DNA of interest was extracted with the QIAEX II Gel Extraction Kit (Quiagen, Hilden) according to the manufacturer's instructions.

2.2.2.8.2. Probe labelling

The probe for centromeric satellite DNA (***AAGAG***)₈ (Metabion, Martinsried) was FITC-labelled with the 3'-end labelling kit (Roche, Mannheim) according to the manufacturer's instructions.

Isolated and purified DNA of vectors containing sequences of ***Ubx*** and ***sd*** loci was labelled with digoxigenin using the Dig DNA labelling kit (Roche, Mannheim) following the manufacturer's instructions. After labelling the ***Ubx*** probe was additionally purified from excess nucleotides using the QIAquick Nucleotide Removal Kit (Quiagen, Hilden).

Isolated and purified DNA of vectors that carried sequences of the ***Abd-B*** gene and the ***Fab-7*** element were biotin- or digoxigenin labelled with nick-translation as described in (2.2.1.6.1).

The DNA sequences of the plasmids that contain sequences of the Polycomb-response elements *Distalless* (*Dll*), *engrailed* (*en*), *homothorax* (*hth*) and *vestigial* (*vg*) (kindly provided by Dr. Leonie Ringrose, ZMBH, Heidelberg) were labelled with biotin or digoxigenin by PCR (Figure 5). The pipetting scheme and the program were kindly provided by Dr. Leonie Ringrose and are described below.

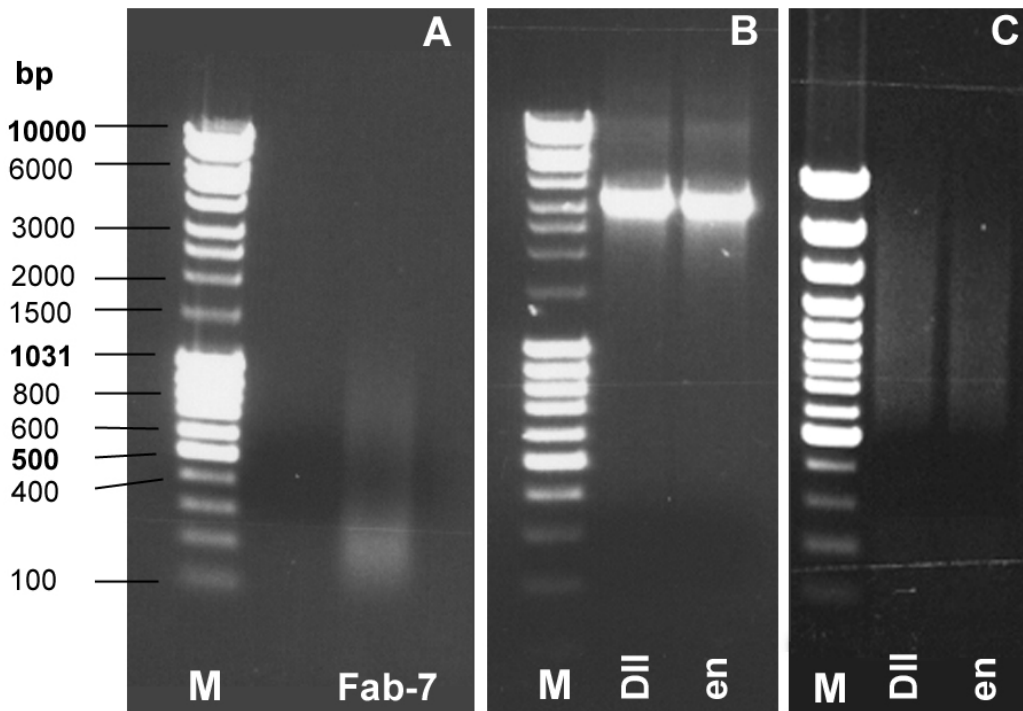


Figure 5. Agarose gel electrophoresis of labelled probes for *Drosophila* PREs. 5 μ l of PCR- /nick-translation product were mixed with 5 μ l of 6x OLD and loaded onto 1% agarose gels together with the marker (M; Mass Ruler, Fermentas). The gels run for ~ 50 min at 100 V. (A) The Fab-7 probe was labelled with biotin by nick-translation. (B) PCR amplification of the *distalless* (*Dll*) and *engrailed* (*en*) probes. (C) Digoxigenin labelling of the *distalless* (*Dll*) and *engrailed* (*en*) probes with nick-translation.

To carry out the PCR reaction some stock solutions have to be prepared in advance (store at -20°C):

- Plasmid DNA for each construct at 2 ng/ μ l
- dNTPs at 3,5 mM
- 5x primer mix: 1 μ l forward primer (100 μ M)
1 μ l reverse primer (100 μ M)
64 μ l dH₂O

PCR mixture (50 µl):

- 5 µl plasmid construct (2 ng/µl)
- 10 µl 5x primer mix
- 5 µl 3,5 mM dNTPs
- 5 µl PCR 10x buffer (Expand high fidelity kit)
- 0,75 µl Taq polymerase (Expand high fidelity kit)
- 25 µl dH₂O

„PRE_PCR“ program

Cycle	Temperature	Time	Number of repeats
1	94°C	3 min	1
2	94°C 55°C 68°C	30 sec 30 sec 3 min	35
3	68°C	7 min	1

All PCR and nick-translation reactions were performed using Hybias Omni Gene PCR-machine (MWG-Biotech, Munich).

2.2.2.8.3. Labelling efficiency and specificity of the probes

To check the efficiency of digoxigenin-labelling of the probes a Dot Blot assay (Figure 6) was performed as follows:

1. 1 µl of the labelled probe (diluted serially 1:10, 1:100 and 1:1000 in dH₂O) was placed onto a positively charged nylon membrane and incubated for 30 min at 80°C in a dry chamber.
2. The membrane was incubated with 1% BSA / 1x PBS for 15 min in a Petri dish.
3. The membrane was incubated with an AP conjugated anti-DIG antibody (1:1000) for 45 min at RT.
4. The membrane was washed 5x 5min with 1x PBS in a Petri dish on a shaker.
5. Washed 2x 2min with AP buffer.
6. Stained for 5 min with NBT / NCIP solution in a dark chamber.
7. Washed 3x 5min with dH₂O.

The specificity of the probes was checked by FISH on polytene chromosomes (Figure 7).

2.2.2.8.4. The enzymatic digestion of the probes was performed as described above (see 2.2.1.6.2.)

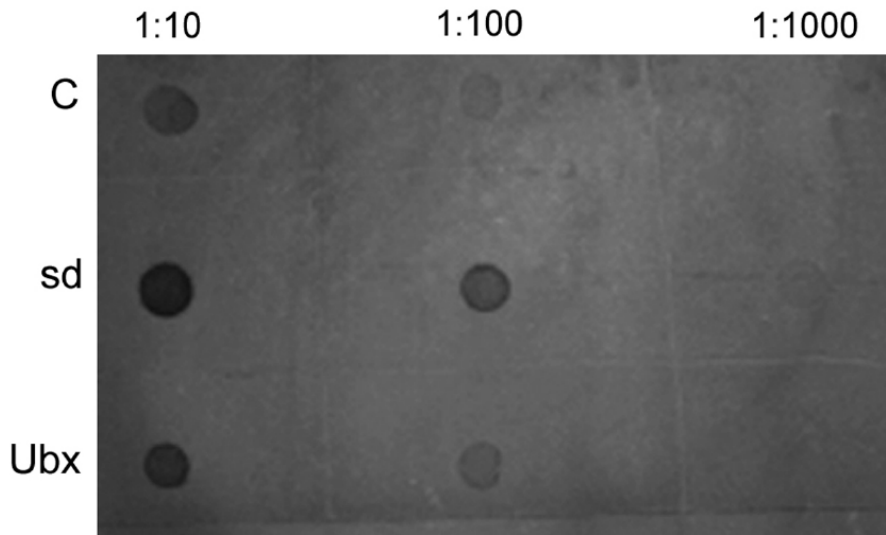


Figure 6. Dot Blot analysis of digoxigenin-labelled *Drosophila* probes. Probes were labelled using the DIG DNA labelling kit (Roche, Mannheim). Dilutions 1:10, 1:100 and 1:1000 are shown. The upper line shows control DNA, the middle line presents the *sd* probe, the lowest shows the *Ubx* probe. The probes were visualized using AP-conjugated anti-digoxigenin antibodies (Roche, Mannheim).

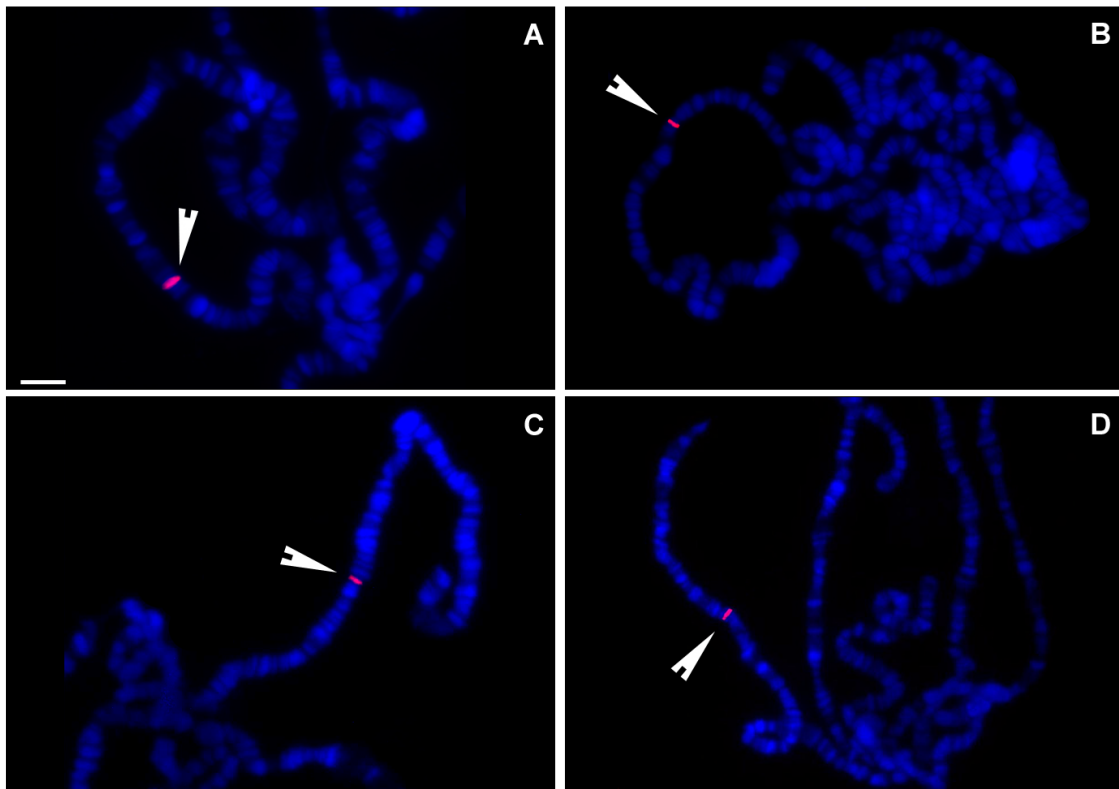


Figure 7. Specificity of probes for *Drosophila* endogenous genes. Digoxigenin- or biotin-labelled probes were hybridized to polytene chromosomes using FISH and detected with Cy3-conjugated antibodies or Cy3-coupled avidin conjugate. FISH signals are shown in red and are indicated by arrowheads. DNA was stained with DAPI and is shown in blue. (A) The *Abd-B* probe, 89 E4-5. (B) The *Fab-7* probe, 89 E2-3. (C) The *sd* probe, 13 F. (D) The *Ubx* probe, 89 D6-9. Scale bar: 10 μ m.

2.2.2.8.5. Precipitation of the probes

Human Cot-1 DNA used for precipitation was enzymatically digested as described in (2.2.1.6.3.). For precipitation the following mixtures were prepared:

(AAGAG)₈:

- 50 μ l probe DNA (10 pM/ μ l)
- 1 μ l yeast tRNA (25 μ g/ μ l)
- 1,5 μ l Cot-1 DNA (digested)
- 5,25 μ l 3M Sodium acetate
- 142,5 μ l dH₂O
- 600 μ l EtOH

Fab-7, PREs:

- 50 μ l labelled probe DNA
- 4 μ l yeast tRNA (25 μ g/ μ l)
- 10 μ l Cot-1 DNA (digested)
- 6,4 μ l 3M Sodium acetate
- 130 μ l dH₂O
- 600 μ l EtOH

Abd-B, sd, Ubx:

- 100 μ l labelled digested probe DNA
- 4 μ l yeast tRNA (25 μ g/ μ l)
- 10 μ l Cot-1 DNA (digested)
- 6,4 μ l 3M Sodium acetate
- 80 μ l dH₂O
- 600 μ l EtOH

All precipitations were carried out overnight at -20°C or for 2 h at -80°C .

2.2.2.8.6. FISH on polytene chromosomes

was performed according to the following protocol, kindly provided by Dr. Donna Arndt-Jovin (MPI for Biophysical Chemistry, Goettingen) (with minor changes):

Probe preparation

1. After precipitation (see 2.2.2.8.5.) centrifuge the probe for 30 min at 14000 RPM in cooled centrifuge.
2. Remove supernatant, add 150 μ l of 70% EtOH, centrifuge 10 min at 14000 RPM.
3. Remove supernatant, place the Eppendorf tube in a termo mixer at 42°C and let the pellet dry until all ethanol has evaporated.
4. Add 10 μ l of ultra-pure formamide pre-warmed to 42°C and gently vortex the Eppendorf tube until the pellet is dissolved.

5. Add 10 μl of the mixture: 4xSSC, 100mM Na-PO₄ pH 7.0, 0.2% Tween 20 (42°C), vortex gently:
6. Denature 10 min in boiling water.
7. Use 20 μl per slide.

Preparation of the slides and hybridization

1. Wash the slides with polytene chromosomes (see 2.2.2.3) 3x10 min in 95% EtOH and let them air dry.
2. Harden chromosomes in 2xSSC at 65°C for 1 h.
3. Incubate 2x 5 min in 70% EtOH, RT.
4. Incubate 2x 5 min in 95% EtOH, RT.
5. Air dry.
6. Incubate 2 min in denaturation mixture (10mM Tris-HCl, pH 7.0, 5mM MgCl₂) at 100°C.
7. Incubate 2x 3 min in 70% EtOH, RT.
8. Incubate 2x 5 min in 95% EtOH, RT.
9. Air dry shortly and add denatured probes (see above).
10. Cover with a coverslip and seal with rubber cement.
11. Incubate overnight at 37°C in a humid chamber.
12. Using fine forceps, carefully remove rubber cement without moving the coverslip (it will slide off during the washing steps).
13. Wash 2x 5 min in 50% formamide, 2xSSC, 5mM Na-PO₄ at 37°C.
14. Shortly rinse in PBT at RT. If the probes are fluorescently labelled proceed to the mounting step.

Detection of biotin- or digoxigenin labelled probes

1. Incubate with 3% BSA for 30 min at 37°C in a humid chamber.
2. Shortly rinse in PBT.
3. Incubate with fluorochrome conjugated anti-DIG antibodies or an avidin fluorochrome conjugate (50 μl per slide) for 1 h at 37°C in a humid chamber.
4. Wash 3x 5 min with 1xPBS at RT.
5. Stain with DAPI (1:4000) or another DNA dye for 5 min in a dark humid chamber.
6. Wash 3x 5min with 1xPBS.
7. Mount the slide with Vectashield and seal with transparent nail polish.

2.2.2.8.7. FISH on tissue samples

was performed according to a protocol, kindly provided by Dr. Donna Arndt-Jovin (MPI for Biophysical Chemistry, Goettingen) (with minor changes):

Hybridization

1. Fix dissected tissues (see 2.2.2.4.) with 4% FA / 0,2% pluronic / Buffer A for 20 min on a rotating wheel. Triton X-100 may be used instead of pluronic.
2. Incubate with 5% BSA / PBT for 5 min to stop the fixation.
3. Wash 2x5 min with PBT. If the tissues are not used immediately they can be prepared for storage (see 2.2.2.7.).
4. Incubate in PBT with 500 µg/ml RNase A for 3 h at RT.
5. Wash 2x 10 min with PBT.
6. Fix with 4% FA / 1xPBS for 20 min on a rotating wheel.
7. Incubate 3x 10 min with 5% BSA / PBT.
8. Transfer stepwise into hybridization mixture (see 2.1.7, Hybridization mixture for *Drosophila* tissues), 15 min each step: 40% mixture / 60% 1xPBS, 70% mixture / 30% 1xPBS, 2x 100% mixture.
9. Denature the tissues in hybridization mixture for 15 min at 83°C in a water bath.
10. Remove as much liquid as possible and add the denatured probe (see 2.2.2.8.6.).
11. Hybridize the tissues overnight at 37°C with gentle shaking.
12. Wash the tissues, 10 min each step:
 - 50% formamide, 2xSSC, 0.1% TritonX-100, 0.3% CHAPS at 45°C.
 - 50% formamide, 2xSSC, 0.1% TritonX-100, 0.3% CHAPS at 37°C.
 - 40% formamide, 0.1xSSC, 0.1% TritonX-100, 0.3% CHAPS at 37°C.
 - 20% formamide, 1xPBS.
 - PBS twice.
13. If the probes are fluorescently labelled, proceed to the mounting step.

Detection of biotin- or digoxigenin labelled probes

1. Incubate the tissues with 5% BSA / PBT for 30 min at RT.
2. Incubate with fluorochrome conjugated anti-DIG antibodies or an avidin fluorochrome conjugate for 2h at RT or overnight at 4°C.
3. Wash 3x 5 min with PBT.
4. Stain with DAPI (1:4000) or another DNA dye for 5 min in a dark humid chamber.

5. Wash 5 min with PBT.
6. Mount and seal the slide as described in 2.2.2.7.

2.2.2.8.8. ImmunoFISH on tissue samples

This procedure was performed using 2 different protocols:

1. The tissue samples were denatured with NaOH (adapted from Brown (2002)) (**protocol A**). In this case immunostaining precedes the FISH procedure.
2. The tissue samples were heat-denatured (adapted from a protocol kindly provided by Dr. Donna Arndt-Jovin (MPI for Biophysical Chemistry, Goettingen)) (**protocol B**). In this case the immunostaining can precede or follow the FISH procedure, depending on the nature of the visualized proteins.

2.2.2.8.8.1. Protocol A

This protocol was used for simultaneous visualization of pericentromeric satellite DNA, dimethylated lysine 9 of histone H3 and nuclear lamina.

1. Fix the dissected tissues (2.2.2.4.) with buffer B for 50 min.
2. Wash 2x 5 min with PBT.
3. Wash 2x 20 min with NaBH₄ (1 mg/ml, prepared immediately before use).
4. Block with 10% goat serum for 40 min.
5. Incubate with primary antibodies for 1.5 h at 37°C.
6. Wash 2x 5 min with PBT.
7. Incubate with fluorescently labelled secondary antibodies for 1.5 h at 37°C.
8. Wash 2x 5 min with PBT.
9. Fix with EGS (100 mM in PBS) for 20 min at 37°C.
10. Wash 3x 5 min with PBT.
11. Incubate with RNase A (500 µg/ml) for 1.5 h at 37°C.
12. Denature with 0.07 N NaOH for 1,5 min and immediately neutralize by 3 brief washes with ice-cold PBS.
13. Add denatured probe (place on ice briefly before combining with tissues) and hybridize overnight at 37°C.
14. Wash briefly with 4xSSC.
15. Wash with 2xSSC for 30 min at 37°C.
16. Wash with 2xSSC for 30 min at RT.
17. Wash with 1xSSC for 30 min at RT. If the probe is fluorescently labelled, proceed directly to step 22.

18. Block with 10% natural goat serum for 30 min at 37°C.
19. Incubate with fluorochrome conjugated anti-DIG antibodies or an avidin fluorochrome conjugate for 1.5 h at 37°C.
20. Wash 3x 5 min with 4xSSC / 0,05% Tween 20.
21. Wash 3 min with 1xPBS.
22. Stain with DAPI (1:4000) or another DNA dye for 5 min in a dark humid chamber.
23. Mount and seal the slide as described in 2.2.2.7.

2.2.2.8.8.2. Protocol B

For a number of antigens, for example certain histone modifications and β -galactosidase, immunostaining must be performed before the FISH:

1. Fix the dissected tissues (2.2.2.4.) with 4% FA / 0,2% pluronic / Buffer A for 20 min on a rotating wheel. Triton X-100 may be used instead of pluronic.
2. Incubate with 5% BSA / PBT for 5 min to stop the fixation.
3. Wash 2x5 min with PBT.
4. Incubate with 5% BSA / PBT for 30 min at RT.
5. Incubate with primary antibodies for 2h at 37°C with gentle shaking.
6. Wash 2x 5 min with PBT.
7. Incubate with fluorescently labelled secondary antibodies overnight at 4°C.
8. Wash 3x 5 min with PBT.
9. Fix with 4% FA / 1xPBS.
10. Incubate 5 min with 5% BSA / PBT.
11. Incubate with 500 μ g/ml RNase A for 2 h at RT.
12. Proceed with the FISH protocol as described in 2.2.2.8.7.

Other proteins, like the *Drosophila* lamin, should be detected after the FISH procedure. In this case the protocol is modified in the following way:

1. Perform FISH and detect the probes as described in 2.2.2.8.7.
2. Wash 3x 5 min with PBT.
3. Incubate with primary antibodies for 1 h at RT.
4. Wash 3x 5 min with PBT.
5. Incubate with fluorescently labelled secondary antibodies for 1 h at RT.
6. Wash 3x 5 min with PBT.
7. Stain with DAPI (1:4000) or another DNA dye for 5 min at RT.
8. Mount and seal the slide as described in 2.2.2.7.

2.2.3. Image analysis

2.2.3.1. Image analysis of methanol / acetic acid fixed nuclei

Images were acquired using a CCD-camera (MicroMax, Princeton Instruments Monmouth, USA), mounted on a microscope equipped for epifluorescence (Axiovert 135 TV, Zeiss), Images were obtained with a Plan-Apochromat 63x oil objective (N.A. 1,4) and recorded using Metamorph 4.0 software. The pixel size was 0,1x0,1 μm .

2.2.3.1.1. 2D erosion analysis

2D erosion analyses were performed as described in Zink et al. (2004) using Adobe Photoshop software (7.0) and a macro created by Dr. Nicolas Sadoni (LMU Munich).

2.2.3.1.2. Distance measurements between the signal and a chromocenter

The measurements were made using ImageJ software. The x;y coordinates of the intensity center of the signal were determined by the software, and a line was drawn from this point to the border of the closest chromocenter. The length of the line (μm) was entered into an Excel table, and the following analyses were made using Excel software.

2.2.3.2. Image analysis of formaldehyde fixed nuclei

All 3D distance measurements and analyses of nuclear positions of gene loci were performed on images obtained by confocal laser scanning microscopy with the voxel size of 0,10 x 0,10 x 0,25 μm

Every image stack was recorded as a series of tiff-files. 3D stacks were assembled using ImageJ 1.34, Metamorph 4.0/4.6 or LCS-Lite 2.5 softwares. All distance measurements were performed with ImageJ software.

In most experiments secondary antibodies used for the detection of the nuclear lamina were Cy5-conjugated goat-anti-mouse antibodies. Therefore, lamina was false- coloured in blue. However, sometimes secondary antibodies were FITC- or Cy3- coupled and consequently the lamina fluorescence was green or red. But for the convenience of the analysis and presentation, the lamina was always false-coloured in blue using Adobe Photoshop 7.0.

2.2.3.2.1. Measuring the distance between two gene loci

For this type of measurement, a RGB stack has to be split so that each colour/channel is represented by a monochromatic stack. For each locus the threshold was adjusted manually (Figure 8) so that only the gene signal was marked, and the intensity center of each locus was determined (in x; y; z coordinates). Then the distance between two centers of mass was defined automatically by ImageJ and is shown in the resulting table. After performing a set of measurements the distance values were copied into an Excel table, and further analyses were performed using Excel software.

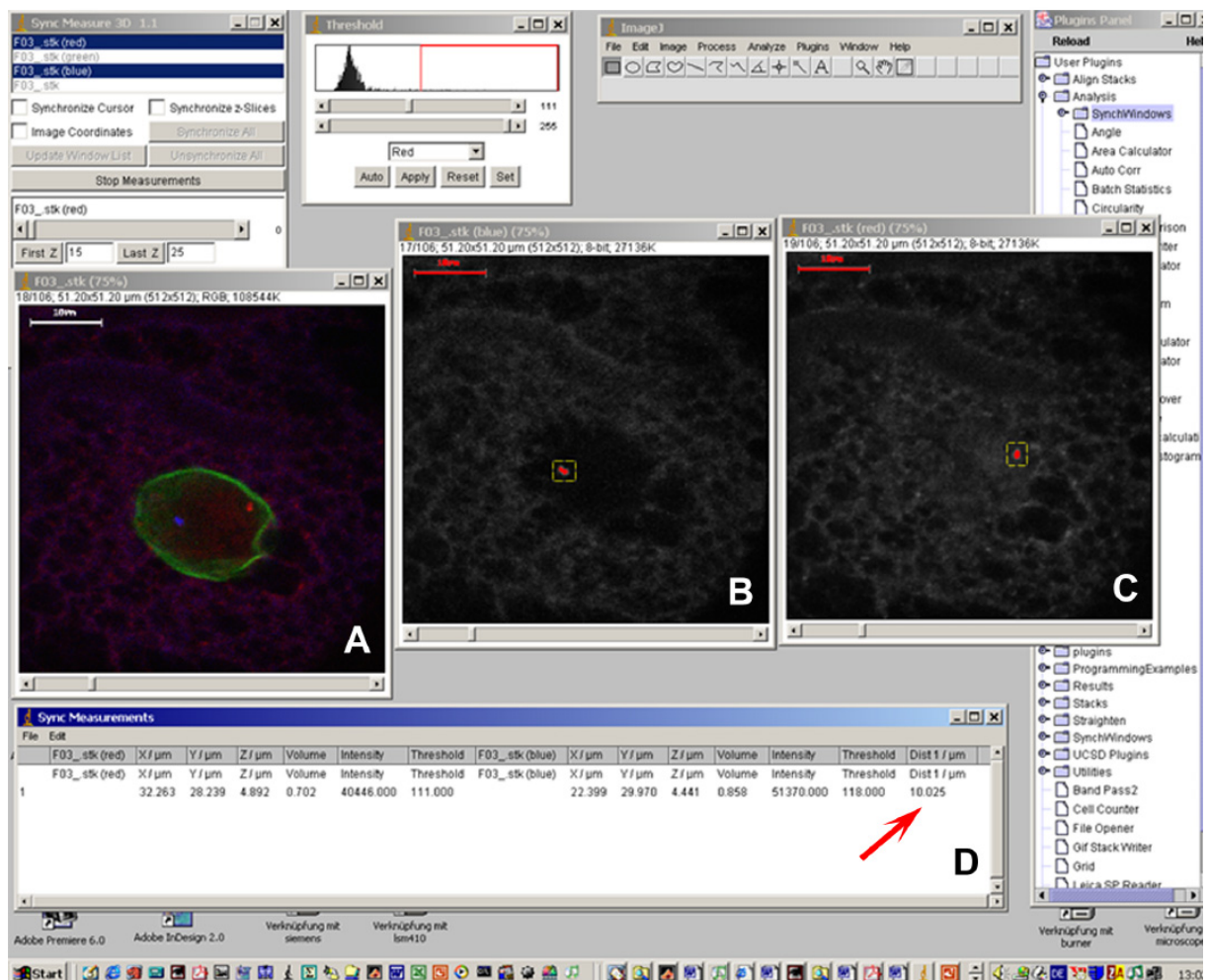


Figure 8. Distance measurements between two gene loci with ImageJ software. A screenshot of a measuring process is shown. (A) The original RGB stack with two gene loci (blue and red) and the nuclear lamina (green). (B), (C) Monochromatic stacks for each locus. The threshold is adjusted to mark only the gene signal (shown in red). (D) The resulting table of distance measurements shows (x; y; z) coordinates of the intensity center of each locus, the threshold value and the distance between the two intensity centers (red arrow).

2.2.3.2.2. Measuring the distance between a gene locus and the nuclear lamina / heterochromatin

In such measurements always the shortest distance was determined. The intensity center of the gene locus was defined as described above. The border of the heterochromatic compartment was determined using the Threshold function of ImageJ, whereas the lamina was defined visually, judging by its immunostaining intensity (Figure 9).

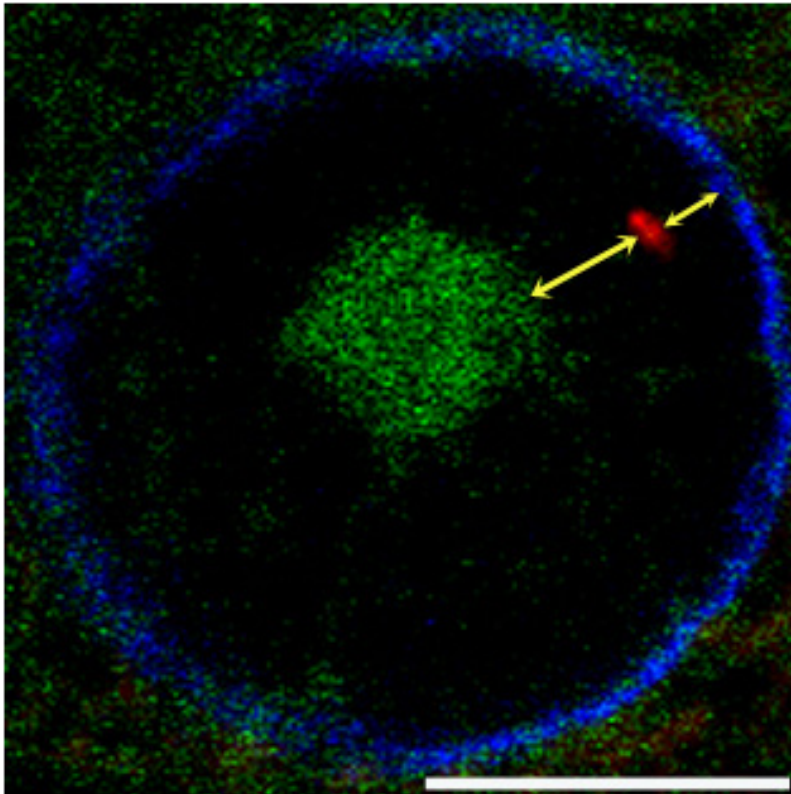


Figure 9. Distance measurements between a gene locus and the nuclear lamina or heterochromatin, performed with ImageJ. A single light optical section of a nucleus, where the intensity center of the signal was situated, was selected. The gene signal is shown in red, heterochromatin in green, and the nuclear lamina in blue. The shortest distances between the gene locus and the lamina or heterochromatin were determined and are indicated with yellow arrows. Scale bar: 10 μm .

The measurement started on the light optical section which corresponded to the z coordinate of the intensity center of the locus. A line was drawn starting from the intensity center. Using the mouse cursor, the free end was placed to the closest border of the nuclear lamina / heterochromatin and the length of the line (in μm) was determined (result R1). If the gene locus was close to the top or bottom of the nucleus, the vertical distance to the lamina was also defined by counting the number of optical sections between the intensity center and the lamina, and dividing it by 4 (as the z-

distance was always 0.25 μm) (result R2). Results R1 and R2 were compared and the smaller value was entered into an Excel table for further analyses. The same type of analysis was used to measure the distance to the heterochromatin if the signal was on a straight line below or above it. Otherwise, the intensity center was projected onto the slice where the heterochromatic border first appeared, and the distance to it was measured (a). The number of slices between the real and the projected center was counted and divided by 4 (b). Finally, the distance was calculated as the square root from the sum of a^2 and b^2 (Pythagoras theorem).

Distance measurements between a transgene and the heterochromatic compartment in tissues from FLW-1, fLW-1 and FLFW-1 transgenic larvae after embryonic and larval heat-shocks were performed with Metamorph 4.0/4.6 software. Association was determined on each individual section where signals from both the *sd* locus and heterochromatin were present. For this analysis the FISH signal was manually thresholded, whereas the threshold value (T) for the immunostaining signal was a function of the fluorescence intensity distribution in the corresponding images and was calculated as follows: **T = Mean fluorescence intensity \pm X x Standard Deviation of fluorescence intensity distribution (M and S.D. values were determined by the software).** The factor X was determined experimentally in the beginning and was then maintained for all analysed nuclei. All data were imported into Excel for further analyses.

2.2.3.2.3. Distance corrections

Taking into account that nuclei sometimes have a wide size range even within one tissue, in several experiments the measured distances were corrected for the approximate nuclear volume. After the correction the distances were expressed in „relative distance units“.

To perform the correction, real distances (in μm) were divided by the approximate volume of the nucleus. The approximate nuclear volume was calculated in the following way: using „Z projection“ function of ImageJ, the largest mid-nuclear plane was defined based on the lamina staining. and the area of this plane was measured (Figure 10). This value was multiplied by the height of the nucleus (which is equal to the number of stacks divided by 4, because the Z distance was always 0.25 μm). The resulting coefficient N reflected the volume of the nucleus and the real measured distances were divided by this value. For convenience of perception the resulting values were multiplied by 1000 (Table 1).

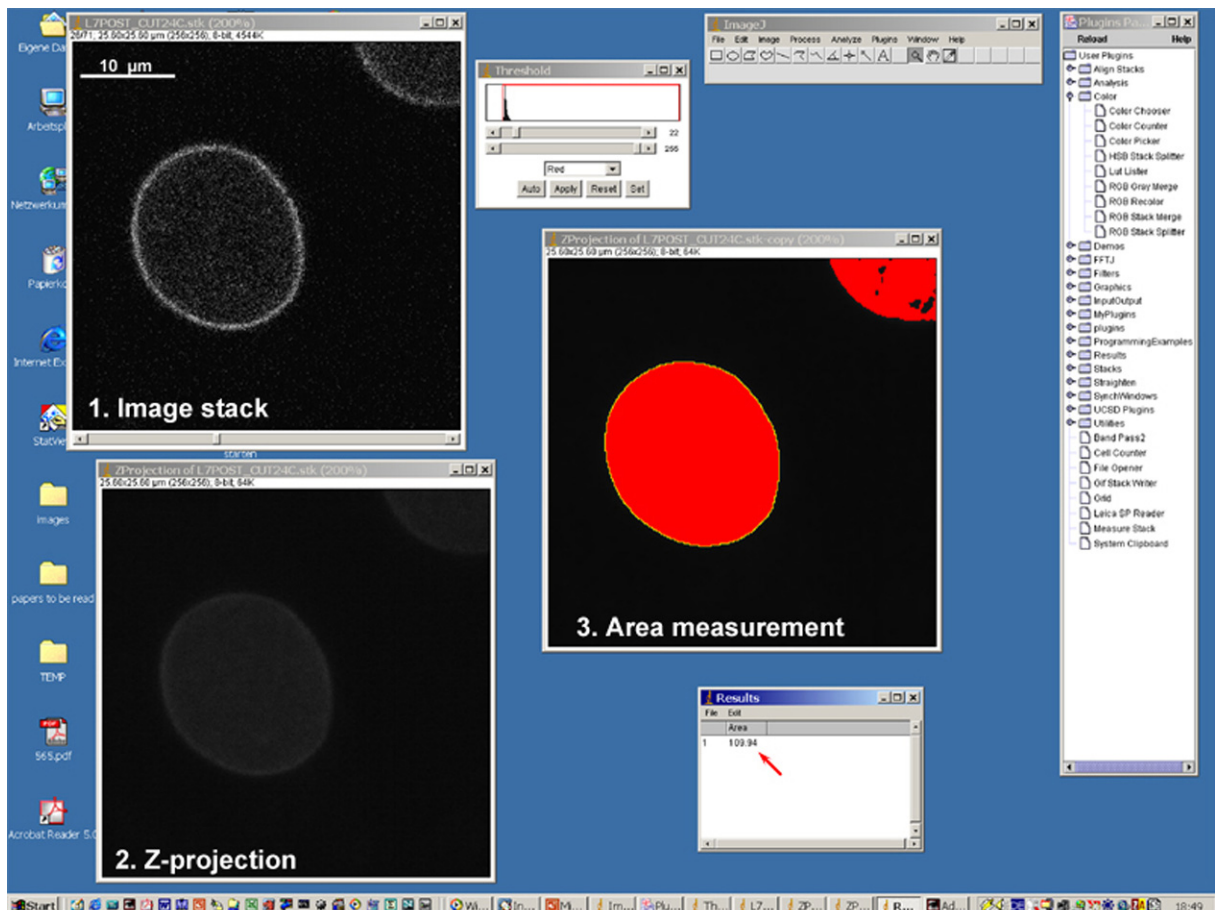


Figure 10. Measurement of the area of the largest mid-nuclear plane of a nucleus using ImageJ. (1) A single confocal section of an entire stack of a nucleus displaying nuclear lamina staining is shown. (2) The z-projection function of ImageJ determined on the basis of the lamina staining the largest mid-nuclear plane of the nucleus. (3) The threshold was adjusted and the size of the marked area was calculated. The result is shown in the table and is indicated with the red arrow.

2.2.3.3. Analysis of the 3D organization of PcG bodies

To analyse numbers, sizes and nuclear localization of Polycomb bodies in different *Drosophila* tissues 3D stacks were assembled using ImageJ, and the numbers of PcG foci were counted by the software for each nucleus. The threshold was adjusted as described in 2.2.3.2.2. As ImageJ operates with single optical sections, the area of each PcG aggregation was measured rather than volume.

In addition, 3D reconstructions were made using Amira 3.0 software. For all confocal images the voxel size was standard: 0.1x0.1x0.25 µm. The threshold was determined as described in 2.2.3.2.2. A Polycomb aggregation or a binding site was defined as a structure consisting of at least nine (for salivary glands) or six (for other tissues) adjacent voxels. The numbers and volumes of Polycomb aggregations were calculated by the software.

nucleus	sd-H3K9 (SK9), μm	sd-lamina (SL), μm	square (S), μm^2	slices	height (H), μm	square*H (SH)	(SK9/SH)*1000	(SL/SH)*1000
malp1	0,13	1,2	50,23	21	5,04	253,1592	0,513510866	4,740100301
malp2	0,08	1,2	50,91	19	4,56	232,1496	0,344605375	5,169080627
malp3	0	0,72	68,95	23	5,52	380,604	0	1,891729987
malp4	0,2	0,22	32,07	36	8,64	277,0848	0,721800691	0,79398076
malp5-1	2,43	0	30,5	43	10,32	314,76	7,720167747	0
malp5-2	2,68	0,78	35,53	35	8,4	298,452	8,979668422	2,613485586
malp6-1	2,54	0	44,78	26	6,24	279,4272	9,090024164	0
malp6-2	0,09	1,69	48,57	24	5,76	279,7632	0,321700638	6,040823096
malp7-1	0,24	0,5	32,13	26	6,24	200,4912	1,197060021	2,493875043
malp7-2	2,71	0,34	37,44	24	5,76	215,6544	12,56640254	1,576596629
malp7-3	1	0,41	35,46	24	5,76	204,2496	4,895970421	2,007347872
malp8-1	1,02	0,57	31,74	21	5,04	159,9696	6,37621148	3,563177004
malp8-2	1,06	0,72	45,25	23	5,52	249,78	4,243734486	2,882536632
malp8-3	3,82	0,45	33,91	33	7,92	268,5672	14,2236282	1,675558296
malp9-1	2,66	0	43,6	30	7,2	313,92	8,473496432	0
malp9-2	1,44	0,46	29,68	27	6,48	192,3264	7,487271638	2,391767329
malp9-3	0,98	0,9	25,65	26	6,24	160,056	6,122857	5,623031939
malp10-1	0,55	0,1	29,25	21	5,04	147,42	3,730837064	0,678334012
malp10-2	0,64	0,25	26,98	25	6	161,88	3,953545836	1,544353842
malp10-3	0,61	0	27,96	25	6	167,76	3,636146876	0
malp10-4	1,81	0,55	30,31	24	5,76	174,5856	10,36740716	3,150317094
malp12-1	2,23	0	26,02	40	9,6	249,792	8,92742762	0
malp12-2	2,43	0,65	36,35	33	7,92	287,892	8,440665249	2,257791116
malp13	0	0,96	40,1	37	8,88	356,088	0	2,695962796
malp15	3,07	0,1	64,67	22	5,28	341,4576	8,990867387	0,29286213
malp16	0	0,72	41,43	14	3,36	139,2048	0	5,17223544
malp17	0	0,8	68,54	20	4,8	328,992	0	2,431670071
malp18	3,69	0,7	101,53	20	4,8	487,344	7,571653698	1,43635707
malp19-1	0,89	0,4	71,07	20	4,8	341,136	2,608930163	1,172552882
malp19-2	0	0,6	71,07	20	4,8	341,136	0	1,758829323
malp19-3	0	0,96	70,28	19	4,56	320,4768	0	2,995536665
malp20-1	0,96	0,8	63,45	23	5,52	350,244	2,740946312	2,284121926
malp20-2	1,05	0,95	63,09	24	5,76	363,3984	2,889390817	2,61421074
malp21-1	1,67	0,75	55,57	23	5,52	306,7464	5,444236672	2,44501647
malp21-2	1,6	0	53,96	28	6,72	362,6112	4,41243955	0
malp21-3	2,7	0	57,82	27	6,48	374,6736	7,206272339	0
malp22-1	2,8	0,1	37,18	39	9,36	348,0048	8,045866034	0,287352358
malp22-2	2,83	0	57,58	26	6,24	359,2992	7,876443922	0
malp23	3,26	1,2	56,39	31	7,44	419,5416	7,770385583	2,860264632
malp24	0,89	0,96	46,02	30	7,2	331,344	2,686030228	2,897291033
malp25	0,37	1,28	56,68	28	6,72	380,8896	0,971410088	3,360553819
malp26	3,05	1,95	56,65	29	6,96	394,284	7,735540879	4,945673677
malp27	3,87	0,48	50,12	29	6,96	348,8352	11,0940639	1,376007926
malp28	3,08	0,7	42,86	21	5,04	216,0144	14,25830871	3,240524706
malp29-1	0,4	0,1	66,23	18	4,32	286,1136	1,398046091	0,349511523
malp29-2	0,33	0,15	82,36	15	3,6	296,496	1,112999838	0,505909017
malp30	0,3	0	56,39	19	4,56	257,1384	1,166686889	0
malp32	0,37	1,55	43,98	28	6,72	295,5456	1,251921869	5,24453756
malp33-1	1,47	0,8	45,99	33	7,92	364,2408	4,035791707	2,196349228
malp33-2	1,53	0,15	48,82	27	6,48	316,3536	4,836360326	0,474152973
malp34	1,82	0,4	63,08	23	5,52	348,2016	5,226857085	1,148759799
malp35-1	1,2	0,8	72,58	13	3,12	226,4496	5,299192403	3,532794935
malp35-2	3,99	0	69,74	12	2,88	200,8512	19,86545263	0
malp36-1	4,55	0,3	67,09	14	3,36	225,4224	20,18432951	1,330834913
malp36-2	2,29	0,6	65,07	16	3,84	249,8688	9,164809692	2,401260181
malp36	3,73	0,1	57,15	24	5,76	329,184	11,3310489	0,303781472
malp37	1,56	0,45	62,11	23	5,52	342,8472	4,550131954	1,312538064
malp38-1	1,34	0,9	46,47	33	7,92	368,0424	3,640884855	2,445370425
malp38-2	1,41	0,14	49,03	28	6,72	329,4816	4,279449899	0,424909919
malp39-1	0,66	0,05	56,42	31	7,44	419,7648	1,572309065	0,119114323
malp39-2	4,09	0	36,5	42	10,08	367,92	11,11654708	0
malp40-1	0,6	0,5	37,71	39	9,36	352,9656	1,699882368	1,41656864
malp40-2	1,68	0,1	26,28	33	7,92	208,1376	8,071583414	0,480451394
malp40-3	1,35	1,05	38,15	32	7,68	292,992	4,607634338	3,583715596

Table 1. Example of an Excel table filled with results of one set of measurements performed with ImageJ. This table shows results of distance measurements for *sd*-lamina and *sd*-heterochromatin in nuclei from WT malpighian tubules as well as corresponding distance corrections for nuclear sizes. From left to right the columns show: the name of the nucleus; distance between *sd* and heterochromatin in μm ; the distance between *sd* and lamina in μm ; the area of the largest mid-nuclear plane in μm^2 ; the number of slices in this nucleus; the height of the nucleus; the „nuclear size“ factor; the distance between *sd* and heterochromatin, divided by the „nuclear size“ factor and multiplied by 1000; the distance between *sd* and lamina, divided by the „nuclear size“ factor and multiplied by 1000.

Some tissues were imaged with the SPIM microscope and corresponding 3D reconstructions were made by Dr. Francesco Pampaloni (EMBL Heidelberg) in MatLab 7.0 using a custom routine written by Dr. Jim Swoger (EMBL Heidelberg). Nuclei in these reconstructions were then analysed visually for the number of PcG aggregations and their spatial distribution.

3. Results

3.1 Nuclear positioning of endogenous genes and transgenes in nuclei of larval tissues of *Drosophila melanogaster*

3.1.1. Spatial organization of chromatin in *Drosophila* nuclei

The aim of the studies performed with *Drosophila melanogaster* was to analyze the nuclear organization of endogenous genes (*Abd-B*, *sd*, *Ubx*) as well as of Fab-7-containing transgenes (5F3, 5F24, 24F6; see Figure 2). The studies focused on larval tissues and one of the questions addressed was whether gene loci associate at defined functional states with heterochromatic compartments. Therefore, it was necessary first to study the nuclear organization of heterochromatin and euchromatin. These analyses were performed with 3rd instar larvae from WT as well as transgenic FLW-1 and fLW-1 flies (Cavalli and Paro, 1998). Both transgenic lines harbour a construct which contains the Fab-7 element and the reporter genes *lacZ* and mini-*white*. FLW-1 harbours the 5F24 transgene where Fab-7 has dorsal-proximal orientation, while fLW-1 contains the 5F3 transgene with proximal-dorsal oriented Fab-7 (Cavalli and Paro, 1998; Zink and Paro, 1995). Nuclei from anterior epidermis, malpighian tubules, fat body cells, anterior midgut and salivary glands were investigated.

In a first set of experiments anterior epidermis, malpighian tubules, fat body cells, and salivary glands of WT as well as transgenic FLW-1 and fLW-1 3rd instar larvae were used. Heterochromatin was visualized by immunostaining with antibodies against histone H3 dimethylated at lysine 9 (dimH3K9), as it was previously shown that this histone modification is strongly enriched in chromocentric heterochromatin and the fourth chromosome (Byrd and Shearn, 2003; Schotta et al., 2002). The nuclear lamina was visualized with specific antibodies against *Drosophila* lamin (kindly provided by Prof. H. Saumweber, University of Berlin). About 300 nuclei were scanned using confocal laser scanning microscopy (see 2.1.8.) and analysed with ImageJ software. Nuclei from malpighian tubules from WT and FLW-1 larvae are shown in Figure 11. Usually heterochromatin enriched in dimH3K9 formed one large compartment, which occupied up to 30% of the nuclear volume. This compartment was often, but not always, associated with the nuclear lamina (Figure 11 A, B). In about 15% of nuclei heterochromatin was split into 2-3 domains (data not shown).

Next, I visualized acetylated isoforms of histone H4 (H4ac) as a mark for euchromatin together with dimH3K9 and the nuclear lamina in interphase nuclei of 3rd WT and FLW-1 instar larvae. Antibodies (Upstate) were used which recognize all forms of acetylation at all four lysines. I found that eu- and heterochromatin occupied mutually exclusive and non-overlapping compartments within the nucleus, and

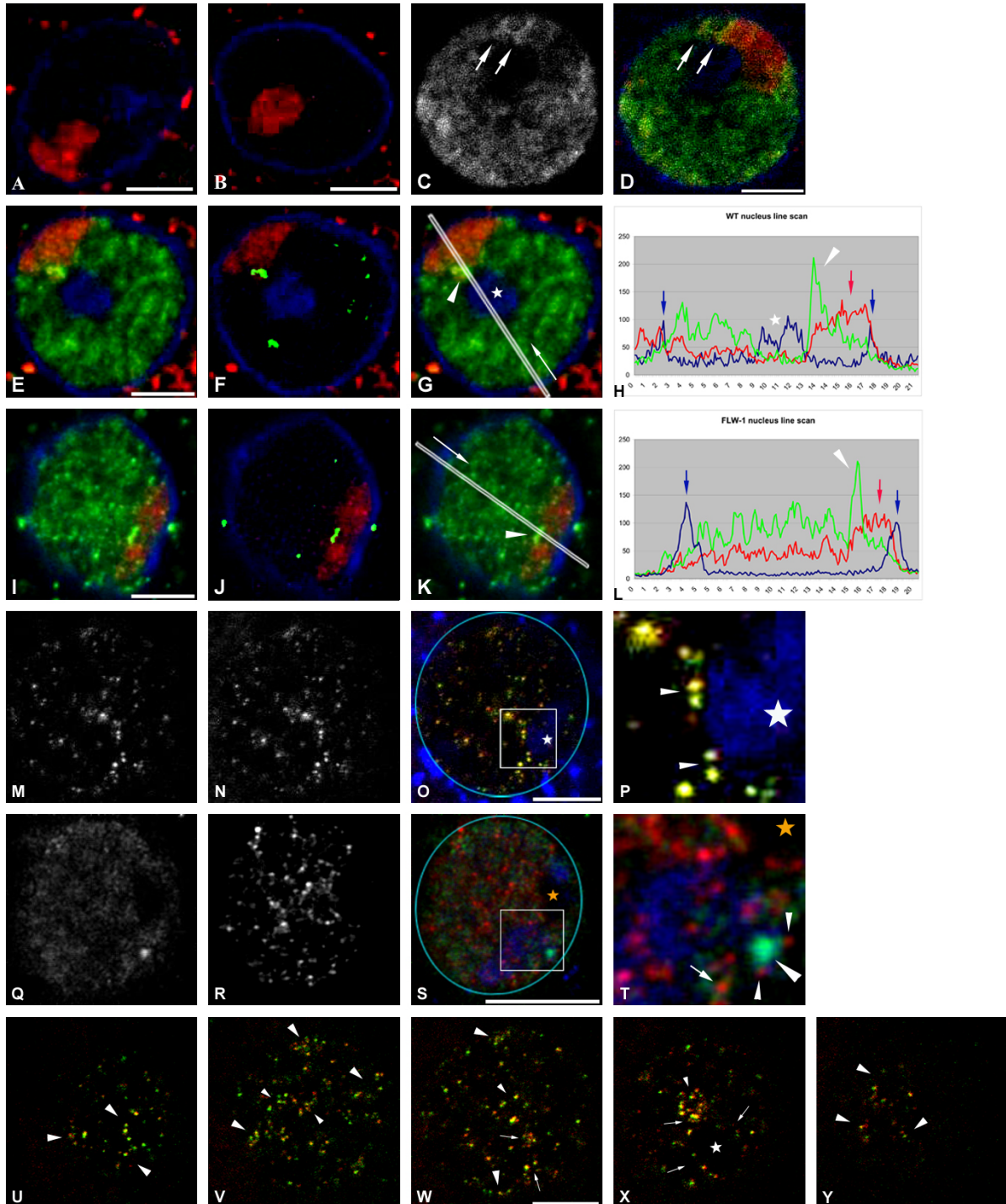


Figure 11. Organization of hetero- and euchromatin in malpighian tubules of 3rd instar larvae. Single light optical sections of nuclei are shown. All histone modifications and the nuclear lamina were visualized with specific antibodies. Anti-lamin antibodies often gave rise to background staining in the nucleolus. (A, B) Nuclei from WT and transgenic FLW-1 larvae, respectively. Heterochromatin was visualized using antibodies against dimH3K9 and is shown in red, whereas the nuclear lamina is shown in blue. Scale bars: 5 μ m. (C, D) A nucleus from a FLW-1 larva. H4ac (C, green in D), dimH3K9 (red in D) and the nuclear lamina (blue in D) were immunostained. Arrows mark domains enriched in H4ac at the boundary of heterochromatin. Scale bar: 5 μ m. (E-L) Relative positioning of sites enriched in dimH3K4 (green) and dimH3K9 (red) in nuclei from WT (E-H) and FLW-1 (I-L) larvae, respectively. The nuclear lamina is shown in blue. To identify sites most enriched in dimH3K4 a high threshold was applied to the corresponding signal so that only the most intensely stained regions remained visible (green).

Original (E, I) as well as processed (F, J) images are shown. Additionally, line scans were performed on the same nuclei (G, K). The direction of the scan along the framed line is shown with white arrows, while arrowheads indicate the regions most enriched in dimH3K4. (H, L) The corresponding fluorescence intensity profiles. The colour code of the diagrams corresponds to that of the images. White arrowheads mark the domains highly enriched in dimH3K4 at the boundary of the dimH3K9-enriched domains (red arrows). The nuclear lamina is indicated by blue arrows. Asterisks in (G, H) mark the nucleolus. Scale bars: 5 μm . (M-P) Sites enriched in trimH3K4 (M, green in O, P), RNA pol II (active form) (N, red in O, P; colocalization of red and green results in yellow in P) and dimH3K9 (blue marked with an asterisks in O, P) in a nucleus from a FLW-1 larva were visualized. The nuclear rim is indicated in light blue (O) and the framed section of the nucleus is shown enlarged in (P), where arrowheads point to sites enriched in trimH3K4 and pol II (colocalizing at most sites) at the boundary of the dimH3K9-positive domain. Scale bar: 5 μm . (Q-T) A nucleus from a FLW-1 larva. DimH3K4 (Q, green in S, T), pol II (active form) (R, red in S, T) and dimH3K9 (blue in S, T) were visualized; the nucleolus is marked with an orange asterisk in (S, T). The nuclear rim is indicated in light blue (S) and the framed section of the nucleus is shown enlarged in (T), where the large arrowhead points to the dimH3K4-enriched domain at the boundary of heterochromatin and small arrowheads mark typical sites where loci enriched in dimH3K4 and pol II at the boundary of the nucleolus are not colocalized but juxtaposed. The arrow marks one of the few sites enriched in both dimH3K4 and pol II. Scale bar: 10 μm . (U-Y) Other light optical sections from the nucleus displayed in (M-P) are shown. The asterisk marks the nucleolus. Large arrowheads mark transcriptionally active foci at the nuclear periphery (U, V, W, Y), arrows mark perinucleolar foci (W, X) and small arrowheads mark intranuclear concentrations of active foci (V, W, X). Scale bar: 5 μm .

one large nucleolus was clearly visible as space that remained unstained by these antibodies. Figure 11 (C, D) shows a typical nucleus from a FLW-1 larva (similar results were obtained with WT tissues). In the majority of nuclei, H4ac was detected in different amounts at numerous sites throughout the euchromatic compartment. Most of the heterochromatic domain was weakly stained by the antibody against H4ac, which was probably due to H4K12 acetylation. Usually 1-3 brightly stained domains were detected at the boundary of dimH3K9-enriched chromatin (arrows in Figure 11 C, D). No such brightly stained sites were found within the dimH3K9-positive domain or the nucleolus. Hyperacetylation of histone H4 is generally associated with transcriptionally competent and active domains (Cavalli and Paro, 1999; Schubeler et al., 2004; Turner, 2000).

In the next series of experiments, histone modifications typical for euchromatin were visualized using antibodies against histone H3 di- and trimethylated at lysine 4 together with dimH3K9 and the nuclear lamina in interphase nuclei of WT and FLW-1 3rd instar larvae. In a first subset of experiments H3 dimethylated at lysine 4 (dimH3K4) was detected. Similar results were obtained for WT and transgenic flies and for different tissues. Although most of the euchromatin was stained with the antibody against dimH3K4, some sites were particularly enriched in this modification (Figure 11 E, I). To address the nuclear localization of these sites, images of nuclei from epidermis and malpighian tubules were analyzed with ImageJ software. Each RGB stack was split and the monochromatic stack, which corresponded to the anti-dimH3K4 staining, was smoothed to increase the signal-to-noise ratio. A very high threshold (defined

individually for each nucleus) was applied to this stack so that only the most brightly stained regions were left. Then the RGB stack was reassembled and the positioning of such sites relative to dimH3K9-enriched heterochromatin was inspected. Figure 11 (E, F, I, J) shows examples of the original as well as processed images from WT and FLW-1 3rd larval malpighian tubules. Single light optical sections are shown which demonstrate in each nucleus a large domain strongly enriched in dimH3K4 at the boundary of heterochromatin. Additionally, line scans with unprocessed raw images were performed using Image J (Figure 11 G, K). Diagrams in (H, L) show the corresponding fluorescence intensity profiles. In both cases the main peak of green fluorescence (anti-dimH3K4 staining) (arrowheads) was located at the boundary of heterochromatin. Loci strongly enriched in dimH3K4 at the border of the dimH3K9-positive domain were observed in about 85% of nuclei from epidermis and malpighian tubules in both analysed fly lines.

In the next subset of experiments I simultaneously detected trimethylated lysine 4 of histone H3 (trimH3K4), the active form of RNA polymerase II (CTD7 phosphorylated at Ser 2, antibody kindly provided by Prof. Dirk Eick and Prof. Elisabeth Kremmer, GSF, Munich) and dimH3K9 in nuclei from malpighian tubules of WT and FLW-1 3rd instar larvae. I concentrated on malpighian tubules because the nuclei in this tissue are large and almost spherical, in contrast to rather flat nuclei of epidermis, and therefore allow a more accurate analysis. Nuclei were imaged using a Zeiss LSM 410 confocal microscope. Assembly of 3D stacks and correction for the shift between channels were performed with ImageJ software. I analyzed ~15 nuclei, and Figure 11 (M-P and U-Y) shows a typical example of a nucleus from a FLW-1 larva (I observed similar patterns in WT nuclei, data not shown). Mostly, trimH3K4 and pol II were colocalized at the same sites (yellow in Figure 11 O, P, U-Y). Some loci, however, showed only presence of either trimH3K4 or pol II (green and red in O, P, U-Y, respectively). No indication of transcriptional activity was found within the heterochromatic domain, while at its boundary there were usually multiple loci which were enriched in trimH3K4 and active pol II (arrowheads in Figure 11 P). These loci had sizes and shapes similar to those distributed elsewhere in the nucleus, small and dot-like. I never observed large elongated sites like those enriched in dimH3K4 at the boundary of heterochromatin (see above), which suggested that di- and trimethylated forms of lysine 4 could occupy different or only partially overlapping euchromatic sites, at least at the boundary of heterochromatin. To address this question, I simultaneously detected dimH3K4, pol II and dimH3K9 in nuclei from WT and FLW-1 3rd larval malpighian tubules. Figure 11 (Q-T) shows an example of a nucleus from a FLW-1 larva (I observed similar patterns in WT nuclei, data not shown). The large domain strongly enriched in dimH3K4 at the boundary of heterochromatin (indicated with the large arrowhead in T) was depleted in RNA pol II which was instead present at adjacent sites at the boundary of heterochromatin (small arrowheads in T). Mostly, sites enriched in pol II (active form)

showed some dimH3K4 staining but were not specifically enriched in this modification. These results suggest that dimH3K4 occurs at both inactive and active euchromatic genes, while trimH3K4 marks only the active ones. Interestingly, transcriptionally active foci were not distributed evenly in euchromatin but were organized into clusters, which often looked like rings or beads on a string (Figure 11 U-Y; Figure S1 on the supplementary CD). Apart from being enriched at the boundary of heterochromatin, many of the clusters were located at the nuclear and nucleolar periphery (U, V, X, Y). Together, these results suggest that active transcription and corresponding histone modifications, associated with transcriptionally competent or active chromatin, were distributed not evenly throughout the euchromatic domain and were enriched at specific sites, in particular at the boundary of heterochromatin.

In a second set of experiments I studied spatial relationships between pericentromeric DNA and the whole heterochromatic compartment. Pericentromeric DNA was detected by FISH using the (AAGAG)₈ repeat as a probe while the bulk of heterochromatin was detected with an antibody against dimH3K9. These experiments were performed with nuclei from anterior epidermis, malpighian tubules, fat body cells and anterior midgut. The tissues were taken from 3rd instar larvae of WT and FLW-1 flies. About 200 nuclei were imaged using confocal laser scanning microscopy and analysed. Figure 12 (A, B) shows single light optical sections of nuclei from WT malpighian tubules and FLW-1 anterior midgut, respectively. Other analysed tissues displayed the same

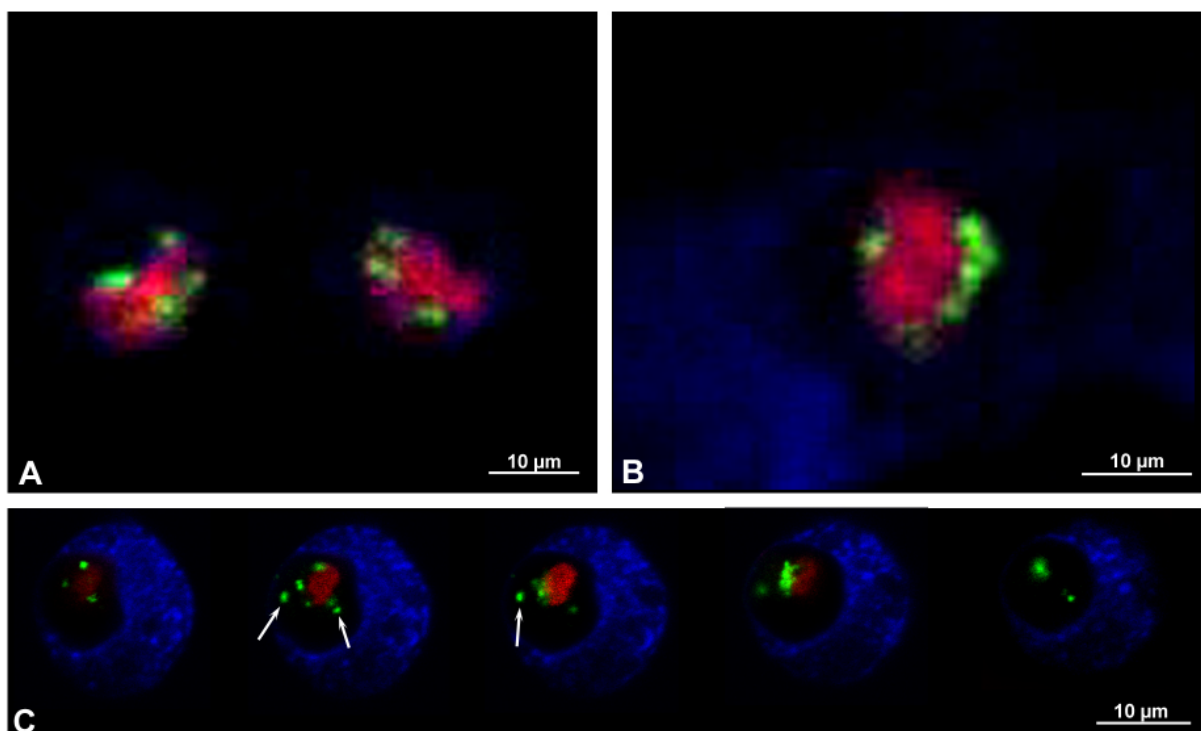


Figure 12. Spatial organization of the heterochromatic domain. The heterochromatic domain was visualized with antibodies against dimH3K9 and is shown in red, whereas pericentromeric satellite DNA was detected by FISH using (AAGAG)₈ as a probe (see 2.2.2.8.2). The FISH signal is shown in green. The nuclear lamina is shown in blue (in Kc cells

also the cytoplasm displayed a high level of background staining). (A), (B) Single confocal sections of nuclei from WT malpighian tubules and FLW-1 anterior midgut, respectively. (C) A series of consecutive light optical sections of a Kc cell. The arrows point at small aggregations of the repetitive DNA, disconnected from the main bulk of heterochromatin.

organization (data not shown). In all analysed nuclei pericentromeric satellite DNA was exposed on the surface of the heterochromatic compartment, forming several domains of variable numbers and sizes. The pericentromeric DNA was never found enclosed within the chromocenter. I also studied the organization of pericentromeric DNA in Kc cells. The satellite DNA and dimH3K9-positive heterochromatin were visualized in the same way as in larval nuclei (see above). About 100 nuclei were analysed. Figure 12 C shows a series of consecutive single confocal sections of a Kc cell nucleus. In Kc cells, like in nuclei from larval tissues, pericentromeric satellite DNA was localized at the boundary of the heterochromatic compartment. In some Kc nuclei small aggregations of satellite DNA were found well apart from the chromocenter (indicated by arrows in Figure 12 C).

In summary, the data showed that eu- and heterochromatin occupy distinct and mutually exclusive compartments in *D. melanogaster* nuclei. The boundary between these two compartments is made up by specific components of eu- and heterochromatin. Pericentric satellite DNA encloses the heterochromatic compartment and is exposed at its boundary. In addition, sites enriched in active pol II and trimH3K4 as well as domains enriched in dimH3K4 are concentrated at this boundary.

3.1.2. Nuclear positioning of endogenous gene loci and transgenic constructs

After addressing the nuclear organization of eu- and heterochromatic domains, the nuclear positioning of three endogenous genes (*Abdominal-B*, *scalloped* and *Ultrabithorax*) and three Fab-7 containing transgenic constructs (5F3, 5F24 and 24F6, see 2.1.10.2.1) was studied. As the relative positioning to heterochromatin and the nuclear lamina appears to play an important role in gene regulation (Brown et al., 1999; Brown et al., 1997; Kosak and Groudine, 2004; Kosak et al., 2002; Misteli, 2004), I first studied the positioning of loci with regard to these domains. All genetic elements were visualized with specific DNA probes using FISH, while the nuclear lamina and heterochromatin were detected with specific antibodies against *Drosophila* lamin and dimH3K9, respectively. All nuclei were scanned using a Leica confocal microscope and analysed with ImageJ software.

The analysis was performed with nuclei from anterior epidermis and malpighian tubules. In these tissues all analysed endogenous loci were inactive. The tissues were taken from 3rd instar larvae of wild type (WT) as well as FLW-1, fLW-1, FLFW-1 and

5F24 25,2 transgenic lines (Cavalli and Paro, 1998)(the latter line is also known as Fab-X (Bantignies et al., 2003)) and fixed with formaldehyde. Transgenic flies were raised and kept under standard conditions (18°C) to keep the transgenes in their inactive state. From transgenic flies only female larvae were taken to exclude influences of the dosage compensation effect.

3.1.2.1. Nuclear positioning of inactive endogenous loci in *Drosophila* tissues

3.1.2.1.1. *Abdominal-B* (*Abd-B*)

Nuclear positioning of the *Abd-B* gene (Figure 13 A) was analysed in nuclei from anterior epidermis and malpighian tubules of WT and transgenic FLW-1 and FLFW-1 flies. In each nucleus the distance between *Abd-B* and the closest border of lamina or heterochromatin, respectively, was measured using Image J (for details see 2.2.3.2.). The results of the measurements are shown in Figures 14 and 15.

In WT flies, nuclei from epidermis showed a peripheral localization of *Abd-B*: ~80% of signals were found within 1 µm from the lamina. In contrast, nuclei from malpighian tubules showed a different positioning of *Abd-B* regarding the nuclear

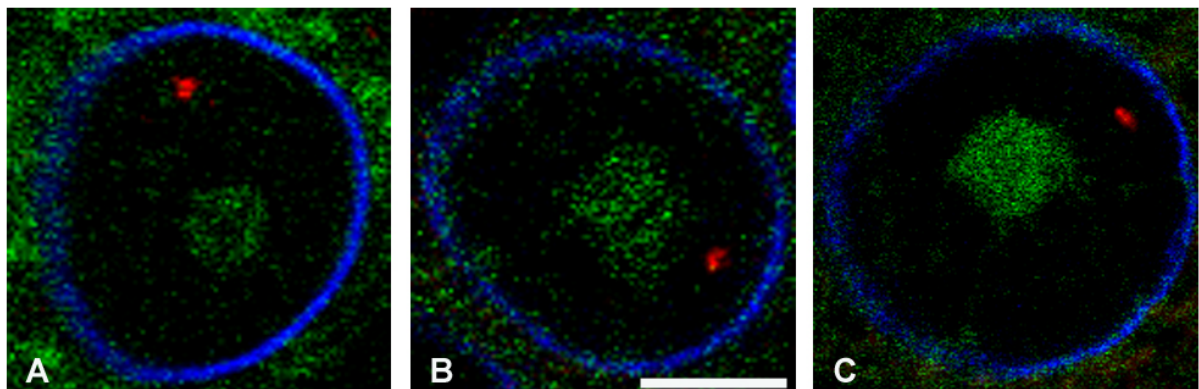


Figure 13. *Abd-B*, *sd* and *Ubx* in nuclei from malpighian tubules of WT and transgenic flies. Genes were detected by FISH using specific probes and the FISH signals are shown in red. Heterochromatin was immunostained with antibodies against dimH3K9 and is shown in green, while the nuclear lamina was visualized using antibodies against *Drosophila* lamin and is shown in blue. (A) *Abd-B* and heterochromatin in a nucleus of a FLFW-1 transgenic larva. (B) *sd* and heterochromatin in a nucleus of a FLW-1 transgenic larva. (C) *Ubx* and heterochromatin in a nucleus of a WT larva. Scale bar: 5 µm.

lamina: only ~35% of nuclei displayed *Abd-B* within 1 µm from the lamina and ~35% between 1 and 2 µm from it (Figure 14, top left diagram). After correction for the size of the nuclei (for details see 2.2.3.2.3.), 50% (epidermis) and 70% (malpighian tubules), respectively, of loci were within the smallest distance interval. This result can be explained by the fact that larger distances in malpighian tubules were mostly measured in relative large nuclei.

In FLW-1 flies ~45% of nuclei from malpighian tubules showed the signal within 1 μm from the lamina and ~47% of nuclei between 1 and 2 μm from it. But in nuclei from epidermis *Abd-B* showed no preferential association with the lamina when real distances were measured, as the gene signal displayed larger distances from the lamina in general and showed a much wider range of distances (Figure 14, left hand side, middle). However, after correction for the nuclear sizes both tissues displayed a similar peripheral positioning of the gene in terms of relative distance units (RDU) (Figure 14, right hand side, middle). Once again, the discrepancy between the real

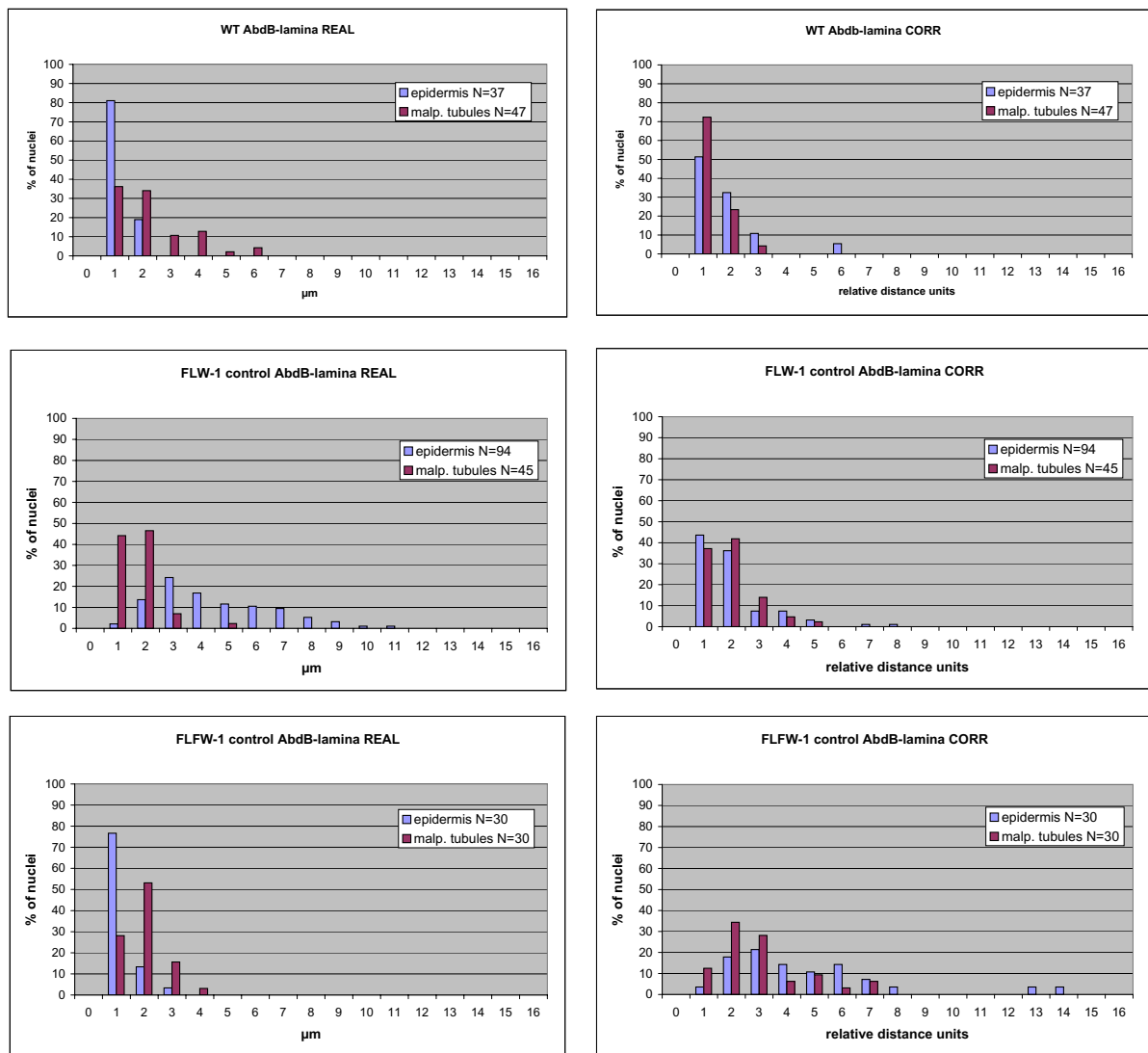


Figure 14. Results of distance measurements between *Abd-B* and the nuclear lamina in tissues from WT, FLW-1, and FLW-1 flies. *Abd-B* was detected by FISH using a specific DNA probe while the nuclear lamina was immunostained with specific antibodies against *Drosophila* lamin. Nuclei were scanned using a Leica SP2 confocal microscope. 3D reconstructions of image stacks and distance measurements were performed with ImageJ 1.34 software. The distance between the intensity center of the FISH signal and the closest part of the lamina was measured in each nucleus. The X axis indicates distance intervals. Interval 1 represents distances from 0,05 μm to 1 μm , interval 2 distances from 1,05 μm to 2 μm etc. The bars indicate the percentages (scale on the Y-axis) of nuclei with measured / corrected distances within

the indicated interval. The diagrams show distances measured in WT (top), FLW-1 (middle), and FLFW-1 (bottom) flies. Diagrams on the left hand side present the distances in microns as directly measured (REAL), while those on the right hand side show the distances in relative distance units after correction for the nuclear size (CORR). N indicates the numbers of analysed nuclei from epidermis (blue) and malpighian tubules (red).

and corrected distances can be explained by the fact that generally larger physical distances were observed in larger nuclei of the epidermis.

In FLFW-1 flies almost 80% of nuclei from epidermis displayed the *Abd-B* signal within 1 μm from the lamina. In malpighian tubules ~30% of nuclei showed the gene signal within 1 μm from the lamina, and over 50% between 1 and 2 μm from it (Figure 14, bottom left). After correction of the distances for the nuclear sizes, a quite variable range of distances was observed in both tissues, and especially in epidermis (Figure 14, bottom right). This can be explained by the fact that small distances were measured in nuclei of all size ranges. In summary, the data revealed a tendency towards a preferential peripheral positioning of *Abd-B*. However, the results showed in addition strong tissue- and fly line-specific influences and a preferential peripheral positioning was not observed consistently.

The positioning of the *Abd-B* locus relative to heterochromatin was analysed in WT and FLFW-1 flies. In WT flies, *Abd-B* showed a similar positioning in both tissues (Figure 15, top left diagram). In FLFW-1 flies, *Abd-B* was positioned differently in epidermis and malpighian tubules (bottom left diagram) and within a smaller range of distances than in WT flies. After correction of the distances for the nuclear sizes, nuclei from epidermis of both fly lines as well as malpighian tubules from FLFW-1 flies displayed an almost uniform distribution of the signal (Figure 15, right diagrams). In malpighian tubules of WT flies the distribution of *Abd-B* was affected by correcting for nuclear sizes but also here *Abd-B* did not show preferential associations with heterochromatin. In summary, the data indicated again some tissue- and fly line-specific influences and no preferential association of the inactive *Abd-B* locus with the heterochromatic domain.

3.1.2.1.2. *Scalloped (sd)*

The nuclear localization of the *sd* locus (Figure 13 B) was studied in nuclei from epidermis and malpighian tubules from WT, FLW-1 and fLW-1 flies. Distances between the *sd* locus and nuclear lamina or heterochromatin, respectively, were measured with ImageJ software. The results of distance measurements are shown in Figures 16 and 17.

In all cases the *sd* locus was preferentially associated with the nuclear periphery, as revealed by the diagrams displaying real distances in μm (Figure 16, left

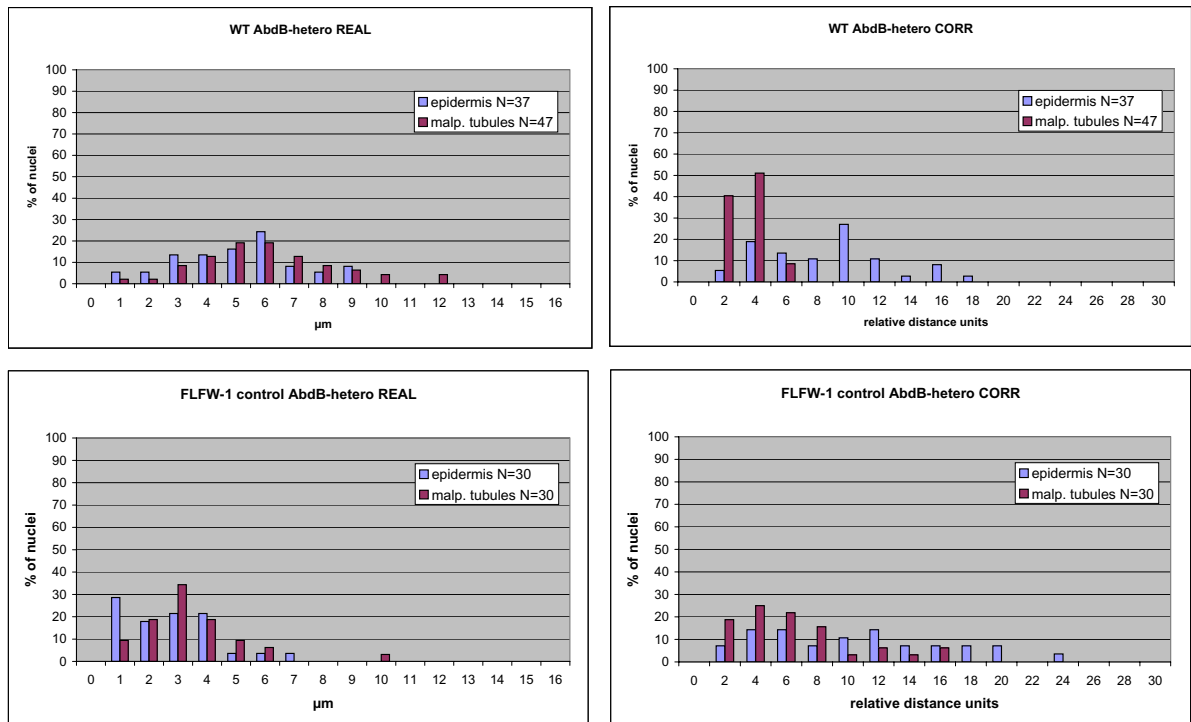


Figure 15. Results of distance measurements between *Abd-B* and heterochromatin in tissues from WT and FLOW-1 flies. *Abd-B* was detected by FISH with a specific DNA probe and heterochromatin was visualized by immunostaining with antibodies against dimH3K9. The distance between the intensity center of the FISH signal and the closest part of the boundary of heterochromatin was measured in each nucleus. The diagrams show results from WT (top) and FLOW-1 (bottom) flies. Diagrams on the left hand side present distances in microns as directly measured (REAL), while those on the right hand side show the distances in relative distance units after correction for the nuclear size (CORR). The bars indicate the fractions of nuclei (%) displaying distances between *Abd-B* and heterochromatin within a given distance interval as indicated on the X-axis. N indicates the numbers of analysed nuclei from epidermis (blue) and malpighian tubules (red).

hand diagrams). After correcting for the nuclear sizes the distance distribution became more variable, which shows that *sd* was closely associated with the nuclear periphery in nuclei of all size ranges (Figure 16, right hand diagrams).

The results of distance measurements between the *sd* locus and heterochromatin are shown in Figure 17. In all cases the distances were quite variable, which did not change when distances were corrected for nuclear sizes. This shows that there was no tendency towards association with heterochromatin.

Together, the results showed that the inactive *sd* locus preferentially associated with the nuclear periphery but not with heterochromatin. This was similar in WT flies and two different transgenic lines and in nuclei from epidermis and malpighian tubules.

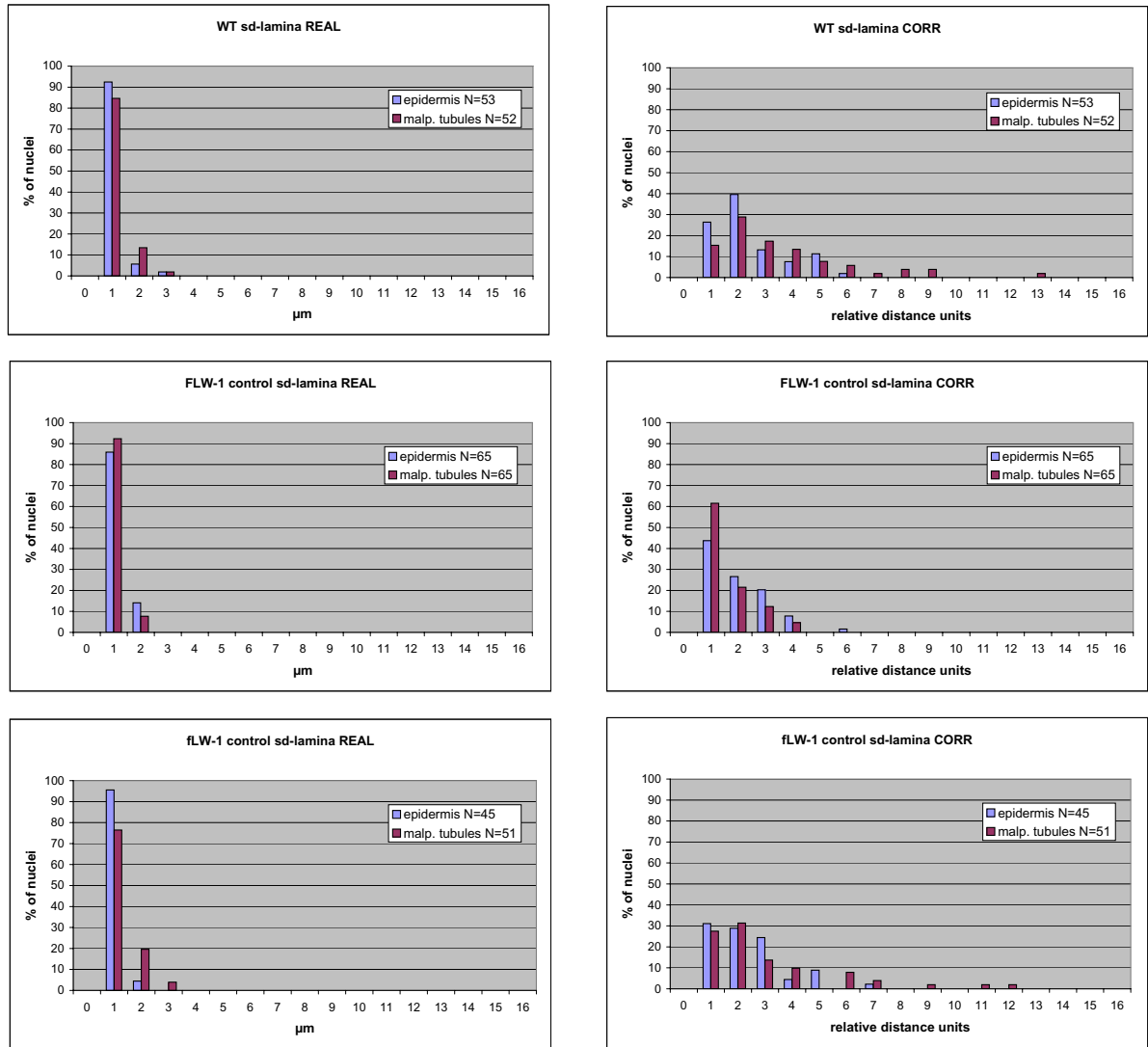


Figure 16. Results of distance measurements between *sd* and the nuclear lamina in tissues from WT, FLW-1, and fLW-1 flies. The *sd* locus was detected by FISH with a specific DNA probe and the nuclear lamina was visualized using specific antibodies against *Drosophila* lamin. The diagrams show distances measured in WT (top), FLW-1 (middle), and fLW-1 (bottom) flies. Diagrams on the left hand side display the distances in microns (REAL), while diagrams on the right hand side display distances after correction for the nuclear size (CORR). N indicates the numbers of analysed nuclei in epidermis (blue) and malpighian tubules (red).

3.1.2.1.3. *Ultrabithorax* (*Ubx*)

The localization of the *Ubx* locus (Figure 13C) relative to the nuclear lamina and heterochromatin was analysed in nuclei from epidermis and malpighian tubules of WT, FLW-1 and 5F24 25,2 flies. In this case only the direct physical distances (REAL) were measured as the previous results showed that correction for nuclear sizes did not contribute very much to the interpretation of the data. The results of the distance measurements between the *Ubx* locus and the nuclear lamina or heterochromatin, respectively, are shown in Figure 18.

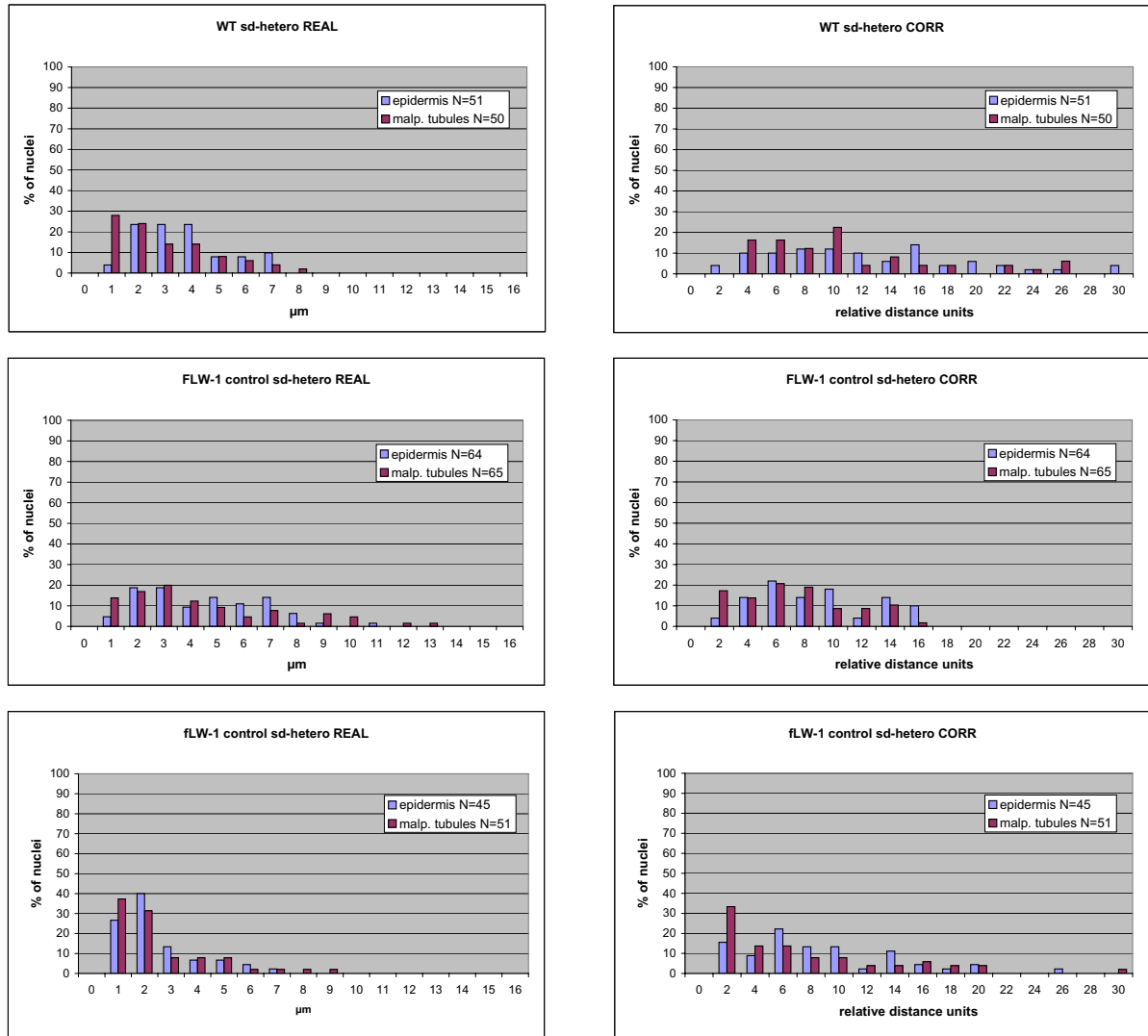


Figure 17. Results of distance measurements between *sd* and heterochromatin in tissues from WT, FLW-1, and fLW-1 flies. The *sd* locus was visualized with FISH using a specific DNA probe, while heterochromatin was detected using antibodies against dimH3K9. The diagrams show distances measured in WT (top), FLW-1 (middle), and fLW-1 (bottom) flies. Diagrams on the left hand side display the distances in microns (REAL), while diagrams on the right hand side display distances after correction for the nuclear size (CORR). N indicates the numbers of analysed nuclei in epidermis (blue) and malpighian tubules (red).

In WT larvae, in about 60% (epidermis) or 43% (malpighian tubules) of nuclei, respectively, the *Ubx* locus was positioned within 1 μm from the lamina. In addition, in about 35% of nuclei the *Ubx* locus displayed distances between 1 and 2 μm from the lamina in epidermis as well as in malpighian tubules (Figure 18, top left diagram). In both transgenic lines *Ubx* displayed an increased peripheral localization and this effect was dramatic in FLW-1 larvae, where *Ubx* was localized within 1 μm from the lamina in almost all cases (Figure 18, left hand side, middle). In contrast, in only about 70% of nuclei the *Ubx* locus showed such small distances to the lamina in 5F24 25,2 flies (left hand side, bottom). This is surprising, as the transgenic lines FLW-1 and 5F24 25,2 carry the same 5F24 transgene and the only difference between these lines

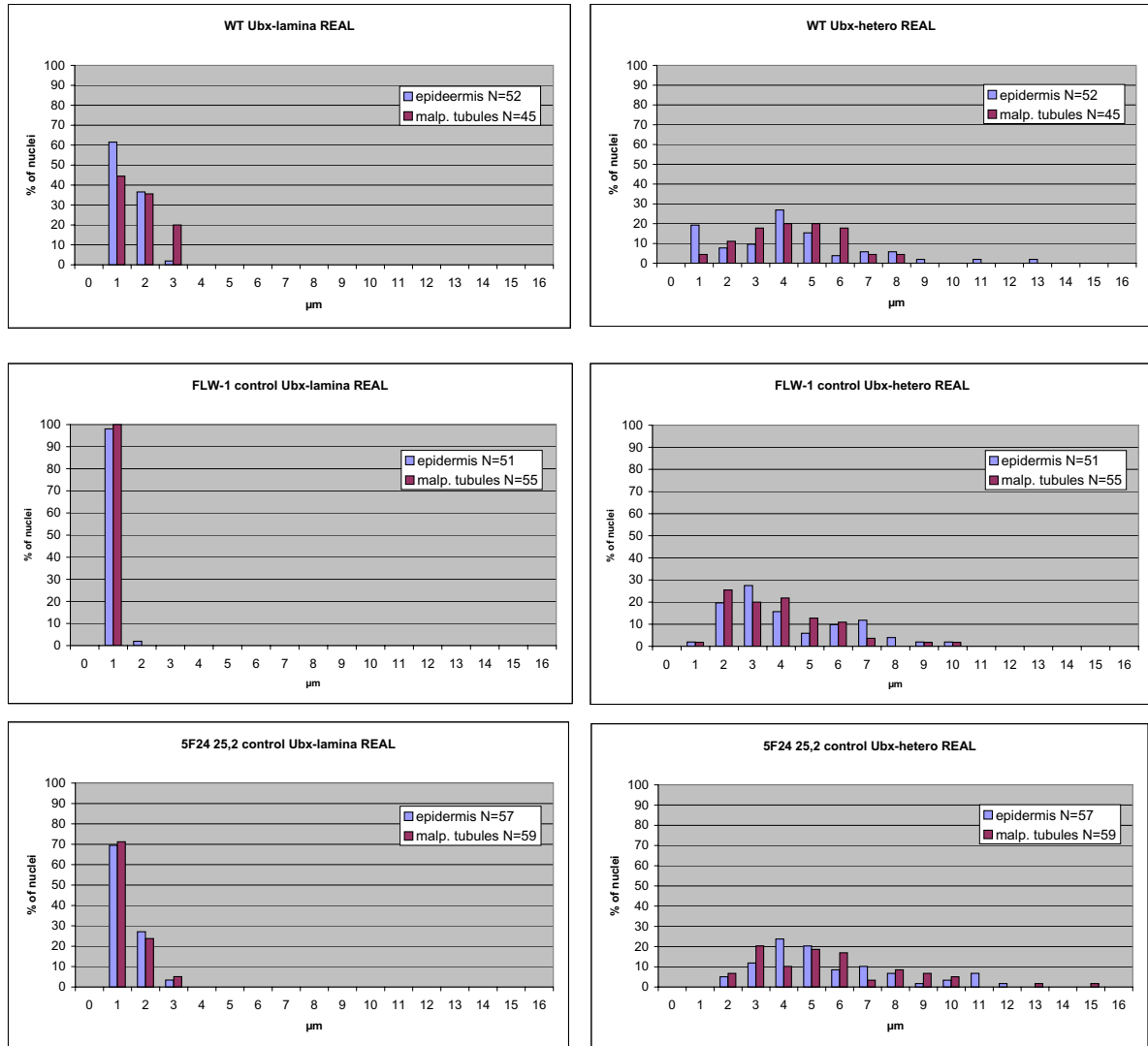


Figure 18. Results of distance measurements between *Ubx* and the nuclear lamina and heterochromatin in tissues from WT, FLW-1, and 5F24 25,2 flies. The *Ubx* locus was detected by FISH using a specific DNA probe, while the nuclear lamina and heterochromatin were immunostained with specific antibodies against *Drosophila* lamin and dimH3K9, respectively. The bars indicate the fractions of nuclei (%) displaying distances between *Ubx* and lamina or heterochromatin within a given distance interval as indicated on the X-axis (REAL). The distances were measured in WT (top), FLW-1 (middle), and 5F24 25,2 (bottom) larvae. The distances between *Ubx* and the nuclear lamina (left panels) or heterochromatin (right panels) are shown. N indicates the numbers of analysed nuclei in epidermis (blue) and malpighian tubules (red).

is the presence of the GAL4 driver located on a balancer CyO chromosome (Cavalli and Paro, 1998; Zink and Paro, 1995).

Together, the data indicated a preferential association of *Ubx* with the nuclear lamina and showed that the peripheral localization of *Ubx* strongly depends on the genetic and chromosomal background. The presence of the GAL4 driver located on the CyO balancer chromosome has a stronger effect on the peripheral localization of *Ubx* (~30% difference in the 1 μm range between 5F24 25,2 and FLW-1 larvae) than the presence of the 5F24 transgenic construct (10% (epidermis) and 25% (malpighian

tubules), respectively, difference in the 1 μm range between WT and 5F24 25,2 flies). In all cases, no specific association between *Ubx* and the heterochromatic domain could be observed (Figure 18, right hand panels).

As a whole, the data indicated a preferential positioning of *Abd-B*, *sd*, and *Ubx* in their inactive states close to the lamina but not close to the heterochromatic domain. The peripheral localization of *Abd-B* and *Ubx* was strongly influenced by the genetic and chromosomal background and also showed tissue-specific effects. Interestingly, the nuclear positioning of *Ubx* and *Abd-B* displayed major differences (particularly pronounced in FLW-1 larvae) (Figures 14, 18). This suggests that these two loci of the Bithorax Complex (BX-C) localized independently from each other. Previous data showed that already intergenic regions of only 50 kb provide enough flexibility for independent nuclear positioning of genes mapping to the same chromosomal region (Zink et al., 2004). On the background of results suggesting pairing between PREs (Bantignies et al., 2003; Vazquez et al., 2006) the question arises whether the extreme peripheral positioning of *Ubx* in FLW-1 flies might be due to pairing with the 5F24 transgene, which is inserted into the *sd* locus in this transgenic line, which also shows here an extreme peripheral position (Figure 16). However, the results obtained here imply that the distinct positioning of *Ubx* in FLW-1 larvae is not due to pairing of PREs, and particularly Fab-7 elements, for two reasons. Firstly, *Abd-B*, which contains Fab-7 in its regulatory region, does not display a pronounced peripheral positioning in FLW-1 larvae (Figure 14). Secondly, the data show that the presence of the balancer chromosome with the GAL4 driver but not the presence of the Fab-7 containing transgene has the most pronounced effect on the peripheral positioning of *Ubx* (Figure 18). Thus, the data suggest that the genetic, chromosomal, and tissue background but not pairing with transgenic Fab-7 elements has a major impact on the nuclear positioning of *Ubx* and *Abd-B*.

3.1.2.2. Nuclear localization of Fab-7 containing transgenes at different states of activity

Next, the nuclear localization of 5F24, 5F3 and 24F6 transgenes was addressed. This part of the research was also performed with nuclei from epidermis and malpighian tubules from FLW-1, fLW-1 and FLFW-1 transgenic female 3rd instar larvae. In FLW-1 and fLW-1 flies transgenes are inserted into the 13F locus of chromosome X within a 5 kb region encompassing the *sd* promoter (Zink and Paro, 1995) and differ only by the orientation of the Fab-7 element (Figure 2, 5F24 and 5F3 transgenes, respectively). As the probe for the Fab-7 element is small (~3 kb) and was not always reliably detectable, a probe for *sd* was used to visualize the integration site (Figure 19 A, B). In FLFW-1 flies the 24F6 transgene, containing 2 copies of the Fab-7 element (Figure 2), was

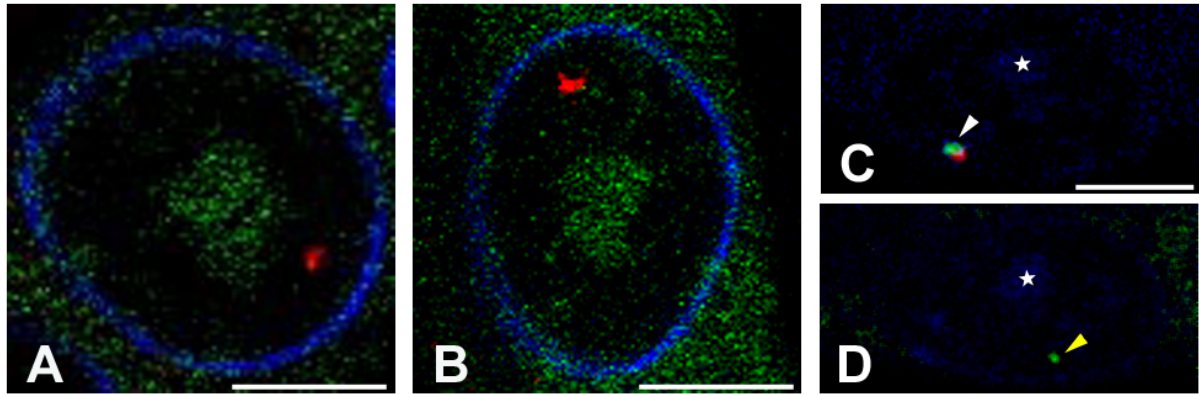


Figure 19. Visualization of transgenes in nuclei from FLW-1, fLW-1, and FLFW-1 flies. Single light optical sections of nuclei from malpighian tubules are shown. Corresponding genetic elements were visualized by FISH using specific DNA probes, while heterochromatin and the nuclear lamina were immunostained with specific antibodies against dimH3K9 and *Drosophila* lamin, respectively. (A), (B) The *sd* locus (red) in FLW-1 and fLW-1 nuclei, respectively. Heterochromatin is shown in green and the nuclear lamina is shown in blue. (C, D) Two light optical sections with a distance of $\Delta z=1 \mu\text{m}$ from the same FLFW-1 nucleus. The Fab-7 probe (green in C, D) was used to visualize the 24F6 transgene (white arrowhead in C) and the endogenous Fab-7 element (yellow arrowhead in D), while the Abd-B probe (red in C) was used to distinguish between transgenic and endogenous copies of Fab-7. Here, the heterochromatin (indicated with an asterisk in C, D) and the nuclear lamina were visualized with Cy5-conjugated secondary antibodies and are both shown in blue. Scale bar: 5 μm .

detectable with the Fab-7 probe. In these flies, the *Abd-B* probe was used in addition to distinguish between the endogenous and transgenic copies of Fab-7 (Figure 19, C).

The localization of transgenes was studied at their inactive state as well as in their stably and transiently active states. Stable activation was achieved by applying an embryonic heat-shock (HS) and after further development 3rd instar larvae were prepared more than a week after the initial HS. Larval HS resulted in transient activation (Figure 1) and 3rd instar larvae were prepared 2 hours after the HS. All genetic elements were visualized by FISH, while nuclear lamina and heterochromatin were detected using specific antibodies against *Drosophila* lamin and dimH3K9, respectively. Activation of the transgene was monitored by β -galactosidase expression in larval tissues (data not shown). Nuclei were imaged using a Leica SP2 confocal microscope and analysed with ImageJ software.

3.1.2.2.1. Nuclear positioning of the 5F24 transgene in FLW-1 larvae

Distance measurements between the 5F24 transgene (inserted in FLW-1 flies into the *sd* locus, which was used as a probe for FISH) and the nuclear lamina or heterochromatin, respectively, were performed in nuclei from female larval anterior epidermis and malpighian tubules, taken from several animals. The results of the

measurements are shown in Figures 20 and 21.

Control tissues (no HS) of FLW-1 larvae, like WT tissues, showed a very peripheral localization of the *sd* locus: ~88% of epidermis nuclei and ~93% of malpighian tubules nuclei displayed the *sd* signal within 1 μ m from the lamina (Figure 20, left hand diagrams). After stable activation of the transgene (embryonic HS), the *sd* locus became less tightly associated with the nuclear lamina and occupied more frequently interior positions (Figure 20, left hand diagrams). This positional shift was most pronounced in malpighian tubules. (For completeness, here and in the following diagrams always the corrected distances are displayed in addition on the right hand side. However, correcting the distances did not contribute to a clearer interpretation and therefore these data are not further discussed). Also after transient activation (Figure 20, bottom, left) a shift towards more interior positioning was observed in nuclei of malpighian tubules, compared to the inactive state.

Distance measurements between the *sd* locus and heterochromatin were performed in the same nuclei as the measurements regarding the nuclear lamina. Nuclei from control tissues of FLW-1 flies did not display any particular association of the *sd* locus with heterochromatin (Figure 21, left hand diagrams). After stable or transient activation of the transgene the data indicated a shift of *sd* towards heterochromatin (Figure 21). This trend was observed in both tissues in real distances as well as after distance corrections. Unfortunately, in these experiments the lamina staining was not very good and thus distance corrections were possible only in a subset of nuclei. However, during image collection and subsequent distance measurements I noticed that after activation of the transgene *sd* was often located at the boundary of the heterochromatic domain. Thus, the percentages of such associations between the *sd* locus and heterochromatin were counted in a larger fraction of nuclei (irrespective of their lamina staining).

The results of the association analyses are shown in Table 2. In FLW-1 flies, after stable activation of the transgene 40% (epidermis) to 48% (malpighian tubules) of nuclei displayed *sd* associated with the boundary of the dimH3K9 positive domain or within 2 pixels from it (Figure 22, Table 2). In contrast, in control FLW-1 larvae only ~10 % of *sd* loci were associated with heterochromatin in both tissues. After transient activation *sd* was less frequently associated with heterochromatin than after stable activation and the degrees of association differed between tissues: while in epidermis ~27% of nuclei displayed *sd* associated with the boundary of the dimH3K9-positive domain, only ~13% of nuclei from malpighian tubules did so. It is noteworthy that the *sd* signal was never observed within heterochromatin, but always at its boundary in case of association.

Taken together, these data suggest that while the inactive 5F24 transgene in FLW-1 larvae was frequently associated with the nuclear lamina, this association was less tight after activation of the transgene. Instead the active transgene frequently

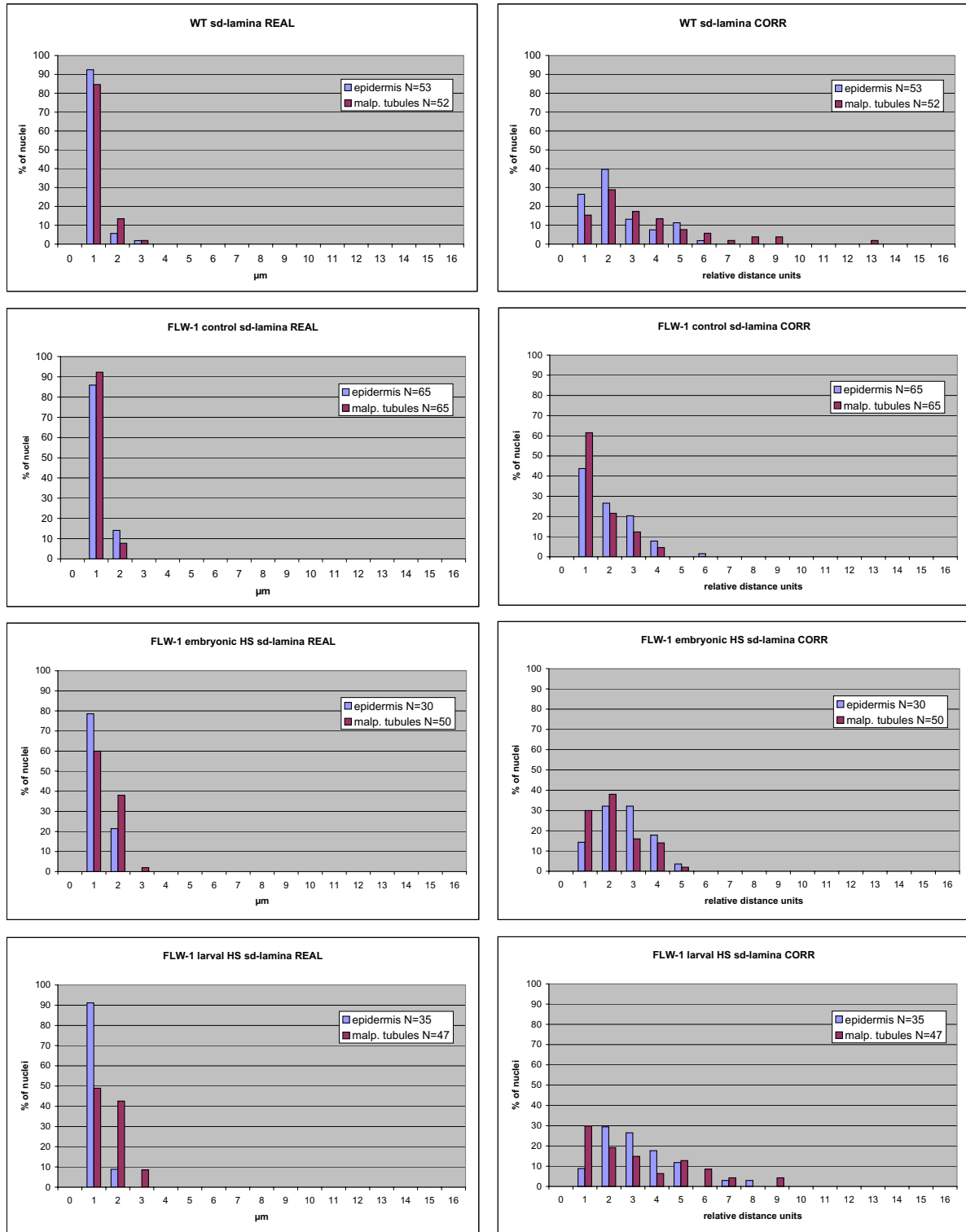


Figure 20. Results of distance measurements between *sd* and the nuclear lamina in FLW-1 tissues. *Sd* was detected by FISH using a specific DNA probe and the nuclear lamina was immunostained with specific antibodies against *Drosophila* lamin. The X axis indicates distance intervals, while bars show corresponding percentages (%; Y-axis) of nuclei displaying a given distance interval between *sd* and the lamina. The diagrams display results from WT larvae (top) and FLW-1 larvae at inactive (control, no heat-shock, second row), stably active (embryonic HS, third row) and transiently active (larval HS, bottom) states of the transgene. Diagrams on the left hand side display the distances in microns (REAL), while diagrams on the right hand side display distances after correction for the nuclear size (CORR). N indicates the numbers of analysed nuclei in epidermis (blue) and malpighian tubules (red).

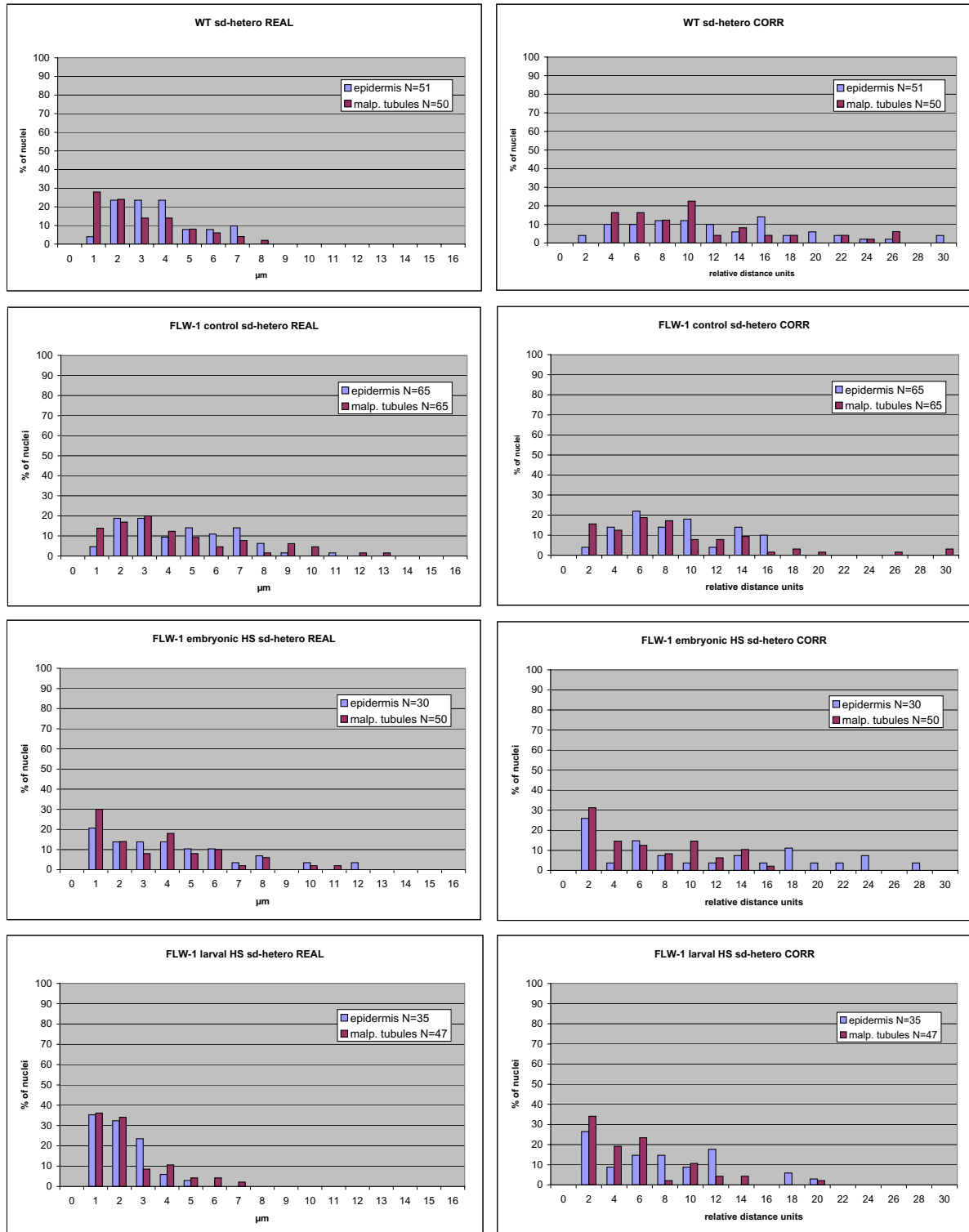


Figure 21. Results of distance measurements between *sd* and heterochromatin in FLW-1 tissues. *Sd* was detected by FISH using a specific DNA probe and heterochromatin was immunostained with specific antibodies against dimH3K9. The X axis indicates distance intervals, while bars show corresponding percentages (%; Y-axis) of nuclei displaying a given distance interval between *sd* and heterochromatin. The diagrams display results from WT larvae (top) and FLW-1 larvae at inactive (control, no heat-shock, second row), stably active (embryonic HS, third row) and transiently active (larval HS, bottom) states of the transgene. Diagrams on the left hand side display the distances in microns (REAL), while diagrams on the right hand side display distances after correction for the nuclear size (CORR). N indicates the numbers of analysed nuclei in epidermis (blue) and malpighian tubules (red).

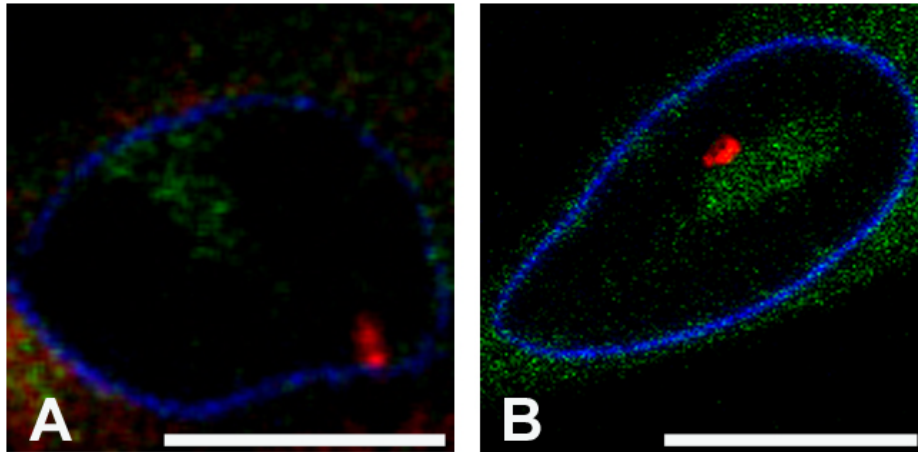


Figure 22. Nuclear localization of the *sd* locus in FLW-1 larval nuclei at inactive and stably active states of the transgene. Single light optical sections of nuclei from malpighian tubules are shown. The *sd* locus was detected using a specific DNA probe and is shown in red. Heterochromatin was immunostained with antibodies against dimH3K9 and is shown in green while the nuclear lamina was visualized with antibodies against *Drosophila* lamin and is shown in blue. (A) A nucleus from a control animal where the *sd* locus was frequently associated with the nuclear lamina and not with heterochromatin. (B) A nucleus from an animal after embryonic heat-shock. *Sd* frequently lost its association with the nuclear lamina and localized at the border of heterochromatin. Scale bar: 10 μ m.

associated with the boundary of the heterochromatic domain, and the highest degree of association was observed after stable activation.

In order to confirm the effects observed with FLW-1 flies with a second transgenic line I selected fLW-1 flies. In this transgenic line the transgenic construct was inserted into the same chromosomal locus as in FLW-1 flies, namely the *sd* locus. fLW-1 flies harbour the 5F3 construct.

3.1.2.2.2. Nuclear positioning of the 5F3 construct in fLW-1 larvae

Distance measurements between the 5F3 transgene integration site (visualized with the *sd* probe) and the nuclear lamina were performed in nuclei from female larval anterior epidermis and malpighian tubules, taken from several animals (Figure 23). Control fLW-1 as well as WT tissues displayed a very peripheral positioning of the *sd* locus (Figure 23, left hand diagrams). As in FLW-1 larvae, an embryonic as well as a larval HS led to a more interior positioning of the *sd* locus. After an embryonic HS the integration site was less tightly associated with the lamina in nuclei of the epidermis. After a larval HS the effect was most pronounced in malpighian tubules. Thus, in fLW-1 as well as in FLW-1 larvae transient and stable activation led to a more interior positioning of the transgene and in both transgenic lines the extent of the effect showed some tissue-specific differences.

Distance measurements between the *sd* locus and heterochromatin were

Tissue	nuclei	association	% of assoc.
WT epi	30	4	13.3
WT malp	64	10	15.6
FLW-1 control epi	62	6	9.7
FLW-1 control malp	61	6	9.8
FLW-1 HSE epi	50	20	40
FLW-1 HSE malp	50	24	48
FLW-1 HSL epi	34	9	26.5
FLW-1 HSL malp	47	6	12.8
fLW-1 control epi	45	1	2.2
fLW-1 control malp	51	7	13.7
fLW-1 HSE epi	49	4	8.2
fLW-1 HSE malp	45	5	11.1
fLW-1 HSL epi	48	2	4.2
fLW-1 HSL malp	46	10	21.7
FLFW-1 control epi	29	3	10.3
FLFW-1 control malp	32	0	0
FLFW-1 HSE epi	42	4	9.5
FLFW-1 HSE malp	37	2	5.4
FLFW-1 HSL epi	48	5	10.4
FLFW-1 HSL malp	39	6	15.4

Table 2. Analysis of the association of Fab-7-containing transgenes with the boundary of heterochromatin. The table shows the percentages of associations of Fab-7-containing transgenic constructs with dimH3K9 positive domains. The measurements were made at inactive (control) and stably (embryonic heat-shock, HSE) and transiently (larval heat-shock, HSL) active states of the transgenes in epidermis (epi) and malpighian tubules (malp) of different fly lines. In WT tissues the association between the *sd* locus and heterochromatin was analysed. In FLW-1 and fLW-1 the *sd* locus was detected to indicate the position of the transgene. In FLFW-1 the transgenic construct itself was visualized. Tissues, numbers of analysed nuclei, frequencies of associations with heterochromatin and the percentages of such nuclei are indicated for each line and tissue (from left to right). A transgene was regarded as associated when 0 - 2 pixels distance between the borders of the heterochromatic domain and the FISH signal were observed. The pixel size was 0.1 x 0.1 μm .

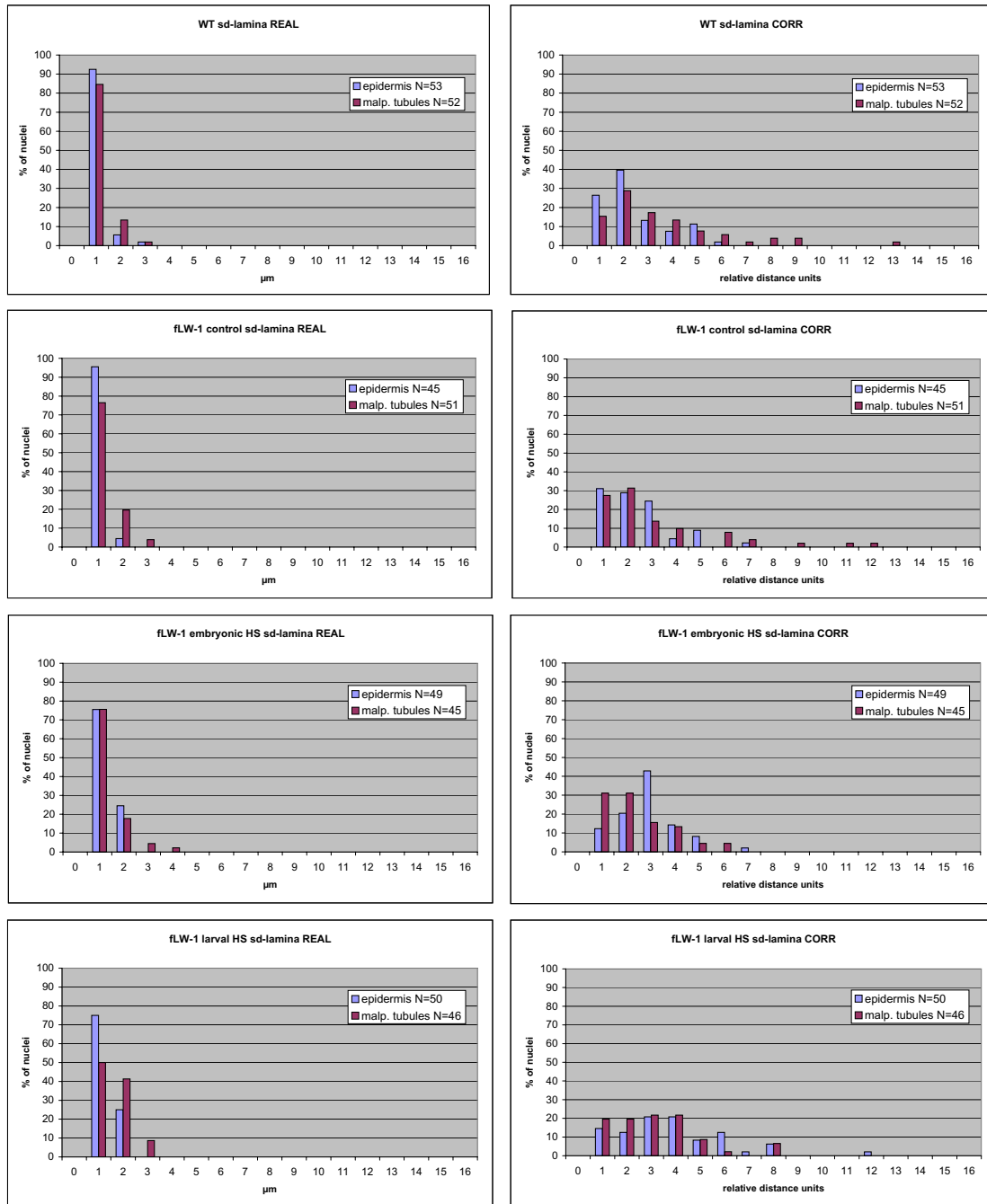


Figure 23. Results of distance measurements between *sd* and the nuclear lamina in fLW-1 tissues. *Sd* was detected by FISH with a specific DNA probe, while the nuclear lamina was immunostained with specific antibodies against *Drosophila* lamin. The X axis indicates distance intervals, while bars show corresponding percentages (%; Y-axis) of nuclei displaying a given distance interval between *sd* and the lamina. The diagrams display results from WT larvae (top) and fLW-1 larvae at inactive (control, second row), stably active (embryonic HS, third row) and transiently active (larval HS; bottom) states of the transgene. Diagrams on the left hand side display the distances in microns (REAL), while diagrams on the right hand side display distances after correction for the nuclear size (CORR). N indicates the numbers of analysed nuclei in epidermis (blue) and malpighian tubules (red).

performed in the same nuclei as the measurements regarding the nuclear lamina. These distance measurements did not indicate a clear shift towards heterochromatin after larval or embryonic HS (Figure 24). Direct inspection of the image data

revealed a slight increase in the frequency of association between the *sd* locus and heterochromatin after an embryonic HS in epidermis nuclei (Table 2, 2,2% in control nuclei vs. 8,2% after embryonic HS). Also, a slight increase in the frequency of association with heterochromatin was observed in malpighian tubules after a larval HS

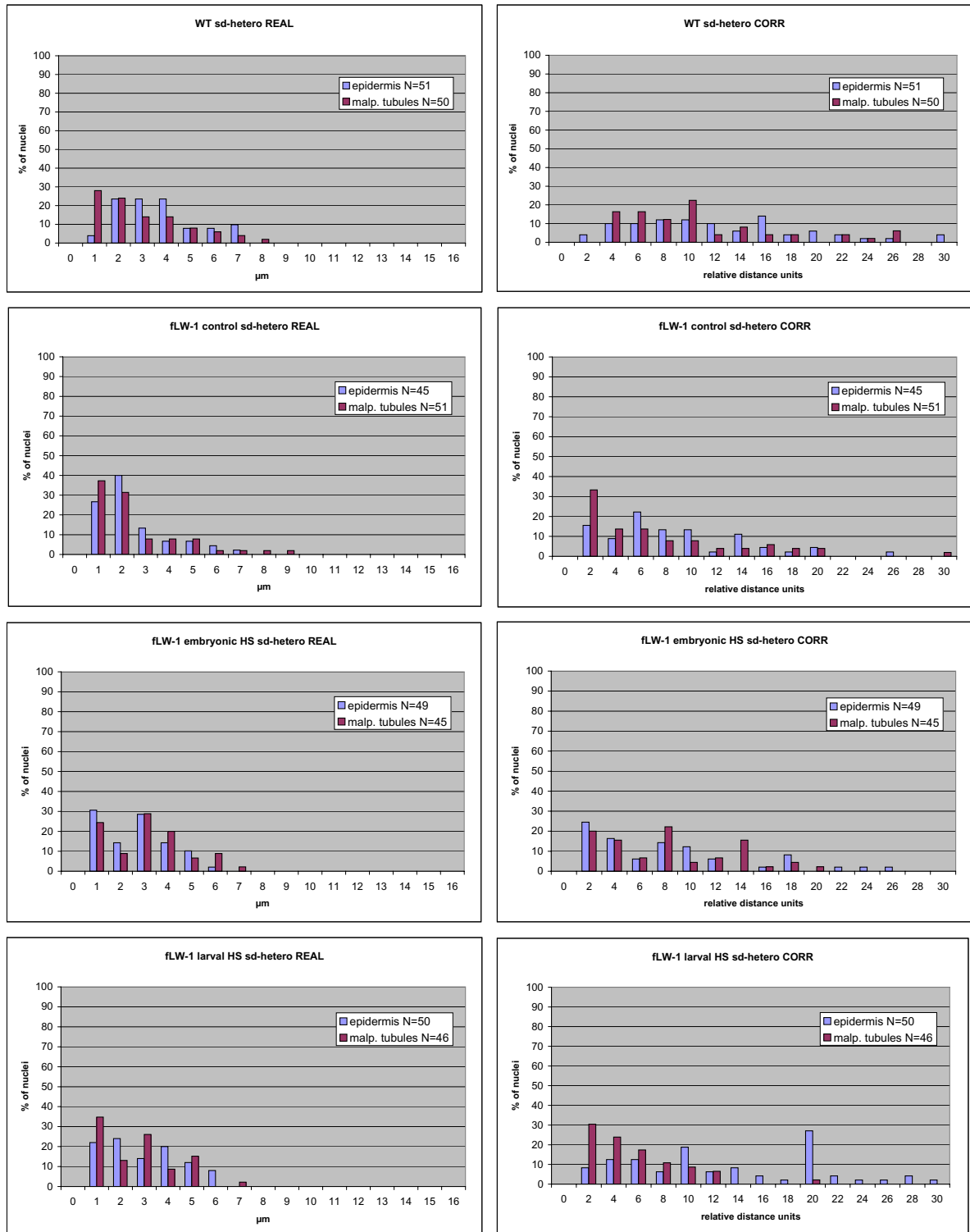


Figure 24. Results of distance measurements between *sd* and heterochromatin in fLW-1 tissues. The *sd* locus was detected by FISH with a specific DNA probe, while heterochromatin was immunostained with specific antibodies against dimH3K9. The X axis indicates distance intervals, while bars show corresponding percentages (% , Y-axis) of nuclei displaying a given

distance interval between *sd* and heterochromatin. The diagrams display results from WT larvae (top) and fLW-1 larvae at inactive (control, second row), stably active (embryonic HS, third row) and transiently active (larval HS; bottom) states of the transgene. Diagrams on the left hand side display the distances in microns (REAL), while diagrams on the right hand side display distances after correction for the nuclear size (CORR). N indicates the numbers of analysed nuclei in epidermis (blue) and malpighian tubules (red).

(13,7% in control nuclei vs. 21,7% after larval HS). In these two cases, where a higher frequency of association with heterochromatin was observed, a marked decrease in short distances to the nuclear lamina was found (Figure 23, left hand diagrams). Thus, also here, as in FLW-1 larvae, a more interior positioning of the transiently or stably activated transgene corresponded to a higher frequency of association with the boundary of heterochromatin. However, this effect was much more pronounced in the FLW-1 transgenic line.

In order to further address the reproducibility of the effects observed a third transgenic line was investigated, where the transgenic construct was integrated into a different chromosome.

3.1.2.2.3. Nuclear localization of the 24F6 construct in FLW-1 larvae

In the FLW-1 line the 24F6 transgene (Figure 2) was located on chromosome 3. Thus, the dosage compensation effect cannot directly affect its activity or positioning. However, for consistency only female larval tissues were used. Distance measurements between the 24F6 transgene and the nuclear lamina were performed in nuclei from anterior epidermis and malpighian tubules, taken from several animals (Figure 25). Real distances showed a peripheral localization of the transgene at all states of activity in both tissues (Figure 25, left hand diagrams). An even more pronounced peripheral localization of the transgene was observed in malpighian tubules after stable and transient activation, respectively.

Distance measurements (Figure 26) and visual inspection of the image data (Table 2) revealed that the positional shift of the transgene in malpighian tubules led to an increased association with the boundary of heterochromatin. In epidermis about 10% of nuclei displayed the transgene at the boundary of the heterochromatic domain at any state of activity (Table 2). However, in malpighian tubules the percentage of association changed from 0% in the inactive to 5% in the stably active to 15,4% in the transiently active state.

Thus, in all three transgenic lines stable or transient activation of the transgene increased the frequency of its association with the boundary of heterochromatin. It is important to note that the transgenic construct never became engulfed in heterochromatin but always associated with its boundary as shown in Figure 22.

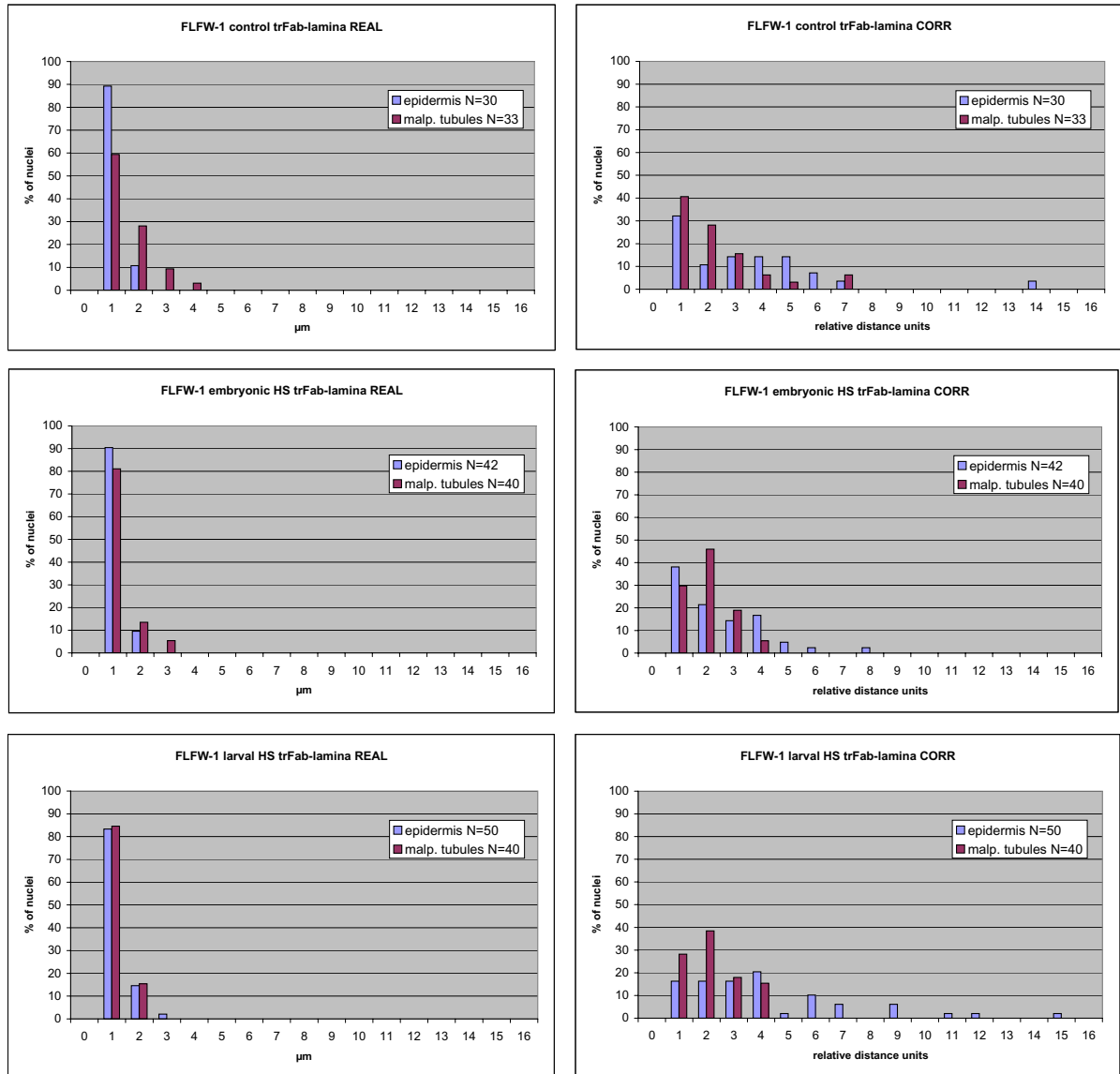


Figure 25. Results of distance measurements between the 24F6 transgene and the nuclear lamina in FLOW-1 tissues. The transgene (trFab) was visualized with a DNA probe for Fab-7, and the lamina was immunostained using specific antibodies against *Drosophila* lamin. The X axis indicates distance intervals, while bars show corresponding percentages (% , Y-axis) of nuclei displaying a given distance interval between the transgene and the lamina. The diagrams display results from FLOW-1 larvae at inactive (control, top), stably active (embryonic HS, middle) and transiently active (larval HS, bottom) states of the transgenic construct. Diagrams on the left hand side display the distances in microns (REAL), while diagrams on the right hand side display distances after correction for the nuclear size (CORR). N indicates the numbers of analysed nuclei in epidermis (blue) and malpighian tubules (red).

The extent of this effect was dependent on the transgenic line and in each line on the particular tissue. It is also important to note that stable and transient activation led to positional shifts relative to the lamina, but not necessarily to a more interior positioning.

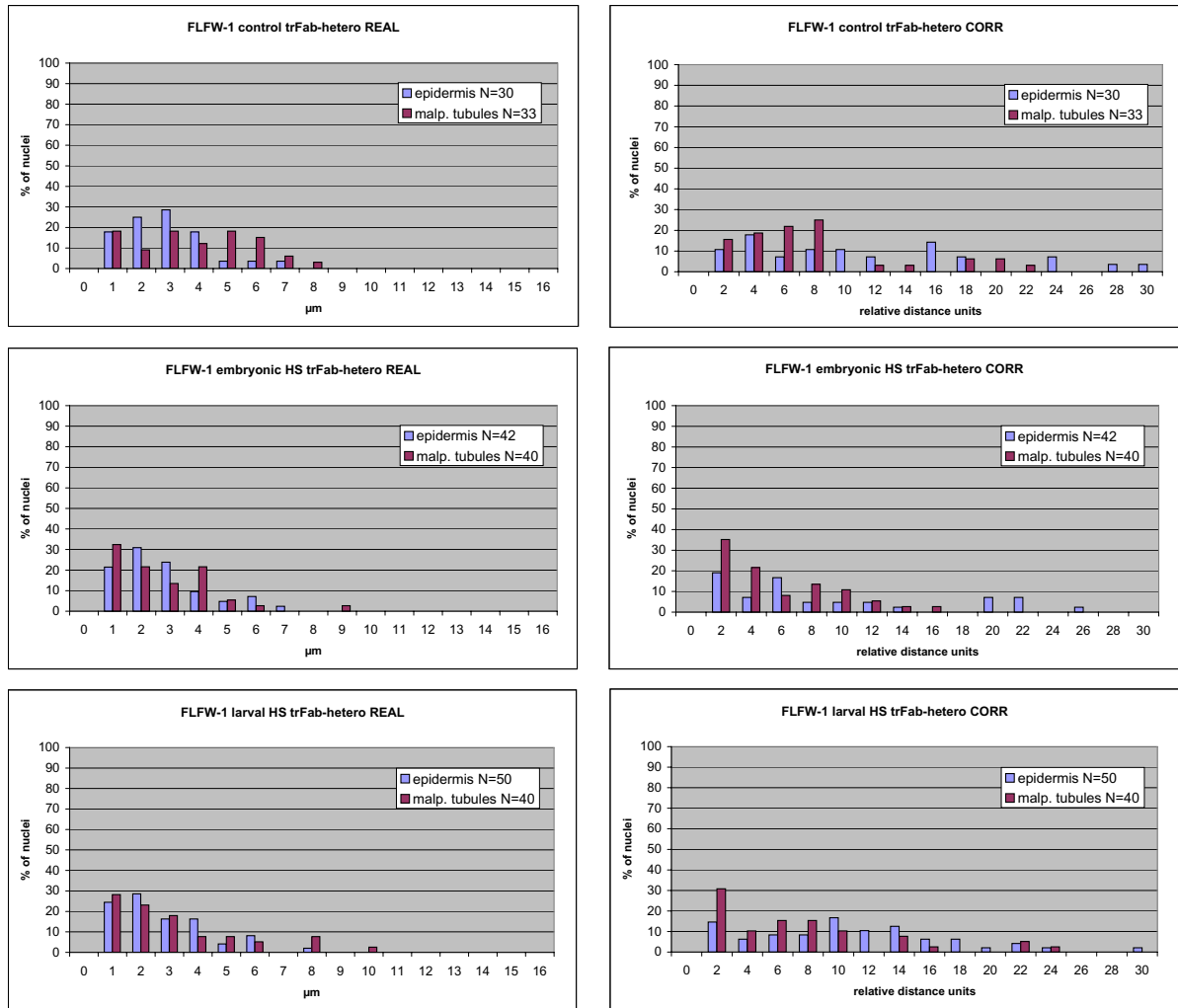


Figure 26. Results of distance measurements between the 24F6 transgene and heterochromatin in FLFW-1 tissues. The transgene (trFab) was visualized with a DNA probe for Fab-7, while heterochromatin was immunostained using specific antibodies against dimH3K9. The X axis indicates distance intervals, while bars show corresponding percentages (% of nuclei, Y-axis) of nuclei displaying a given distance interval between the transgene and heterochromatin. The diagrams display results from FLFW-1 larvae at inactive (control, top), stably active (embryonic HS, middle) and transiently active (larval HS, bottom) states of the transgenic construct. Diagrams on the left hand side display the distances in microns (REAL), while diagrams on the right hand side display distances after correction for the nuclear size (CORR). N indicates the numbers of analysed nuclei in epidermis (blue) and malpighian tubules (red).

3.1.2.3. Nuclear positioning of other PREs in their active and inactive states

In addition to Fab-7, I have tried to study the nuclear positioning of other PREs. Probes for PREs located in the regulatory regions of *Distalless* (*Dll*), *engrailed* (*en*), *homothorax* (*hth*) and *vestigial* (*vg*) were kindly provided by Dr. Leonie Ringrose (ZMBH, Heidelberg). Each DNA probe had a size of ~3 kb and was thus of similar size as the Fab-7 probe (Figure 5). These PREs were selected because it was known in which parts of imaginal discs they are active or inactive, and these areas were easily discernible during microscopy (Figure 27). It was planned to study the nuclear

positioning of these endogenous PREs in imaginal discs of WT larvae. Unfortunately, two sorts of problems made this study not possible. Firstly, DNA probes produced

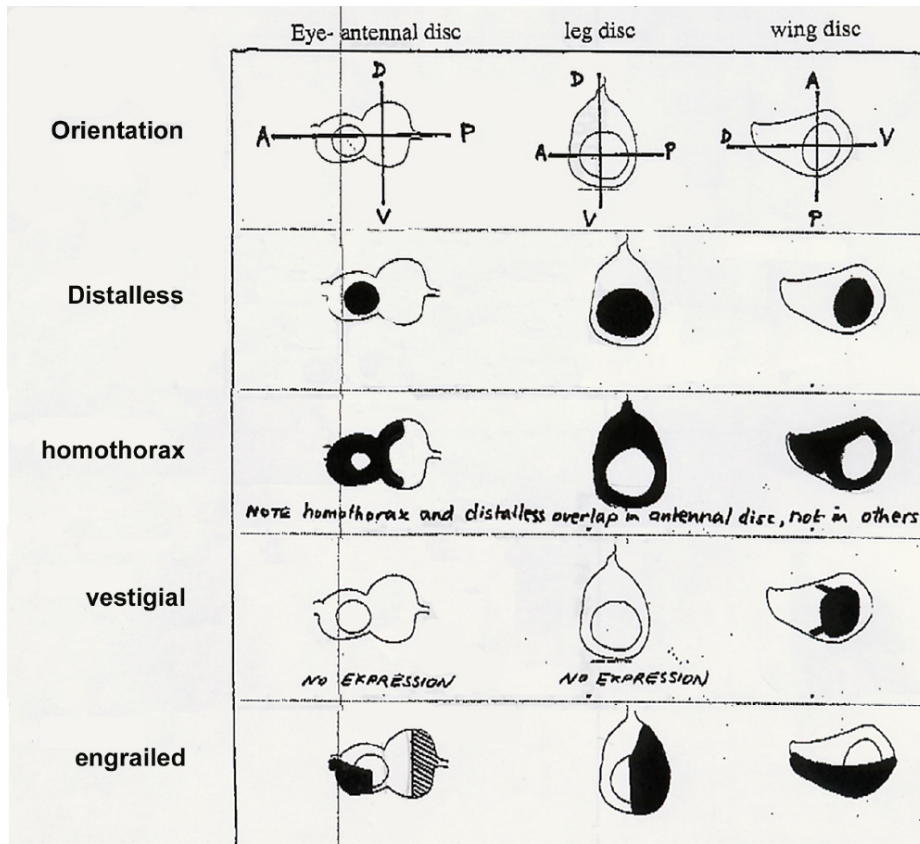


Figure 27. Expression patterns of *Distalless*, *homothorax*, *vestigial* and *engrailed* in eye-antennal, leg and wing imaginal discs from 3rd instar larvae (from: *Imaginal discs*, by Lewis I. Held, Jr. Cambridge University Press). The regions where one of the listed genes is expressed in imaginal discs of the type indicated are shown in black. A-P and D-V show the anterior-posterior and dorso-ventral axes, respectively.

very weak FISH signals, which were at best visible as tiny bands on polytene chromosomes of salivary gland nuclei (data not shown). Consequently, FISH signals in the small nuclei of imaginal discs were difficult to recognize. Secondly, the high level of autofluorescence in imaginal discs, and especially wing discs, made it impossible to reliably identify these FISH signals. Thus, although experiments were repeated several times and it was tried to improve the results in different ways reliable results could not be obtained.

3.1.3. Do homologous PREs interact physically?

Next, a series of experiments was performed to address the question whether the nuclear positioning of Fab-7-containing transgenic constructs might be affected by pairing with the endogenous Fab-7 locus. Recent results suggested such interactions

(Bantignies et al., 2003). A first series of experiments was performed with the transgenic lines FLW-1 and FLFW-1. In both cases chromosomal loci with endogenous and transgenic copies of Fab-7 could be distinguished with the FISH probes available. In addition, the transgenic line 5F24 25,2 was chosen because this line (under the name Fab-X) was used in another study, which suggested pairing of endogenous and transgenic copies of Fab-7 (Bantignies et al., 2003). The transgenic line 5F24 25,2 is essentially the same as FLW-1, but lacks the GAL4-driver on the balancer chromosome (2.1.10.2.2.).

3.1.3.1. Relative positioning of transgenic and endogenous Fab-7 elements in FLW-1 larvae

All analyses were performed at the inactive state of the transgene (no HS). In order to visualize the integration site of the transgenic copy of the Fab-7 element the *sd* locus was used as a probe. The chromosomal site of the endogenous Fab-7 element was detected by using the *Abd-B* locus as a probe in immunoFISH experiments. The nuclear lamina was detected by using antibodies against *Drosophila* lamin. Nuclei were imaged using a Leica SP2 confocal microscope. The reconstruction of 3D data sets and the image analyses were performed with ImageJ software.

In the first set of experiments distance measurements between *Abd-B* and *sd* were performed in nuclei from anterior epidermis and malpighian tubules of female FLW-1 3rd instar larvae (Figure 28). Colocalization or direct association (which means that FISH signals would visibly touch each other) of the different FISH signals was

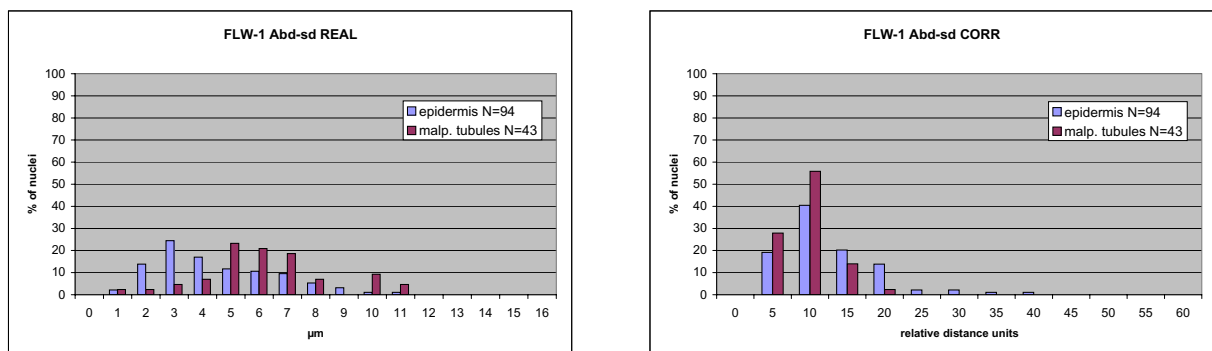


Figure 28. Results of distance measurements between *Abd-B* and *sd* in FLW-1 larvae. *Abd-B* and *sd* were detected by FISH using specific DNA probes, while the nuclear lamina was immunostained with antibodies against *Drosophila* lamin. The X axis indicates distance intervals, while bars show corresponding percentages (%; Y-axis) of nuclei displaying a given distance interval between the intensity centers of *Abd-B* and *sd* FISH signals. Distances were measured at the inactive state of the transgenic construct. The left hand diagram displays distances in microns for epidermis and malpighian tubules (REAL), the right hand diagram shows corrected distances (CORR). Please note that the scaling on the X axis of the right hand diagram (the corrected distances) is different from the scaling of the left hand diagram. N indicates the numbers of analysed nuclei in epidermis (blue) and malpighian tubules (red).

never observed. The minimal distance between the intensity centers of the *Abd-B* and *sd* FISH signals in epidermis was 0,7 μm (found in 1 nucleus) and in malpighian tubules 1.0 μm (found in 1 nucleus). In epidermis ~60% of nuclei displayed *Abd-B* and *sd* 2-4 μm apart from each other. In almost all other nuclei the distances were even larger (Figure 28, the left hand diagram). In malpighian tubules, in less than 15% of nuclei *Abd-B* and *sd* were closer than 4 μm and in the majority of nuclei (~60%) the loci were 5-7 μm apart from each other. Corrected distances showed the same distribution in both epidermis and malpighian tubules (Figure 28, the right hand diagram). This was due to the fact that the nuclei from epidermis have a rather flat shape, in contrast to the almost spherical nuclei from malpighian tubules, and generally have a smaller volume. Thus, the results of the distance corrections suggest that in epidermis generally smaller distances were measured due to the small size of nuclei. Typical examples of *Abd-B* and *sd* in nuclei from epidermis and malpighian tubules are shown in Figure 29 A and B. Nuclei from epidermis are also shown in Figure 31 A.

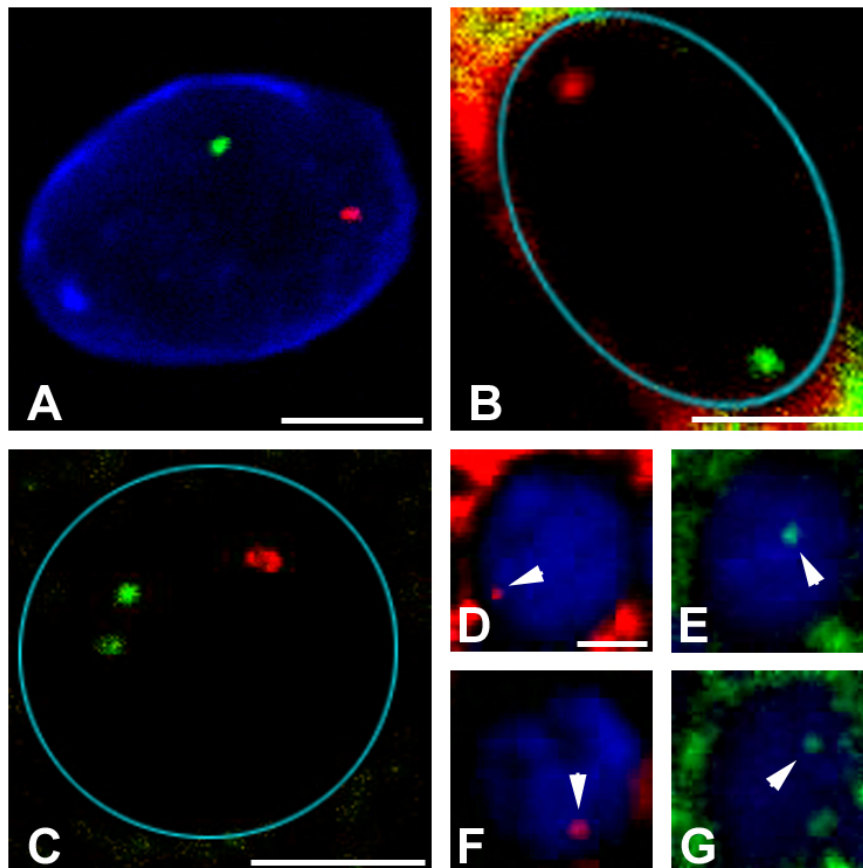


Figure 29. Positioning of *Abd-B* and *sd* in nuclei from FLW-1 female larvae. Single light optical sections of nuclei from epidermis (A), malpighian tubules (B), fat body (C) and brain (D-G) are shown. *Abd-B* (green) and *sd* (red) were visualized by FISH with specific DNA probes. Arrowheads in D-G point at corresponding FISH signals. In nuclei from brain (D-G) the FISH signals were present in different optical planes and therefore they are shown separately for each nucleus (D, E and F, G). The nuclear lamina (blue in (A)) was immunostained with antibodies against *Drosophila* lamin. In (B, C) the lamina immunostaining was not performed, and the nuclear rim is indicated in light blue. In (D-G) DNA was visualized with DAPI and is shown in blue. Scale bars: in (A-C) 5 μm , in (D-G) 2 μm .

To further investigate possible interactions between endogenous and transgenic copies of Fab-7 in these transgenic flies, more tissues were included into the analyses, which were brain, fat body and anterior midgut. 40-45 nuclei from each tissue were imaged using a Leica confocal microscope and the positioning of the loci was visually inspected. In nuclei that displayed a proximal positioning of *Abd-B* and *sd* the distance was measured with ImageJ software and the nucleus with the shortest distance between the two loci was identified in this way. Table 3 summarizes these shortest distances. No colocalization, overlap or association of the two different FISH signals within one nucleus was observed. Typical examples of fat body cell and brain nuclei are shown in Figure 29°C and D-G, respectively. The closest distance between *Abd-B* and *sd* in these tissues was observed in a nucleus from the brain and amounted to 1.1 μm (Table 3).

FLW-1			
tissue	nuclei	pairing, %	closest distance, μm
brain	40	0	1.1
epidermis	93	0	0.7
fat body	40	0	1.6
anterior midgut	45	0	2.7
malp. tubules	45	0	1.0
5F24 25,2 18°C			
tissue	nuclei	pairing, %	closest distance, μm
epidermis	49	0	1.7
fat body	51	0	4.7
anterior midgut	42	0	3.7
malp. tubules	56	0	2.8
5F24 25,2 29°C			
tissue	nuclei	pairing, %	closest distance, μm
epidermis	90	0	3.8
fat body	40	0	2.5
anterior midgut	56	0	2.6
malp. tubules	67	0	4.2
FLFW-1			
tissue	nuclei	pairing, %	closest distance, μm
epidermis	120	0	0.6
malp. tubules	108	0	0.6

Table 3. Relative positioning of endogenous and transgenic copies of the Fab-7 element in tissues of different transgenic fly lines. The table shows the data obtained with FLW-1, 5F24 25,2 and FLFW-1 transgenic 3rd instar larvae. In FLW-1 and 5F24 25,2 tissues *Abd-B* and *sd* were detected to visualize loci adjacent to endogenous and transgenic copies of Fab-7, respectively. In FLFW-1, the detection of the endogenous Fab-7 element was ensured with

the *Abd-B* probe, and the transgenic construct was visualized using the Fab-7 probe. Nuclei were scanned using confocal microscopy and the closest distances between the loci were measured. FLW-1 and FLFW-1 flies were raised and kept under standard conditions (18°C), while for 5F24 25,2 flies possible temperature effects were addressed and the flies were raised and kept at 18°C and 29°C, respectively. For each fly line analysed tissues, numbers of analysed nuclei in each tissue, percentages of pairing and the closest distances between endogenous and transgenic copies of Fab-7 observed for each tissue are indicated. Pairing was defined as colocalization, overlap, or direct contact between the different FISH signals in one nucleus.

Taken together, the data show that in the analysed tissues of FLW-1 larvae the *Abd-B* and *sd* loci were never found closer than 0.7 µm apart from each other (found once in epidermis). Therefore, the findings suggest that endogenous and transgenic copies of the Fab-7 element did not physically interact in these tissues.

3.1.3.2. Endogenous and transgenic copies of Fab-7 in 5F24 25,2 larvae: do temperature and the chromosomal background influence presumable interactions?

This line, 5F24 25,2, is also known as Fab-X from the work of Bantignies et al. (2003), but in this study I will use its original name 5F24 25,2 (Zink and Paro, 1995). This line differs from FLW-1 (see above) only by the absence of the GAL4 driver on a corresponding balancer chromosome. In fact, FLW-1 has been derived from 5F24 25,2 by crossing in the GAL4 driver and thus both lines carry an identical Fab-7-containing construct integrated into 13F. Bantignies et al. (2003) found that in one of the tissues of female 3rd instar larvae, the wing imaginal disc (other larval tissues were not investigated by Bantignies et al.), *Abd-B* and *sd* were paired in 43% of nuclei. To exclude the possibility that in control tissues of FLW-1 flies as investigated before the GAL4 driver leaked and thus influenced the position of the *sd* locus and the interaction of the two Fab-7 elements, I analysed a number of tissues from female 5F24 25,2 larvae with regard to the relative positioning of *Abd-B* and *sd* loci. The analysis of wing imaginal discs was difficult due to the strong autofluorescence and background staining and the extremely small size of nuclei (about 4 µm in diameter). Although experiments were repeated several times and it was tried in different ways to improve results reliable detection of FISH signals was very difficult. Figure 30 shows one of the best results obtained. Here, clear FISH signals were obtained with the *Abd-B* probe (Figure 30 C). The *sd* locus, which was detected with the brightest fluorochrome, Cy3, could not be reliably detected. Although nuclei look „clean“ in the example shown, often bright red nuclear spots, which were due to autofluorescence and background staining, made a reliable detection of Cy3-FISH signals impossible. Detection with other fluorochromes than Cy3 is less sensitive and did also not lead to reliable results

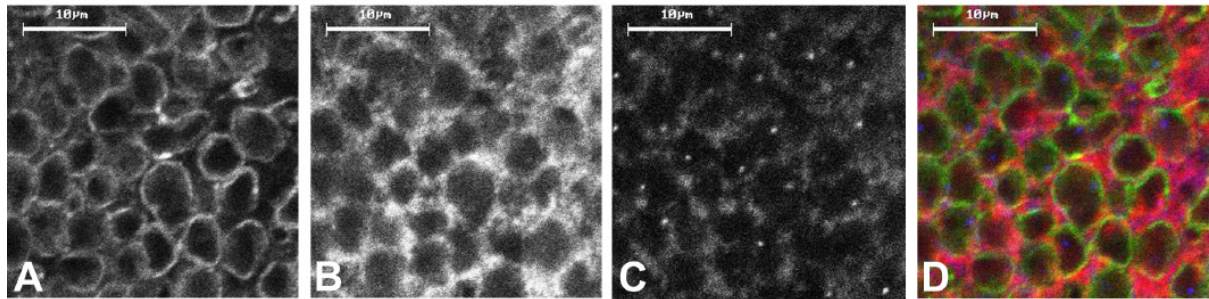


Figure 30. ImmunofISH with a wing imaginal disc of a 5F24 25,2 female larva. Single light optical sections are shown. The nuclear lamina was immunostained with antibodies against *Drosophila* lamin (A). *Sd* (B) and *Abd-B* (C) loci were visualized by FISH using specific dig- or bio-dUTP labelled DNA probes, followed by detection with Cy3 conjugated anti-dig antibodies (*sd*) or Cy5-coupled avidin (*Abd-B*). (D) RGB merge. The nuclear lamina is shown in green, signals from Cy3 in red, and signals from *Abd-B* in blue. Scale bar: 10 µm. A certain level of autofluorescence and background staining was observed in all channels, but this was particularly strong in the Cy3 channel. This made it difficult to distinguish between bright spots that were caused by the autofluorescence and potential FISH signals from the *sd* probe. Nevertheless, note that no Cy3-spots, which could be potential *sd* FISH-signals, colocalize with *Abd-B*.

in case of *sd*. Although reliable detection of FISH signals per se was difficult in case of *sd*, *Abd-B* signals were examined for colocalization or association with potential *sd* signals in cases of low red background fluorescence in nuclei, as in the example shown in Figure 30. However, also in this way no potential colocalizing signals could be detected. Due to these difficulties, distance measurements and pairing analyses could not be performed with this tissue. Therefore four other tissues were chosen, which were also analysed in FLW-1 flies: anterior epidermis, malpighian tubules, fat body and anterior midgut.

The first part of this analysis was performed with tissues from larvae which were raised and kept under standard conditions (18°C). About 50 nuclei from each tissue were imaged and the relative positioning of the *Abd-B* and *sd* loci was evaluated visually and measured in cases of proximal positioning. In this way the closest distances between the loci were identified for each tissue and the results are shown in Table 3. The shortest distance between the loci was observed in a nucleus from epidermis and was equal to 1.7 µm (Table 3). No case of pairing was found, and typical examples of nuclei from epidermis are shown in Figure 31 C, D.

PcG-mediated silencing is temperature-dependent and thus it was addressed whether increased temperature influences potential physical interactions of Fab-7 elements. Also, in experiments of Bantignies et al. (2003) such interactions were found in wing imaginal discs of larvae which were raised and kept at 29°C (Bantignies et al., 2003; F. Bantignies, personal communication). Therefore, in our next series of experiments eggs were laid and larvae were raised and constantly kept at 29°C and the analyses were performed with epidermis, fat body, anterior midgut, and malpighian

tubules from female 3rd instar larvae. 90 nuclei from anterior epidermis and 40 to 67 nuclei from other tissues were imaged with a Leica SP2 confocal laser scanning microscope and analysed. Distances were measured with ImageJ software (Table 3). The closest proximity of *Abd-B* and *sd* loci was found in a fat body nucleus: 2.5 μm (Table 3). No pairing was observed in any case, and a typical example for the positioning of *Abd-B* and *sd* in epidermis nuclei is shown in Figure 31 E, F.

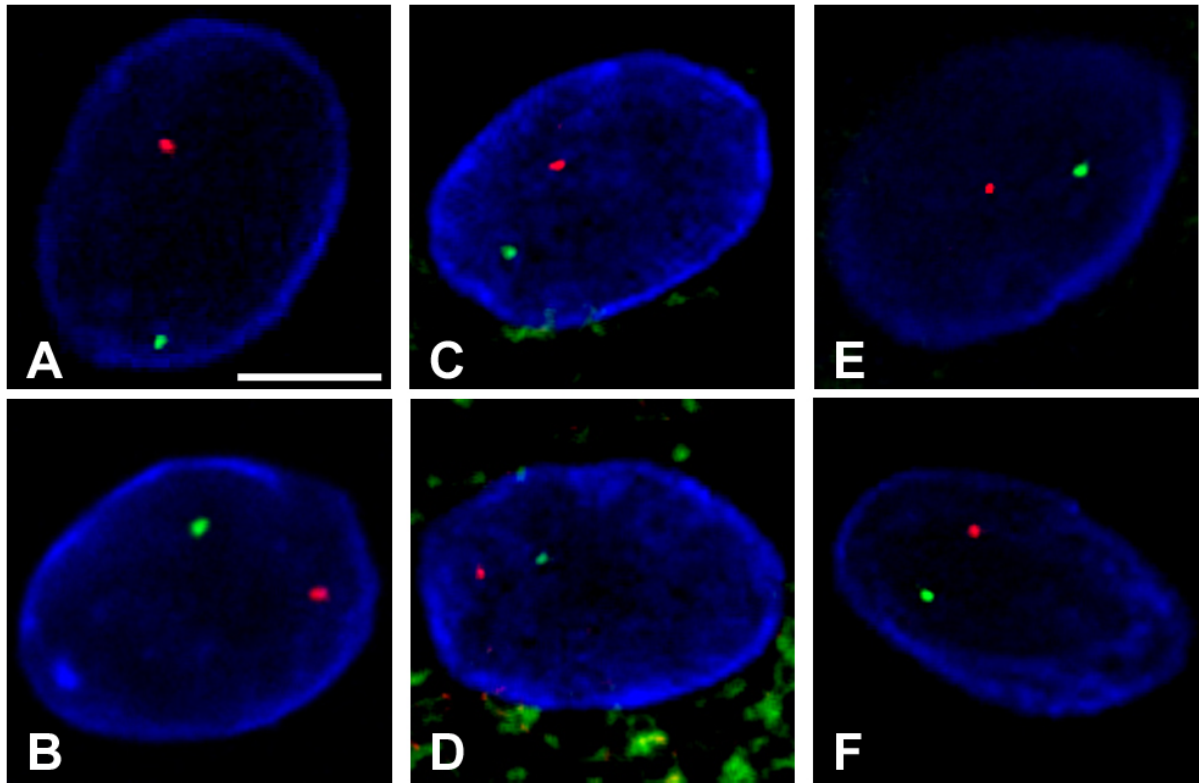


Figure 31. *Abd-B* and *sd* in epidermis nuclei from FLW-1 and 5F24 25,2 larvae. Single light optical sections from epidermis nuclei are shown. *Abd-B* (green) and *sd* (red) loci were visualized by FISH, while the nuclear lamina (blue) was visualized using antibodies against *Drosophila* lamin. (A, B) FLW-1 flies were raised and kept under standard conditions (18°C). (C-F) 5F24 25,2 (Fab-X) flies were raised and kept at 18°C (C, D) and 29°C (E, F).

Thus the data obtained with 5F24 25,2 larvae corresponded to the results obtained with tissues from FLW-1 larvae. No pairing or direct contact of *Abd-B* and *sd* loci was observed. This suggests that in the tissues analysed the endogenous and transgenic Fab-7 elements did not interact physically.

3.1.3.3. Is the chromosomal localization of the transgenic copy of Fab-7 important? Distance measurements between transgenic and endogenous Fab-7 elements in FLW-1 larvae

As a third transgenic line FLW-1 flies were analysed. In this line the 24F6 transgene (Figure 2) is located on the same chromosome as the endogenous Fab-7

element (2.1.10.2.2.). This transgenic construct contains two copies of Fab-7 and was easily detectable by FISH with the Fab-7 probe. The endogenous copy, however, did not always produce a strong signal. Nevertheless, this signal could be identified due to additional use of the *Abd-B* probe (Figure 19 C, D). Distance measurements between the endogenous (eFab) and transgenic (trFab) copies of Fab-7 were performed in nuclei from anterior epidermis and malpighian tubules.

Figure 32 displays the results of the analysis performed with FLW-1 control tissues (bottom, 18°C). For comparison the results from FLW-1 flies are also displayed again (as in Figure 28, top). Please note that the scaling of the X axis is different for

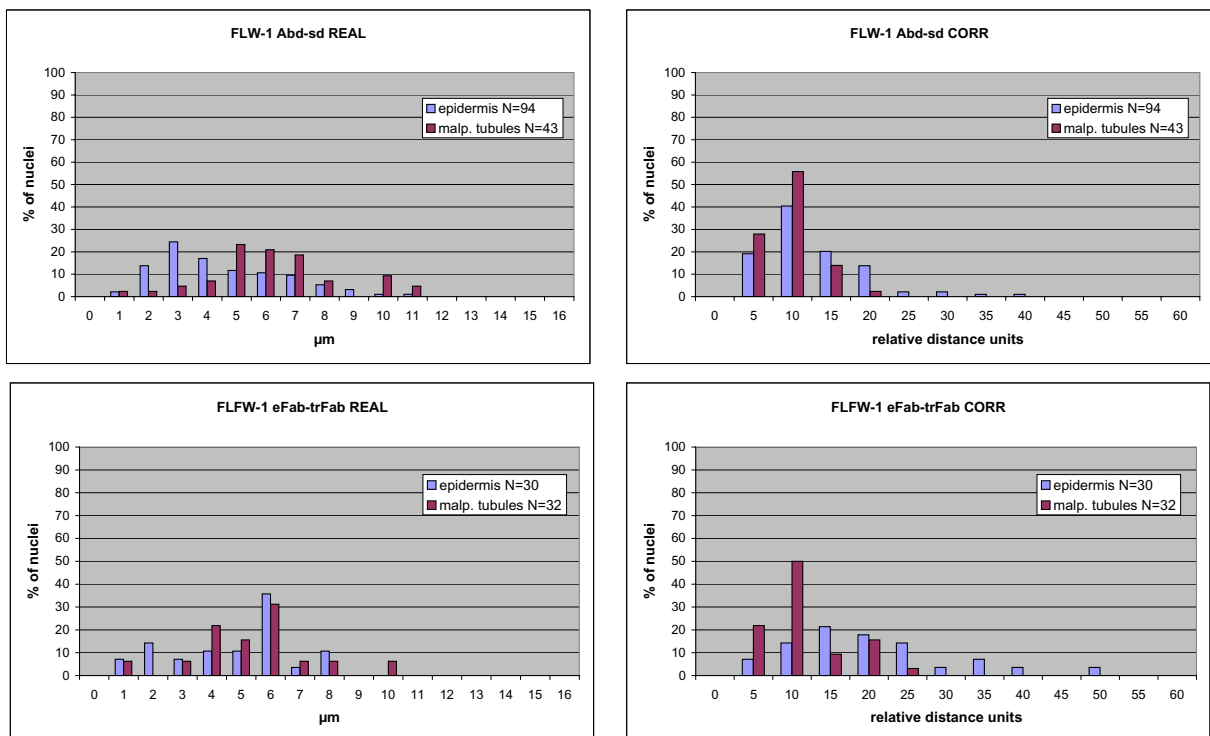


Figure 32. Results of distance measurements between endogenous and transgenic copies of Fab-7 in FLW-1 and FLOW-1 larvae. Distances were measured at the inactive state of the transgenes. The X axis indicates distance intervals, while bars show corresponding percentages (% , Y-axis) of nuclei displaying a given distance interval between FISH signals. The diagrams display the results in microns (REAL) and in relative distance units (CORR) for FLW-1 (top) and FLOW-1 (bottom) flies. N indicates the numbers of nuclei analysed in epidermis (blue) and malpighian tubules (red).

the real and corrected distances in both cases. In FLOW-1 tissues only 2 nuclei from epidermis and malpighian tubules, respectively, displayed the endogenous (eFab) and transgenic (trFab) elements within 1 μm from each other. The closest distances measured were 0.6 μm in both tissues (Table 3). In more than 30% of nuclei in each tissue the eFab and trFab were located $\sim 6 \mu\text{m}$ apart from each other (see major peaks in Figure 32, bottom left). Also here no cases of colocalization, overlap, or direct association between the two FISH signals were observed. Thus, no pairing between endogenous and transgenic copies of the Fab-7 element was observed in both tissues from FLOW-1 flies at the inactive state of the transgene.

The distances between the endogenous and transgenic copies of the Fab-7 element in epidermis and malpighian tubules were also measured at different states of activity of the transgene (Figure 33). Please note that the scaling of the X axis is different for the real and corrected distances. No pairing was registered at any state of activity of the transgene. Only 1-2 nuclei showed the eFab and trFab elements within 1 μm from each other at each state of activity of the trFab element, and the distance between them was always more than 0.5 μm .

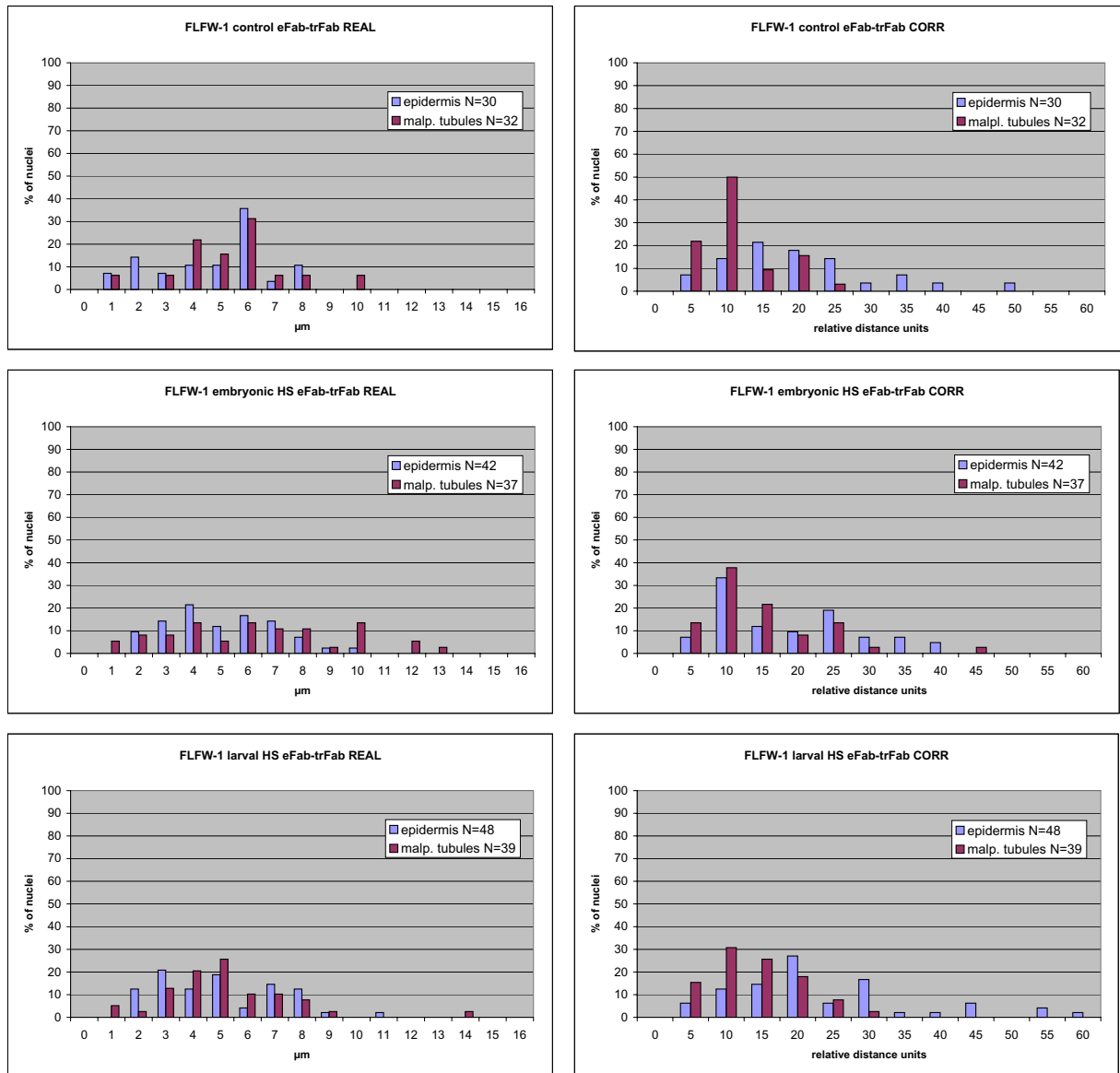


Figure 33. Results of distance measurements between endogenous and transgenic copies of Fab-7 in FLFW-1 larvae at different states of activity of the 24F6 transgene. The X axis indicates distance intervals, while bars show corresponding percentages (% , Y-axis) of nuclei displaying a given distance interval between FISH signals. The diagrams display results from FLFW-1 larvae at inactive (control, top), stably active (embryonic HS, middle) and transiently active (larval HS, bottom) states of the transgene. Diagrams on the left hand side display the distances in microns (REAL), while diagrams on the right hand side display distances after correction for the nuclear size (CORR). N indicates the numbers of nuclei analysed in epidermis (blue) and malpighian tubules (red).

In summary, no pairing could be observed between the endogenous and transgenic copies of the Fab-7 element in FLW-1 flies at any state of activity of the transgene in the analysed tissues. This result corresponds to the data obtained with FLW-1 and 5F24 25,2 larvae.

3.1.4. The spatial distribution of the Polycomb protein in larval interphase nuclei

Given the lack of evidence for pairing of Fab-7 elements the question arose how the Polycomb (Pc) protein was distributed in corresponding nuclei. If indeed PREs, the binding sites for Pc, would not physically interact one would expect more than 100 Pc foci per nucleus since it was previously shown that there are over 100 Pc binding sites in embryonic nuclei (Buchenau et al., 1998) and on polytene chromosomes from larval salivary glands (Rastelli et al., 1993; Zink and Paro, 1989). On the other hand, a smaller number of Pc-enriched sites and the presence of large aggregations or „Pc-bodies“ would indicate clustering of PREs. To study the spatial organization of Pc in nuclei I analysed WT 3rd instar larvae and a transgenic line stably expressing a fusion between Pc and the green fluorescent protein (GFP) (Dietzel et al., 1999). Tissues with different levels of polyteny were selected: leg and eye-antennal imaginal discs (leg ID and eye ID, respectively) as diploid tissues, anterior epidermis, middle midgut, and malpighian tubules as tissues with an intermediate level of polyteny, and highly polytenic salivary glands (Ashburner, 1989). Dissection and fixation procedures were performed as described in 2.2.2.4 and 2.2.2.7. WT tissues were immunostained with specific antibodies against Pc and *Drosophila* lamin. Detection of the lamina was especially important in case of imaginal discs, owing to the small size and tight packing of their nuclei (Figure 34 D - I). Tissues from Pc-GFP larvae (malpighian tubules and salivary glands) were immunostained with an Alexa-488-conjugated anti-GFP antibody to enhance the GFP fluorescence, since these nuclei are large and imaging requires long exposure times. Nuclei from all tissues were imaged using a Leica SP2 or Zeiss 410 confocal microscope. While examining the images visually we had the impression that Pc forms aggregations of different sizes and numbers in nuclei from different tissues and, moreover, that there are less than 100 of such aggregations. This suggested clustering of Pc-binding sites. To find out whether this is the case, we performed quantitative analyses of nuclear sites enriched in Pc.

First, I analysed nuclei from epidermis and eye ID. 3D image stacks were assembled using ImageJ software, and total numbers of Pc aggregations were counted in several nuclei from each tissue (Table 4; see also 2.2.3.3.). The analysis showed that nuclei from eye ID had from 4 to 10 Pc aggregations, while in epidermis, from 8 to 30 such aggregations were found (Table 4). This result suggested that polyploid

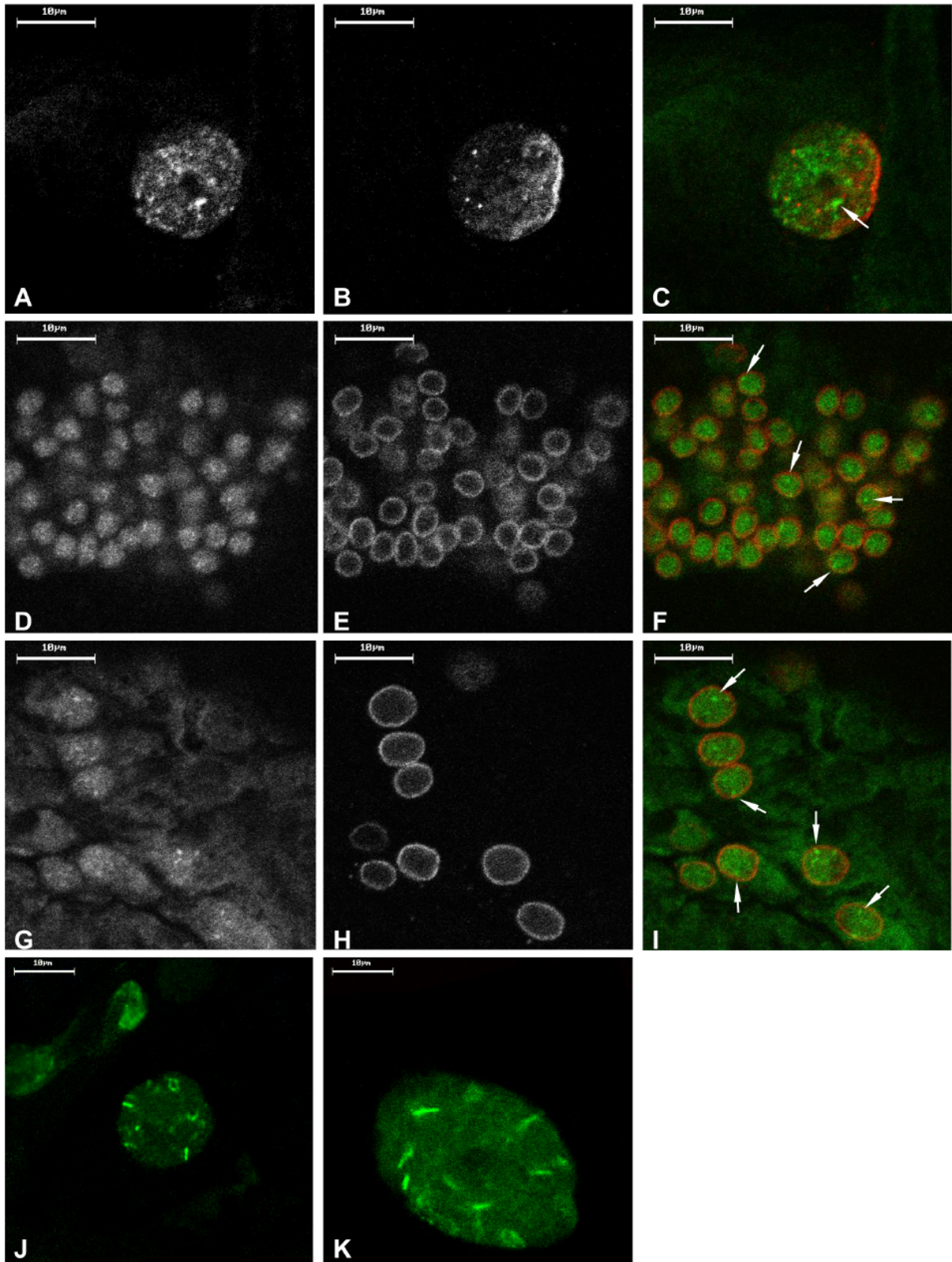


Figure 34. Distribution of Pc in nuclei from WT larval tissues. Nuclei were imaged using a Leica SP2 confocal laser scanning microscope and single light optical sections are shown. (A - I) Pc was detected using specific anti-Pc antibodies and FITC-coupled secondary antibodies (left hand panels). The nuclear lamina was immunostained with antibodies against *Drosophila* lamin and Cy3-coupled secondary antibodies (middle). The right hand panels shows merges (Pc: green, lamina: red) from nuclei of epidermis (A - C), eyeID (D - F), and legID (G - I). Arrows mark sites of the brightest anti-Pc staining. (J, K). Nuclei from a malpighian tubule (J) and

a salivary gland (K) from Pc-GFP transgenic larvae are shown. The GFP fluorescence was additionally enhanced with an Alexa-488-coupled anti-GFP antibody. Scale bar: 10 μ m.

epidermis nuclei had larger numbers of Pc aggregations than diploid nuclei of eye ID.

To further address differences between tissues we took advantage of Amira software for 3D reconstructions (kindly performed by Jeannette Koch, LMU Munich) and counted the numbers of Polycomb aggregations in nuclei from different tissues (2.2.3.3.). It is known that there are more than 100 binding sites of Pc protein on polytene salivary gland chromosomes (Rastelli et al., 1993; Zink and Paro, 1989).

eye ID		
Nucleus	threshold	Total N of particles
eye_2-1	222-255	5
eye_2-2	200-255	6
eye_2-3	192-255	6
eye_2-4	203-255	7
eye_2-5	188-255	10
eye_2-6	191-255	6
eye_3-1	180-255	8
eye_3-2	198-255	4
eye_3-3	207-255	7
eye_3-4	189-255	9
eye_3-5	210-255	5
eye_7-1	188-255	5
eye_7-2	178-255	7
eye_7-3	199-255	6
eye_9-1	182-255	4
eye_9-2	195-255	9
epidermis		
Nucleus	threshold	Total N of particles
epi_3-1	154-255	15
epi_3-2	149-255	11
epi_4-1	113-255	8
epi_7-1	157-255	30
epi_8-1	174-255	16
epi_9-1	131-255	8
epi_9-2	155-255	10
epi_9-3	160-255	18
epi_9-4	170-255	15
epi_10-1	177-255	19
epi_10-2	206-255	11
epi_10-3	142-255	15
epi_10-4	147-255	16
epi_11-1	164-255	10
epi_11-2	184-255	8
epi_11-3	193-255	21
epi_12-1	154-255	8
epi_12-2	119-255	6
epi_12-3	134-255	10

Table 4. Polycomb aggregations in nuclei from WT eye ID and epidermis. The table shows results of ImageJ analyses of numbers of Pc aggregations in WT eye ID and epidermis. Pc protein was visualized using specific antibodies, nuclei were scanned with a Leica SP2 confocal microscope, and the resulting stacks were analysed with ImageJ software. The names of nuclei, applied thresholds, and numbers of Pc aggregations are indicated.

Therefore, a salivary gland nucleus was analysed first to address the reliability of the Amira reconstructions and analysis of Pc binding sites. Figure 35 (A, D) shows a snapshot from the Amira reconstruction and a single confocal section of the analysed nucleus, respectively. One can see that while most of the bands occupy a distinct position within the nucleus, some are localized very close together or lay across each other. Simultaneous inspection of the original image and the reconstruction revealed that some of such closely positioned bands were counted as one by the software

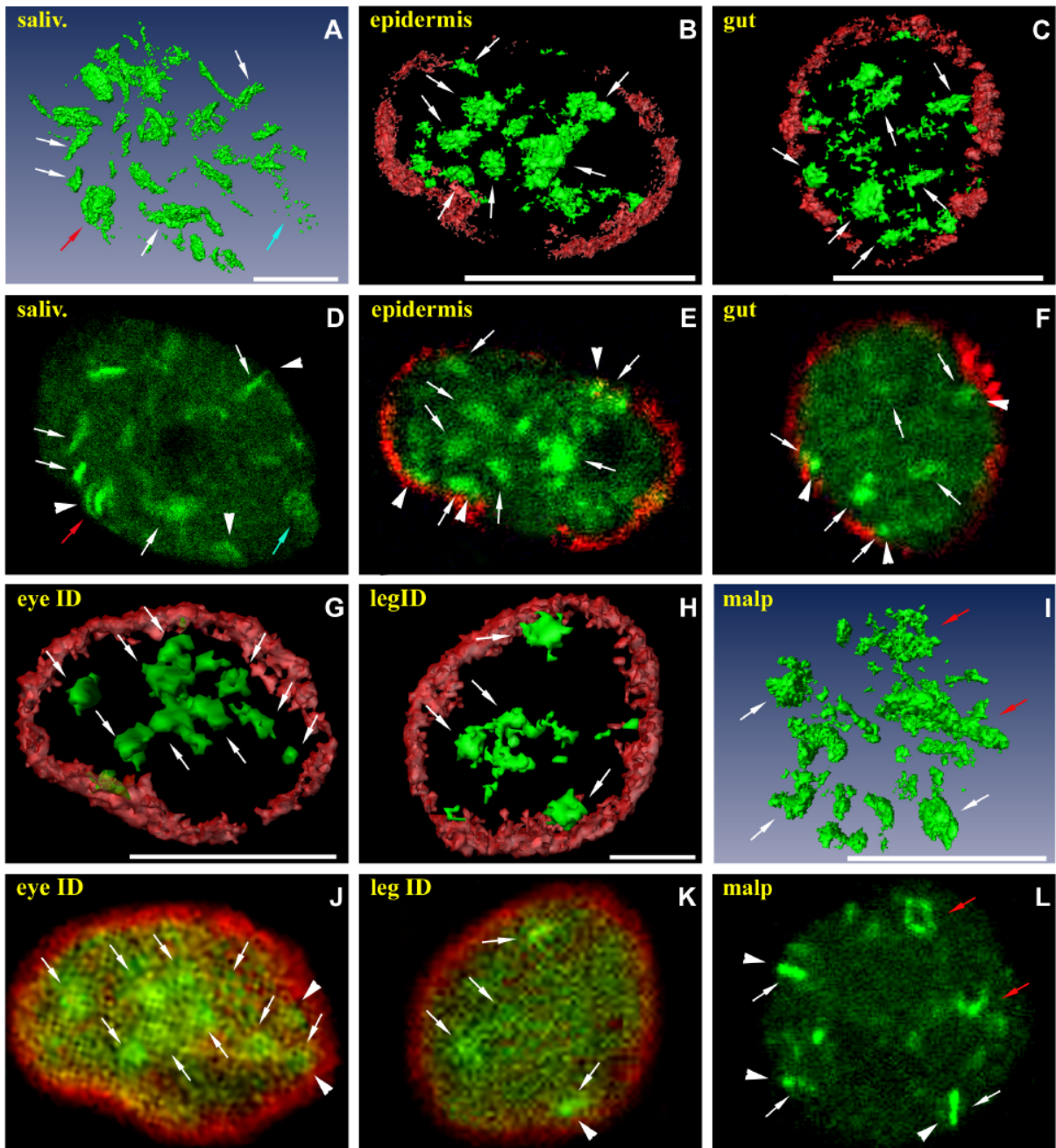


Figure 35. 3D reconstructions of Polycomb aggregations in Pc-GFP and WT larval tissues. (A, D, I, L) In nuclei from Pc-GFP transgenic larvae GFP fluorescence was additionally enhanced with an Alexa-488-coupled anti-GFP antibody and is shown in green. All other nuclei were from WT larvae where Pc was visualized using specific antibodies and is shown in green, while the nuclear lamina was visualized with antibodies against *Drosophila* lamin and is shown

in red. All nuclei were scanned using a Leica SP2 confocal microscope and 3D reconstructions were built with Amira 3.0 software. The voxel size was 0.1x0.1x0.25 μm . Here snapshots from the reconstructions are shown. Tissue types are indicated. For the convenience of perception all snapshots have the same size, although nuclei from imaginal discs (G, H, J, K, scale bars: 2 μm) are much smaller than nuclei from salivary gland (A, D), epidermis (B, E), middle midgut (C, F), and malpighian tubules (I, L) (scale bars: 10 μm). Below each reconstruction a single light optical section from the original nucleus is shown. Arrows indicate corresponding Pc foci on the reconstructions and light optical sections. Red arrows indicate closely positioned bands which were counted as one large aggregation by the software. Light blue arrows in (A, D) indicate a weakly stained region which divided into a number of small aggregations after the threshold was applied. Arrowheads indicate Pc binding sites associated with the nuclear periphery.

(red arrows in Figure 35 A, D). On the other hand, an extremely weakly stained band was divided into a few smaller „islands“ after the threshold was applied and thus was counted as several bands (light blue arrows). On the whole, the number of these artificial „islands“ equalized the number of false aggregations (adjacent double bands counted as 1) and the total number counted was in the expected range (105, Table 5). However, it should be noted that already under these optimal conditions in salivary gland nuclei, where there is a relatively wide spacing between Pc-binding sites and a high signal-to-noise ratio, the software produced a number of artefacts. Therefore, the reliability of results obtained under less optimal conditions is questionable. Table 5 (top line) also shows the total numbers and volumes of Pc binding sites from this

Tissue	Number of Pc binding sites	Volumes ($\mu\text{m}^3 \times 10^{-3}$) of Pc-binding sites				
		<0.01	0.01-0.1	0.1-1	1-10	>10
Salivary gland	105	0	51	28	19	7
Anterior epidermis	34	3	17	7	6	1
Middle midgut	66	7	44	12	3	0
Eye ID	6	0	4	1	1	0
Leg ID	8	0	5	3	0	0
Malp. tubule	74	0	25	28	19	2

Table 5. Polycomb aggregations in nuclei after Amira 3D reconstruction. The table displays numbers and sizes of Pc aggregations of the nuclei whose snapshots are shown in Figure 35. 3D reconstructions were built with Amira software. Voxel size was 0.1x0.1x0.25 μm . Calculations of numbers and volumes of Pc bodies were made by Amira software. Tissues, total number of Pc aggregations and numbers of aggregations in each volume group are indicated in the table.

nucleus. For the convenient comparison of nuclei from different tissues, not only the total numbers of Pc foci were counted, but they were also divided into 5 groups by their volume.

Next, we performed the same analysis with nuclei from epidermis, middle midgut, eye ID, leg ID, and malpighian tubules (Figure 35, Table 5). The total number of Pc foci found in different tissues corresponded to the level of ploidy and the size of the nucleus (Table 5): diploid nuclei from eye ID and leg ID had 6-8 foci, epidermis with an intermediate level of polyteny had 34 foci, and more highly polyploid middle midgut and malpighian tubules had 66 and 74 foci, respectively. The distribution of Pc aggregations in different volume groups appeared to be tissue-specific. One could conclude that these results indicated tissue-specific clustering of PREs and formation of „Pc bodies“ analogous to those described in mammalian cells (Saurin et al., 1998). However, differences in nuclear sizes and signal-to-noise ratios between tissues, which are especially pronounced when diploid nuclei from imaginal discs (Figure 35 G, K) are compared to extremely polyploid salivary gland nuclei (A), had to be taken into account. To address influence of such differences on the visual perception of Pc-binding sites (which is still more reliable than computer assisted image analysis) I chose a leg ID nucleus and a salivary gland nucleus, which were used in reconstructions, for further analyses (Figure 36). Initially, both nuclei had two large and brightly stained Pc-binding sites (indicated with arrows), but the salivary gland nucleus showed much less background and more Pc bands were visible than in the leg ID nucleus (Figure 36 A, B). Then I artificially increased the level of noise in the salivary gland nucleus, using the „Add noise“ function of the Image J software, so that it resembled the background level of the leg ID nucleus. The result is shown in Figure 36 C: only the largest and brightest sites are still reliably detectable, while smaller and weaker bands

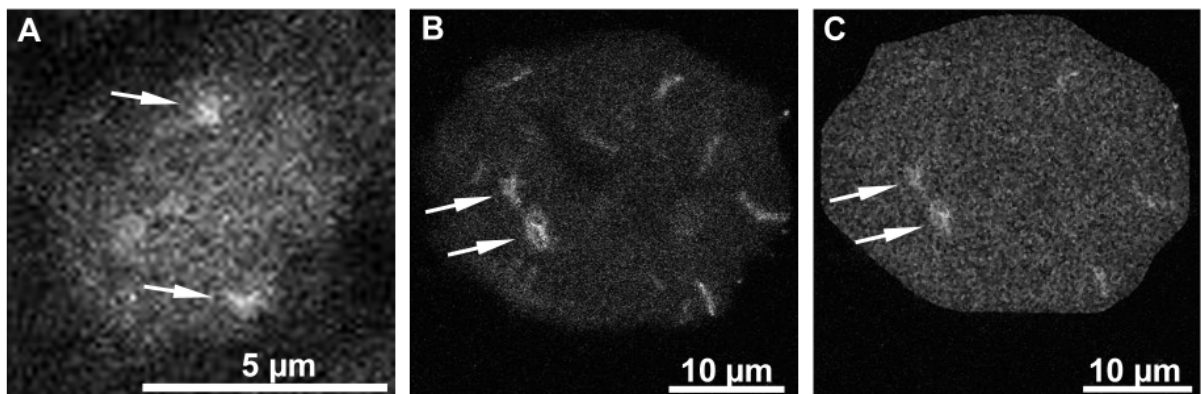


Figure 36. Influence of the signal-to-noise ratio on the detection of Pc-binding sites. Single light optical monochromatic sections are shown as grey-scale images. (A) A nucleus from a leg ID of a WT 3rd instar larva, where Pc was visualized using specific antibodies. Two brightly stained Pc-binding sites are marked with arrows. Scale bar: 5 µm. (B) A nucleus from a salivary gland of a Pc-GFP transgenic 3rd instar larva. An Alexa-488 anti-GFP antibody was used to enhance the GFP fluorescence. Several Pc binding sites are visible, and arrows mark

the two brightest sites. Scale bar: 10 μm . (C) The same light optical section of the salivary gland nucleus. The level of the background noise was artificially increased using the „Add noise“ function of Image J software so that it corresponded to the background level of the leg ID nucleus. Scale bar: 10 μm .

are camouflaged by the background. This result suggests that in diploid nuclei, where the signal-to-noise ratio was relatively low, only a few of the existing Pc binding sites could be detected. The difference in nuclear sizes also plays an important role. In both diploid and polyploid nuclei there were two particularly large and bright Pc binding sites, which probably represent the Bithorax Complex (BX-C) and the Antennapedia Complex (ANT-C) since these two regions are known to contain many PREs (Orlando and Paro, 1995; Ringrose and Paro, 2004) and are brightly stained on salivary gland chromosomes by anti-Pc antibodies (Zink and Paro, 1989). In the salivary gland nucleus these regions had volumes of more than $10 \mu\text{m}^3 \times 10^{-3}$, and the majority of other Pc binding sites were noticeably smaller and more weakly stained and were not reliably detectable when the level of the background noise was artificially increased. In the leg ID nucleus even those large regions had only volumes between 0.1 and $1 \mu\text{m}^3 \times 10^{-3}$ (Table 5). This suggests that in diploid nuclei of imaginal discs the majority of the Pc-binding sites have a very small volume, and they could not be reliably detected and reconstructed. In addition, the close spacing of Pc-binding sites in small nuclei makes a reliable detection of individual sites difficult.

Next, I compared a salivary gland nucleus and a malpighian tubule nucleus (Figure 37). Both of these tissues are polytenic, although malpighian tubules have a lower degree of polyteny than salivary glands (Ashburner, 1989). Nuclei of malpighian tubules are about 2.5 times smaller than salivary gland nuclei, and in the 3D reconstruction there were 74 Pc foci found (Table 5). Careful visual inspection revealed that most of the Pc binding sites in this nucleus were clearly individual bands and not aggregations (single light optical sections of the same nucleus are shown in Figure 35 I, L and Figure 37 F-I). Moreover, what appeared as clusters in the reconstruction were, in fact, single bands which were located too close together or laid across each other (red arrows in Figure 35 I, L). Together with the fact that the signal-to-noise ratio in nuclei from malpighian tubules was lower than in salivary glands, it is likely that in these nuclei all individual Pc binding sites could not be counted as single sites (see Movie 1 on the supplementary CD).

In malpighian tubules from Pc-GFP larvae, the dimH3K9-containing heterochromatin was additionally visualized with specific antibodies (Figure 37 H, I). Interestingly, in all analysed nuclei there were several bright Pc binding sites at the boundary of the dimH3K9-positive domain (Figure 37 I, J, arrows point to Pc-binding sites which are in contact with heterochromatin), but not within it. In addition, in all tissues analysed Pc-binding sites were frequently located at the nuclear periphery (arrowheads

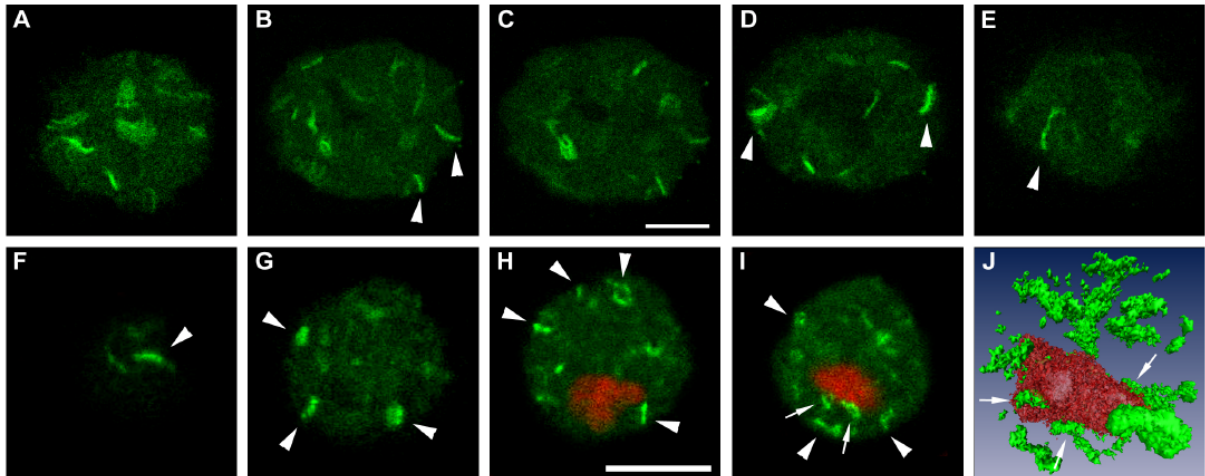


Figure 37. Polycomb-binding sites in larval polytene tissues. Light optical sections of a salivary gland nucleus (A-E) and a malpighian tubule nucleus (F-I) from Pc-GFP transgenic 3rd instar larvae are shown. Tissues were immunostained with an Alexa-488-conjugated anti-GFP antibody (green). In the malpighian tubule nucleus the dimH3K9-positive domain was visualized additionally with specific antibodies (red). (J) A snapshot from the Amira reconstruction from the malpighian tubule nucleus. Arrows in (I, J) mark corresponding Pc binding sites at the boundary of heterochromatin. Arrowheads indicate Pc binding sites associated with the nuclear periphery. Scale bars: 10 μ m.

in Figures 35 and 37). This is in accordance with our previous results showing PREs located at the nuclear periphery and at the boundary of heterochromatin.

To obtain more information about the native spatial organization of Pc in nuclei from different *Drosophila* tissues, I used the Pc-GFP transgenic line (2.1.10.2.2.), which allowed imaging without preceding fixation and antibody detection of Pc, thus minimizing the number of possible artefacts. I tried to scan unfixed tissues with a confocal microscope, but the GFP fluorescence diminished rapidly and it was only possible to image a small subset of nuclei from tissues like malpighian tubules or salivary glands. Therefore, we took advantage of the selective plane illumination microscope (SPIM) (courtesy of Dr. Ernst Stelzer, EMBL Heidelberg), which allows imaging of large unfixed specimen with sufficient resolution during a very short time period (Huisken et al., 2004; Keller et al., 2006). We imaged nuclei from different 3rd instar larval tissues: eye and leg imaginal discs, malpighian tubules, a nerve and a part of a salivary gland. Each tissue sample was imaged from several angles, and then multiview reconstructions were made using MatLab 7.0 software (kindly performed by Dr. Francesco Pampaloni, EMBL Heidelberg). Unfortunately, the resolution was not sufficient to distinguish single Pc binding sites in small nuclei of imaginal discs. Imaging of malpighian tubules was also problematic, because any specimen which was large enough for SPIM microscopy coiled in the dissection buffer or in the cylinder of agarose gel used to embed the specimen. This made the creation of multiview reconstructions impossible. But a part of a salivary gland and a nerve were successfully imaged and reconstructed. From the reconstructions it was possible to make projections which gave

a very realistic 3D view of the tissue (see Movies 2 and 3 on the supplementary CD). Figure 38 shows snapshots from the projections of a salivary gland (A-D) and a nerve (E-H). Snapshots were taken as the projections were turned around the X (horizontal) axis. In agreement with the previous results, in nuclei from both tissues numerous Pc binding sites were visible, with variable sizes and fluorescence intensities.

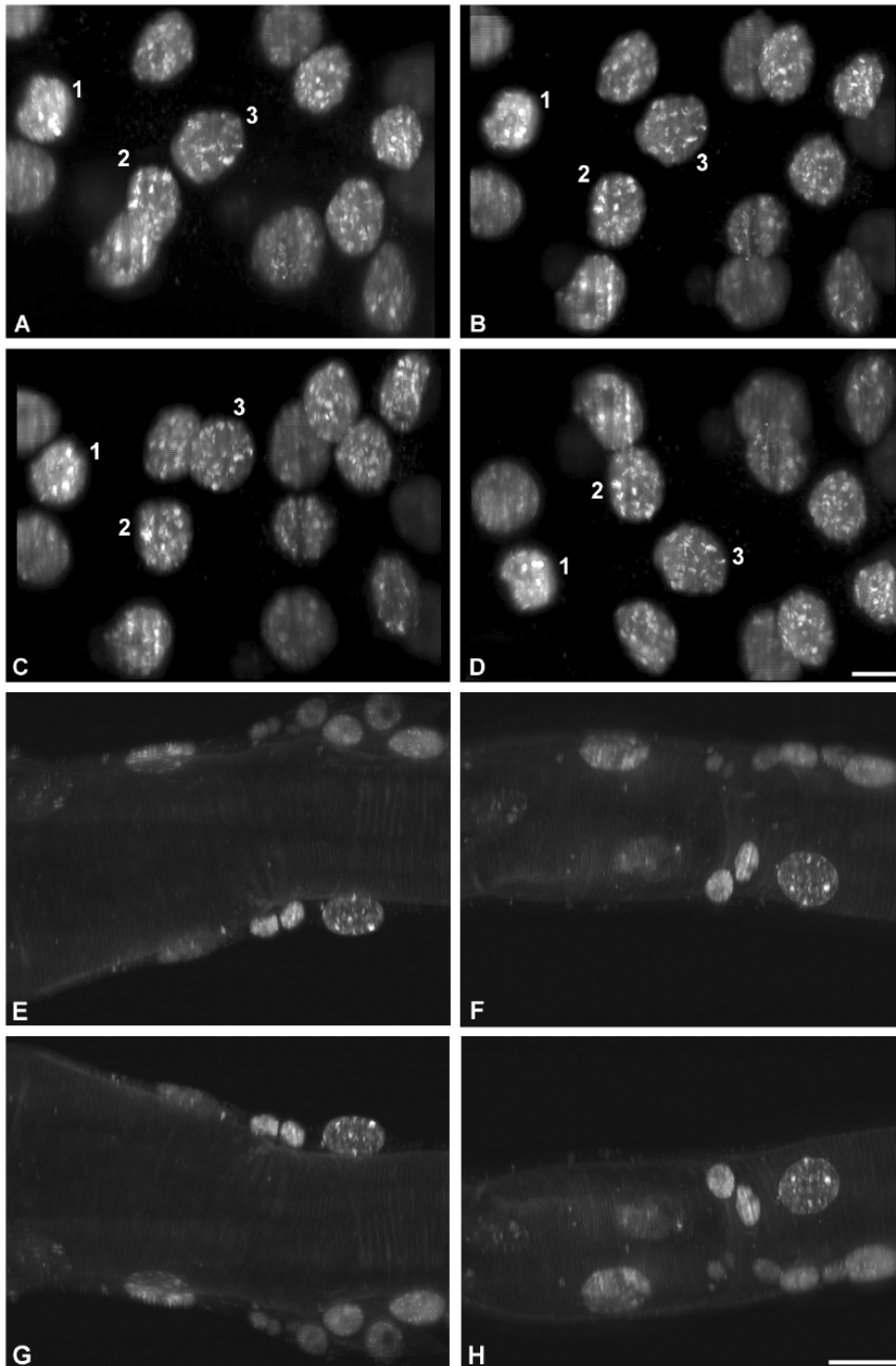


Figure 38. Native distribution of the Pc-GFP fusion protein. Tissues from Pc-GFP transgenic 3rd instar larvae were imaged using the SPIM microscope. No fixation or immunostaining steps were performed. 3D data sets were collected at every 30° by rotating the sample and the total of 360° was covered. Using MatLab software the 3D data sets were combined into a multiview reconstruction, and a maximum intensity projection was made. Here, snapshots from the projections are shown. They were taken at different angles of rotation around the X axis of the

projection. (A-D) A section of a salivary gland was imaged. Snapshots were made at 0° (A), +40° (B), +60° (C), and +200° (D) of rotation relative to the starting point, respectively. Three nuclei were numbered to facilitate tracking single of nuclei through rotations. Scale bar: 20 µm. (E-H) Part of a nerve. Snapshots were taken approx. every 90°. Scale bar: 10 µm.

3.1.4.1. Endogenous Pc-GFP binding sites associate with the active form of RNA pol II at the boundary of the heterochromatic domain

Results, obtained here with different transgenic fly lines showed that transgenes, which contained one or two copies of the Fab-7 PRE, were frequently associated with the boundary of the heterochromatic domain in their transcriptionally active states (3.1.2.2.). I have also shown that a number of sites, enriched in dimH3K4, trimH3K4 and the active form of RNA pol II, are present at the boundary of heterochromatin (3.1.1.). An independent earlier study on spreads of polytene salivary gland chromosomes of FLOW-1 transgenic larvae (see also 3.1.2.2.3.) showed that the transgenic Fab-7 element was associated with Pc not only in its inactive but, surprisingly, also in its stably active state (Cavalli and Paro, 1999). On the other hand, in embryonic nuclei it was shown that Pc and other members of Polycomb-group proteins (PcG) did not coincide with transcriptionally active chromatin loci (Buchenau et al., 1998). To address the spatial relationships between Pc and transcriptionally active or inactive euchromatic sites in larval interphase nuclei, I performed a series of immunostaining experiments with malpighian tubules from Pc-GFP transgenic 3rd instar larvae. Nuclei were imaged with a Zeiss 410 confocal laser scanning microscope. 3D data sets were assembled and the shifts between channels were corrected using Image J. First, the nuclei were immunostained with specific antibodies against dimH3K4 and dimH3K9. In all analysed nuclei, the dimH3K4-enriched sites, whether large or small, at the boundary of heterochromatin were not associated with Pc-binding sites. In turn, Pc-binding sites at the boundary of heterochromatin were devoid of dimH3K4 (data not shown). Rarely, a PRE elsewhere in the nucleoplasm was associated, but not colocalized, with a small dimH3K4-domain, but mostly these PREs were also depleted in dimH3K4 (data not shown). This suggests that PREs are not associated with dimH3K4-enriched sites in interphase larval nuclei.

Next, in nuclei from Pc-GFP larvae I visualized the active form of RNA pol II (phosphorylated at Ser 2, see also 3.1.1.) and dimH3K9 with specific antibodies. Surprisingly, in all analysed nuclei many Pc-binding sites were associated with pol II, at the boundary of heterochromatin as well as elsewhere in the nucleoplasm (Figure 39). In the majority of cases, pol II-enriched sites were localized at both „ends“ of Pc-binding bands. These results show that a number of PREs in the interphase larval

nucleus associate with sites of transcriptional activity, including the PREs at the boundary of heterochromatin.

In summary, I analysed sites of enrichment of Pc in a number of larval tissues from different fly lines, using different methods to visualize Pc and Pc-GFP. Different microscopy techniques and software tools were applied. The data showed consistently

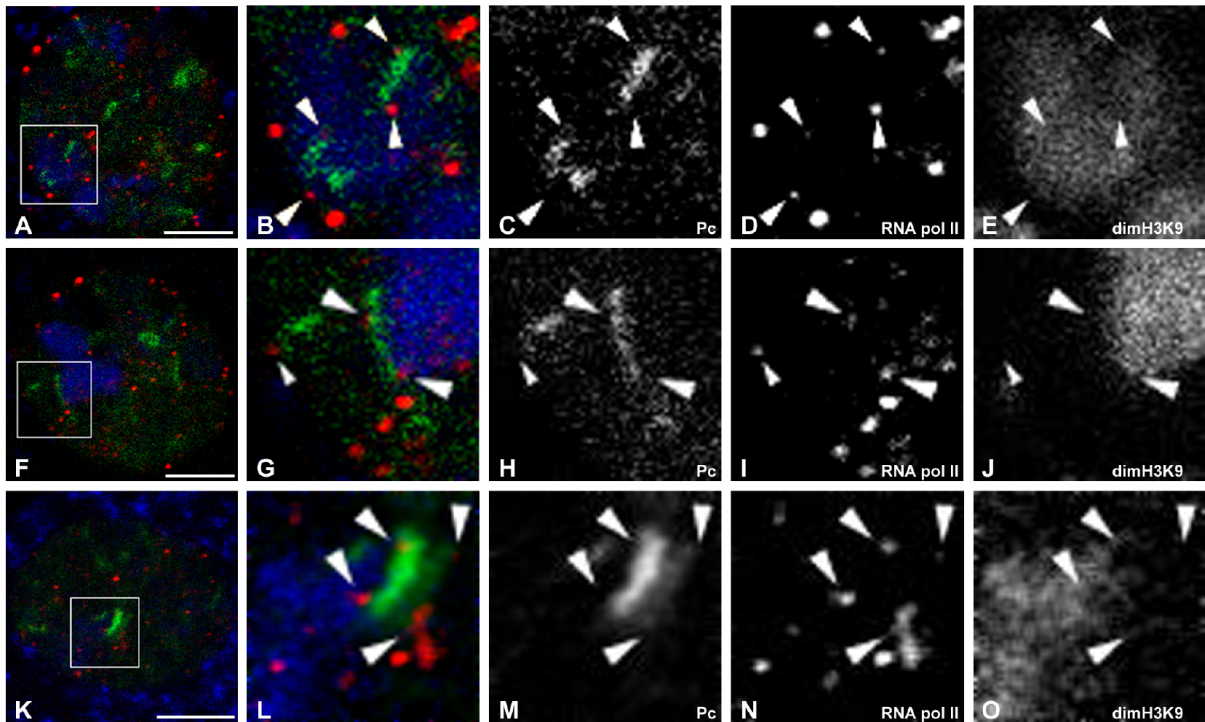


Figure 39. Pc-binding sites at the boundary of heterochromatin associate with the active form of RNA pol II. The panels show single light optical sections from nuclei of malpighian tubules from Pc-GFP transgenic 3rd instar larvae. Histone modifications and RNA pol II (phosphorylated at Ser2) were visualized using specific antibodies. GFP fluorescence was additionally enhanced with an Alexa-488-coupled anti-GFP antibody. Nuclei were imaged with a Zeiss 410 confocal microscope. Each row (A-E, F-J and K-O) represents one nucleus. A, F and K show corresponding merges (Pc-GFP: green, RNA pol II (Phosphorylated at Ser.2): red, dimH3K9: blue). Framed areas of nuclei in A, F and K are shown enlarged in B, G and L, respectively. Images in (D-E) show the Pc-GFP-binding sites at the very top of the heterochromatic domain but not colocalizing with it. Images in (K-O) were smoothed using ImageJ to increase signal-to-noise ratio. Grey-scale images of the green fluorescence (Pc-GFP: C, H and M), red fluorescence (RNA pol II: D, I and N) and blue fluorescence (dimH3K9: E, J and O) are shown in addition. Large arrowheads in (B-E, G-J and L-O) indicate RNA pol II-enriched sites associated with Pc-GFP-binding sites at the boundary of heterochromatin. The small arrowhead in (G-J) points at a RNA pol II-enriched site associated with a Pc-binding site elsewhere in the nucleus. Scale bars: 5 μ m.

that in nuclei from all tissues analysed numerous sites enriched in Pc (or Pc-GFP) with variable sizes and fluorescence intensities were present. These findings are in agreement with results obtained by immunostaining of spreads of polytene salivary gland chromosomes with anti-Pc antibodies (Rastelli et al., 1993; Zink and Paro, 1989) and the results suggest that at least in polytene tissues each nuclear site of enrichment represents a single chromosomal binding site of Pc. Although it is problematic to analyse small diploid nuclei with the current methodology available, no evidence for clustering of chromosomal Pc-binding sites in the 3D nuclear space could be obtained. The nuclear distribution of Pc-binding sites was in agreement with our previous results, which showed frequent association of PREs with the nuclear periphery and the boundary of heterochromatin. I have also found that PREs, positioned at the boundary of heterochromatin, were associated with sites enriched in the active form of RNA pol II, which is in accordance with my previous observation that Fab-7-containing transgenes were frequently associated with the boundary of heterochromatin in their active states.

3.2. Nuclear localization of active versus inactive LV-PGK transgenes in porcine fibroblasts obtained from transgenic animals (*Sus scrofa scrofa*)

The results obtained with transgenic *Drosophila* lines suggested that the chromosomal localization of a transgene, its nuclear positioning and its transcriptional activity are interrelated (3.1.2.2.). To address the relationships between these features in mammals we took advantage of transgenic pigs produced by the team of Prof. Alexander Pfeifer, LMU Munich (Hofmann et al., 2003). Transgenic pigs carried the same LV-PGK transgenic construct (see Figure 3, (Follenzi et al., 2000)) but the site of its integration as well as its transcriptional activity differed. For my studies only animals with a single integration were chosen. Southern blot analyses were performed to check the number of integrants in each pig (Hofmann et al., 2006). Skin fibroblasts from several pigs with different expression levels were cultured in vitro and their GFP expression was monitored to check the state of activity of the transgene.

3.2.1. Immortalized cells

To find out whether the LV-PGK construct was positioned differently in nuclei of high- and low-expressing porcine cells, in the first part of these experiments I used fibroblasts immortalized with the T-large antigen. All cell lines and FISH probes were provided by the Pfeifer group. SFF 8777 were high-expressing, while SFF 8779 were low-expressing cells, SFF WT TAg were immortalized WT cells (2.1.11.3.). Cells were fixed with methanol-acetic acid and FISH was performed. The LV-PGK construct was visualized with the full-length LV-PGK probe labelled with biotin or digoxigenin (2.2.1.6.1.), which was then detected with Cy3-conjugated anti-digoxigenin antibodies or a Cy3-coupled avidin conjugate. Surprisingly, there were multiple FISH signals in nuclei from all cell lines, including WT cells (Figure 40, first 3 pictures on the top, left). Typically up to 5 signals were found in each nucleus. On metaphase chromosomes there were mostly doublet signals on both sister chromatids, confirming that the signals represented true FISH signals. These multiple signals were unexpected since it was firmly established that each transgenic cell line had one integrant only. But most puzzling of all were FISH signals in WT nuclei where there was no transgene integrated.

Our first working hypothesis was that the full-length LV-PGK probe, which was used for detection of the transgene, also visualized some of the endogenous retroviruses, which are present in the porcine genome (Patience et al., 2001). To test this possibility I performed FISH with the full-length LV-PGK probe on human SH-EP N14 cells, as the human genome also harbours a vast number of retroviruses.

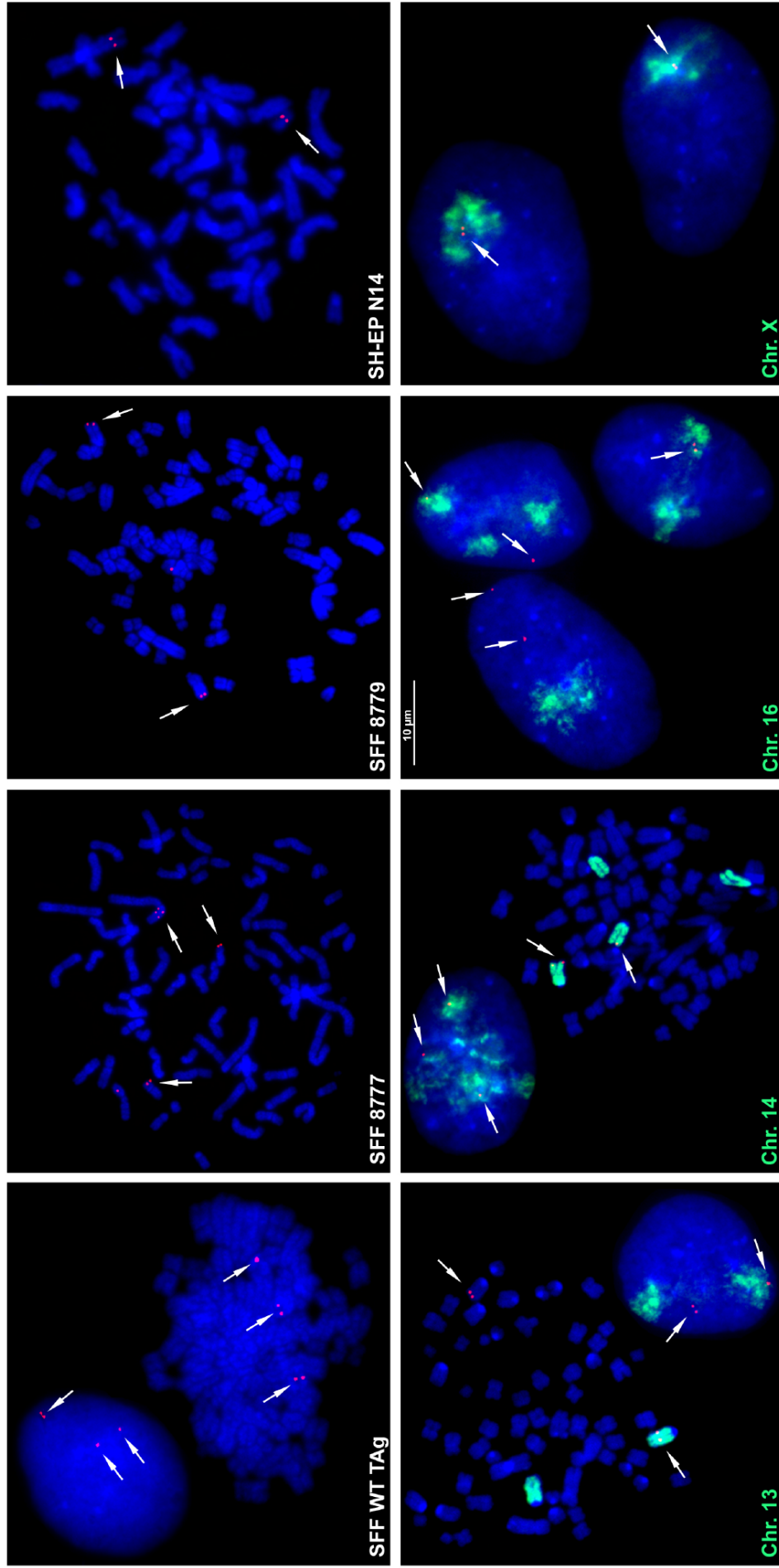


Figure 40. Localization of FISH signals obtained with the LV-PGK construct in immortalized porcine and human tumour cells. FISH was performed with the dig-labelled full-length LV-PGK probe and the probe was detected with Cy3-conjugated anti-dig antibodies. FISH signals are shown in red and are indicated with arrows. DNA was stained with DAPI and is shown in blue. Chromosome paints were labelled with FITC and are shown in green. Images on the top show LV-PGK signals in immortalized porcine cells, from left to right: SFF WT TAG, SFF 8777 and SFF 8779. The right image in the top row shows results obtained with human SH-EP N14 cells. Images on the bottom show interphase nuclei and metaphase spreads of SFF 8779 cells, where the LV-PGK construct was visualized together with different chromosome paints (indicated on corresponding figures). Scale bar: 10 µm.

Corresponding results are illustrated in Figure 40 (top, right). Remarkably, in SH-EP N14 nuclei there were always two signals: one on chromosome 1 and another on chromosome 19. The location of the signals corresponded to known hotspots for retroviral integration in human genome (Schroder et al., 2002). This result indeed suggested that unspecific FISH signals in porcine cells resulted from endogenous viruses.

Analysis of the structure of the LV-PGK probe (Figure 3) revealed three fragments which were not expected to hybridize with endogenous retroviruses. The eGFP sequence has no match in the porcine genome, and ppt-PGK and W-3'LTR fragments were significantly changed in the construct compared to WT viruses. These fragments were isolated, labelled (Figure 4) and mixed together as a probe for FISH. With this pooled probe multiple signals were detected in all three cell lines (data not shown). It was assumed that the ppt-PGK or W-3'LTR fragment or both of them were the source of unspecific signals. Therefore, we concentrated on the eGFP fragment. Its sequence was BLASTed against known sequences from the porcine genome and no hits were registered, suggesting that there were no complementary elements in the genome. The eGFP probe was labelled with Cy3-, digoxigenin- or biotin-dUTP using PCR or nick-translation (2.2.1.6.1, Figure 4) and then used for FISH. After using the dig-/bio-labelled probe with subsequent antibody detection or the Cy3-dUTP labelled probe no signals were registered (data not shown). As the GFP fragment was only ~800 bp long I tried to enhance the signal from the biotin-labelled probe with the Tyramide Signal Amplification kit (2.2.1.6.5.). The drawback of this method was that in the majority of the nuclei there was a high level of background noise which made detection of specific FISH signals impossible. In some cases there was only one bright spot which might have been the FISH signal but the percentage of such nuclei was low, ~5% (data not shown). Thus, we were forced to use the full-length probe.

Unfortunately, the integration sites of the construct were not mapped. One possible way to distinguish between FISH signals from the LV-PGK construct and endogenous retroviruses appeared to be the use of chromosome paints (kindly provided by Dr. Roscoe Stanyon, University of Florence). It was expected that signals with the same chromosomal localization in all three cell lines would be due to endogenous retroviruses, while a signal whose location differed in SFF 8777 and SFF 8779 lines was expected to result from the LV-PGK construct. After identifying the chromosomal localization of the transgene it would be possible to identify it in further experiments using the corresponding chromosome paint. To execute this strategy, I first performed FISH with the LV-PGK probe in combination with painting probes for chromosomes 13-18, X and Y on SFF 8779 cells. Figure 40 (bottom panels) shows typical results obtained with painting probes for chromosomes 13, 14, 16 and X. With painting probes for chromosomes 13 and 14 the results were consistent in most of the nuclei: there were one or two signals on the painted chromosomes and one or two signals

somewhere else. The use of painting probes for chromosome 16 revealed a huge diversity between nuclei: some had no signals on the painted chromosome (left nucleus in Figure 40), some had signals on chromosome 16 as well as somewhere else (upper right nucleus) while others had FISH signals only on the painted chromosome (lower right nucleus). With other chromosome paints (data not shown) similarly inconsistent results were obtained. After obtaining these results I got the suspicion that the cell lines provided by the Pfeifer lab might not be suitable for these experiments and might contain other retroviral vectors. Dr. Andreas Hofmann from the Pfeifer group confirmed that the T-large antigen used for immortalization of these cell lines was delivered to the cells using a LV-PGK construct which differed from the original one only by ~700 bp (eGFP versus T-large antigen). This fact explained the number of signals and the inconsistency of their chromosomal localization. Therefore, since I could not visualize the construct with the eGFP fragment alone and could not use the full-length probe, we performed another series of experiments with primary fibroblasts.

3.2.2. Primary cells

To investigate the nuclear positioning of the LV-PGK construct at its active and inactive states we used in vitro cultured primary fibroblasts obtained from different animals: SFF 9338 fibroblasts were highly expressing, SFF 9206 cells had a variegated expression pattern (~20% of the cells were expressing), SFF 9193 cells were weakly expressing, SFF 9192 and 9196 were non-expressing and SFF WT were wild type cells (2.1.11.3.3, Figure 41). More data regarding mean eGFP fluorescence in these cell lines can be found in (Hofmann et al., 2006). All cell lines and the eGFP expression data were provided by Dr. Andreas Hofmann (LMU Munich). Each fibroblast strain had a single and unique site of integration of the transgenic construct but the chromosomal localization had been determined in only two cases: chromosome X in 9192 cells and chromosome 11 in 9196 cells.

Cells were fixed with methanol-acetic acid and FISH was performed with the dig-labelled full-length probe which was detected with Cy3-conjugated anti-dig antibodies. There was only one FISH signal in each transgenic cell line and no signal in WT cells (Figure 42). 2D erosion analyses were performed (~ 90 nuclei in each case). The results of the analyses are shown in Figure 43 (for details concerning the interpretation of such diagrams see (Zink et al., 2004)). The two strains containing highly expressing cells (9338 and 9206) displayed the most interior localization of FISH signals (majority of signals in shell 3). FISH signals displayed a more peripheral localization in 9193 cells (majority of signals in shell 2), which showed only low levels of expression. The most peripheral localization was observed in 9192 and 9196 cells, which were non-expressing. In these cells the majorities of FISH signals were found in the outermost

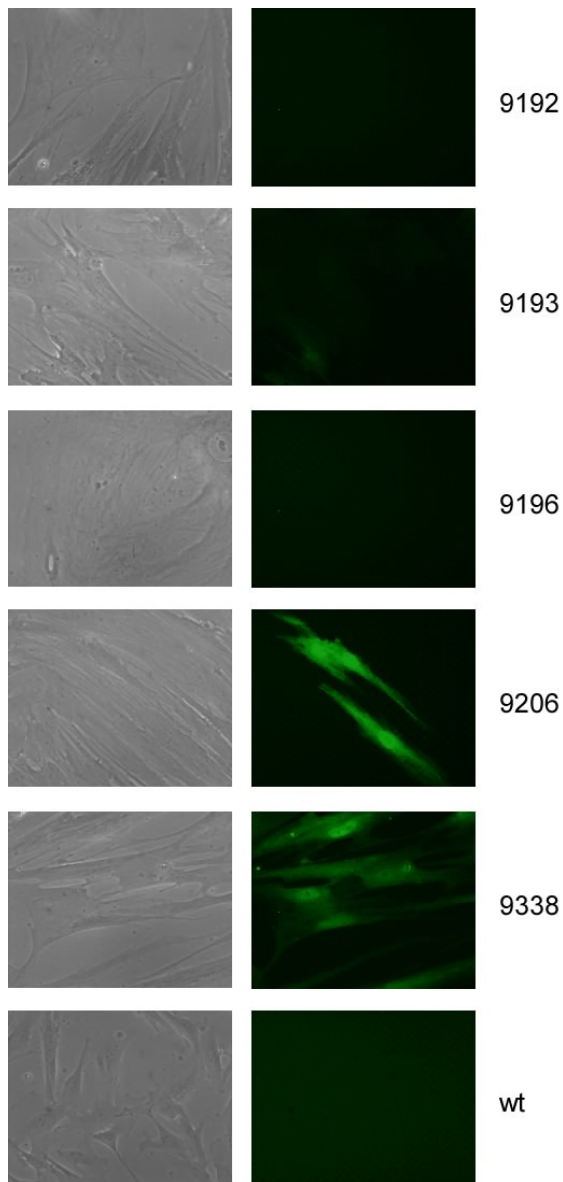


Figure 41. eGFP expression in primary skin fibroblasts from transgenic pigs (provided by Dr. Andreas Hofmann, LMU Munich). Phase contrast images of live cells are shown on the left hand side and the corresponding images on the right hand side show the eGFP fluorescence. The name of each fibroblast strain is indicated. WT cells showed no GFP expression.

shell 1 and the numbers of FISH signals constantly declined towards the nuclear interior. These results show a correlation between the level of activity of the LV-PGK transgene and its nuclear localization: inactive transgenes were closest to the nuclear periphery while active constructs were found at more interior positions. In highly expressing cells the transgenic constructs occupied the most extreme interior positions and the transgenic constructs with low levels of activity occupied an „intermediate“ position. The results also demonstrated that the nuclear position depended not only on the activity of the construct but also on its chromosomal localization and, probably, on surrounding chromatin. In the two non-expressing strains, 9192 and 9196, the positioning of the transgenic construct was slightly different. Furthermore, the transgenic construct displayed the most extreme interior positioning in 9206 cells, although only ~20% of cells were expressing in this case. It should be noted that in these cells only ~5% of FISH signals showed a pronounced peripheral positioning (localization in shell 1), although about 80% of cells were non-expressing in this strain.

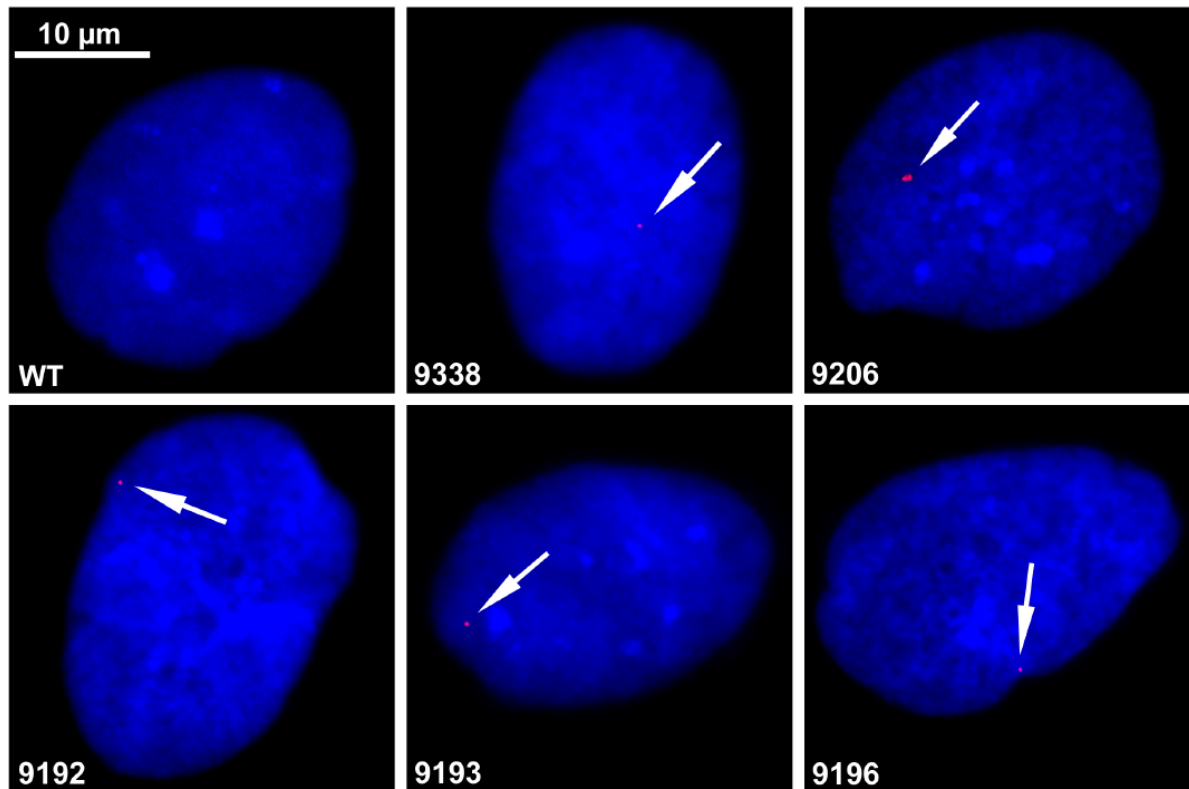


Figure 42. Detection of the LV-PGK transgenic construct in primary WT and transgenic pig fibroblasts. The transgenic construct was visualized by FISH using the full-length LV-PGK dig-labelled probe which was detected with Cy3-conjugated anti-dig antibodies. The FISH signals are shown in red and are indicated by arrows. The LV-PGK probe was only ~3,5 kb long and the FISH signals in transgenic cells were small. There was no FISH signal in WT cells. DNA was stained by DAPI and is shown in blue. The name of each cell line is indicated on the corresponding image. Scale bar: 10 μ m.

While collecting images for the erosion analysis I noticed that only in two cases (9206 and 9193) chromocenters could be recognized after DAPI staining (Figure 42). During the erosion analysis of 9206 cells I got the impression that FISH signals were frequently associated with a chromocenter. In 9193 nuclei I did not notice such a preferential localization of the FISH signal. To further address this, I performed distance measurements between the signal and the nearest border of a chromocenter in 81 nuclei from 9206 cells and in 88 nuclei from 9193 cells. The results of the measurements are shown in Figure 44 A. In nuclei of 9193 cells (right hand diagram) the results revealed no specific association with chromocenters and the distribution of distances showed one major peak (15%) at 3.5 μ m. Concerning 9206 cells the distance distribution (left hand diagram) showed two major peaks at 0.5 μ m and 3 μ m (~ 16% in each case). ~22% of the FISH signals were found within 1 μ m from the closest chromocenter. Remarkably, the FACS analysis of eGFP expression in 9206 cells showed that ~ 21% of the cells expressed eGFP at a high level while the rest of the cells were not expressing (Figure 44 B). This suggested that, as in transgenic flies, expressed transgenes were located at the boundary of heterochromatin. Unfortunately, in porcine cells the eGFP

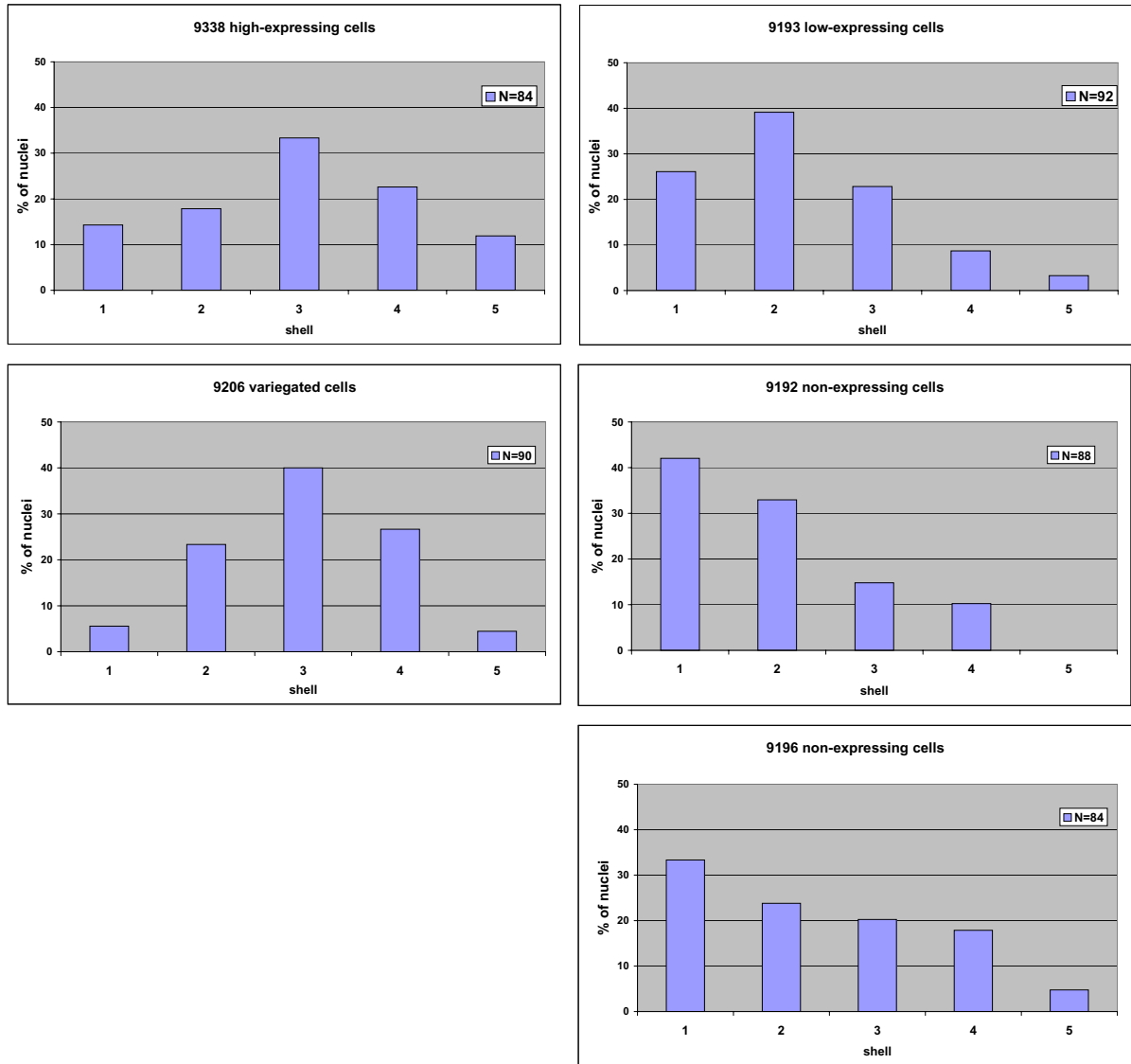


Figure 43. Results of 2D erosion analyses with transgenic pig cell lines. Cells were fixed with methanol-acetic acid and FISH was performed using the full-length LV-PGK probe. Nuclei were imaged with a Zeiss Axiovert epifluorescence microscope and then analysed with Photoshop 7.0 software (see also 2.2.3.1.1). Nuclei were divided into 5 concentric shells and the numbers of signals in each shell were counted. Shells are indicated on the X axis: 1 is the outermost shell and 5 the innermost. The bars show corresponding percentages (%; Y-axis) of FISH signals in a given shell. N indicates the number of analysed nuclei.

fluorescence did not survive the FISH procedure in methanol-acetic acid fixed cells and it was not possible to perform single-cell analyses to find out whether the active LV-PGK construct was indeed localized in the vicinity of a chromocenter. We tried to perform 3D FISH with formaldehyde-fixed 9206 cells, as this method preserves the eGFP fluorescence. However, this procedure gives rise to weaker FISH signals and since the LV-PGK probe was short (3.5 kb), the signal it produced was not reliably detectable on confocal images. Therefore, it was not possible to test whether indeed the transgenic construct associated with heterochromatin only in its active state.

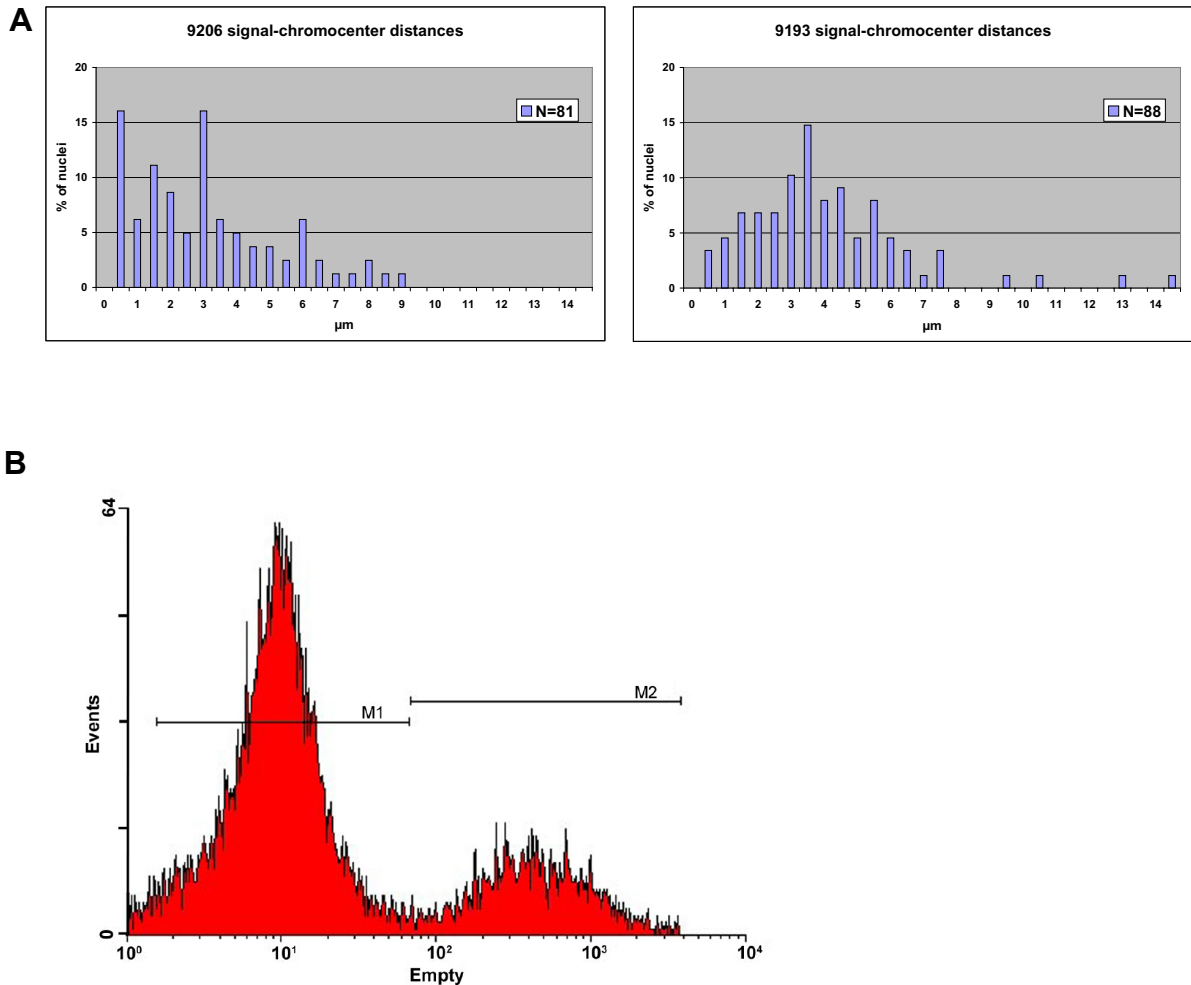


Figure 44. A. Results of distance measurements between the LV-PGK construct and the closest chromocenter in 9206 and 9193 cells. The LV-PGK transgenic construct was visualized with FISH while chromocenters were identified by DAPI staining. X axis shows distances in microns. The bars indicate the fractions of nuclei (%) displaying distances between the FISH signal and the nearest chromocenter within a given distance interval as indicated on the X-axis. N indicates the number of analysed signals.

B. The result of FACS analysis of the GFP expression in 9206 cells (kindly provided by Dr. Andreas Hofmann, LMU Munich). The X axis shows the intensity of GFP fluorescence, while the Y axis (“events”) shows the number of counted cells. 76% of cells were in area M1 (no expression), 21% of cells were in area M2 (high expression).

3.2.3. Activation of the LV-PGK transgene with 5-azacytidine

Our results showed that the transgene in its inactive state localized close to the nuclear periphery while in the active state it was found in the nuclear interior. Did the state of activity define the nuclear position of the transgene, or *vice versa*? One way to address this question was to activate the transgene in non- or low level

expressing cells and test whether this changed its nuclear positioning. It was shown previously that 5-azacytidine (5-azaC) treatment of 8779 fibroblasts (non-expressing cells, 2.1.11.3.3.) significantly increased their mean eGFP fluorescence intensity (Hofmann et al., 2006). Therefore, we treated 9206 and 9193 cells with 5-azaC for 5 days as described in Hofmann et al. (2006). (After performing the previous set of experiments all cells were frozen. Unfortunately, non-expressing 9192 and 9196 cells did not survive the freezing procedure and could not be used for 5-azaC treatment). Subsequently, examination of the eGFP fluorescence confirmed that after 5-azaC treatment all cells were highly expressing (data not shown) (these two procedures were kindly performed by Dr. Andreas Hofmann, LMU Munich). Then 5-azaC treated and control cells were fixed with methanol-acetic acid, FISH was performed as before, and 2D erosion analyses were performed (Figure 45). The freezing-melting procedure

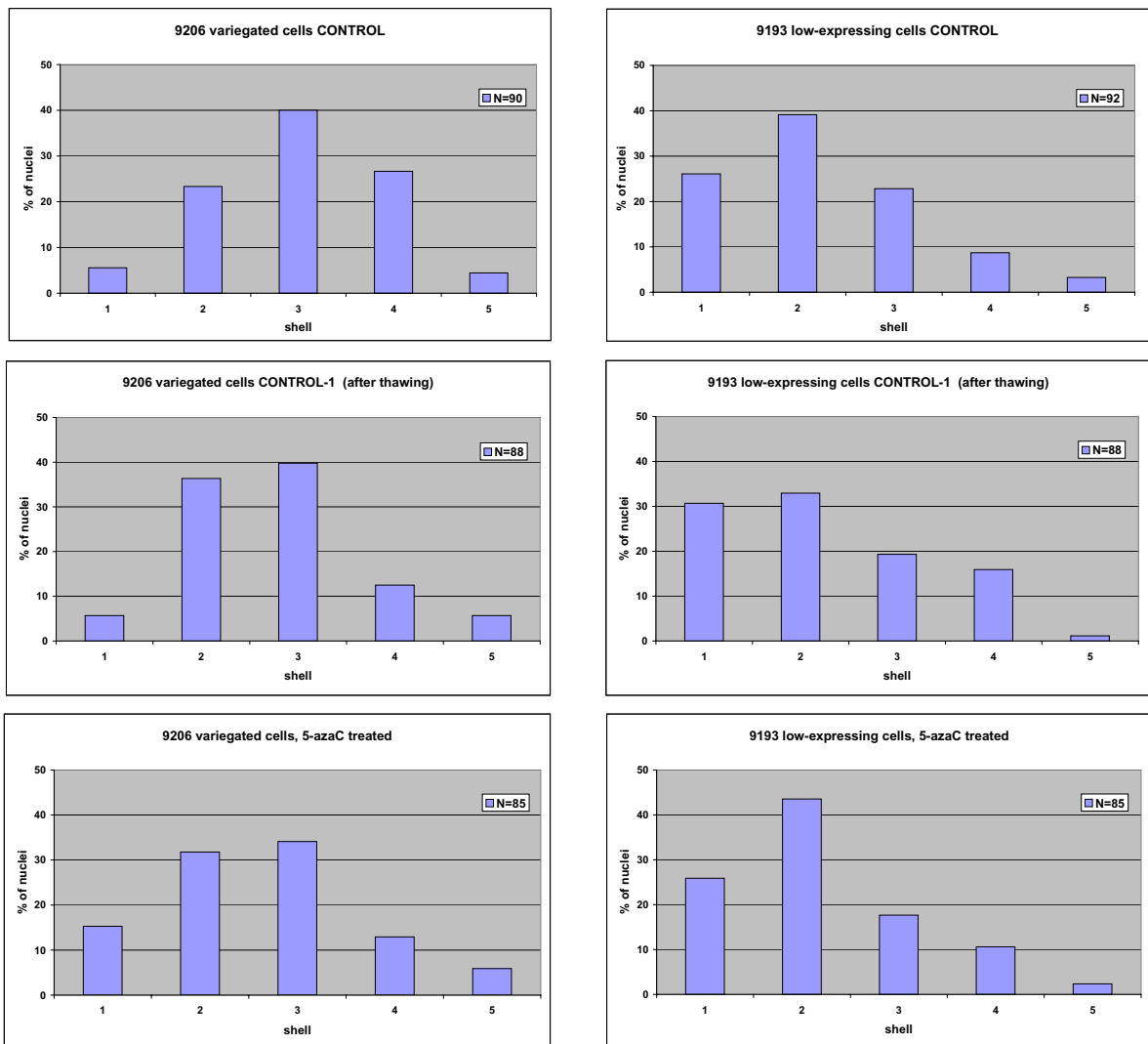


Figure 45. Results of 2D erosion analyses in control and 5-azaC treated transgenic pig cell lines. The data from CONTROL cells are the same as shown in Figure 43. CONTROL-1 cells correspond to CONTROL cells which were frozen, stored in liquid nitrogen for ~1 month, thawed and put into culture again. 5-azaC treatment was performed on CONTROL-1 cells as described in Hofmann et al. (2006). Cells were fixed with methanol-acetic acid and FISH was

performed using the full-length LV-PGK probe. Nuclei were imaged with a Zeiss Axiovert epifluorescence microscope and then analysed with Photoshop 7.0 software (see also 2.2.3.1.1). Nuclei were divided into 5 concentric shells and the number of signals in each shell was counted. Shells are indicated on the X axis: 1 is the outermost shell and 5 the innermost. The bars show corresponding percentages (% , Y-axis) of FISH signals in a given shell. N indicates the number of analysed nuclei.

seemed to slightly affect the localization of the transgene in control cells, probably due to stress-induced reactions. However, in both cases 5-azaC treatment did not lead to a more interior positioning of the transgenic construct. This might be explained by the fact that the transgenic construct in these cell lines already localized in the interior transcriptionally permissive area.

3.2.4. Localization of the active LV-PGK construct in infected WT cells

To further address nuclear positioning and transcriptional activity of the LV-PGK retroviral construct primary WT fibroblasts were freshly infected in *in vitro* culture with the LV-PGK retrovirus (made by Dr. Andreas Hofmann, LMU Munich). As a result each cell had its own unique number of integrants, site of integration, and level of activity of the transgene. Highly expressing cells (data not shown) were selected and cultivated separately. After ~3 weeks the level of activity did not change and cells were fixed with methanol-acetic acid. FISH was performed as before using the full-length LV-PGK probe to visualize the transgene. Figure 46 A-D demonstrates that the number of integrants in infected cells was variable as expected but only nuclei with only 1 integrant (A) were selected for the erosion analysis. The result of the erosion analysis is shown in Figure 46. Most of the signals, ~ 40%, were found in the 2nd shell and ~ 30% were found in the 1st shell. The rest was found in 3rd, 4th and 5th shells (~ 5% - 15%). This result showed an interior positioning of the transgenic constructs. Together, these findings also suggested that the transgenic construct localized in the nuclear interior in its active state.

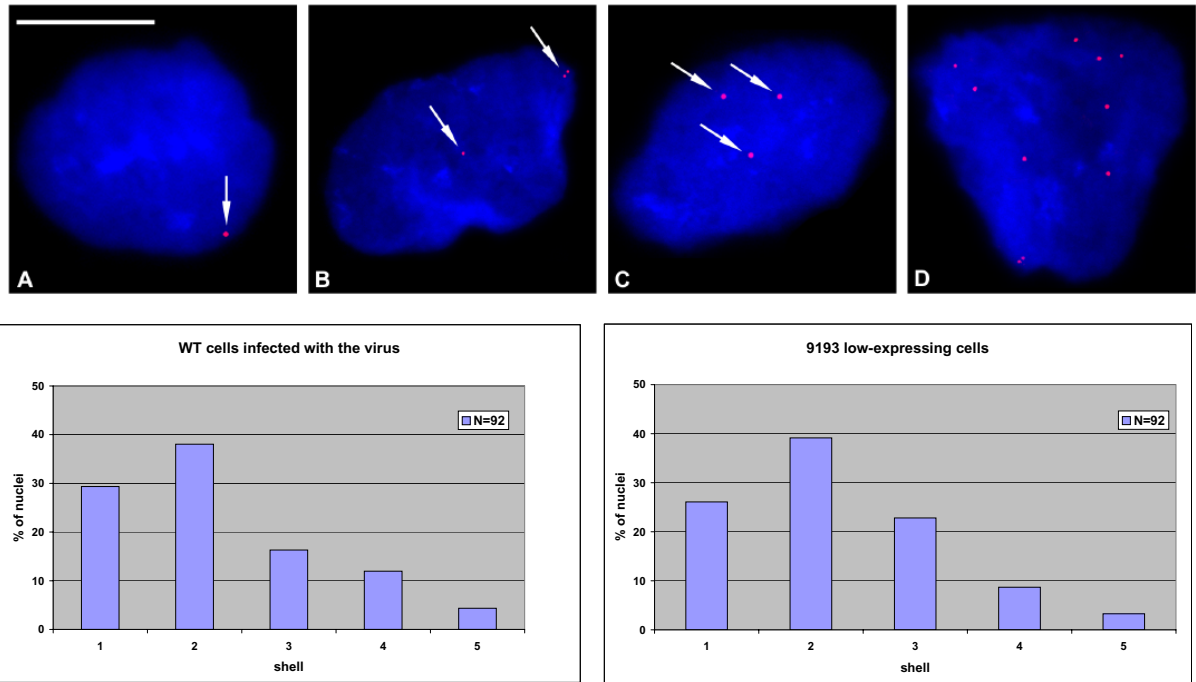


Figure 46. Nuclear position of the LV-PGK transgene in infected WT primary fibroblasts. Cells were fixed with methanol-acetic acid and FISH was performed using the full-length LV-PGK probe. FISH signals are shown in red, on images A-C they are additionally indicated with arrows. DNA was stained with DAPI and is shown in blue. Scale bar: 10 μ m. A - one integrant in a nucleus. B - two integrants, one doublet FISH signal. C - three integrants. D - multiple integrants in one nucleus. Epifluorescence images of WT nuclei with 1 FISH signal were analysed with Photoshop 7.0 (see also 2.2.3.1.1). Nuclei were divided into 5 concentric shells and the number of signals in each shell was counted. Shells are indicated on the X axis: 1 is the outermost shell and 5 the innermost. The bars show corresponding percentages (% , Y-axis) of FISH signals in a given shell. The left diagram shows the result of 2D erosion analyses of WT infected cells. The right diagram shows one of the previous results (Figure 43) obtained with the 9193 low-expressing transgenic cell line. N indicates the number of analysed nuclei.

3.3. The role of the Tpr protein in the nuclear positioning of the CFTR locus in HeLa cells

RNA interference (RNAi) is a highly conserved post-transcriptional gene silencing mechanism that uses double-stranded RNA (dsRNA) as a signal to trigger the degradation of homologous mRNAs (Elbashir et al., 2001a; Elbashir et al., 2002; Elbashir et al., 2001b). Moreover, RNAi can be efficiently applied to *in vitro* cultured cells to study gene function (Elbashir et al., 2001a). Here, I applied RNAi to knock-down the Tpr protein localizing at the nuclear periphery (Cordes et al., 1997). Previous studies suggested that such peripheral proteins and the nuclear lamina play an important role in gene positioning (Englmann, 2005; Goldman et al., 2002; Segura-Totten and Wilson, 2004; Vlcek et al., 2001). However, evidence for such a role *in vivo* is lacking. Recently it was shown that knock-down of Lamin A/C and lamina-associated proteins Lap2 β and Emerin leads to repositioning of the cystic fibrosis transmembrane conductance regulator (CFTR) locus from the nuclear periphery to the nuclear interior (Englmann, 2005). To investigate whether other proteins at the nuclear periphery also contribute to the spatial organization of chromatin, we studied the effect of downregulation of Tpr on the nuclear positioning of the CFTR locus in HeLa cells. Tpr is a filamental protein attached to the nuclear basket (Cordes et al., 1997). CFTR was chosen as a model system because its peripheral localization has been studied in detail (Zink et al., 2004).

3.3.1. The effect of the knock-down of Tpr on the nuclear localization of CFTR in HeLa cells

The knock-down of Tpr was performed with 25-nt siRNAs provided by Invitrogen (Karlsruhe, Germany). Two different Tpr siRNAs were tested (see also 2.1.3): sequence A which starts at nt 3352 of sequence U69668, and sequence C which starts at nt 4828 of sequence U69668 (Cordes et al., 1997). Transfection of HeLa cells (kindly provided by Dr. Volker Cordes, ZMBH, Heidelberg) with these siRNAs was carried out as described for other cell lines (Englmann, 2005). After treatment with A or C variants in about 75% of cells Tpr was present in very low amounts, often not detectable by immunostaining with a specific antibody (kindly provided by Dr. Volker Cordes, DKFZ, Heidelberg) (Figure 47). Cells which were not affected by the treatment usually formed small patches. This suggested that they were daughter cells of those few cells which were not transfected. Transfection with Tpr siRNA had a slight cytotoxic effect which appeared as reduced viability of cells. This effect was more pronounced for siRNA variant A. FISH worked better on cells transfected with siRNA variant C. For these two reasons siRNA variant C was used for the whole assay.

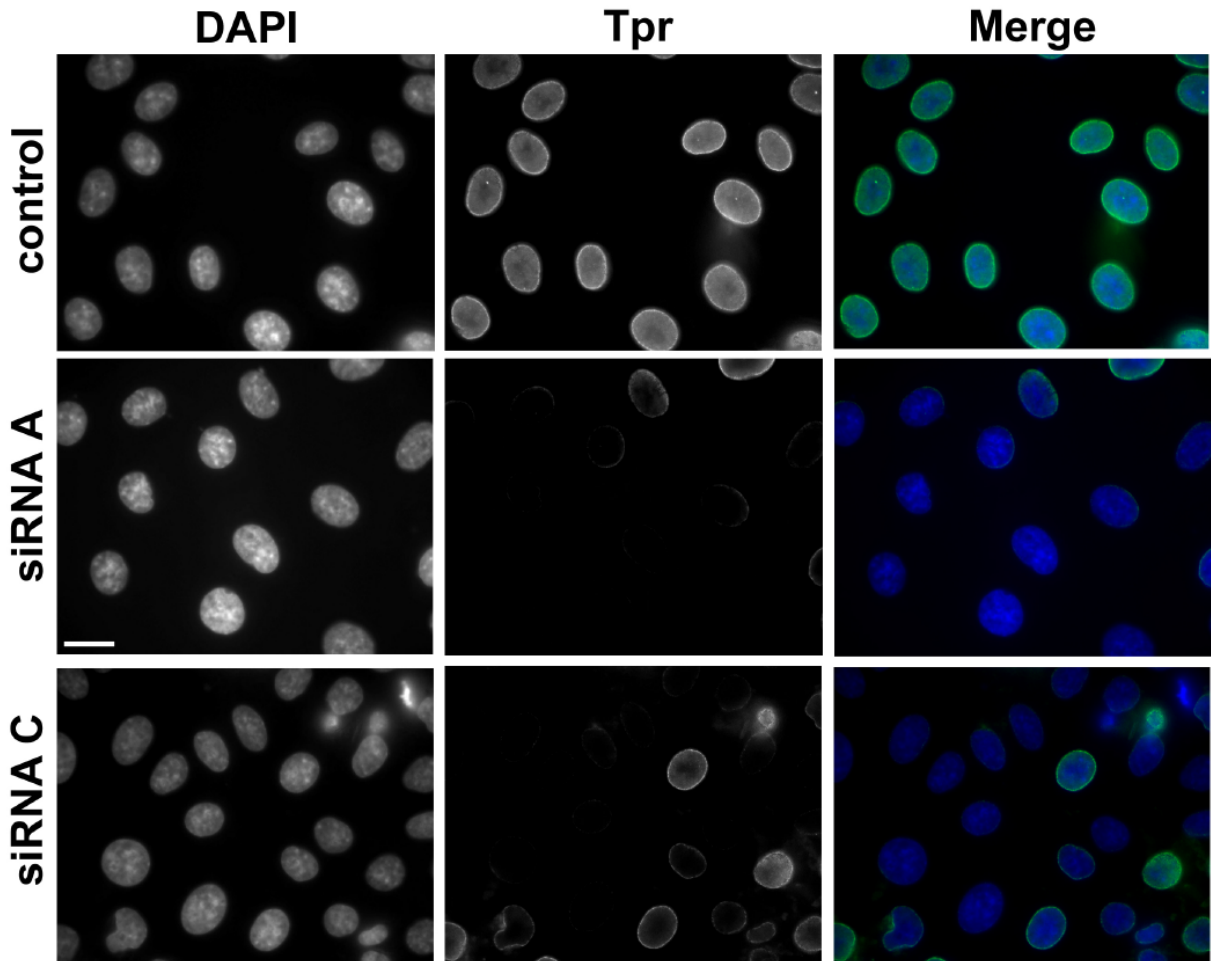
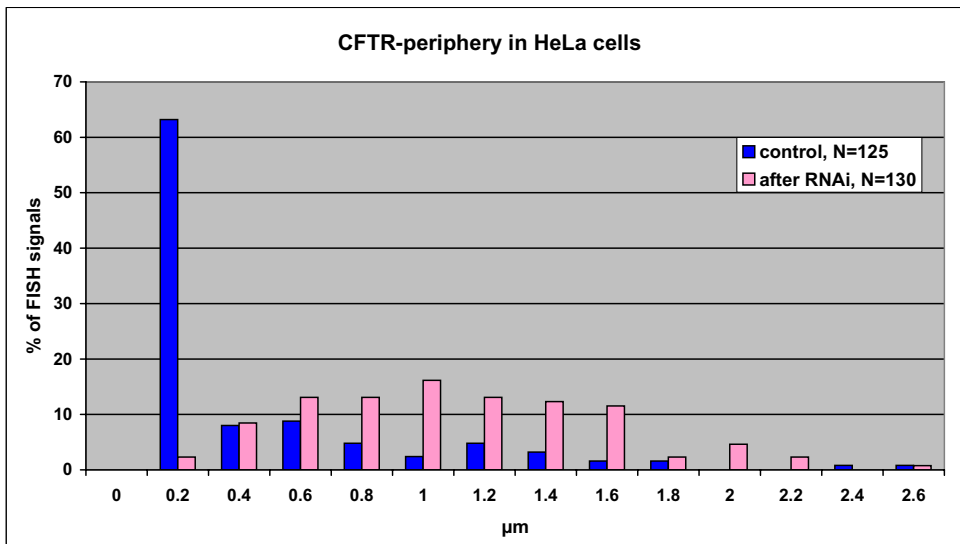
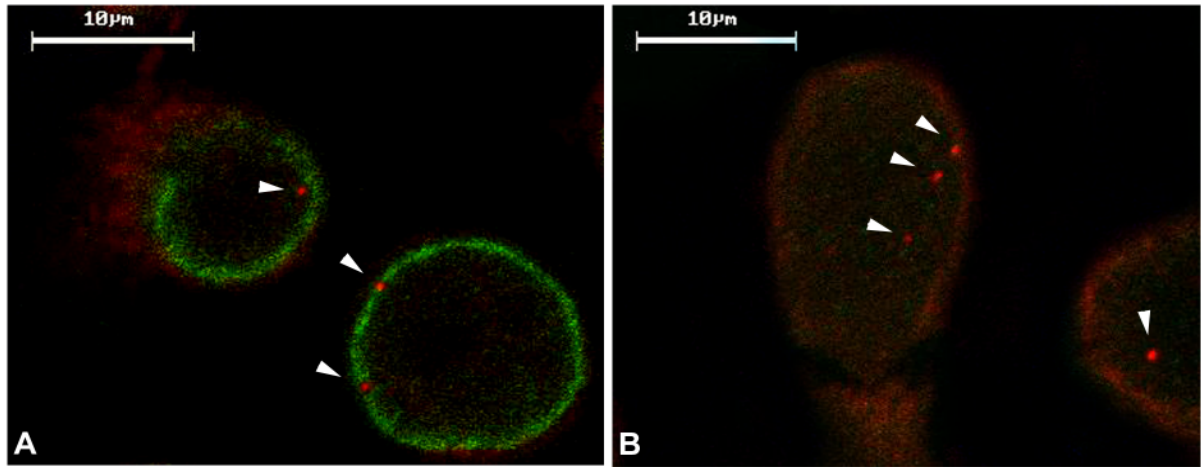


Figure 47. Knock-down of Tpr in HeLa cells. HeLa cells were transfected with two different siRNAs homologous to Tpr, sequences A and C. Cells were incubated with ~5 μ g of siRNA for 4 days in 6-well dishes, fixed with 3,7% formaldehyde and immunostained against Tpr (shown in green). DNA was visualized with DAPI and is shown in blue. The top row shows untreated cells while the middle and bottom rows show results obtained after incubation with siRNAs A and C, respectively. Scale bar: 10 μ m.

To find out whether the Tpr protein plays a role in the nuclear positioning of CFTR I compared the localization of CFTR in control and RNAi-treated HeLa cells. The CFTR locus was visualized with FISH using the CF1 probe (kindly provided by Dr. Andreas Englmann, LMU Munich) (Zink et al., 2004). Tpr was immunostained with specific anti-Tpr antibodies. After 3D immunoFISH nuclei were scanned using a Zeiss LSM 410 confocal microscope. From RNAi-treated cells only nuclei without Tpr staining were imaged and analysed. Assembly of 3D stacks and image analyses were performed with ImageJ software. The nuclear positioning of CFTR in control and RNAi-treated cells was evaluated by distance measurements between CFTR and the nuclear rim as described in 2.2.3.2.2. HeLa cells are hypotriploid and carry 3 copies of chromosome 7 on which the CFTR gene is located. Therefore up to 3 signals from CFTR were detected in each nucleus, and the analysis was performed for each signal independently.

The results of the distance measurements are shown in Figure 48 together with typical examples of control and RNAi-treated HeLa nuclei. In control cells CFTR was



Experiment	CFTR-periphery aver., µm	CFTR-periphery max., µm
Control cells	0.31	2.5
RNAi-treated cells	0.97	2.55

Figure 48. The nuclear localization of CFTR in control and RNAi-treated HeLa cells. Single light optical sections of control (A) and RNAi-treated (B) HeLa nuclei are shown. There are 3 copies of CFTR in HeLa cells, which are often not visible together on a single light optical section. The CFTR locus (red; indicated also with arrowheads) was visualized by FISH with the dig-labelled CF1 probe, which was detected with Cy3-conjugated anti-dig antibodies. Nuclei were immunostained with antibodies against Tpr. The corresponding secondary antibodies were FITC-conjugated and Tpr is shown in green (A). Note the absence of Tpr staining in RNAi-treated cells (B). Here, the nuclear border was still clearly detectable due to unspecific binding of Cy3-conjugated anti-dig antibodies. Nuclei were scanned using a Zeiss LSM 410 confocal microscope and analysed with ImageJ software. Results of distance measurements between the CFTR signals and the nuclear border are shown in the diagram. The X-axis shows distance intervals in microns. The bars indicate the percentages (% Y-axis) of FISH signals within a given distance interval to the nuclear periphery. N indicates numbers of FISH signals analysed in control (blue) and RNAi-treated (pink) cells. The average and maximal distances between CFTR and he nuclear periphery (in microns) are shown for each case in the table below the diagram.

preferentially associated with the nuclear periphery: more than 60% of FISH signals were within 0.2 μm from the nuclear rim (Figure 46, blue in the diagram). The average distance between CFTR and the nuclear border was 0.31 μm (see the table below the diagram). After RNAi treatment, the localization of CFTR changed dramatically (pink in the diagram): only ~20% of signals were found within 0.6 μm , and most of them were 1 to 1.6 μm apart from the nuclear border. The average distance between CFTR and the nuclear rim in RNAi-treated cells was 0.97 μm (the table below the diagram). Examples of control (A) and RNAi-treated (B) HeLa cells are shown above the diagram, displaying a clear difference in the localization of CFTR. These results suggest that Tpr plays a role in the peripheral positioning of CFTR.

As a control I performed a transfection of HeLa cells with FITC-labelled non-specific siRNA as described in Englmann (2005) and analysed the position of the CFTR locus in comparison to untreated cells. No positional shift occurred after transfection with the non-specific siRNA (data not shown).

3.3.2. The knock-down of Tpr induced a positional shift of CFTR without changing its transcriptional activity

The knock-down of Tpr resulted in repositioning of CFTR into the nuclear interior. To test whether localization in this transcriptionally permissive nuclear environment led to induction of CFTR we used semiquantitative RT-PCR analyses. However, first Western Blot analyses were made (kindly performed by Dr. Andreas Englmann, LMU Munich) to ensure that Tpr was successfully knocked down after siRNA transfection (Figure 49). Cells transfected with 5 μg of siRNA (the same amount was used for RNAi treatment for the immunoFISH experiments described above) showed ~75% reduction of the amount of the Tpr protein (Figure.49, lane 3). The quantification of the intensity of the bands was evaluated by measuring their mean grey values with Image J and Photoshop 7.0 as described in (Englmann, 2005). This result was in agreement with the visual evaluation of immunostaining intensities (Figure 47).

Semiquantitative RT-PCR analyses in control and RNAi-treated HeLa cells were kindly performed by Dr. Nicolas Sadoni, LMU Munich. The results of these analyses are shown in Figure 50. β -actin cDNA was used as a control. Calu3 cells, where CFTR is highly expressed (Zink et al., 2004), were used as a positive control. CFTR expression was not detected in control or RNAi-treated HeLa cells (Figure 50, lanes 5-12). Thus, RNAi-treatment of HeLa cells led to a positional shift of CFTR towards the nuclear interior but did not induce transcriptional activity.

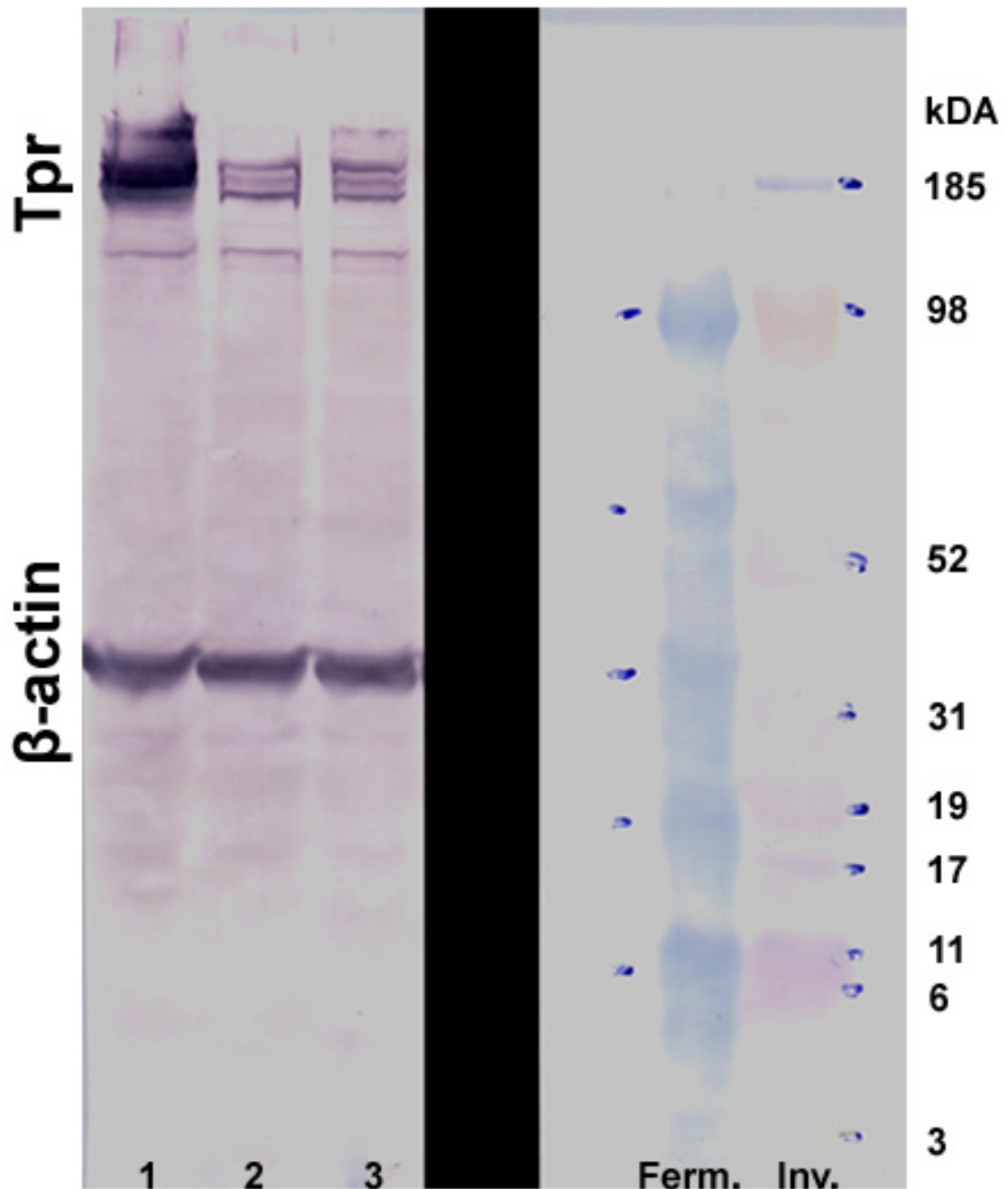


Figure 49. Western Blot analysis of HeLa cells after transfection with siRNA C (courtesy of Dr. Andreas Englmann, LMU Munich). HeLa cells were grown to ~60% confluency in a 6-well dish, transfected with 0 nM (lane 1), 125 nM or 250 nM (lanes 2 and 3, respectively) siRNA C and harvested after 4 days. β-actin was used as a control. Tpr was detected with the same mouse monoclonal antibody as was used in immunostaining and immunoFISH experiments (kindly provided by Dr. Volker Cordes, ZMBH, Heidelberg). Two markers were used: Fermentas Prestained (Ferm.) and Invitrogen MultiMark (Inv.). Molecular weights (kDa) are indicated for the Invitrogen marker. Several bands were detected with the anti-Tpr antibody. Only the band at the very top (molecular mass ~270 kDa) correspond to Tpr. The other bands are putative degradation products (Cordes et al., 1997).

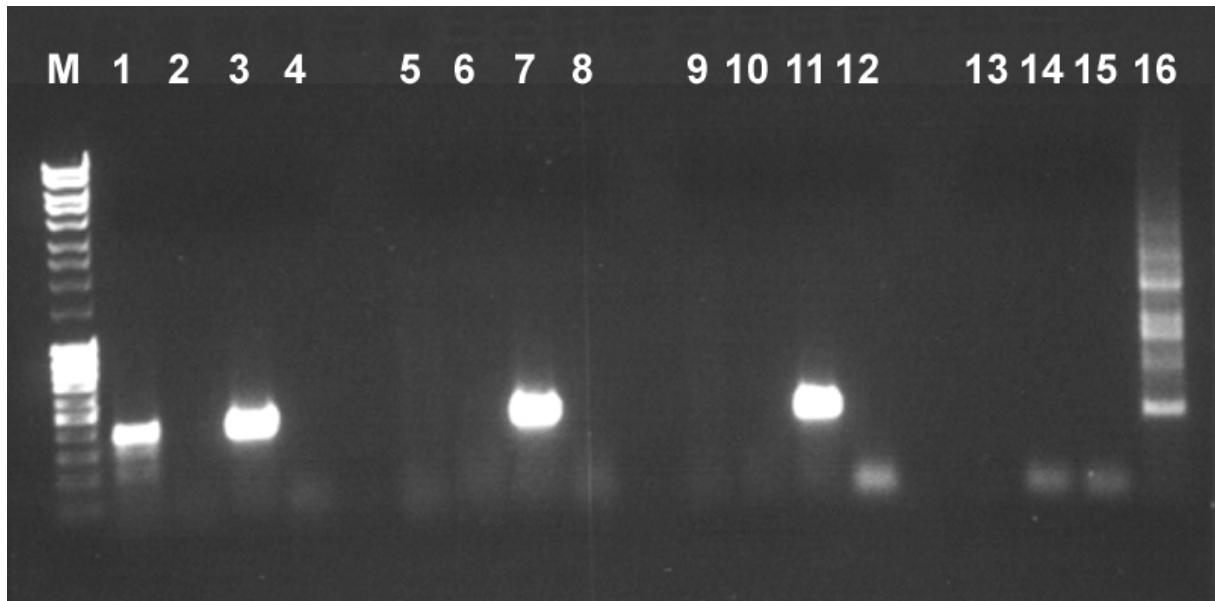


Figure 50. Semi-quantitative RT-PCR analyses of CFTR expression in RNAi-treated HeLa cells (courtesy of Dr. Nicolas Sadoni, LMU Munich). Total cellular mRNA from Calu-3 control cells (CFTR is expressed), HeLa control cells (CFTR is not expressed) and RNAi-treated HeLa cells was extracted using the RNeasy Mini Kit (Quiagen, Hilden, Germany) according to manufacturer's instructions. mRNA was reverse transcribed into cDNA. cDNA or RNA (control), respectively, were incubated with specific primers to generate ~600 bp fragments of CFTR or β -actin (control). 20 μ l of the reaction products were mixed with 5 μ l of 6x OLD and loaded into 1% agarose gel together with the marker (M; Mass Ruler, Fermentas). The lanes show PCR products from following templates with corresponding primers: 1. cDNA from Calu cells with primers specific for CFTR (see 2.1.3.). 2. Total RNA from Calu cells with primers specific for CFTR (control). 3. cDNA from Calu cells with primers specific for β -actin. 4. Total RNA from Calu cells with primers specific for β -actin (control). 5. cDNA from control HeLa cells with primers specific for CFTR. 6. Total RNA from control HeLa cells with primers specific for CFTR (control). 7. cDNA from control HeLa cells with specific primers for β -actin. 8. Total RNA from control HeLa cells with primers specific for β -actin (control). 9. cDNA from RNAi-treated HeLa cells with primers specific for CFTR. 10. Total RNA from RNAi-treated HeLa cells with primers specific for CFTR (control). 11. cDNA from RNAi-treated HeLa cells with primers specific for β -actin. 12. Total RNA from RNAi-treated HeLa cells with primers specific for β -actin (control). 13. No template, primers specific for CFTR (control). 14. No template, primers specific for β -actin (control). 15. Distilled water from the 1st strand cDNA synthesis kit, no template, primers specific for β -actin (control). 16. neo cDNA (synthesized from the control neo RNA with primers, provided with the kit).

4. Discussion

4.1. Positioning of the PRE Fab-7 in nuclei of *Drosophila melanogaster*

In the first part of this thesis the spatial organization of the PRE Fab-7 in interphase nuclei of *Drosophila* larval tissues was investigated. The results showed that transgenic copies of Fab-7 did not associate with endogenous copies of Fab-7 in nuclei of brain, anterior epidermis, anterior midgut, malpighian tubules and fat body cells. Active transgenic copies often located at the boundary of heterochromatin. Also active endogenous PREs were found in close association with this boundary. The boundary of the heterochromatic domain was enriched in histone H3 di- and trimethylated at lysine 4, the active form of RNA pol II (phosphorylated at Ser 2), and the pericentromeric satellite repeat (AAGAG)_n. These findings suggest that enrichment of heterochromatic repeats and factors associated with active chromatin states at the boundary between heterochromatin and euchromatin plays a role in the functional separation of these two different chromatin fractions. The euchromatic side of this boundary enriched in factors associated with active chromatin states might provide a favourable environment for PREs in active state.

4.1.1. The spatial organisation of different chromatin fractions in nuclei of *Drosophila melanogaster*

In order to address the spatial organization of different chromatin fractions in nuclei of *Drosophila melanogaster*, antibodies specific for a variety of different histone modifications and chromatin associated proteins were used here for immunostaining experiments with larval nuclei. In *Drosophila*, localization of many different epigenetic marks was studied previously by immunofluorescence on larval polytene chromosomes from salivary glands (Chinwalla et al., 1995; Rastelli et al., 1993; Rozovskaia et al., 1999; Schotta et al., 2002; Turner et al., 1992), by CHIP experiments on Kc cells (Schubeler et al., 2004), also in chromatin from embryonic nuclei (Czermin et al., 2001; Giancotti et al., 1984). The spatial nuclear organization of centric heterochromatin has been described previously in several larval tissues of *Drosophila*: salivary gland, prothoracic gland, hindgut and middle midgut (Hochstrasser and Sedat, 1987a; Hochstrasser and Sedat, 1987b; Schotta et al., 2002), brain (Huang et al., 1998), and eye imaginal disc (Thakar and Csink, 2005). Since it was shown that histone H3 dimethylated at lysine 9 (dimH3K9) is mainly concentrated in pericentromeric heterochromatin (Byrd and Shearn, 2003; Schotta et al., 2002), I used antibodies against dimH3K9 to visualize this domain in nuclei from anterior epidermis, malpighian tubules, fat body cells, anterior midgut

and salivary glands. I found that in all analysed tissues heterochromatin usually forms one huge and distinct compartment which occupies up to 30% of the nuclear volume and is often in contact with the nuclear lamina. In the present work, similar data were obtained for larval tissues and Kc cells, and these observations are in agreement with previously published results (Ahmad and Henikoff, 2001; Ahmad and Henikoff, 2002; Hochstrasser and Sedat, 1987a; Schotta et al., 2002; Sullivan and Karpen, 2001). My data showed that the nucleoli were often associated with the heterochromatic domain (Figure 11 D, S), which is in agreement with previous observations in *Drosophila* salivary gland nuclei (Hochstrasser and Sedat, 1987b; Kaufmann, 1938) and with the fact that nucleolar-organizing regions (NORs) are localized in the heterochromatin of the X chromosome (Appels and Hilliker, 1982; Hochstrasser and Sedat, 1987a). It had been suggested that heterochromatin somehow shields NORs and centromeres (Manuelidis, 1990).

Centromeric DNA in *Drosophila* is flanked by highly repetitive satellite DNAs, which are packaged into heterochromatin (Csink and Henikoff, 1998b), and it was proposed that this forms a compartment at interphase stage in which centromeres are embedded in heterochromatin (Ahmad and Henikoff, 2002). Most of the pericentromeric satellite DNAs are chromosome-specific, but one of them, the (AAGAG)_n repeat, is found in pericentromeric regions of all chromosomes (Dernburg et al., 1996; Lohe et al., 1993). In the present study, we visualized the AAGAG repeat by FISH and the heterochromatic domain with an antibody against dimH3K9. In nuclei from larval tissues and Kc cells we found that the satellite DNA was exposed at the boundary of the heterochromatic compartment, forming several aggregations at this position (see 3.1.1 and Figure 12). The localization of pericentromeric satellite repeats with regard to heterochromatin was not studied before. In studies of other research groups, only the positioning of centromeres relative to the heterochromatic domain was investigated in Kc and S2 cell cultures, and the obtained results were contradicting. In some studies, centromeres were found enclosed within heterochromatin (Ahmad and Henikoff, 2001; Ahmad and Henikoff, 2002), while another research group showed that centromeres were widely distributed throughout interphase nuclei and were not sequestered to a single nuclear location (Sullivan and Karpen, 2001). Since the localization of the pericentromeric DNA does not necessarily reflect the localization of centromeres, it is difficult to say how results of the present work correspond to the data of previous studies.

Nevertheless, the results obtained here show that the chromocenter in *Drosophila* nuclei has a defined spatial organization. Intriguingly, also mouse chromocenters have a comparable radial organization: minor satellites and centromeres are exposed at the periphery of chromocenters (which consist of major satellites of different chromosomes, associated in clusters) as several individual spots (Guenatri et al., 2004; Martin et al., 2006; Weidtkamp-Peters et al., 2006). It was proposed that distinct replication timing

and / or epigenetic barriers exist between major and minor satellite domains, which would allow them to assemble different chromatin components according to their role (Guenatri et al., 2004). Together, these data suggest that *Drosophila* and mouse heterochromatic domains have specific spatial organizations that appear to be of functional significance.

4.1.2. The spatial organization of factors associated with euchromatin

Isoforms of histone H3 methylated at lysine 4 of histone H3 and hyperacetylation of histone H4 are typical marks of active chromatin domains (Cavalli and Paro, 1999; Noma et al., 2001; Santos-Rosa et al., 2002; Schubeler et al., 2004). Therefore, I used antibodies against histone H3 di- and trimethylated at lysine 4 (dimH3K4 and trimH3K4, respectively) and hyperacetylated histone H4 (H4ac) to investigate the spatial distribution of these characteristic marks. The relationships between dimH3K4 and trimH3K4 were especially interesting for me, since previous studies suggested that their distribution is different in yeast and *Drosophila*. In *S. cerevisiae*, it was shown that dimH3K4 is a modification which is typical for euchromatic regions (Noma et al., 2001) and occurs at both transcriptionally active and silent euchromatic genes, while trimH3K4 is restricted to active loci (Santos-Rosa et al., 2002). In *Drosophila*, however, both of these modifications showed a similar distribution and were preferentially associated with active loci (Schubeler et al., 2004). I simultaneously visualized trimH3K4 and the active form of RNA pol II (phosphorylated at Ser 2) and found that almost all transcriptionally active sites carried the trimH3K4 mark (3.1.1., Figure 11 M-P). Also, only very few trimH3K4 domains did not colocalize with local enrichments of the active form of RNA pol II. However, simultaneous detection of dimH3K4 and RNA pol II showed that dimH3K4-enriched sites were rarely transcriptionally active (Figure 11, Q-T). Thus, the results obtained here imply that in interphase nuclei of *D. melanogaster* di- and trimethylated isoforms of H3K4 occur in different fractions of euchromatin, corresponding to the results obtained with yeast (Santos-Rosa et al., 2002). The fact that our results are not in accordance with the data obtained with Kc cells by Schubeler et al. (2004) could be explained by differences between *in vitro* cultured cells of embryonic origin and larval tissues.

I found that transcriptionally active sites enriched in trimH3K4 were not evenly distributed throughout the nucleoplasm but formed specific patterns in all nuclei analysed (Figure 11 U-Y, see also Figure S1 on the supplementary CD). In some cases these active sites accumulated into larger clusters (Figure 11 V, the upper arrowhead), but mostly they were arranged into distinct large circles or semicircles in the nuclear interior and at the nuclear periphery (Figure 11 U-Y, see also Figure S1). These circles were often connected to each other and might outline some kind of subcompartments within

nuclei. Multiple active sites and even clusters of them decorated the whole periphery of the nucleolus, and one of the most massive aggregations of active sites observed in all nuclei was also connected to the nucleolar periphery (Figure 11, W, X; see also Figure S1). Such patterns of active sites have not been described in larval nuclei so far. In embryonic nuclei, however, distribution of NONA (a protein colocalizing with the active form of RNA pol II on polytene chromosomes) and Hrb57A (a protein strongly associated with transcriptionally active loci), resembled large bending and looping patterns comparable to those we observed in larval nuclei with respect to trimH3K4 and RNA pol II (phosphorylated at Ser 2), although the loops formed by NONA and Hrb57A were fewer in number and smaller in sizes (Buchenau et al., 1993; Buchenau et al., 1998). Interestingly, NONA was also preferentially found at the nuclear periphery, although the distribution of this protein, observed *in vivo*, was very dynamic in some nuclei. It was also proposed that the arrangement of NONA in looping patterns reflects the organization of interphase chromatin (Buchenau et al., 1993). In this respect it is interesting that one of the models concerning the arrangement of interphase chromatin proposes that 30 nm fibers of chromatin are organized into flexible giant loops which contain several Mbp of DNA (Yokota et al., 1995). However, it is unclear whether this model can be applied to *Drosophila* nuclei, because it is based on results obtained with nuclei of human cells, and transcription sites in mammalian cells have a different spatial organization. Here, RNA pol II-mediated transcription was detected in up to two thousand domains which have the average diameter of 71 nm and are scattered throughout the nucleoplasm (Iborra et al., 1996; Jackson et al., 1993; Wei et al., 1999) but are not associated with perinuclear or perinucleolar regions (Sadoni et al., 1999). The specific organisation of active sites, which I observed in larval interphase nuclei, could also be caused by a specific arrangement of polytene chromosomes in the analysed tissue larval nuclei.

4.1.3. The association of active sites with the boundary of heterochromatin

Most interestingly, we found that all histone modifications typical for euchromatin, which were analysed here, were enriched at the boundary of the heterochromatic compartment. The numbers and shapes of these sites at the heterochromatic boundary were characteristic for each analysed modification: H4ac formed band-like structures, dimH3K4 was usually enriched in one large domain, whereas sites enriched in trimH3K4 were small and dot-like and there were several of them at the boundary of heterochromatin (Figure 11). The large dimH3K4-enriched domain did not appear to be transcriptionally active: pol II (phosphorylated at Ser 2) sites were found in its vicinity but colocalization was rarely observed (Figure 11, S). Sites enriched in trimH3K4 seemed to be transcriptionally active since they colocalized with RNA pol II

(phosphorylated at Ser 2) (Figure 11, P). Quantitative analyses should be performed in addition to characterize the degree of enrichment of trimH3K4 and RNA pol II at the boundary of heterochromatin. H4ac-enriched domains were not tested for association with pol II, but we suppose that they should also be transcriptionally active, since H4 hyperacetylation was shown to be one of epigenetic marks of transcriptionally active sites (Cavalli and Paro, 1999; Schubeler et al., 2004).

Localization of active euchromatic sites at the boundary of heterochromatin was rather unexpected since it is known that silent loci associate with heterochromatin in *Drosophila* as well as in mammals (Brown et al., 1997; Csink and Henikoff, 1996; Csink and Henikoff, 1998a; Dernburg et al., 1996; Schubeler et al., 2000; Zink et al., 2004). On the other hand, there exist about 40 of so-called heterochromatic genes in *Drosophila*, which reside in heterochromatin, require a heterochromatic environment for proper expression (Lu et al., 2000; Sun et al., 2001) and are prone to PEV if repositioned into an euchromatic environment (Weiler and Wakimoto, 1995). One of these genes, *light*, is located in the centromeric heterochromatin of chromosome 2 and is expressed in a number of larval tissues, including malpighian tubules (Devlin et al., 1990), the tissue which was used in the experimental work performed here. Being transcriptionally active, *light* should carry the corresponding epigenetic marks, or at least associate with pol II-enriched sites. However, in nuclei from malpighian tubules we did not observe pol II (phosphorylated at Ser 2)-enriched sites within the heterochromatic domain. Instead, active sites were consistently found at the boundary of heterochromatin. This suggests that *light* and maybe other heterochromatic genes are exposed at the surface of heterochromatin in order to be expressed. Such positioning would provide them with the proper heterochromatic surrounding and might make them at the same time accessible to the transcription machinery. This idea is supported by results of a recent study performed with a heterochromatic $\lambda 5$ transgene in mice. The transgene was integrated into pericentromeric chromatin and was visualized with FISH. In its inactive state it resided within heterochromatin, while upon transcriptional activation it was relocated to the boundary of heterochromatin but still remained in contact with it (Lundgren et al., 2000).

Here, it was investigated whether chromatin domains displaying other epigenetic marks were also associated with heterochromatin in *Drosophila* larval nuclei, and if yes, whether they would be enclosed within heterochromatin or associate with its border. To address this question, I investigated the spatial organization of Pc-binding sites with regard to the heterochromatic compartment. In all nuclei analyzed we consistently found several Pc-binding sites closely associated with the boundary of heterochromatin (Figure 37 H-J; see also Figure S2 on the supplementary CD). It should be noted that in contrast to nuclei from malpighian tubules (Figure 37), on polytene salivary gland chromosomes the Pc-binding sites were not directly adjacent to heterochromatin (Figure S2). Pc was not observed within heterochromatin, which

corresponds to results obtained with polytene salivary gland chromosomes and SL2 cells (Fischle et al., 2003; Zink and Paro, 1989). It was shown that although HP1 and Pc proteins harbour a chromodomain, the chromodomains of these proteins show different binding specificities and the chromodomain of Pc does not bind with high affinity to histone H3 methylated at lysine 9, which is enriched in heterochromatin (Fischle et al., 2003),

I also found that Pc-binding sites at the boundary of heterochromatin are associated with the active form of RNA pol II (Figure 39) but not with dimH3K4 (data not shown). The fact that endogenous sites simultaneously contain Pc (a repressor protein) and RNA pol II (a hallmark of transcriptional activity) is not very surprising. It was shown in one of the transgenic fly lines that the transgenic Fab-7 binds Pc in both inactive and transcriptionally active states (Cavalli and Paro, 1999). Recently it was also shown that PcG protein complexes PhoRC, PRC1 and PRC2 are constitutively bound to PREs of the Ubx locus in the ON as well as OFF stages (Papp and Muller, 2006). I also showed that Fab-7-containing transgenes are frequently associated with the boundary of heterochromatin in three transgenic fly lines after transcriptional activation (see 3.1.2.2., 4.3.). Thus, both transgenic and endogenous Pc-binding sites appear to associate with the boundary of heterochromatin in their active states.

Association with actively transcribed genes was also shown in *Drosophila* Schneider cells for two other members of the PcG, Polyhomeotic (Ph) and Posterior Sex Combs (Psc) (Strutt and Paro, 1997). In addition, Psc was found closely associated or even partially colocalizing with centromeric heterochromatin in *Drosophila* embryos, while Pc only showed a few spots of colocalization (Buchenau et al., 1998). Interestingly, a similar observation was made in human cells. There, proteins of the human PcG complex formed large aggregations in certain areas of the nucleus, which were termed "PcG bodies". In three cell lines PcG bodies were associated with pericentromeric heterochromatin of several chromosomes (Saurin et al., 1998). As discussed above, I showed that in *Drosophila* nuclei pericentromeric satellite DNA is exposed at the surface of the heterochromatic compartment. Although I did not perform simultaneous detection of the satellite DNA and Pc-binding sites, it is arguable that Pc-binding sites at the boundary of heterochromatin could be associated with the pericentromeric repeats. However, the organization of PcG proteins in *Drosophila* (a multitude of single binding sites) and human (large aggregations) nuclei appears to be very different, and thus it is unclear to which extent these two organisms are comparable in this regard.

In summary, my results demonstrated that the boundary of heterochromatin has a complex organization, with intermingling euchromatic and heterochromatic sites. Figure 51 shows a schematic representation of the sites which we found at the boundary of heterochromatin. The (AAGAG)_n pericentromeric repeat was observed exclusively at the surface of the heterochromatic domain, while euchromatic sites were also found elsewhere in the nucleus (Figure 51). We propose that the complex

architecture of the boundary of heterochromatin is involved in maintaining the equilibrium between euchromatin and heterochromatin and, consequently, the balance between transcriptional activation and repression (red arrows in Figure 51). The data showed that inactive Pc-binding sites are localized at the nuclear periphery, while they were found at the boundary of heterochromatin at transcriptionally active states. We suggest that this region, enriched in active factors, provides a favourable environment for such active sites.

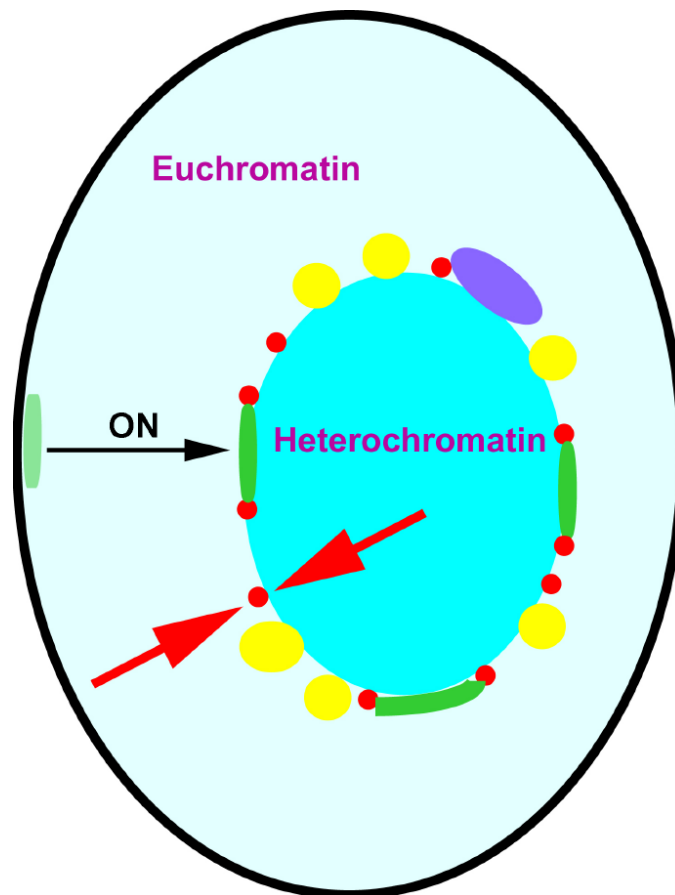


Figure 51. The model shows schematically factors found in close association and enriched at the boundary of heterochromatin (cyan; euchromatin: light blue). Yellow: (AAGAG)_n pericentromeric satellite repeat, violet oval: dimh3K4, red: the active form of RNA pol II (these sites are also enriched in trimH3K4), and dark green: Pc-binding sites associated with sites enriched in RNA pol II (phosphorylated at Ser 2). Inactive Pc-binding sites (light green) are often associated with the nuclear periphery (black). In accordance with results obtained in this work it is suggested that inactive Pc-binding sites relocate from the nuclear periphery to the boundary of heterochromatin upon activation (black arrow, ON). The boundary of heterochromatin enriched in factors associated with active chromatin might provide a favourable environment for active PREs. It is suggested that the specific enrichment and arrangement of satellite repeats and active and / or distinctly marked euchromatic sites helps to maintain the equilibrium between activation and repression (red arrows) at this boundary between eu- and heterochromatin.

Complex spatial interactions between the euchromatic and heterochromatic domains, which we discovered in *Drosophila*, were not observed before either in mammals or in flies. Recently, however, striking results were obtained with 3D *in*

in vitro cultures of chicken cells (Berchtold et al., submitted). In this study, rosetted retinospheroids (RS) derived from embryonic chicken retinal cells were used as a model for cells organized into 3D environments. It was shown that in RS nuclei GC-rich microchromosomes, which contain in chickens most of the transcribed genes, were enriched around chromocenters, in contrast to AT-rich macrochromosomes which occupied peripheral positions (Berchtold et al., submitted). Most interestingly, in monolayer cells no such higher order organization was observed. Results of this and other experiments demonstrated that nuclear organization in 2D and 3D *in vitro* cultures of chicken cells has different levels of complexity (Berchtold et al., submitted). Together with these data, the results of the present work suggest two possible explanations of the fact that the complex organization of heterochromatin was not observed before. In mammals, monolayer *in vitro* cell cultures are used in the absolute majority of cases. In the light of results obtained by Berchtold et al. (submitted) it is likely that investigation of 3D cultures or tissue samples will reveal new aspects of the nuclear organization, and probably also with regard to the spatial organization of heterochromatin. In flies, *in vitro* Kc cell cultures are used as well as embryos, larval imaginal discs and larval brain, all of which have very small and densely packed nuclei. Together with limitations of the currently available light microscopy, a detailed analysis of the boundary of heterochromatin is difficult in these popular model systems. Therefore, results of the present study also indicate that other than the preferentially used larval tissues might be better model systems to address nuclear organization.

4.1.4. Factors that contribute to the subnuclear localization of chromatin in *Drosophila*

In this thesis I also investigated the nuclear positioning of inactive endogenous loci in *Drosophila* larval tissues. I performed for the first time a quantitative evaluation of distances between three endogenous loci and the nuclear lamina / heterochromatic compartment. The results indicated that the nuclear periphery and not pericentric heterochromatin might contribute to the silencing of these genes, and that gene positioning in *Drosophila* might be regulated at the level of individual genes in a tissue-specific way.

4.1.4.1. The nuclear envelope and the localization of inactive endogenous loci in *Drosophila*

Since it became clear that the nuclear localization of gene loci might be an important determinant of their functional regulation, the role of different nuclear

compartments in gene regulation was investigated. Many studies, performed with yeast and mammalian cells suggest that particularly two nuclear compartments participate in gene silencing: the nuclear periphery (Andrulis et al., 1998; Dietzel et al., 2004; Kosak et al., 2002; Tumber and Belmont, 2001; Zink et al., 2004) and heterochromatic domains (Brown et al., 1997; Skok et al., 2001; Schubeler et al., 2000). Also corresponding studies performed with *Drosophila* suggested that the nuclear periphery and heterochromatin are involved in gene silencing (Csink et al., 2002; Pickersgill et al., 2006). At the moment, only three studies performed with *Drosophila* tissues or cells include 3D distance measurements between a gene locus and a nuclear compartment. In embryos and larval neuroblasts, distances between the *bw* locus and a fraction of heterochromatin represented by the (AACAC)_n satellite repeat were measured in 3D data sets acquired by epifluorescence microscopy and subsequent deconvolution (Csink et al., 2002; Dernburg et al., 1996). Further development of microscopic and software tools, which allow more precise distance measurements, provided possibilities to study more closely the role of gene positioning in functional regulation. Recently, very precise 3D distance measurements between a FISH signal and the nuclear rim were performed in nuclei from Kc cells with data sets obtained with confocal laser scanning microscopy (Pickersgill et al., 2006).

I investigated in anterior larval tissues the nuclear localization of *Abd-B*, *Ubx* and *sd* relative to the nuclear lamina and heterochromatin. In these nuclei from anterior epidermis and malpighian tubules all three genes were inactive. Gene loci were detected by FISH, while the nuclear lamina and heterochromatin were immunostained with specific antibodies against *Drosophila* lamin Dm₀ and dimH3K9, respectively. Nuclei were imaged using a Leica SP2 confocal laser scanning microscope and distances between FISH signals and the nuclear lamina or heterochromatin were measured in 3D data sets. These two compartments were selected because they are regarded as the major repressive domains in the nucleus. Such measurements in larval tissues of *Drosophila* were performed for the first time.

Ubx and *Abd-B* belong to the Bithorax Complex (BX-C) and are positioned close to each other on the right arm of chromosome 3 (loci 89 D6-9 and 89 E4-5, respectively), while *sd* maps to the band 13F on the X chromosome. Thus, using these three genes it was possible to compare the positioning of two neighbouring genes as well as the positioning of loci located on different chromosomes. The results showed that all three genes were preferentially associated with the nuclear lamina in both tissues and all analysed fly lines. However, the exact nuclear positioning of the genes was tissue- and fly line-specific (3.1.2.1.). As neither of these genes displayed any particular association with pericentromeric heterochromatin (3.1.2.1.), we concluded that this compartment did not play a major role in silencing of the endogenous loci.

In *Drosophila melanogaster*, several components of the nuclear envelope were identified, including derivatives of the lamin Dm₀ protein, YA (“young arrest”), otefin

and lamin C (see (Goldberg et al., 1999) for review). Lamin Dm₀ plays an important role in nuclear organization: it was shown that flies homozygous for mutations in the lamin Dm₀ gene have aberrant nuclear structure and die early in development, after depletion of the maternal pool of lamin Dm₀ (Harel, 1998). *In vitro* studies demonstrated that the C-terminal (tail) domain of lamin Dm₀ binds chromatin and histones H2A and H2B (Goldberg et al., 1999). Studies in *C. elegans* and mammalian cells suggested that lamins and their associated proteins are indeed involved in chromatin organization *in vivo* (Englmann, 2005; Liu et al., 2000). In the light of these data our results indicate that *Drosophila* lamin Dm₀ probably contributes to the organization of chromatin in larval tissues.

Our observations are also in agreement with data obtained recently with *Drosophila* Kc cells (Pickersgill et al., 2006). In this study, Pickersgill et al. (2006) performed a genome-wide search for genes which interact with the nuclear lamina. Using the DamID method to detect binding sites of *Drosophila* lamin, about 500 genes were identified which interact with the nuclear lamina in Kc cells. Several features were characteristic for lamina-binding genes in Kc cells. (a) Genes were transcriptionally repressed; (b) they were often clustered, and (d) they were not bound by HP1 and Su(var)3-9, two markers of pericentric heterochromatin. Pickersgill et al. also compared their results to the pattern of nuclear envelope contacts of polytene chromosomes, which was previously analysed in nuclei from salivary glands, prothoracic glands and midgut (Hochstrasser and Sedat, 1987b). The correspondence in gene positioning between diploid Kc cells and polyploid larval tissues was high but incomplete, suggesting cell type-dependent factors that regulate the association with the nuclear periphery (Dernburg et al., 1996; Pickersgill et al., 2006). Also this was in accordance with our results, which indicated tissue-specific influences on the localization of genes at the nuclear periphery (3.1.2.1.). It is known that chromatin in interphase nuclei is very mobile, as demonstrated by data from yeast cells (Heun et al., 2001; Marshall et al., 1997), *Drosophila* embryos (Buchenau et al., 1993; Marshall et al., 1997) and larval tissues (Csink and Henikoff, 1998a; Hochstrasser and Sedat, 1987b; Thakar and Csink, 2005). Such movements of chromatin could influence the frequency of association with the nuclear periphery and account for the tissue- and cell type-specific organization of chromatin.

To obtain more information about the role of the nuclear architecture in the functional regulation of endogenous genes in *Drosophila*, it would have been interesting to perform the same measurements in tissues where these endogenous genes are transcriptionally active. Unfortunately, after the experiments described above were completed, we ran out of probes and could not perform these additional experiments within a reasonable time period.

In summary, our results together with the data from Pickersgill et al. (2006) show that repressed loci preferentially associate with the nuclear periphery and that these

associations are mediated by lamin Dm₀. Furthermore, the results suggest that the same mechanisms operate in embryonic Kc cells and in nuclei from larval tissues.

4.1.4.2. The positioning of *Abd-B* and *Ubx* in transgenic flies

Distance measurements between FISH signals from genes and the nuclear lamina revealed a noticeable difference between gene loci located on different chromosomes. *Sd* (chromosome X) was positioned extremely peripherally in both tissues of all analysed fly lines, WT as well as transgenic (Figure 16). On the contrary, the peripheral localization of *Abd-B* and *Ubx*, which are juxtaposed on 3R, showed strong tissue- and fly line-specific influences (Figures 14 and 18, respectively). This result indicated a possible influence of the chromosomal background on gene positioning. Interestingly, *Abd-B* and *Ubx* showed major differences in nuclear positioning. This indicates that these two loci localize independently from each other, which is in accordance with data obtained with the CFTR locus in human cells (Zink et al., 2004). In that study, it was shown that intergenic regions of only 50 kb provide enough flexibility for independent positioning of three genes from the CFTR locus. In the BX-C of *Drosophila* intergenic regions are much larger, and the distance between the midpoints of the probes used here for *Abd-B* and *Ubx* is ~250 kb (Lewis et al., 1995), which suggests that these genes can indeed be positioned according to their individual properties. In fact, even distances between *Abd-B* and its regulatory element Fab-7, measured in individual nuclei of FLW-1 larvae, ranged from 0.2 µm to 0.73 µm (data not shown). These distances exceed those measured between CFTR and adjacent genes (Zink et al., 2004)

Positional differences between *Abd-B* and *Ubx* were particularly pronounced in tissues from FLW-1 transgenic larvae (Figures 14 and 18). FLW-1 transgenic flies carry two transgenic constructs: the Fab-7-containing 5F24 construct (Figure 2) at the *sd* locus (Zink and Paro, 1995) and a GAL4 driver on a balancer chromosome (Cavalli and Paro, 1998). *Ubx* showed an extreme peripheral positioning in FLW-1 flies. Could this be caused by pairing with the 5F24 transgene? Results obtained by two different research groups indicated pairing of PREs in *Drosophila* larval imaginal discs (Bantignies et al., 2003; Vazquez et al., 2006). My results showed that the *sd* locus, where the transgene is inserted, displayed a very peripheral localization in FLW-1 flies (Figure 16). Therefore, if endogenous and transgenic Fab-7 PREs were paired also in the tissues analysed here, this interaction could be the reason for a more peripheral localization of *Ubx*. However, since the endogenous Fab-7 element is localized in the regulatory region of *Abd-B*, one would expect a similar or even more peripheral positioning of the *Abd-B* locus. This, however, was not observed. Instead, in nuclei from malpighian tubules *Abd-B* showed an even more interior positioning in comparison to

WT flies (Figure 14). This result implied that presumable interactions between Fab-7 PREs do not influence the localization of the *Ubx* gene. However, pairing between the transgenic Fab-7 element and other PREs from the *Ubx* regulatory region cannot be excluded.

Next, I analysed *Ubx* positioning in tissues from 5F24 25,2 transgenic larvae (Zink and Paro, 1995). This line differs from FLW-1 only by the absence of the GAL4 driver on a corresponding balancer chromosome. In fact, the FLW-1 line has been derived from 5F24 25,2 flies by crossing in the GAL4 driver (Cavalli and Paro, 1998) and thus both lines carry an identical Fab-7-containing construct integrated into the *sd* locus. Surprisingly, in these flies *Ubx* showed a similar positioning as in WT flies (Figure 18). This suggests that the presence of the balancer chromosome with the GAL4 driver, and not the presence of the transgenic Fab-7 element, led to the extreme peripheral positioning of *Ubx* in FLW-1 flies. The mechanism of this interaction is unclear.

Together, the results suggest that Fab-7-containing transgenes do not influence the nuclear positioning of endogenous genes from the BX-C. However, the genetic background appears to be important, since a balancer chromosome can influence the nuclear localization of the *Ubx* gene. These findings underline the complex interactions within the nucleus which regulate the spatial organization of chromatin.

4.1.5. The nuclear localization of active and inactive Fab-7-containing transgenes in larval tissues of *Drosophila*

In this chapter I will discuss the relationships between transcriptional activity and nuclear positioning of transgenic constructs. In this work I used larval tissues from several transgenic fly lines of *Drosophila melanogaster*, and the results showed that inactive transgenes were associated with the nuclear periphery, while in their active states they mostly occupied more interior positions. Surprisingly, active transgenes were often found at the boundary of the heterochromatic domain. The following paragraphs will discuss these findings in detail.

The results of this study showed that inactive endogenous loci occupy peripheral positions in *Drosophila* larval tissues. The genetic background and tissue specificity contributed to the regulation of this localization. An obvious question was whether transcriptional activity of a gene locus also affected its nuclear position in *Drosophila*. To address this issue, we used three transgenic fly lines: FLW-1, fLW-1 and FLFW-1 (Cavalli and Paro, 1998). The corresponding transgenic constructs 5F24, 5F3 and 24F6 (Figure 2) have different orientations and numbers of Fab-7 elements and were inserted into different chromosomal sites (Zink and Paro, 1995). Each of the transgenic constructs could be stably or transiently activated by a pulse of GAL4 at

embryonic or larval stages of development, respectively. Thus, using these transgenic lines it was possible to assess the influence of transcriptional activity, chromosomal localization, orientation and copy number of the transgenic Fab-7 element on the nuclear localization of the transgenic construct. I analysed these relationships in nuclei from anterior epidermis and malpighian tubules from 3rd instar larvae. In each fly line, the construct or its integration site was visualized with FISH (see 3.1.2.2.), while the nuclear lamina and heterochromatin were immunostained using specific antibodies. At each functional state of the transgene, nuclei were imaged with a Leica SP2 confocal microscope, and the distances between the transgene and the nuclear lamina or heterochromatin were measured in 3D data sets.

The results showed that all transgenic constructs displayed a high degree of association with the nuclear lamina in their inactive state (Figures 20, 23 and 25). This is in accordance with the results obtained with inactive endogenous loci, which also occupy peripheral positions in these tissues (3.1.2.1., 4.2.). This is also in accordance with the finding that lamina associated genes are typically silenced in *Drosophila* (Pickersgill et al., 2006). Also the data from other species indicated that the nuclear periphery is a repressive compartment in the nucleus (Andrulis et al., 1998; Dietzel et al., 2004; Tumber and Belmont, 2001; Zink et al., 2004). On the other hand, the localization of transcriptionally active transgenes in our study was dependent on their chromosomal insertion site. 5F24 and 5F3 transgenic constructs, which are inserted in the *sd* locus (X chromosome), displayed more interior localization after both stable and transient activation (Figures 20, 23). This was in agreement with previously obtained results which showed that transcriptionally active loci occupy more interior positions than inactive ones (Kosak et al., 2002; Tumber and Belmont, 2001; Zink et al., 2004). In contrast, the 24F6 transgene, which contains 2 copies of Fab-7 and is inserted into 61C9 (3L chromosome), showed after its activation a similar or even more peripheral (in malpighian tubules) localization in comparison to the inactive state (Figure 25). This result, although unexpected, is in agreement with the emerging view that the nuclear periphery is not simply a repressive nuclear domain but has a more complex role. In yeast cells, relocation of active genes to the nuclear periphery was observed, where they associated with NPCs (Casolari et al., 2004; Ishii et al., 2002). As discussed above, in larval tissues of *Drosophila* we found sites of active transcription not only in the nuclear interior but also at the nuclear periphery (4.1., Figure 11, Figure S1). Together with this observation, the peripheral localization of the 24F6 transgene in its active state suggests that there are transcriptionally permissive as well as repressive regions at the nuclear periphery. It is possible that the chromosomal localization of a transgene determines whether the transgene will move to the nuclear interior or keeps its association with the nuclear periphery after activation.

In agreement with the results discussed above (4.2.1.), inactive transgenes did not display any particular relationships with heterochromatin (Figures 21, 24 and

26). This indicated again that in larval tissues of *Drosophila* heterochromatin does not contribute to the silencing of the inactive loci investigated here. But most unexpectedly, we found that active transgenic constructs were frequently associated with the boundary of the heterochromatic domain. The degree of association was specific for the transgene, the tissue and the state of activity (Table 2). The effect was especially pronounced in FLW-1 flies where association with the boundary of heterochromatin occurred in 40% of epidermis nuclei and 48% of malpighian tubule nuclei after stable activation of the transgene (Table 2, Figure 22). Interestingly, the 5F3 transgene (FLW-1 flies) which differs from the 5F24 transgene (FLW-1 flies) only by the orientation of the Fab-7 element shows a much lesser frequency of association with heterochromatin (Table 2). (In both FLW-1 and fLW-1 lines the transgene is inserted into the *sd* locus). Figures 21 and 24 show different degrees of associations between these transgenes and heterochromatin than are shown in Table 2, because analyses of associations between FISH signals from the *sd* probe and heterochromatin were performed with Metamorph software (2.2.3.2.2.), while the direct distance measurements were made with Image J. Therefore, threshold values for the heterochromatic domain were different in these two analyses. Together, these differences explain the fact that the percentage of associations between *sd* and heterochromatin was much higher than that found by the direct distance measurements.

In all fly lines, an active transgene was never found embedded into heterochromatin. If the association occurred, it was always restricted to the boundary. Why would a domain, which is generally regarded as repressive, be a favourable location for an active transgene? Our investigation of heterochromatin in larval tissues demonstrated the presence of multiple sites enriched in the active form of RNA pol II and trimH3K4 at the boundary of the heterochromatic compartment (Figure 11, M-P). Thus, the repressive nature of this domain does not exclude transcriptional activity at its surface. Furthermore, some of the endogenous Pc-binding sites were also found closely associated with the boundary of heterochromatin (Figure 37 I, J), and most of them were associated with active RNA pol II / trimH3K4-enriched sites (Figure 39). These findings indicate that the boundary of heterochromatin is a favourable environment for active PREs. However, there are many sites of transcriptional activity elsewhere in the nucleoplasm as well (Figure 11, U-Y; Figure S1), and we also observed PREs in association with these nucleoplasmic sites (data not shown). Since the percentage of association of active transgenes with the boundary of the heterochromatic domain did not exceed 50% in the most extreme case, the results suggested that other nucleoplasmic sites are at least equally preferable. Considering these facts, I suggest that an active transgenic construct associates with the closest site of transcriptional activity. 5F24 and 5F3 transgenes (FLW-1 and fLW-1 flies, respectively) dissociate from the nuclear lamina upon activation, and this enables them to associate with a site of active transcription at the boundary of heterochromatin

as well as elsewhere in the nucleoplasm. The 24F6 transgene (FLFW-1 flies) does not relocate from the nuclear periphery upon activation, and also the percentage of its association with heterochromatin is only slightly increased after activation (Table 2). The observed 10% of association with heterochromatin could be explained by the fact that the heterochromatic domain in larval tissues is often associated with the nuclear lamina, and probably in such nuclei the active transgene could associate with a transcription site at its boundary without dissociation from the nuclear periphery.

My results showed that activated Fab-7-containing transgenes not only associate with heterochromatin, but remained active (monitored by β -galactosidase expression, data not shown). In this regard it is interesting that Fab-7 belongs to a group of regulatory sequences called insulators or boundary elements, which are able to protect genes from the influence of neighbouring enhancers or silencers and from position effects (Bell et al., 2001; Busturia and Bienz, 1993; Gerasimova and Corces, 1996; Gyurkovics et al., 1990; Hagstrom et al., 1996; West et al., 2002). Thus, if an active transgene associates with a RNA pol II-enriched site at the boundary of heterochromatin, the insulator property of the transgenic Fab-7 element could protect the transgene from encroachment of heterochromatin and consequent silencing.

Our results demonstrated that the nuclear localization of euchromatic transgenes and their association with specific nuclear compartments correlated with their state of activity. Additional factors appeared to impact on nuclear positioning, which were the integration site, the orientation of the transgenic Fab-7, and tissue specificity. Association of active transgenes with heterochromatin confirmed our previous suggestion that the boundary of the heterochromatic domain might partially be a transcriptionally permissive environment. The exact functional relationships between all these factors, however, have to be addressed in future studies

4.1.6. Associations between homologous PREs in larval tissues of *Drosophila*

It was first demonstrated for a 2.4 kb PRE from the *Drosophila engrailed* gene that it induces pairing-sensitive silencing of the *white* reporter gene (Kassis et al., 1991). Since then, many studies showed that PRE-mediated silencing is pairing-sensitive, which suggests physical interaction between homologous PREs in *Drosophila* (Americo et al., 2002; Bantignies et al., 2003; Kassis, 1994; Muller et al., 1999; Sigrist and Pirrotta, 1997; Vazquez et al., 2006; Zink and Paro, 1995). So far, three studies were performed where physical interaction between PREs was directly addressed (Bantignies et al., 2003; Grimaud et al., 2006; Vazquez et al., 2006). The results of these studies suggested that PREs in *Drosophila* can physically interact and associate with each other over long distances in interphase nuclei (Bantignies et al., 2003; Grimaud et al., 2006; Vazquez et al., 2006). It is expected that such interactions would

not only influence the nuclear localization of PREs but might also affect the nuclear positioning of other genes in their vicinity. My investigation of the spatial organization of two endogenous genes from the BX-C in transgenic flies indicated indirectly that in the analysed tissues Fab-7 PREs did not interact physically (4.2.2.). To address the issue of interactions between endogenous and transgenic Fab-7 elements directly, I visualized corresponding loci in three transgenic fly lines: FLW-1, 5F24 25,2 and FLFW-1 (Cavalli and Paro, 1998; Zink and Paro, 1995). In FLW-1 and 5F24 25,2 flies, *Abd-B* and *sd* loci were detected to visualize sites with endogenous and transgenic copies of Fab-7, respectively. In FLFW-1 flies, both copies of Fab-7 were visualized directly with the same probe, and the *Abd-B* gene was additionally detected to indicate the endogenous copy of Fab-7. Nuclei were imaged using a Leica SP2 confocal laser scanning microscope, and the relative localizations of Fab-7 copies were analysed in 3D data sets. In FLW-1 and FLFW-1 transgenic flies such analyses were made for the first time, while 5F24 25,2 flies were also used in corresponding studies of G. Cavalli's group, where this line was renamed into Fab-X (Bantignies et al., 2003; Grimaud et al., 2006). In all analysed fly lines and larval tissues no pairing between endogenous and transgenic copies of the Fab-7 element was observed. Here, I will discuss in more detail differences in experimental approaches and obtained results between our studies and previously performed experiments.

4.1.6.1. Diploid and polytene tissues and the question of tissue-specific interactions

In the experiments performed in this study, I have used several different larval tissues: brain, anterior midgut, anterior epidermis, malpighian tubules and fat body cells. Except of diploid brain cells, all other tissues were polyploid and contained polytene chromosomes. I have not observed differences between polytene and diploid tissues with regard to associations of Fab-7 elements in our study, since there was no pairing in any tissue (Figure 29). Nevertheless, in the study of Vazquez et al. (2006) such differences in the pairing frequency of PREs have been reported. While in nuclei from eye-antennal imaginal discs (for simplicity, this tissue will be further referred to as eye imaginal disc) the frequency of pairing between copies of Mcp-containing transgenes was as high as ~98%, in polytene tissues such as salivary glands and malpighian tubules or fat body cells there was no pairing of these elements ((Vazquez et al., 2006); J. Vazquez, personal communication). Moreover, similar results were obtained by Bantignies et al. (2003): endogenous and transgenic copies of the Fab-7 element were paired in 43% of the diploid nuclei of wing imaginal discs, while in polyploid nuclei of the peripodial membrane enclosing the wing imaginal disc the frequency of pairing was close to 0% ((Bantignies et al., 2003); F. Bantignies, personal communication).

Thus, the lack of pairing between Fab-7 PREs in polytene tissues, observed in our study, is in agreement with findings of other research groups.

However, in diploid nuclei of larval brain, like in polytene tissues, I also did not observe any pairing of Fab-7 PREs. This might be due to tissue-specific interactions of PREs in diploid tissues. Indeed, the data from two other studies support this possibility. It should be noted that in all tissues used in the present work all of the analysed endogenous and transgenic loci (when no heat-shock was applied) were inactive and mostly occupied peripheral positions, which was especially pronounced in case of the *sd* locus (Figure 14). In contrast, Bantignies et al. (2003) analysed the relative localization of endogenous and transgenic Fab-7 elements (visualized by detection of *Abd-B* and *sd*, respectively) in wing imaginal discs from 5F24 25,2 (Fab-X) 3rd instar larvae (Bantignies et al., 2003). There, pairing between *Abd-B* and *sd* was found in 43% of nuclei. However, the *sd* gene is expressed in larval wing imaginal discs, since its product is required for wing blade formation (Campbell et al., 1992; Campbell et al., 1991; Srivastava et al., 2004). Other larval tissues were not analysed by Bantignies et al. (2003). In the present work we demonstrated that the inactive *sd* locus occupied a very peripheral position (4.2.1., 4.2.2.), but it is probable that the *sd* gene is regulated in a similar way as many other genes and thus exhibits a different positioning at its active state. This might influence the nuclear localization of the transgenic Fab-7 element, which is inserted in the vicinity of the *sd* gene in 5F24 25,2 flies (Zink and Paro, 1995), and account for the observed differences between Fab-7 interactions in wing imaginal discs and brain.

The data obtained by Vazquez et al. (2006) present another example of possibly tissue-specific interactions. There, transgenic Mcp elements were paired in ~98% of nuclei from eye imaginal discs, but in two other diploid larval tissues tested, wing imaginal discs and brain, the frequency of pairing dropped to 20-60% of that observed in eye imaginal discs (Vazquez et al., 2006). Authors offered a possible explanation for such tissue-specific pairing frequencies. The mini-*white* gene, which was present in the Mcp-containing constructs, is normally expressed in the eye. It was suggested that mini-*white* sequences might act together with Mcp elements to increase the level of pairing in this particular tissue (Vazquez et al., 2006). Together with these observations, our data indicate that associations between homologous PREs are regulated in a complex way. Besides sequence homology, also tissue-specific factors, the state of activity of neighbouring genes and the level of ploidy appear to contribute to long-range interactions of PREs.

4.1.6.2. The impact of the chromosomal background and temperature on PRE associations

During comparative analyses of the spatial organization of inactive endogenous loci in tissues from 3rd instar larvae of FLW-1 and 5F24 25,2 transgenic lines, I obtained data which indicated indirectly the absence of pairing between endogenous and transgenic Fab-7 elements in these tissues (4.2.2.). Visualization of both copies of Fab-7 in four different tissues provided direct evidence for their independent localization (Table 3). To exclude the possibility of site-specific behaviour because the insertions in the of the transgenic lines investigated were at the *sd* locus, we analysed the relative localization of endogenous and transgenic Fab-7 elements in another transgenic line, FLFW-1. There, the 24F6 transgene is inserted into 61C9 (3L) and contains two copies of Fab-7 (Zink and Paro, 1995). Nevertheless, despite localization on the same chromosome in both analysed tissues the transgene was not paired with the endogenous copy of Fab-7. It is noteworthy that these flies displayed the closest distance between endogenous and transgenic copies of Fab-7 ever measured in all analysed fly lines, but even this distance of 0.6 μm was found only in one nucleus from epidermis and malpighian tubules each. The majority of nuclei showed much larger distances. Thus, localization of both copies on the same chromosome does not necessarily increase the frequency of their physical association but might result only in closer nuclear positioning.

The issue of chromosomal localization was also addressed in *Drosophila* embryos. Bantignies et al. (2003) analysed frequencies of pairing in embryos of two transgenic lines, where transgenic Fab-7 was inserted either at 13F (chromosome X) or 38F (chromosome 2L), respectively. Pairing frequencies between endogenous and transgenic copies of Fab-7 in embryonic nuclei were 23% and 11%, respectively (Bantignies et al., 2003). This suggests that for Fab-7 the degree of long-range interactions between copies is locus-dependent. The stage of development appeared to be important as well: in 5F24 25,2 embryos, endogenous and transgenic Fab-7 elements were paired in 23% of nuclei, while in wing imaginal discs from 3rd instar larvae the pairing frequency was 43%. Nevertheless, up to 90% of these transgenic flies had a *sd* phenotype and displayed strong variegation of eye colour (Bantignies et al., 2003), which suggests that repression of *sd* is not dependent on pairing of Fab-7 elements. Moreover, it was shown that *sd* repression could be mediated by the transgenic copy of Fab-7 alone (Bantignies et al., 2003). Together, these observations suggest that two more factors influence the spatial relationships between homologous PREs: the stage of development and the chromosomal localization of PREs.

Silencing properties of PREs are temperature-dependent and Pc-mediated silencing is enhanced at higher temperatures (Cavalli and Paro, 1998; Fauvarque and Dura, 1993; Zink and Paro, 1995). Most of the studies of Bantignies et al. (2003)

and Grimaud et al. (2006) were performed under conditions of enhanced Pc-mediated silencing, since the entire development of 5F24 25,2 (Fab-X) flies was carried out at 25°C-29°C ((Bantignies et al., 2003; Grimaud et al., 2006); F. Bantignies, personal communication). My experiments were performed in the beginning with larvae which developed at 18°C. To test whether enhancement of silencing leads to association of PREs I performed comparative analyses of the same tissues from 3rd instar larvae of 5F24 25,2 transgenic flies (Zink and Paro, 1995). Eggs were laid and larvae developed either at 18°C (control) or at 29°C, respectively, and positions of endogenous and transgenic Fab-7 elements were visualized in anterior epidermis, malpighian tubules, anterior midgut and fat body cells from larvae of both samples (Table 3). 5F24 25,2 flies do not carry the heat-shock inducible GAL4 driver, and thus the development at 29°C could not result in activation of the transgenic Fab-7. However, the increase of temperature did not influence the spatial relationships between Fab-7 copies in the analysed tissues, as they remained unpaired in all nuclei (Figure 31, Table 3). This indicates that the strength of Pc-mediated silencing does not affect the relative nuclear positioning of endogenous and transgenic Fab-7 PREs in the analysed larval tissues. It would have been very interesting to perform similar comparisons in embryos and in larval wing imaginal discs, where the PREs were shown to interact under conditions of enhanced Pc-dependent silencing (Bantignies et al., 2003). Unfortunately, we could not obtain reliable results with wing imaginal discs (Figure 30).

The RNAi machinery was very recently identified as another factor which influences interactions between Fab-7 copies in *Drosophila* (Grimaud et al., 2006). In this study mutations of the *AGO1*, *aub*, *piwi*, and *hls* components of the *Drosophila* RNAi machinery were introduced into 5F24 25,2 (Fab-X) flies. In corresponding embryos the frequencies of pairing between endogenous and transgenic copies of Fab-7 did not change in comparison to control 5F24 25,2 embryos (25%). However, in larval wing imaginal discs of *AGO1*, *aub*, and *piwi* mutants no associations between copies of Fab-7 were observed, although Fab-7 elements were associated with PcG proteins as usual (Grimaud et al., 2006). This suggests that the RNAi machinery participates in the maintenance, but not in the establishment, of long-range Fab-7 interactions. This again indicates that the stage of development is an important factor of these interactions.

In summary, I addressed the issue of physical interactions between homologous PREs, using a number of *Drosophila* larval tissues and fly lines which were not studied before in this regard. Together with previously obtained data, our results indicate that pairing of PREs depends on a number of factors, such as tissue type, the level of polyteny, in certain cases on the chromosomal location of copies, and the stage of development. My results also indicate that spatial relationships between copies of Fab-7 do not depend on the temperature. Furthermore, the results suggest that gene silencing occurs in many cases in the absence of physical pairing of corresponding PREs. Thus, physical interactions of homologous PREs are in many cases not a

necessary prerequisite for PRE-dependent silencing.

4.1.7. The 3D nuclear organization of Pc-binding sites in *Drosophila* nuclei: challenges of interpretation

To address pairing of PREs in general, Pc-binding sites were analyzed in interphase nuclei. There are about 100 or more binding sites for Pc on polytene chromosomes from salivary glands of 3rd instar larvae (Rastelli et al., 1993; Zink and Paro, 1989). Their organization in interphase nuclei provides information of whether PREs indeed associate physically: presence of 100 or more small Pc foci would indicate absence of pairing, while smaller numbers of larger foci would suggest clustering of Pc-binding sites. Currently, the data are not clear. Results obtained with tissue culture SL2 cells indicated that the many small Pc foci observed in these cells represented individual chromosomal binding sites (Messmer et al., 1992). However, in this study a careful analysis of the numbers of Pc foci has not been performed. In 1998, the distribution of Pc and other PcG proteins was carefully investigated in wild-type embryos, using high-resolution confocal microscopy with a voxel size of 0.1x0.1x0.3 μm (Buchenau et al., 1998). Indeed, 100 or more discrete spots of Pc per nucleus were found, which had different intensities and volumes. This would be expected if spots represent individual Pc-binding sites, since sizes and intensities of binding sites vary considerably, as the analyses of polytene salivary gland chromosomes revealed (Rastelli et al., 1993; Zink and Paro, 1989). Similar results were obtained for two other investigated PcG proteins, Ph and Psc (Buchenau et al., 1998). However, in embryos from 5F24 25,2 transgenic flies only 45-50 Pc and Ph foci were found (Grimaud et al., 2006). In this study, imaging of Pc and Ph proteins was performed under the same conditions as imaging of endogenous and transgenic Fab-7 copies: epifluorescence microscopy and subsequent deconvolution with a compromised resolution due to a step with of 0.5 μm . Moreover, in larval wing imaginal discs only about 30 such foci were observed. The authors suggested, that these are aggregations of individual binding sites due to the reduced numbers observed, and referred to them as “Pc bodies” (Grimaud et al., 2006). Similar numbers of Pc and Ph loci in larval wing imaginal discs were also found during studies of the dynamics of PcG complexes, although the main aim of that research was not the analysis of numbers of Pc and Ph foci (Ficz et al., 2005). Given these uncertainties and the fact that we did not observe pairing of PREs in analysed larval tissues, I performed a series of experiments addressing the nuclear distribution of Pc in a number of larval tissues.

We analysed a number of diploid and polyploid tissues from 3rd instar larvae of WT and Pc-GFP transgenic flies (Dietzel et al., 1999). All tissues were imaged with a Leica SP2 or Zeiss 410 confocal laser scanning microscope, using a 63x NA 1.4 Plan-

Apochromat oil immersion objective. The xy-pixel size was 100 nm and the distance between planes was $\Delta z=250$ nm. Our goal was to compare the nuclear organization of Pc-binding sites in different tissues and to find out whether they existed as separate binding sites or might form clusters. At first we have tried to analyse these parameters using the ImageJ software: total numbers of Pc foci were counted in several nuclei from eye imaginal discs and anterior epidermis (Table 4). These results showed a strong tissue-specificity of the numbers of detected Pc foci. However, ImageJ did not appear to be suitable for analysing volumes of these foci and their relative positions, since this software operates with single optical sections and at each section calculates the number of Pc-binding sites present. As a result, a Pc-binding site which appears on more than one optical section is counted more than once, and the total number of Pc-binding sites calculated in this way does not reflect the real number of Pc foci present in the nucleus. Therefore, we tried a novel approach. Using the Amira software, 3D reconstructions of individual nuclei were made on the basis of the confocal data sets and numbers and volumes of Pc foci were analysed in these reconstructions.

First, we made a reconstruction of a salivary gland nucleus to test whether we will be able to resolve 100 or more individual Pc-binding sites. Large polytene nuclei of this tissue provide as optimal conditions as possible: regular nuclear shape, very high signal-to-noise ratio, and good spatial separation of Pc-binding sites due to the sheer volume of the nuclei. Based on visual evaluation, we defined a Pc-binding site as a structure of at least 9 adjacent voxels (voxel size was $0.1 \times 0.1 \times 0.25 \mu\text{m}$). Under these conditions the observed number of Pc foci was 105 and therefore in the expected range in case that single Pc-binding sites would be present (Figure 35; Table 5, top). However, even under these optimal conditions the software produced a number of artefacts (for details see 3.1.4.). Therefore, the reliability of results obtained under less optimal conditions was questionable.

Nevertheless, we also made 3D reconstructions and performed subsequent analyses of nuclei from eye and leg imaginal discs (diploid tissues), anterior epidermis, middle midgut and malpighian tubules (polytene tissues). The results, shown in Table 5, at the first glance indicate strong tissue-specific differences and, perhaps, a different organization of Pc-binding sites in diploid and polytene tissues. The most profound differences were found between nuclei from salivary glands and leg imaginal discs. However, visual inspection of confocal data sets and resulting reconstructions showed that in all tissues analyzed not only the nuclear sizes were smaller than in salivary glands, and were smallest in imaginal discs, but also the signal-to-noise ratio was directly proportional to the sizes of nuclei. Subsequent analyses (Figure 36) strongly suggested that indeed in smaller nuclei we could only detect the largest and brightest Pc foci. The majority of Pc foci in such tissues are likely too small and too faintly stained (compared to the background) for a reliable detection and reconstruction. Also, it is very likely that PREs are densely packed in such small nuclei, which makes it difficult

to resolve individual Pc-binding sites.

Nuclei from malpighian tubules were selected for further analyses for several reasons. First, this tissue was used in all our studies of the nuclear localization of PREs and endogenous genes. Second, nuclei from malpighian tubules are rather large (10-13 μm in diameter) and have a regular shape. And third, this tissue has the next highest level of polyteny after salivary glands. Only ~ 74 Pc foci on average were identified in reconstructions of these nuclei (Table 5, bottom). To find out whether the relatively small number of Pc foci was due to clustering of PREs or due to limitations of the applied method, we performed a close visual inspection of several nuclei. Comparative analyses of the raw data and 3D reconstructions revealed that most of the Pc-binding sites are clear bands of different intensity, like in salivary glands (Figure 35 I, L; Figure 37 F-I). Due to the smaller size of nuclei bands were located closer to each other, and closely spaced or neighbouring chromosomal bands were more difficult to resolve given the higher level of background staining compared to salivary glands. Since the software counted such cases as single structures, the total number of counted Pc foci was lower than in salivary gland nuclei. Moreover, among the bands in malpighian tubule nuclei we could reliably identify several individual telomeric and euchromatic Pc-binding sites due to their characteristic staining patterns (data not shown). Taken together, these observations support the view that in analysed tissues PREs do not cluster, but their detection and reliable reconstruction depends on the size of nuclei and the signal-to-noise ratio.

There are two tools in ImageJ which could be applied to the raw data as an attempt to reduce the background and increase the signal-to-noise ratio before building a reconstruction: thresholding and smoothening (Figure 52). Both of them, however, can produce further artefacts. Using the threshold tool, it is possible to reduce the

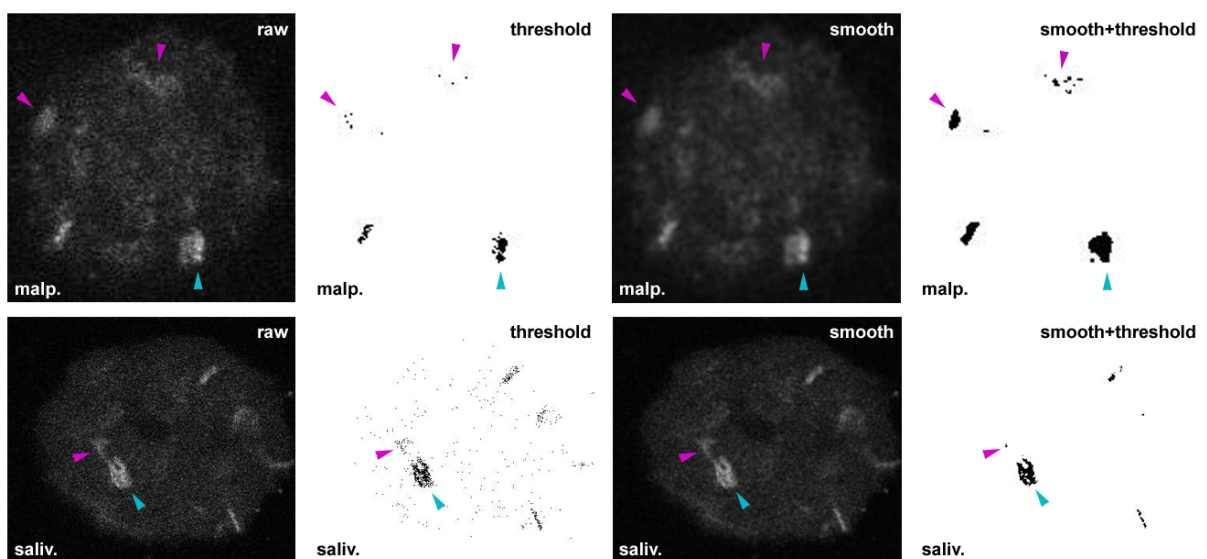


Figure 52. Processing of raw images with ImageJ tools „threshold“ and „smooth“. In nuclei from Pc-GFP transgenic 3rd instar larvae the GFP signal was additionally enhanced with an Alexa-488-conjugated anti-GFP antibody. Single light optical sections from monochromatic

stacks of nuclei from malpighian tubules (malp., top) and a salivary gland (saliv., bottom) are shown. The unprocessed images are shown on the left (raw), and subsequent images show different ways of the processing: thresholding, smoothing and thresholding of an already smoothed image (from left to right, respectively). Blue arrowheads indicate closely situated Pc-binding sites of different (malp.) or similar (saliv.) intensity. Pink arrowheads point at weakly stained bands.

background level while leaving brighter structures intact (Figure 52, threshold, blue arrowheads). This might help to resolve closely positioned bands. However, since not all Pc-binding sites have similar intensity, weaker sites might disappear or might be disintegrated to several smaller structures (pink arrowheads). Smoothing, on the other hand, allows to increase the signal-to-noise ratio. However, in case of closely spaced sites of different brightness this might result in fusion (Figure 52). Smoothing can also produce other artefacts: if several adjacent background voxels have higher staining levels than the rest, smoothing will fuse them together, and a new structure will appear in the reconstruction. This problem can be partially solved by removing all structures with volumes below a certain number of voxels (defined empirically). A careful application of smoothing and subsequent thresholding to the raw data might therefore improve the reconstruction, but careful comparison to the raw data is always obligatory.

Another way of dealing with these problems is to apply more advanced imaging and reconstruction techniques. Here, we applied selective plane illumination microscopy (SPIM) (Huisken et al., 2004), which allows fast imaging of unfixed and unstained specimens (we used tissues from Pc-GFP transgenic larvae (Dietzel et al., 1999)) from different angles. Subsequently, multiview reconstructions were assembled by the MatLab software. Projections of these reconstructions gave a very realistic 3D view of imaged tissues (Figure 38, see also Movies 2 and 3 on the supplementary CD). Unfortunately, the resolution of these reconstructions was not sufficient for the detection of individual Pc-GFP-binding sites in small nuclei of imaginal discs, and for a number of reasons (see 3.1.4.) we could not image malpighian tubules. But two tissues were successfully imaged (a salivary gland and a nerve) and once again these data illustrate the complexity of PRE organization and the resulting current problems with its analysis. Pc-GFP-binding sites were distributed throughout the whole nucleoplasm and have different volumes and brightnesses. Salivary gland nuclei again demonstrate that due to chromosome folding different PREs are often in close contact. It is possible to distinguish between individual bands visually, but for currently available software tools this is a major problem

Our data illustrate that currently the main problem with analyses of the nuclear organization of PREs is not the imaging of nuclei but the interpretation of the data. While 3D reconstructions offer a relatively easy way of calculating the numbers and

volumes of Pc-binding sites in different tissues, the reliability of such analyses is questionable at the moment. Artefacts can be produced at the steps of imaging, image processing and building of the reconstruction.

Despite the described difficulties with the interpretation of the results, the data obtained with regard to the distribution of Pc and Pc-GFP in nuclei of larval tissues are in agreement with the other results of this study obtained by immunoFISH analyses. The results revealed that Pc-binding sites do not cluster in polytene tissues. Evidence for clustering of PREs in diploid tissues could not be obtained.

4.2. Integration site and transcriptional activity determine the nuclear localization of LV-PGK transgenic constructs in porcine cells

The results obtained with transgenic *Drosophila* lines indicated that transcriptional activation of transgenes led to a change in their nuclear localization. Transgenic pigs, created by the team of Prof. Alexander Pfeifer at the LMU Munich (Hofmann et al., 2003), gave us the opportunity to address such relationships in transgenic mammals other than mice. All pig cells investigated here carried the same LV-PGK transgenic construct (see Figure 3, (Follenzi et al., 2000)) but the site of its chromosomal integration as well as its transcriptional activity differed. *In vitro* cultured primary fibroblasts from five different animals with single integrants were used: highly expressing SFF 9338, variegating SFF 9206, low-expressing SFF 9193, and non-expressing SFF 9192 and 9196 cells (Figure 41). Transgenic constructs were visualized with FISH, nuclei were imaged with a Zeiss epifluorescence microscope, and the radial nuclear localization of transgenes was analyzed with 2D erosion analyses (for details of the erosion analysis see (Zink et al., 2004)).

In accordance with the results obtained with *Drosophila* transgenic flies (see above), I observed a clear correlation between the transcriptional activity of the LV-PGK construct and its localization regarding the nuclear periphery. In expressing 9338 and 9206 cells the construct was found in the nuclear interior, while in the non-expressing cells it had more peripheral localization. In low-expressing cells the transgene showed an „intermediate“ position (Figure 43). The nuclear localization of the transgenic construct in two non-expressing lines was slightly different but in both cases a peripheral localization was observed. Interestingly, in 9206 cells where only ~21% of the cells were expressing, the transgene showed a more interior localization than in highly expressing 9338 cells. These findings indicated that the site of chromosomal integration of the transgene also influenced its nuclear position. This would be in agreement with data obtained with human cells, which suggested that in some cases the chromosomal localization of a gene could be the key determinant of its nuclear position. In a corresponding study it was shown that three immunoglobulin genes associated with

different nuclear subvolumes independently on the state of their transcriptional activity, and that this distribution was conserved in different cell types (Parreira et al., 1997). However, the integration sites of the LV-PGK transgenic construct are not mapped yet. It is likely that transcriptional activity and nuclear localization of the construct in each cell line were both defined by the fraction of chromatin in which the construct resided. It is probable that transgenes which integrated into inactive perinuclear chromatin would be transcriptionally silent and exhibit peripheral localization with their whole domain, while constructs integrated into active domains might be positioned with this domain in the nuclear interior and might be active here.

Using DAPI staining, I could detect chromocenters only in 9206 and 9193 cells. In these cells, I performed distance measurements between the transgene and a closest chromocenter. In 9193 cells no specific relationships were found. In 9206 cells, however, ~22% of FISH signals were found within 1 μm from the closest chromocenter (Figure 44). This number is remarkably close to the percentage of expressing cells in this line (~21%). Due to a number of reasons I could not perform the analysis at the level of individual cells (3.2.2.), and so it was not possible to test whether the transgene associated with a chromocenter only in expressing cells. But the results obtained with *Drosophila* transgenic flies and particularly the FLW-1 line suggest that these numbers might reflect a functional link. However, further experiments are necessary to clarify whether porcine chromocenters might have a comparable organization.

In *Drosophila*, transcriptional activation of 5F24 and 5F3 transgenic constructs led to their repositioning into more interior nuclear regions, while the 24F6 construct kept its peripheral position upon activation. It was unclear whether the integration site or differences between transgenes were responsible for these positional distinctions. In porcine cells where only one transgenic construct was used we could address this issue in more detail. We performed activation of the transgene with 5-azacytidine (5-azaC). Unfortunately, only two cell lines were available for this analysis: 9206 (variegated expression pattern) and 9193 (low level of expression). In both cases, treatment with 5-azaC resulted in high levels of activity of the transgene but its nuclear position did not change (Figure 45). This seeming contradiction might be explained by the fact that in these cell lines the transgenic construct already localized in the nuclear interior in the transcriptionally permissive area. So, with the available cell lines it was not possible to evaluate the role of the integration site. Therefore, we used another approach. An *in vitro* culture of primary WT cells was freshly infected with the LV-PGK retrovirus. Then highly expressing cells were selected and cultivated separately, and we analysed the localization of the transgene in nuclei with only one integrant. The analysis showed that the transgenes had an interior distribution, with the majority of signals in the 2nd shell (40%). This result was in accordance with other data obtained in the present study, which indicated that transcriptionally active transgenes are preferentially associated with the transcriptionally permissive nuclear interior.

Interestingly, the distribution of FISH signals in highly expressing freshly infected cells was not similar to the distribution observed in 9338 highly expressing cells line, but instead closely resembled the pattern found in 9193 low-expressing cells (Figure 46). However, it is arguable whether one can directly compare data obtained from primary cells to data from *in vitro* infected WT cells. The transgenic pigs were created by infecting sperm with the LV-PGK retrovirus and these spermatocytes were used to fertilize oocytes. Therefore, there was selection against integrations which disturbed fertilization and further development of animals. One of the safest places for integration in this case is gene-poor heterochromatin, which occupies certain positions in interphase nuclei. Furthermore, the constructs, like the rest of the genome, went through processes of cell division and differentiation which could influence positional and functional properties of chromatin. In contrast to this scenario, the WT cells, which were used for the *in vitro* infection already underwent the process of differentiation and therefore might have more abundant genomic sites, including euchromatic ones, where a retroviral integration does not influence the cell viability. Therefore, it is likely that even though cells from transgenic animals and *in vitro* transfected cells might show a similar behaviour of the transgene, the differences between these systems must be taken into account during the interpretation of the results.

On the whole, the results obtained with transgenic pigs are in agreement with the results obtained with transgenic *Drosophila* lines: transgenes in their inactive state exhibit peripheral nuclear localization, while they occupy more interior positions in their transcriptionally active states. However, further experiments are required to test if other nuclear compartments, such as heterochromatin, contribute to the regulation of transgenes in pigs.

4.3. The Tpr protein, associated with the nuclear pore complex (NPC), contributes to the peripheral positioning of inactive gene loci in human cells

The data obtained with *Drosophila* and porcine cells suggested conserved mechanisms for the positioning of inactive loci at the nuclear periphery. Recent data suggest that in *Drosophila* lamin Dm₀ is involved in the peripheral positioning of inactive gene loci (Pickersgill et al., 2006). A close association with the nuclear periphery has also been observed for the human CFTR gene in its inactive state (Zink et al., 2004). Also here lamin A/C, as well as LAP2 β and emerin appeared to play a role in the positioning of this gene locus (Englmann, 2005). Data from yeast cells imply that also nuclear pore complexes are involved in chromatin positioning. Here, physical tethering of gene loci to the NPC has been observed (Galy et al., 2000; Ishii et al., 2002). To test whether the NPC might have a similar function in mammalian cells,

we have chosen to address the role of the Tpr protein, which is thought to constitute the central architectural element that forms the scaffold of the nuclear basket (Cordes et al., 1997; Krull et al., 2004). Tpr was selected because it was suggested to be an anchor site for perinuclear chromatin (Cordes et al., 1997), and it was shown that its yeast homologs Mlp1 and Mlp2 are involved in the peripheral positioning of inactive loci (Galy et al., 2000). Taking advantage of RNAi we knocked down Tpr in HeLa cells and assessed the effects on the peripheral localization of the CFTR locus, whose nuclear organization was extensively characterized before (Englmann, 2005; Lang, 2003; Zink et al., 2004).

CFTR was detected with FISH using a specific DNA probe and nuclei were imaged with a Zeiss 410 confocal laser scanning microscope. Assembly of 3D data sets and distance measurements were performed with the ImageJ software. In control nuclei CFTR was positioned very peripherally: the mean distance between the CFTR locus and the nuclear rim was 0.31 μm , which is in accordance with data obtained before with HeLa cells, where a corresponding distance of 0.28 μm was measured (Englmann, 2005). The data showed that knock-down of Tpr led to repositioning of CFTR towards the nuclear interior: the mean distance between CFTR and the nuclear rim increased to 0.97 μm (Figure 48, B). HeLa cells contain three copies of chromosome 7 harbouring CFTR (Scherer and Hoogasian, 1954) and up to 3 FISH signals from the CFTR locus were observed in each nucleus. All copies of CFTR showed increased distances to the nuclear rim after Tpr knock-down (Figure 48, A). These findings suggest that Tpr in human cells indeed contributes to the peripheral positioning of silenced gene loci.

Although it is not known whether and how Tpr might interact with chromatin, data obtained from several species suggest possible mechanisms. It was shown that the Tpr yeast homologs Mlp1 and Mlp2 are directly involved in subnuclear positioning of telomeres in interphase nuclei and in telomeric gene repression (Galy et al., 2000). These interactions were probably mediated by chromatin-binding proteins yKu70p and yKu80p, which are also crucial for peripheral localization of telomeres and telomeric silencing (Laroche et al., 1998). Mlp2 physically tethers yKu70 to the nuclear periphery, providing the link between chromatin and the nuclear envelope (Galy et al., 2000).

In *Xenopus*, immunocytochemical studies revealed that chromatin was attached to the intranuclear filaments of the NPC and to the nuclear basket (Arlucea et al., 1998). It was further shown in *Xenopus* oocytes that the terminal ring of the nuclear basket contained nucleoporin Nup153 (see (Krull et al., 2004) and references therein), a protein which has a zinc-finger domain and was shown to bind DNA *in vitro* (Sukegawa and Blobel, 1993). Some data suggest that Nup153 might also interact with chromatin *in vivo* (Bodoor et al., 1999; Daigle et al., 2001). In mammalian cells, Nup153 is directly involved in binding of Tpr to the nuclear coaxial ring of the NPC (Hase and Cordes, 2003) and is also essential for anchoring the NPC to the nuclear envelope (Daigle et al.,

2001). In addition, there are data from mammalian and *Xenopus* cells which indicate that localization of Nup153 and Tpr is not restricted to the nuclear basket, but that they are also located on long filaments which are attached to the nuclear basket and protrude further into the nucleoplasm, interacting with chromatin (Arlucea et al., 1998; Cordes et al., 1993; Cordes et al., 1997). Given these results and our data suggesting that Tpr is functionally involved in tethering inactive gene loci to the nuclear periphery, it might be possible that Tpr interacts with peripheral chromatin through Nup153, which has a DNA-binding and, probably, chromatin binding activity.

Knock-down of Tpr led to a significant increase of the mean distance between CFTR and the nuclear rim (Figure 48, B). A similar effect was observed after knock-down of several proteins of the nuclear envelope, namely lamin A/C, emerin and Lap2 β (Englmann, 2005). In these cases, mean distances between CFTR and the nuclear rim increased from 0.28 μm to 0.8 μm and the maximum distances between CFTR and the nuclear periphery increased from 0.61-0.71 μm to 1.5 μm (control and RNAi-treated cells, respectively). Knock-down of Tpr resulted in a larger increase of the mean distance: from 0.31 μm in control cells to 0.97 μm in RNAi-treated cells. The maximum distance, however, was the same both with and without RNAi: 2.5 μm . This suggests that there are certain limits of chromatin movements, independent of the presence of Tpr. A possible reason for such limitation could be the fact that at least three other proteins of the nuclear envelope appear to be involved in CFTR positioning (Englmann, 2005). It would be interesting to knock-down several proteins simultaneously to test whether the distances between CFTR and the nuclear envelope will further increase in this case.

In summary, in mammalian cells several proteins appear to be involved in anchoring inactive gene loci the nuclear periphery: lamin A/C and two lamin-binding proteins (Englmann, 2005) and Tpr, which is an NPC associated protein (present work). In *Drosophila* Kc cells at least lamin Dm₀ appears to be involved in the perinuclear localization of chromatin (Pickersgill et al., 2006), and the finding that many gene loci tethered to the nuclear periphery in *Drosophila* cells are inactive is in accordance with the results of this study investigating larval tissues. Since a *Drosophila* homolog of Tpr was described, which localizes at the nuclear periphery on or near NPCs and has a striking sequence similarity to the mammalian Tpr (Zimowska et al., 1997), one could suggest that this protein might also participate in chromatin organization in *Drosophila* nuclei. Taking into account the data which demonstrated a role of NPC proteins and Tpr homologs in tethering of inactive loci to the nuclear envelope in yeast (Galy et al., 2000), I suggest that involvement of lamins as well as NPC components and associated proteins in chromatin organization is conserved in many species, from yeast to mammals.

Summary

The goal of the work was to address the role of higher order nuclear architecture in the functional regulation of endogenous genes and transgenes in different species. In the first part of the work, 3D distance measurements were performed to analyze in WT flies and in different transgenic lines of *Drosophila melanogaster* (Cavalli and Paro, 1998; Zink and Paro, 1995) the nuclear localization of endogenous genes and transgenic constructs containing the Polycomb Response Element (PRE) Fab-7 relative to the nuclear periphery and heterochromatin. Transgenic constructs containing the Fab-7 element and three endogenous genes, *Abd-B*, *sd*, and *Ubx*, were first analyzed at their inactive state. The results showed that they were preferentially associated with the nuclear periphery and did not display specific associations with heterochromatin. The localization of the transgenic Fab-7 element was further analyzed at different states of activity. Activation of the transgenic Fab-7 element resulted in frequent (up to ~50%) association with the boundary of the heterochromatic domain. The percentages of such associations were tissue- and fly line-dependent. Further investigations of the boundary of heterochromatin showed that this region has a complex organization, where euchromatic sites enriched in the active form of RNA pol II and trimH3K4, sites enriched in dimH3K4 and Pc-binding sites, as well as pericentromeric satellite DNA are exposed and juxtaposed towards each other. The concentration and specific architecture of such sites at the boundary of heterochromatin might help to maintain the equilibrium between activation and repression at this boundary. This specific environment might be favourable for maintaining PREs in the active state.

I also investigated in three transgenic lines whether endogenous and transgenic copies of the Fab-7 element interact physically, using 3D distance measurements. In five tissues analyzed, no pairing between endogenous and transgenic copies of the Fab-7 element was observed. Also enhancement of Pc-mediated silencing did not induce pairing. Additionally, the general organization of Pc-binding sites was addressed in six larval tissues. We used different methods of microscopy and image analyses to count the numbers of Pc foci in nuclei from these tissues. Our data did not indicate clustering of Pc-binding sites and formation of so called „Pc bodies“. However, corresponding analyses are not without problems at the current stage of methodology and results must be interpreted carefully. Together with the results of previously published studies, which investigated pairing between PREs (Bantignies et al., 2003; Vazquez et al., 2006), my data demonstrated that such pairing is a highly tissue-specific phenomenon and is likely not involved in the regulation of PREs in various tissues.

Activity-related positioning of transgenes was also addressed in transgenic porcine cell lines (Hofmann et al., 2003). Results of 2D erosion analyses showed that the LV-PGK transgene was associated with the nuclear periphery in its inactive state, while it occupied more interior positions in its active state. This corresponds to

my results obtained with transgenic *Drosophila* lines. My data also suggested that the active LV-PGK construct might be associated with heterochromatin in one case. However, further experiments would be necessary to confirm such associations.

The results obtained with *Drosophila* and porcine cells suggested conserved mechanisms for tethering inactive loci to the nuclear periphery. These were further addressed using the human CFTR locus as a model, which is closely associated with the nuclear periphery in its inactive state (Zink et al., 2004). The question was addressed whether Tpr, a protein associated with the nuclear basket, plays a role in the perinuclear localization of the inactive CFTR locus. CFTR showed a high degree of association with the nuclear periphery in control cells in accordance with previous data (Zink et al., 2004). After knock-down of Tpr via RNAi CFTR displayed a more interior positioning. This suggests that Tpr is involved in the organization of inactive gene loci at the nuclear periphery. Moreover, since *Drosophila* Tpr has a high level of homology to the mammalian Tpr (Zimowska et al., 1997) and as it has been shown that the yeast Tpr homologs Mlp1 and Mlp2 are involved in tethering of inactive loci to the nuclear periphery in yeast cells (Galy et al., 2000), it is possible that Tpr is a part of a conserved mechanism anchoring inactive loci to the nuclear periphery in eukaryotic cells.

6. Acknowledgements

Most of all, I wish to thank **Dr. Daniele Zink** for giving me the opportunity to study in Munich, for introducing me into the world of *Drosophila* genetics, and for being such a wonderful supervisor, always cheerful, supportive and very patient. I am very grateful for the great help she provided me during my experimental work and especially during writing of my thesis, and for being my first reviewer.

I thank **Prof. Peter Becker** for fruitful discussions and helpful suggestions regarding *Drosophila* experiments and for critical reading of my doctoral thesis as the second reviewer.

Dr. Donna Arndt-Jovin I thank for providing me with DNA probes and basic protocols at the initial stage of my experimental work and for giving me the opportunity to stay in her lab to learn some critical techniques.

I thank **Dr. Volker Cordes** for collaborating in the investigation of the role of the Tpr protein, for providing me with cells, antibodies and siRNAs, and for helpful suggestions.

I am grateful to **Prof. Renato Paro**, **Dr. Leonie Ringrose** and **Dr. Steffen Dietzel** for fly lines and probes, which they provided for my studies, and for their suggestions regarding the experimental work.

I very much appreciate the help from **Dr. Ina Dahlsveen** in mastering the art of dissecting larval tissues of *Drosophila*.

I thank **Dr. Roscoe Stanyon** for kindly providing painting probes for porcine chromosomes.

I am grateful to **Prof. Ralph Rupp** and **Dr. Gernot Längst** for support during my PhD work.

I especially thank **Dr. Nicolas Sadoni** for helping me greatly with image analyses and for introducing me to microscopes and all complicated software products, which I used during my work, for performing the RT-PCR analyses, for spending much time and effort with the assembly of my PhD thesis, and for being always patient and cheerful.

Dr. Andreas Englmann I thank for his help in the preparation of probes, and for help in performing RNAi and Western Blot analyses, and for his good mood and support in every aspect of my life in the lab and outside it.

I appreciate the help from **Jeannette Koch** in analyses of the organization of Pc-binding sites.

I thank **Joscha Muck**, **Stephani Fesser**, **Kathrin Luther**, **Susanne Lang**, **Doris Berchtold** and **Stephan Mitschik** for their help and laughter, and for making the lab such a wonderful place to work in.

I am grateful to **Dr. Ernst Stelzer** for allowing me to work with the SPIM, and to **Dr. Francesco Pampaloni** for his great help in imaging *Drosophila* specimens and for

building multiview reconstructions.

Dr. Rainer Pepperkok and **Dr. Timo Zimmerman** I thank for providing me with an exclusive access to a Leica SP2 AOBS microscope for 2 seasons.

I thank **Prof. Harald Saumweber**, **Prof. Dirk Eick** and **Dr. Elisabeth Kremmer** for antibodies against *Drosophila* lamin and the active form of RNA pol II, which were of key importance in many of my experiments.

I am grateful to **Prof. Alexander Pfeifer** and **Dr. Andreas Hofmann** for providing transgenic porcine cells and DNA probes for the LV-PGK construct.

I am deeply grateful to **all my friends** from different countries for their help, advices and understanding, and for making my life and work so much fun.

I thank people without whom this work could not have been done: **my parents** and **Sergey, my husband to be**, for helping me in everything I did, for their support and understanding, and for their love, which I always feel.

7. References

- Aagaard, L., G. Laible, P. Selenko, M. Schmid, R. Dorn, G. Schotta, S. Kuhfittig, A. Wolf, A. Lebersorger, P.B. Singh, G. Reuter, and T. Jenuwein. 1999. Functional mammalian homologues of the *Drosophila* PEV-modifier Su(var)3-9 encode centromere-associated proteins which complex with the heterochromatin component M31. *Embo J.* 18:1923-38.
- Ahmad, K., and S. Henikoff. 2001. Centromeres are specialized replication domains in heterochromatin. *J Cell Biol.* 153:101-10.
- Ahmad, K., and S. Henikoff. 2002. Histone H3 variants specify modes of chromatin assembly. *Proc Natl Acad Sci U S A.* 99 Suppl 4:16477-84.
- Akhtar, A., and P.B. Becker. 2000. Activation of transcription through histone H4 acetylation by MOF, an acetyltransferase essential for dosage compensation in *Drosophila*. *Mol Cell.* 5:367-75.
- Akhtar, A., D. Zink, and P.B. Becker. 2000. Chromodomains are protein-RNA interaction modules. *Nature.* 407:405-9.
- Alkema, M.J., M. Bronk, E. Verhoeven, A. Otte, L.J. van ,t Veer, A. Berns, and M. van Lohuizen. 1997. Identification of Bmi1-interacting proteins as constituents of a multimeric mammalian polycomb complex. *Genes Dev.* 11:226-40.
- Allfrey, V.G., R. Faulkner, and A.E. Mirsky. 1964. Acetylation And Methylation Of Histones And Their Possible Role In The Regulation Of RNA Synthesis. *Proc Natl Acad Sci U S A.* 51:786-94.
- Americo, J., M. Whiteley, J.L. Brown, M. Fujioka, J.B. Jaynes, and J.A. Kassis. 2002. A complex array of DNA-binding proteins required for pairing-sensitive silencing by a polycomb group response element from the *Drosophila* engrailed gene. *Genetics.* 160:1561-71.
- Andrulis, E.D., A.M. Neiman, D.C. Zappulla, and R. Sternglanz. 1998. Perinuclear localization of chromatin facilitates transcriptional silencing. *Nature.* 394:592-5.
- Appels, R., and A.J. Hilliker. 1982. The cytogenetic boundaries of the rDNA region within heterochromatin in the X chromosome of *Drosophila melanogaster* and their relation to male meiotic pairing sites. *Genet Res.* 39:149-56.
- Arlucea, J., R. Andrade, R. Alonso, and J. Arechaga. 1998. The nuclear basket of the nuclear pore complex is part of a higher-order filamentous network that is related to chromatin. *J Struct Biol.* 124:51-8.
- Ashburner, M. 1989. *Drosophila: A laboratory handbook.* Cold Spring Harbor Laboratory Press, NY.
- Bannister, A.J., P. Zegerman, J.F. Partridge, E.A. Miska, J.O. Thomas, R.C. Allshire, and T. Kouzarides. 2001. Selective recognition of methylated lysine 9 on histone H3 by the HP1 chromo domain. *Nature.* 410:120-4.
- Bantignies, F., C. Grimaud, S. Lavrov, M. Gabut, and G. Cavalli. 2003. Inheritance of Polycomb-dependent chromosomal interactions in *Drosophila*. *Genes Dev.* 17:2406-20.
- Beisel, C., A. Imhof, J. Greene, E. Kremmer, and F. Sauer. 2002. Histone methylation by the *Drosophila* epigenetic transcriptional regulator Ash1. *Nature.* 419:857-62.
- Bell, A.C., A.G. West, and G. Felsenfeld. 2001. Insulators and boundaries: versatile regulatory elements in the eukaryotic. *Science.* 291:447-50.
- Berchtold, D., Fesser, S., Kaiser, A., Eilert, J.-C., Frohns, F., Sadoni, N., Kremmer, E., Eick, D., Layer, P., and Zink, D. Tissue-specific functional architectures of vertebrate nuclei require a three-dimensional environment. *submitted.*
- Bienz, M., and J. Muller. 1995. Transcriptional silencing of homeotic genes in *Drosophila*. *Bioessays.* 17:775-84.
- Bodoor, K., S. Shaikh, D. Salina, W.H. Raharjo, R. Bastos, M. Lohka, and B. Burke. 1999. Sequential recruitment of NPC proteins to the nuclear periphery at the end of mitosis. *J Cell Sci.* 112 (Pt 13):2253-64.
- Boivin, A., and J.M. Dura. 1998. In vivo chromatin accessibility correlates with gene silencing

- in *Drosophila*. *Genetics*. 150:1539-49.
- Boyle, S., S. Gilchrist, J.M. Bridger, N.L. Mahy, J.A. Ellis, and W.A. Bickmore. 2001. The spatial organization of human chromosomes within the nuclei of normal and emerimutant cells. *Hum Mol Genet*. 10:211-9.
- Braunstein, M., R.E. Sobel, C.D. Allis, B.M. Turner, and J.R. Broach. 1996. Efficient transcriptional silencing in *Saccharomyces cerevisiae* requires a heterochromatin histone acetylation pattern. *Mol Cell Biol*. 16:4349-56.
- Breiling, A., E. Bonte, S. Ferrari, P.B. Becker, and R. Paro. 1999. The *Drosophila* polycomb protein interacts with nucleosomal core particles *In vitro* via its repression domain. *Mol Cell Biol*. 19:8451-60.
- Briggs, S.D., M. Bryk, B.D. Strahl, W.L. Cheung, J.K. Davie, S.Y. Dent, F. Winston, and C.D. Allis. 2001. Histone H3 lysine 4 methylation is mediated by Set1 and required for cell growth and rDNA silencing in *Saccharomyces cerevisiae*. *Genes Dev*. 15:3286-95.
- Brown, J.L., D. Mucci, M. Whiteley, M.L. Dirksen, and J.A. Kassis. 1998. The *Drosophila* Polycomb group gene pleiohomeotic encodes a DNA binding protein with homology to the transcription factor YY1. *Mol Cell*. 1:1057-64.
- Brown, K.E., S. Amoils, J.M. Horn, V.J. Buckle, D.R. Higgs, M. Merckenschlager, and A.G. Fisher. 2001. Expression of alpha- and beta-globin genes occurs within different nuclear domains in haemopoietic cells. *Nat Cell Biol*. 3:602-6.
- Brown, K.E., J. Baxter, D. Graf, M. Merckenschlager, and A.G. Fisher. 1999. Dynamic repositioning of genes in the nucleus of lymphocytes preparing for cell division. *Mol Cell*. 3:207-17.
- Brown, K.E., S.S. Guest, S.T. Smale, K. Hahm, M. Merckenschlager, and A.G. Fisher. 1997. Association of transcriptionally silent genes with Ikaros complexes at centromeric heterochromatin. *Cell*. 91:845-54.
- Brownell, J.E., J. Zhou, T. Ranalli, R. Kobayashi, D.G. Edmondson, S.Y. Roth, and C.D. Allis. 1996. Tetrahymena histone acetyltransferase A: a homolog to yeast Gcn5p linking histone acetylation to gene activation. *Cell*. 84:843-51.
- Buchenau, P., D.J. Arndt-Jovin, and H. Saumweber. 1993. *In vivo* observation of the puff-specific protein no-on transient A (NONA) in nuclei of *Drosophila* embryos. *J Cell Sci*. 106 (Pt 1):189-99.
- Buchenau, P., J. Hodgson, H. Strutt, and D.J. Arndt-Jovin. 1998. The distribution of polycomb-group proteins during cell division and development in *Drosophila* embryos: impact on models for silencing. *J Cell Biol*. 141:469-81.
- Busturia, A., and M. Bienz. 1993. Silencers in abdominal-B, a homeotic *Drosophila* gene. *Embo J*. 12:1415-25.
- Busturia, A., C.D. Wightman, and S. Sakonju. 1997. A silencer is required for maintenance of transcriptional repression throughout *Drosophila* development. *Development*. 124: 4343-50.
- Byrd, K.N., and A. Shearn. 2003. ASH1, a *Drosophila* trithorax group protein, is required for methylation of lysine 4 residues on histone H3. *Proc Natl Acad Sci U S A*. 100:11535-40.
- Campbell, S., M. Inamdar, V. Rodrigues, V. Raghavan, M. Palazzolo, and A. Chovnick. 1992. The scalloped gene encodes a novel, evolutionarily conserved transcription factor required for sensory organ differentiation in *Drosophila*. *Genes Dev*. 6:367-79.
- Campbell, S.D., A. Duttaroy, A.L. Katzen, and A. Chovnick. 1991. Cloning and characterization of the scalloped region of *Drosophila melanogaster*. *Genetics*. 127: 367-80.
- Casolari, J.M., C.R. Brown, S. Komili, J. West, H. Hieronymus, and P.A. Silver. 2004. Genome-wide localization of the nuclear transport machinery couples transcriptional status and nuclear organization. *Cell*. 117:427-39.
- Cavalli, G., and R. Paro. 1998. The *Drosophila* Fab-7 chromosomal element conveys epigenetic inheritance during mitosis and meiosis. *Cell*. 93:505-18.
- Cavalli, G., and R. Paro. 1999. Epigenetic inheritance of active chromatin after removal of the main transactivator. *Science*. 286:955-8.

- Chan, C.S., L. Rastelli, and V. Pirrotta. 1994. A Polycomb response element in the Ubx gene that determines an epigenetically inherited state of repression. *Embo J.* 13:2553-64.
- Chen, T.R. 1977. In situ detection of mycoplasma contamination in cell cultures by fluorescent Hoechst 33258 stain. *Exp Cell Res.* 104:255-62.
- Chinwalla, V., E.P. Jane, and P.J. Harte. 1995. The Drosophila trithorax protein binds to specific chromosomal sites and is co-localized with Polycomb at many sites. *Embo J.* 14:2056-65.
- Cockell, M., and S.M. Gasser. 1999. Nuclear compartments and gene regulation. *Current Opinion in Genetics & Development.* 9:199-205.
- Cordes, V.C., S. Reidenbach, A. Kohler, N. Stuurman, R. van Driel, and W.W. Franke. 1993. Intranuclear filaments containing a nuclear pore complex protein. *J Cell Biol.* 123:1333-44.
- Cordes, V.C., S. Reidenbach, H.R. Rackwitz, and W.W. Franke. 1997. Identification of protein p270/Tpr as a constitutive component of the nuclear pore complex-attached intranuclear filaments. *J Cell Biol.* 136:515-29.
- Cremer, M., J. von Hase, T. Volm, A. Brero, G. Kreth, J. Walter, C. Fischer, I. Solovei, C. Cremer, and T. Cremer. 2001. Non-random radial higher-order chromatin arrangements in nuclei of diploid human cells. *Chromosome Res.* 9:541-67.
- Croft, J.A., J.M. Bridger, S. Boyle, P. Perry, P. Teague, and W.A. Bickmore. 1999. Differences in the localization and morphology of chromosomes in the human nucleus. *J. Cell Biol.* 145:1119-1131.
- Csink, A.K. 2001. Somatic pairing.
- Csink, A.K., A. Bounoutas, M.L. Griffith, J.F. Sabl, and B.T. Sage. 2002. Differential gene silencing by trans-heterochromatin in Drosophila melanogaster. *Genetics.* 160:257-69.
- Csink, A.K., and S. Henikoff. 1996. Genetic modification of heterochromatic association and nuclear organization in Drosophila. *Nature.* 381:529-31.
- Csink, A.K., and S. Henikoff. 1998a. Large-scale chromosomal movements during interphase progression in Drosophila. *J Cell Biol.* 143:13-22.
- Csink, A.K., and S. Henikoff. 1998b. Something from nothing: the evolution and utility of satellite repeats. *Trends Genet.* 14:200-4.
- Czermin, B., R. Melfi, D. McCabe, V. Seitz, A. Imhof, and V. Pirrotta. 2002. Drosophila enhancer of Zeste/ESC complexes have a histone H3 methyltransferase activity that marks chromosomal Polycomb sites. *Cell.* 111:185-96.
- Czermin, B., G. Schotta, B.B. Hulsmann, A. Brehm, P.B. Becker, G. Reuter, and A. Imhof. 2001. Physical and functional association of SU(VAR)3-9 and HDAC1 in Drosophila. *EMBO Rep.* 2:915-9.
- Daigle, N., J. Beaudouin, L. Hartnell, G. Imreh, E. Hallberg, J. Lippincott-Schwartz, and J. Ellenberg. 2001. Nuclear pore complexes form immobile networks and have a very low turnover in live mammalian cells. *J Cell Biol.* 154:71-84.
- Davie, J.R. 1998. Covalent modifications of histones: expression from chromatin templates. *Curr Opin Genet Dev.* 8:173-8.
- Dernburg, A.F., K.W. Broman, J.C. Fung, W.F. Marshall, J. Philips, D.A. Agard, and J.W. Sedat. 1996a. Perturbation of nuclear architecture by long-distance chromosome interactions. *Cell.* 85:745-59.
- Dernburg, A.F., J.W. Sedat, and R.S. Hawley. 1996b. Direct evidence of a role for heterochromatin in meiotic chromosome segregation. *Cell.* 86:135-46.
- Devlin, R.H., B. Bingham, and B.T. Wakimoto. 1990. The organization and expression of the light gene, a heterochromatic gene of Drosophila melanogaster. *Genetics.* 125:129-40.
- Dietzel, S., H. Niemann, B. Bruckner, C. Maurange, and R. Paro. 1999. The nuclear distribution of Polycomb during Drosophila melanogaster development shown with a GFP fusion protein. *Chromosoma.* 108:83-94.
- Dietzel, S., K. Zolghadr, C. Hepperger, and A.S. Belmont. 2004. Differential large-scale chromatin compaction and intranuclear positioning of transcribed versus non-

- transcribed transgene arrays containing beta-globin regulatory sequences. *J Cell Sci.* 117:4603-14.
- Dillon, N., and R. Festenstein. 2002. Unravelling heterochromatin: competition between positive and negative factors regulates accessibility. *Trends Genet.* 18:252-8.
- Echalier, G., and A. Ohanessian. 1970. In vitro culture of *Drosophila melanogaster* embryonic cells. *In Vitro.* 6:162-72.
- Ekwall, K., E.R. Nimmo, J.P. Javerzat, B. Borgstrom, R. Egel, G. Cranston, and R. Allshire. 1996. Mutations in the fission yeast silencing factors *clr4+* and *rik1+* disrupt the localisation of the chromo domain protein Swi6p and impair centromere function. *J Cell Sci.* 109 (Pt 11):2637-48.
- Elbashir, S.M., J. Harborth, W. Lendeckel, A. Yalcin, K. Weber, and T. Tuschl. 2001a. Duplexes of 21-nucleotide RNAs mediate RNA interference in cultured mammalian cells. *Nature.* 411:494-8.
- Elbashir, S.M., J. Harborth, K. Weber, and T. Tuschl. 2002. Analysis of gene function in somatic mammalian cells using small interfering RNAs. *Methods.* 26:199-213.
- Elbashir, S.M., W. Lendeckel, and T. Tuschl. 2001b. RNA interference is mediated by 21- and 22-nucleotide RNAs. *Genes Dev.* 15:188-200.
- Elgin, S.C. 1996. Heterochromatin and gene regulation in *Drosophila*. *Curr Opin Genet Dev.* 6:193-202.
- Elgin, S.C., and S.I. Grewal. 2003. Heterochromatin: silence is golden. *Curr Biol.* 13:R895-8.
- Englmann, A. 2005. Kernpositionierung und funktionelle Regulation von Genen der humanen CFTR-Region auf Chromosom 7. In Fakultät für Biologie. LMU München, München. 161.
- Englmann, A., L.A. Clarke, S. Christan, M.D. Amaral, D. Schindelbauer, and D. Zink. 2005. The replication timing of CFTR and adjacent genes. *Chromosome Res.* 13:183-94.
- Fauvarque, M.O., and J.M. Dura. 1993. polyhomeotic regulatory sequences induce developmental regulator-dependent variegation and targeted P-element insertions in *Drosophila*. *Genes Dev.* 7:1508-20.
- Felsenfeld, G. 1996. Chromatin unfolds. *Cell.* 86:13-19.
- Feuerbach, F., V. Galy, E. Trelles-Sticken, M. Fromont-Racine, A. Jacquier, E. Gilson, J.C. Olivo-Marin, H. Scherthan, and U. Nehrbass. 2002. Nuclear architecture and spatial positioning help establish transcriptional states of telomeres in yeast. *Nat Cell Biol.* 4: 214-21.
- Ficz, G., R. Heintzmann, and D.J. Arndt-Jovin. 2005. Polycomb group protein complexes exchange rapidly in living *Drosophila*. *Development.* 132:3963-76.
- Fischle, W., Y. Wang, S.A. Jacobs, Y. Kim, C.D. Allis, and S. Khorasanizadeh. 2003. Molecular basis for the discrimination of repressive methyl-lysine marks in histone H3 by Polycomb and HP1 chromodomains. *Genes Dev.* 17:1870-81.
- Fletcher, T.M., and J.C. Hansen. 1995. Core histone tail domains mediate oligonucleosome folding and nucleosomal DNA organization through distinct molecular mechanisms. *J Biol Chem.* 270:25359-62.
- Follenzi, A., L.E. Ailles, S. Bakovic, M. Geuna, and L. Naldini. 2000. Gene transfer by lentiviral vectors is limited by nuclear translocation and rescued by HIV-1 pol sequences. *Nat Genet.* 25:217-22.
- Francis, N.J., and R.E. Kingston. 2001. Mechanisms of transcriptional memory. *Nat Rev Mol Cell Biol.* 2:409-21.
- Francis, N.J., A.J. Saurin, Z. Shao, and R.E. Kingston. 2001. Reconstitution of a functional core polycomb repressive complex. *Mol Cell.* 8:545-56.
- Franke, A., M. DeCamillis, D. Zink, N. Cheng, H.W. Brock, and R. Paro. 1992. Polycomb and polyhomeotic are constituents of a multimeric protein complex in chromatin of *Drosophila melanogaster*. *Embo J.* 11:2941-50.
- Galy, V., J.C. Olivo-Marin, H. Scherthan, V. Doye, N. Rascalou, and U. Nehrbass. 2000. Nuclear pore complexes in the organization of silent telomeric chromatin. *Nature.* 403:108-12.
- Gaszner, M., and G. Felsenfeld. 2006. Insulators: exploiting transcriptional and epigenetic

- mechanisms. *Nat Rev Genet.* 7:703-13.
- Gemkow, M.J., P.J. Verveer, and D.J. Arndt-Jovin. 1998. Homologous association of the Bithorax-Complex during embryogenesis: consequences for transvection in *Drosophila melanogaster*. *Development.* 125:4541-52.
- Gerasimova, T.I., K. Byrd, and V.G. Corces. 2000. A chromatin insulator determines the nuclear localization of DNA. *Mol Cell.* 6:1025-35.
- Gerasimova, T.I., and V.G. Corces. 1996. Boundary and insulator elements in chromosomes. *Curr Opin Genet Dev.* 6:185-92.
- Giancotti, V., E. Russo, F. de Cristini, G. Graziosi, F. Micali, and C. Crane-Robinson. 1984. Histone modification in early and late *Drosophila* embryos. *Biochem J.* 218:321-9.
- Gilbert, D.M. 2002. Replication timing and transcriptional control: beyond cause and effect. *Curr Opin Cell Biol.* 14:377-83.
- Goldberg, M., A. Harel, M. Brandeis, T. Rechsteiner, T.J. Richmond, A.M. Weiss, and Y. Gruenbaum. 1999. The tail domain of lamin Dm0 binds histones H2A and H2B. *Proc Natl Acad Sci U S A.* 96:2852-7.
- Goldman, R.D., Y. Gruenbaum, R.D. Moir, D.K. Shumaker, and T.P. Spann. 2002. Nuclear lamins: building blocks of nuclear architecture. *Genes Dev.* 16:533-47.
- Grant, P.A., A. Eberharter, S. John, R.G. Cook, B.M. Turner, and J.L. Workman. 1999. Expanded lysine acetylation specificity of Gcn5 in native complexes. *J Biol Chem.* 274:5895-900.
- Grewal, S.I., and S.C. Elgin. 2002. Heterochromatin: new possibilities for the inheritance of structure. *Curr Opin Genet Dev.* 12:178-87.
- Grimaud, C., F. Bantignies, M. Pal-Bhadra, P. Ghana, U. Bhadra, and G. Cavalli. 2006. RNAi components are required for nuclear clustering of Polycomb group response elements. *Cell.* 124:957-71.
- Gruenbaum, Y., A. Margalit, R.D. Goldman, D.K. Shumaker, and K.L. Wilson. 2005. The nuclear lamina comes of age. *Nat Rev Mol Cell Biol.* 6:21-31.
- Guenatri, M., D. Bailly, C. Maison, and G. Almouzni. 2004. Mouse centric and pericentric satellite repeats form distinct functional heterochromatin. *J Cell Biol.* 166:493-505.
- Gunster, M.J., D.P. Satijn, K.M. Hamer, J.L. den Blaauwen, D. de Bruijn, M.J. Alkema, M. van Lohuizen, R. van Driel, and A.P. Otte. 1997. Identification and characterization of interactions between the vertebrate polycomb-group protein BMI1 and human homologs of polyhomeotic. *Mol Cell Biol.* 17:2326-35.
- Gyurkovics, H., J. Gausz, J. Kummer, and F. Karch. 1990. A new homeotic mutation in the *Drosophila* bithorax complex removes a boundary separating two domains of regulation. *Embo J.* 9:2579-85.
- Hagstrom, K., M. Muller, and P. Schedl. 1996. Fab-7 functions as a chromatin domain boundary to ensure proper segment specification by the *Drosophila* bithorax complex. *Genes Dev.* 10:3202-15.
- Hagstrom, K., M. Muller, and P. Schedl. 1997. A Polycomb and GAGA dependent silencer adjoins the Fab-7 boundary in the *Drosophila* bithorax complex. *Genetics.* 146:1365-80.
- Hanson, R.D., J.L. Hess, B.D. Yu, P. Ernst, M. van Lohuizen, A. Berns, N.M. van der Lugt, C.S. Shashikant, F.H. Ruddle, M. Seto, and S.J. Korsmeyer. 1999. Mammalian Trithorax and polycomb-group homologues are antagonistic regulators of homeotic development. *Proc Natl Acad Sci U S A.* 96:14372-7.
- Harel, A., Goldberg, M., Ulitzur, N., and Gruenbaum, Y. 1998. Structural organization and biological roles of the nuclear lamina. In *Textbook of gene therapy and molecular biology: from basic mechanism to clinical applications*. Vol. 1. P.A. T. Boulikas, editor. Gene Therapy Press. 529-542.
- Hartl, D.L., D.I. Nurminsky, R.W. Jones, and E.R. Lozovskaya. 1994. Genome structure and evolution in *Drosophila*: applications of the framework P1 map. *Proc Natl Acad Sci U S A.* 91:6824-9.
- Hase, M.E., and V.C. Cordes. 2003. Direct interaction with nup153 mediates binding of Tpr to the periphery of the nuclear pore complex. *Mol Biol Cell.* 14:1923-40.

- Hebbes, T.R., A.W. Thorne, and C. Crane-Robinson. 1988. A direct link between core histone acetylation and transcriptionally active chromatin. *Embo J.* 7:1395-402.
- Heitz, E. 1928. Das Heterochromatin der Moose. *I. Jahrb. Wiss. Botanik.* 69:762-818.
- Henikoff, S. 1997. Nuclear organization and gene expression: homologous pairing and long-range interactions. *Curr Opin Cell Biol.* 9:388-95.
- Heun, P., T. Laroche, K. Shimada, P. Furrer, and S.M. Gasser. 2001. Chromosome dynamics in the yeast interphase nucleus. *Science.* 294:2181-6.
- Hochstrasser, M., and J.W. Sedat. 1987a. Three-dimensional organization of *Drosophila melanogaster* interphase nuclei. I. Tissue-specific aspects of polytene nuclear architecture. *J Cell Biol.* 104:1455-70.
- Hochstrasser, M., and J.W. Sedat. 1987b. Three-dimensional organization of *Drosophila melanogaster* interphase nuclei. II. Chromosome spatial organization and gene regulation. *J Cell Biol.* 104:1471-83.
- Hofmann, A., B. Kessler, S. Ewerling, A. Kabermann, G. Brem, E. Wolf, and A. Pfeifer. 2006. Epigenetic regulation of lentiviral transgene vectors in a large animal model. *Mol Ther.* 13:59-66.
- Hofmann, A., B. Kessler, S. Ewerling, M. Weppert, B. Vogg, H. Ludwig, M. Stojkovic, M. Boelhaue, G. Brem, E. Wolf, and A. Pfeifer. 2003. Efficient transgenesis in farm animals by lentiviral vectors. *EMBO Rep.* 4:1054-60.
- Huang, D.W., L. Fanti, D.T. Pak, M.R. Botchan, S. Pimpinelli, and R. Kellum. 1998. Distinct cytoplasmic and nuclear fractions of *Drosophila* heterochromatin protein 1: their phosphorylation levels and associations with origin recognition complex proteins. *J Cell Biol.* 142:307-18.
- Huisken, J., J. Swoger, F. Del Bene, J. Wittbrodt, and E.H. Stelzer. 2004. Optical sectioning deep inside live embryos by selective plane illumination microscopy. *Science.* 305:1007-9.
- Iborra, F.J., A. Pombo, D.A. Jackson, and P.R. Cook. 1996. Active RNA polymerases are localized within discrete transcription „factories“ in human nuclei. *J Cell Sci.* 109:1427-36.
- Ingham, P.W., and A. Martinez Arias. 1992. Boundaries and fields in early embryos. *Cell.* 68:221-35.
- Ishii, K., G. Arib, C. Lin, G. Van Houwe, and U.K. Laemmli. 2002. Chromatin boundaries in budding yeast: the nuclear pore connection. *Cell.* 109:551-62.
- Ivanova, A.V., M.J. Bonaduce, S.V. Ivanov, and A.J. Klar. 1998. The chromo and SET domains of the Clr4 protein are essential for silencing in fission yeast. *Nat Genet.* 19:192-5.
- Jackson, D.A., A.B. Hassan, R.J. Errington, and P.R. Cook. 1993. Visualization of focal sites of transcription within human nuclei. *Embo J.* 12:1059-65.
- Jenuwein, T. 2001. Re-SET-ting heterochromatin by histone methyltransferases. *Trends Cell Biol.* 11:266-73.
- Jenuwein, T., and C.D. Allis. 2001. Translating the histone code. *Science.* 293:1074-80.
- Jenuwein, T., G. Laible, R. Dorn, and G. Reuter. 1998. SET domain proteins modulate chromatin domains in eu- and heterochromatin. *Cell Mol Life Sci.* 54:80-93.
- Kal, A.J., T. Mahmoudi, N.B. Zak, and C.P. Verrijzer. 2000. The *Drosophila* brahma complex is an essential coactivator for the trithorax group protein zeste. *Genes Dev.* 14:1058-71.
- Kassis, J.A. 1994. Unusual properties of regulatory DNA from the *Drosophila* engrailed gene: three „pairing-sensitive“ sites within a 1.6-kb region. *Genetics.* 136:1025-38.
- Kassis, J.A. 2002. Pairing-sensitive silencing, polycomb group response elements, and transposon homing in *Drosophila*. *Adv Genet.* 46:421-38.
- Kassis, J.A., E.P. VanSickle, and S.M. Sensabaugh. 1991. A fragment of engrailed regulatory DNA can mediate transvection of the white gene in *Drosophila*. *Genetics.* 128:751-61.
- Kaufmann, B.P. 1938. Nucleolus-organizing regions in salivary gland chromosomes of *Drosophila melanogaster*. *Cell and Tissue Research.* 28:1-11.
- Keller, P.J., F. Pampaloni, and E.H. Stelzer. 2006. Life sciences require the third dimension.

- Curr Opin Cell Biol.* 18:117-24.
- Klymenko, T., B. Papp, W. Fischle, T. Kocher, M. Schelder, C. Fritsch, B. Wild, M. Wilm, and J. Muller. 2006. A Polycomb group protein complex with sequence-specific DNA-binding and selective methyl-lysine-binding activities. *Genes Dev.* 20:1110-22.
- Koonin, E.V., S. Zhou, and J.C. Lucchesi. 1995. The chromo superfamily: new members, duplication of the chromo domain and possible role in delivering transcription regulators to chromatin. *Nucleic Acids Res.* 23:4229-33.
- Kornberg, R.D. 1974. Chromatin structure: a repeating unit of histones and DNA. *Science.* 184:868-71.
- Kosak, S.T., and M. Groudine. 2004. Form follows function: The genomic organization of cellular differentiation. *Genes Dev.* 18:1371-84.
- Kosak, S.T., J.A. Skok, K.L. Medina, R. Riblet, M.M. Le Beau, A.G. Fisher, and H. Singh. 2002. Subnuclear compartmentalization of immunoglobulin loci during lymphocyte development. *Science.* 296:158-62.
- Kouzarides, T. 2002. Histone methylation in transcriptional control. *Curr Opin Genet Dev.* 12:198-209.
- Krull, S., J. Thyberg, B. Bjorkroth, H.R. Rackwitz, and V.C. Cordes. 2004. Nucleoporins as components of the nuclear pore complex core structure and Tpr as the architectural element of the nuclear basket. *Mol Biol Cell.* 15:4261-77.
- Kuo, M.H., J.E. Brownell, R.E. Sobel, T.A. Ranalli, R.G. Cook, D.G. Edmondson, S.Y. Roth, and C.D. Allis. 1996. Transcription-linked acetylation by Gcn5p of histones H3 and H4 at specific lysines. *Nature.* 383:269-72.
- Kuo, M.H., J. Zhou, P. Jambeck, M.E. Churchill, and C.D. Allis. 1998. Histone acetyltransferase activity of yeast Gcn5p is required for the activation of target genes in vivo. *Genes Dev.* 12:627-39.
- Lachner, M., D. O'Carroll, S. Rea, K. Mechtler, and T. Jenuwein. 2001. Methylation of histone H3 lysine 9 creates a binding site for HP1 proteins. *Nature.* 410:116-20.
- Lachner, M., R.J. O'Sullivan, and T. Jenuwein. 2003. An epigenetic road map for histone lysine methylation. *J Cell Sci.* 116:2117-24.
- Lamond, A.I., and W.C. Earnshaw. 1998. Structure and function in the nucleus. *Science.* 280:547-53.
- Lang, S. 2003. Untersuchung zur Lokalisierung von drei benachbarten Genen der humanen „Cystic Fibrosis Transmembrane Conductance Regulator“-Region im Zellkern. In Department Biology II. LMU Munich, Munich. 1-89.
- Laroche, T., S.G. Martin, M. Gotta, H.C. Gorham, F.E. Pryde, E.J. Louis, and S.M. Gasser. 1998. Mutation of yeast Ku genes disrupts the subnuclear organization of telomeres. *Curr Biol.* 8:653-6.
- Lengauer, C., E.D. Green, and T. Cremer. 1992. Fluorescence in situ hybridization of YAC clones after Alu-PCR amplification. *Genomics.* 13:826-8.
- Levine, S.S., A. Weiss, H. Erdjument-Bromage, Z. Shao, P. Tempst, and R.E. Kingston. 2002. The core of the polycomb repressive complex is compositionally and functionally conserved in flies and humans. *Mol Cell Biol.* 22:6070-8.
- Lewis, E.B. 1954. The theory and application of a new method of detecting chromosomal rearrangements in *Drosophila melanogaster*. *American Naturalist.* 88:255-239.
- Lewis, E.B., J.D. Knafels, D.R. Mathog, and S.E. Celniker. 1995. Sequence analysis of the cis-regulatory regions of the bithorax complex of *Drosophila*. *Proc Natl Acad Sci U S A.* 92:8403-7.
- Liu, J., T. Rolef Ben-Shahar, D. Riemer, M. Treinin, P. Spann, K. Weber, A. Fire, and Y. Gruenbaum. 2000. Essential roles for *Caenorhabditis elegans* lamin gene in nuclear organization, cell cycle progression, and spatial organization of nuclear pore complexes. *Mol Biol Cell.* 11:3937-47.
- Lohe, A.R., A.J. Hilliker, and P.A. Roberts. 1993. Mapping simple repeated DNA sequences in heterochromatin of *Drosophila melanogaster*. *Genetics.* 134:1149-74.
- Lu, B.Y., P.C. Emtage, B.J. Duyf, A.J. Hilliker, and J.C. Eissenberg. 2000. Heterochromatin protein 1 is required for the normal expression of two heterochromatin genes in

- Drosophila*. *Genetics*. 155:699-708.
- Lucchesi, J.C. 1996. Dosage compensation in *Drosophila* and the „complex‘ world of transcriptional regulation. *Bioessays*. 18:541-7.
- Luger, K., and T.J. Richmond. 1998. The histone tails of the nucleosome. *Curr Opin Genet Dev*. 8:140-6.
- Lundgren, M., C.M. Chow, P. Sabbattini, A. Georgiou, S. Minaee, and N. Dillon. 2000. Transcription factor dosage affects changes in higher order chromatin structure associated with activation of a heterochromatic gene. *Cell*. 103:733-43.
- Manuelidis, L. 1990. A view of interphase chromosomes. *Science*. 250:1533-40.
- Marshall, W.F., A. Straight, J.F. Marko, J. Swedlow, A. Dernburg, A. Belmont, A.W. Murray, D.A. Agard, and J.W. Sedat. 1997. Interphase chromosomes undergo constrained diffusional motion in living cells. *Curr Biol*. 7:930-9.
- Martin, C., N. Beaujean, V. Brochard, C. Audouard, D. Zink, and P. Debey. 2006. Genome restructuring in mouse embryos during reprogramming and early development. *Dev Biol*. 292:317-32.
- Messmer, S., A. Franke, and R. Paro. 1992. Analysis of the functional role of the Polycomb chromo domain in *Drosophila melanogaster*. *Genes Dev*. 6:1241-54.
- Misteli, T. 2004. Spatial positioning; a new dimension in genome function. *Cell*. 119:153-6.
- Muller, J., C.M. Hart, N.J. Francis, M.L. Vargas, A. Sengupta, B. Wild, E.L. Miller, M.B. O‘Connor, R.E. Kingston, and J.A. Simon. 2002. Histone methyltransferase activity of a *Drosophila* Polycomb group repressor complex. *Cell*. 111:197-208.
- Muller, J., and J.A. Kassis. 2006. Polycomb response elements and targeting of Polycomb group proteins in *Drosophila*. *Curr Opin Genet Dev*. 16:476-484.
- Muller, M., K. Hagstrom, H. Gyurkovics, V. Pirrotta, and P. Schedl. 1999. The mcp element from the *Drosophila melanogaster* bithorax complex mediates long-distance regulatory interactions. *Genetics*. 153:1333-56.
- Myers, F.A., D.R. Evans, A.L. Clayton, A.W. Thorne, and C. Crane-Robinson. 2001. Targeted and extended acetylation of histones H4 and H3 at active and inactive genes in chicken embryo erythrocytes. *J Biol Chem*. 276:20197-205.
- Ng, J., C.M. Hart, K. Morgan, and J.A. Simon. 2000. A *Drosophila* ESC-E(Z) protein complex is distinct from other polycomb group complexes and contains covalently modified ESC. *Mol Cell Biol*. 20:3069-78.
- Noma, K., C.D. Allis, and S.I. Grewal. 2001. Transitions in distinct histone H3 methylation patterns at the heterochromatin domain boundaries. *Science*. 293:1150-5.
- Orlando, V. 2003. Polycomb, epigenomes, and control of cell identity. *Cell*. 112:599-606.
- Orlando, V., E.P. Jane, V. Chinwalla, P.J. Harte, and R. Paro. 1998. Binding of trithorax and Polycomb proteins to the bithorax complex: dynamic changes during early *Drosophila* embryogenesis. *Embo J*. 17:5141-50.
- Orlando, V., and R. Paro. 1993. Mapping Polycomb-repressed domains in the bithorax complex using in vivo formaldehyde cross-linked chromatin. *Cell*. 75:1187-98.
- Orlando, V., and R. Paro. 1995. Chromatin multiprotein complexes involved in the maintenance of transcription patterns. *Curr Opin Genet Dev*. 5:174-9.
- Papoulas, O., S.J. Beek, S.L. Moseley, C.M. McCallum, M. Sarte, A. Shearn, and J.W. Tamkun. 1998. The *Drosophila* trithorax group proteins BRM, ASH1 and ASH2 are subunits of distinct protein complexes. *Development*. 125:3955-66.
- Papp, B., and J. Muller. 2006. Histone trimethylation and the maintenance of transcriptional ON and OFF states by trxG and PcG proteins. *Genes Dev*. 20:2041-54.
- Parekh, B.S., and T. Maniatis. 1999. Virus infection leads to localized hyperacetylation of histones H3 and H4 at the IFN-beta promoter. *Mol Cell*. 3:125-9.
- Paro, R., and P.J. Harte. 1996. The role of Polycomb group and trithorax group chromatin complexes in the maintenance of determined cell states. In *Epigenetic Mechanisms of Gene Regulation*. V.E.A. Russo, R.A. Martienssen, and A.R. Riggs, editors. Cold Spring Harbor Laboratory Press, Cold Spring Harbor, NY. 507-528.
- Paro, R., and D.S. Hogness. 1991. The Polycomb protein shares a homologous domain with a heterochromatin-associated protein of *Drosophila*. *Proc Natl Acad Sci U S A*. 88:

263-7.

- Parreira, L., M. Telhada, C. Ramos, R. Hernandez, H. Neves, and M. Carmo-Fonseca. 1997. The spatial distribution of human immunoglobulin genes within the nucleus: evidence for gene topography independent of cell type and transcriptional activity. *Hum Genet.* 100:588-94.
- Patience, C., W.M. Switzer, Y. Takeuchi, D.J. Griffiths, M.E. Goward, W. Heneine, J.P. Stoye, and R.A. Weiss. 2001. Multiple groups of novel retroviral genomes in pigs and related species. *J Virol.* 75:2771-5.
- Pawley, J.B. 1995. Handbook of Biological Confocal Microscopy. Plenum Press, New York.
- Peters, A.H., J.E. Mermoud, D. O'Carroll, M. Pagani, D. Schweizer, N. Brockdorff, and T. Jenuwein. 2002. Histone H3 lysine 9 methylation is an epigenetic imprint of facultative heterochromatin. *Nat. Genet.* 30:77-80.
- Peters, A.H., D. O'Carroll, H. Scherthan, K. Mechtler, S. Sauer, C. Schofer, K. Weipoltshammer, M. Pagani, M. Lachner, A. Kohlmaier, S. Opravil, M. Doyle, M. Sibilia, and T. Jenuwein. 2001. Loss of the Suv39h histone methyltransferases impairs mammalian heterochromatin and genome stability. *Cell.* 107:323-37.
- Petruk, S., Y. Sedkov, S. Smith, S. Tillib, V. Kraevski, T. Nakamura, E. Canaani, C.M. Croce, and A. Mazo. 2001. Trithorax and dCBP acting in a complex to maintain expression of a homeotic gene. *Science.* 294:1331-4.
- Pickersgill, H., B. Kalverda, E. de Wit, W. Talhout, M. Fornerod, and B. van Steensel. 2006. Characterization of the Drosophila melanogaster genome at the nuclear lamina. *Nat Genet.*
- Pirrotta, V. 1995. Chromatin complexes regulating gene expression in Drosophila. *Curr Opin Genet Dev.* 5:466-72.
- Pirrotta, V. 1998. Polycomb the genome: PcG, trxG, and chromatin silencing. *Cell.* 93:333-6.
- Pirrotta, V. 1999. Transvection and chromosomal trans-interaction effects. *Biochim Biophys Acta.* 1424:M1-8.
- Platero, J.S., T. Hartnett, and J.C. Eissenberg. 1995. Functional analysis of the chromo domain of HP1. *Embo J.* 14:3977-86.
- Ramalho, A.S., S. Beck, M. Meyer, D. Penque, G.R. Cutting, and M.D. Amaral. 2002. Five percent of normal cystic fibrosis transmembrane conductance regulator mRNA ameliorates the severity of pulmonary disease in cystic fibrosis. *Am J Respir Cell Mol Biol.* 27:619-27.
- Rastelli, L., C.S. Chan, and V. Pirrotta. 1993. Related chromosome binding sites for zeste, suppressors of zeste and Polycomb group proteins in Drosophila and their dependence on Enhancer of zeste function. *Embo J.* 12:1513-22.
- Rea, S., F. Eisenhaber, D. O'Carroll, B.D. Strahl, Z.W. Sun, M. Schmid, S. Opravil, K. Mechtler, C.P. Ponting, C.D. Allis, and T. Jenuwein. 2000. Regulation of chromatin structure by site-specific histone H3 methyltransferases. *Nature.* 406:593-9.
- Reuter, G., and P. Spierer. 1992. Position effect variegation and chromatin proteins. *Bioessays.* 14:605-12.
- Ringrose, L., and R. Paro. 2004. Epigenetic regulation of cellular memory by the Polycomb and Trithorax group proteins. *Annu Rev Genet.* 38:413-43.
- Ringrose, L., M. Rehmsmeier, J.M. Dura, and R. Paro. 2003. Genome-wide prediction of Polycomb/Trithorax response elements in Drosophila melanogaster. *Dev Cell.* 5:759-71.
- Ross, R.A., B.A. Spengler, and J.L. Biedler. 1983. Coordinate morphological and biochemical interconversion of human neuroblastoma cells. *J Natl Cancer Inst.* 71:741-7.
- Rozovskaia, T., S. Tillib, S. Smith, Y. Sedkov, O. Rozenblatt-Rosen, S. Petruk, T. Yano, T. Nakamura, L. Ben-Simchon, J. Gildea, C.M. Croce, A. Shearn, E. Canaani, and A. Mazo. 1999. Trithorax and ASH1 interact directly and associate with the trithorax group-responsive bxd region of the Ultrabithorax promoter. *Mol Cell Biol.* 19:6441-7.
- Rundlett, S.E., A.A. Carmen, R. Kobayashi, S. Bavykin, B.M. Turner, and M. Grunstein. 1996. HDA1 and RPD3 are members of distinct yeast histone deacetylase complexes that

- regulate silencing and transcription. *Proc Natl Acad Sci U S A*. 93:14503-8.
- Sadoni, N., S. Langer, C. Fauth, G. Bernardi, T. Cremer, B.M. Turner, and D. Zink. 1999. Nuclear organization of mammalian genomes. Polar chromosome territories build up functionally distinct higher order compartments. *J Cell Biol*. 146:1211-26.
- Santos-Rosa, H., R. Schneider, A.J. Bannister, J. Sherriff, B.E. Bernstein, N.C. Emre, S.L. Schreiber, J. Mellor, and T. Kouzarides. 2002. Active genes are tri-methylated at K4 of histone H3. *Nature*. 419:407-11.
- Saurin, A.J., Z. Shao, H. Erdjument-Bromage, P. Tempst, and R.E. Kingston. 2001. A Drosophila Polycomb group complex includes Zeste and dTAFII proteins. *Nature*. 412:655-60.
- Saurin, A.J., C. Shiels, J. Williamson, D.P. Satijn, A.P. Otte, D. Sheer, and P.S. Freemont. 1998. The human polycomb group complex associates with pericentromeric heterochromatin to form a novel nuclear domain. *J Cell Biol*. 142:887-98.
- Scherer, W.F., and A.F. Hoogasian. 1954. Preservation at subzero temperatures of mouse fibroblasts (strain L) and human epithelial cells (strain HeLa). *Proc Soc Exp Biol Med*. 87:480-7.
- Schneider, R., A.J. Bannister, F.A. Myers, A.W. Thorne, C. Crane-Robinson, and T. Kouzarides. 2004. Histone H3 lysine 4 methylation patterns in higher eukaryotic genes. *Nat Cell Biol*. 6:73-7.
- Schotta, G., A. Ebert, V. Krauss, A. Fischer, J. Hoffmann, S. Rea, T. Jenuwein, R. Dorn, and G. Reuter. 2002. Central role of Drosophila SU(VAR)3-9 in histone H3-K9 methylation and heterochromatic gene silencing. *EMBO J*. 21:1121-31.
- Schotta, G., M. Lachner, K. Sarma, A. Ebert, R. Sengupta, G. Reuter, D. Reinberg, and T. Jenuwein. 2004. A silencing pathway to induce H3-K9 and H4-K20 trimethylation at constitutive heterochromatin. *Genes Dev*. 18:1251-62.
- Schroder, A.R., P. Shinn, H. Chen, C. Berry, J.R. Ecker, and F. Bushman. 2002. HIV-1 integration in the human genome favors active genes and local hotspots. *Cell*. 110: 521-9.
- Schubeler, D., C. Francastel, D.M. Cimbor, A. Reik, D.I. Martin, and M. Groudine. 2000. Nuclear localization and histone acetylation: a pathway for chromatin opening and transcriptional activation of the human beta-globin locus. *Genes Dev*. 14:940-50.
- Schubeler, D., D.M. MacAlpine, D. Scalzo, C. Wirbelauer, C. Kooperberg, F. van Leeuwen, D.E. Gottschling, L.P. O'Neill, B.M. Turner, J. Delrow, S.P. Bell, and M. Groudine. 2004. The histone modification pattern of active genes revealed through genome-wide chromatin analysis of a higher eukaryote. *Genes Dev*. 18:1263-71.
- Segura-Totten, M., and K.L. Wilson. 2004. BAF: roles in chromatin, nuclear structure and retrovirus integration. *Trends Cell Biol*. 14:261-6.
- Selig, S., K. Okumura, D.C. Ward, and H. Cedar. 1992. Delineation of DNA replication time zones by fluorescence in situ hybridization. *Embo J*. 11:1217-25.
- Shao, Z., F. Raible, R. Mollaaghababa, J.R. Guyon, C.T. Wu, W. Bender, and R.E. Kingston. 1999. Stabilization of chromatin structure by PRC1, a Polycomb complex. *Cell*. 98: 37-46.
- Sigrist, C.J., and V. Pirrotta. 1997. Chromatin insulator elements block the silencing of a target gene by the Drosophila polycomb response element (PRE) but allow trans interactions between PREs on different chromosomes. *Genetics*. 147:209-21.
- Simon, J., A. Chiang, W. Bender, M.J. Shimell, and M. O'Connor. 1993. Elements of the Drosophila bithorax complex that mediate repression by Polycomb group products. *Dev Biol*. 158:131-44.
- Simon, J.A., and J.W. Tamkun. 2002. Programming off and on states in chromatin: mechanisms of Polycomb and trithorax group complexes. *Curr Opin Genet Dev*. 12: 210-8.
- Skok, J.A., K.E. Brown, V. Azuara, M.L. Caparros, J. Baxter, K. Takacs, N. Dillon, D. Gray, R.P. Perry, M. Merkenschlager, and A.G. Fisher. 2001. Nonequivalent nuclear location of immunoglobulin alleles in B lymphocytes. *Nat Immunol*. 2:848-54.
- Srivastava, A., A.J. Simmonds, A. Garg, L. Fossheim, S.D. Campbell, and J.B. Bell. 2004.

- Molecular and functional analysis of scalloped recessive lethal alleles in *Drosophila melanogaster*. *Genetics*. 166:1833-43.
- Strahl, B.D., and C.D. Allis. 2000. The language of covalent histone modifications. *Nature*. 403:41-5.
- Strahl, B.D., R. Ohba, R.G. Cook, and C.D. Allis. 1999. Methylation of histone H3 at lysine 4 is highly conserved and correlates with transcriptionally active nuclei in *Tetrahymena*. *Proc Natl Acad Sci U S A*. 96:14967-72.
- Strutt, H., G. Cavalli, and R. Paro. 1997. Co-localization of Polycomb protein and GAGA factor on regulatory elements responsible for the maintenance of homeotic gene expression. *Embo J*. 16:3621-32.
- Strutt, H., and R. Paro. 1997. The polycomb group protein complex of *Drosophila melanogaster* has different compositions at different target genes. *Mol Cell Biol*. 17: 6773-83.
- Sukegawa, J., and G. Blobel. 1993. A nuclear pore complex protein that contains zinc finger motifs, binds DNA, and faces the nucleoplasm. *Cell*. 72:29-38.
- Sullivan, B., and G. Karpen. 2001. Centromere identity in *Drosophila* is not determined in vivo by replication timing. *J Cell Biol*. 154:683-90.
- Sun, F.L., M.H. Cuaycong, and S.C. Elgin. 2001. Long-range nucleosome ordering is associated with gene silencing in *Drosophila melanogaster* pericentric heterochromatin. *Mol Cell Biol*. 21:2867-79.
- Telenius, H., N.P. Carter, C.E. Bebb, M. Nordenskjold, B.A. Ponder, and A. Tunnacliffe. 1992. Degenerate oligonucleotide-primed PCR: general amplification of target DNA by a single degenerate primer. *Genomics*. 13:718-25.
- Thakar, R., and A.K. Csink. 2005. Changing chromatin dynamics and nuclear organization during differentiation in *Drosophila* larval tissue. *J Cell Sci*. 118:951-60.
- Thorne, A.W., D. Kmiecik, K. Mitchelson, P. Sautiere, and C. Crane-Robinson. 1990. Patterns of histone acetylation. *Eur J Biochem*. 193:701-13.
- Tie, F., T. Furuyama, J. Prasad-Sinha, E. Jane, and P.J. Harte. 2001. The *Drosophila* Polycomb Group proteins ESC and E(Z) are present in a complex containing the histone-binding protein p55 and the histone deacetylase RPD3. *Development*. 128: 275-86.
- Tumbar, T., and A.S. Belmont. 2001. Interphase movements of a DNA chromosome region modulated by VP16 transcriptional activator. *Nat Cell Biol*. 3:134-9.
- Turner, B.M. 2000. Histone acetylation and an epigenetic code. *Bioessays*. 22:836-45.
- Turner, B.M., A.J. Birley, and J. Lavender. 1992. Histone H4 isoforms acetylated at specific lysine residues define individual chromosomes and chromatin domains in *Drosophila* polytene nuclei. *Cell*. 69:375-84.
- van Holde, K. 1989. Chromatin. New York: Springer Press.
- Vazquez, J., M. Muller, V. Pirrotta, and J.W. Sedat. 2006. The Mcp element mediates stable long-range chromosome-chromosome interactions in *Drosophila*. *Mol Biol Cell*. 17: 2158-65.
- Vlcek, S., T. Dechat, and R. Foisner. 2001. Nuclear envelope and nuclear matrix: interactions and dynamics. *Cell Mol Life Sci*. 58:1758-65.
- Wallrath, L.L., and S.C. Elgin. 1995. Position effect variegation in *Drosophila* is associated with an altered chromatin structure. *Genes Dev*. 9:1263-77.
- Wei, X., S. Somanathan, J. Samarabandu, and R. Berezney. 1999. Three-dimensional visualization of transcription sites and their association with splicing factor-rich nuclear speckles. *J Cell Biol*. 146:543-58.
- Weidtkamp-Peters, S., H.P. Rahn, M.C. Cardoso, and P. Hemmerich. 2006. Replication of centromeric heterochromatin in mouse fibroblasts takes place in early, middle, and late S phase. *Histochem Cell Biol*. 125:91-102.
- Weiler, K.S., and B.T. Wakimoto. 1995. Heterochromatin and gene expression in *Drosophila*. *Annu Rev Genet*. 29:577-605.
- Wenzel, A., C. Cziepluch, U. Hamann, J. Schurmann, and M. Schwab. 1991. The N-Myc oncoprotein is associated in vivo with the phosphoprotein Max(p20/22) in human

- neuroblastoma cells. *Embo J.* 10:3703-12.
- West, A.G., M. Gaszner, and G. Felsenfeld. 2002. Insulators: many functions, many mechanisms. *Genes Dev.* 16:271-88.
- Wu, R.S., H.T. Panusz, C.L. Hatch, and W.M. Bonner. 1986. Histones and their modifications. *CRC Crit Rev Biochem.* 20:201-63.
- Yokota, H., G. van den Engh, J.E. Hearst, R.K. Sachs, and B.J. Trask. 1995. Evidence for the organization of chromatin in megabase pair-sized loops arranged along a random walk path in the human G0/G1 interphase nucleus. *J Cell Biol.* 130:1239-49.
- Zhang, J., F. Xu, T. Hashimshony, I. Keshet, and H. Cedar. 2002. Establishment of transcriptional competence in early and late S phase. *Nature.* 420:198-202.
- Zimowska, G., J.P. Aris, and M.R. Paddy. 1997. A Drosophila Tpr protein homolog is localized both in the extrachromosomal channel network and to nuclear pore complexes. *J Cell Sci.* 110 (Pt 8):927-44.
- Zink, B., and R. Paro. 1989. In vivo binding pattern of a trans-regulator of homoeotic genes in *Drosophila melanogaster*. *Nature.* 337:468-71.
- Zink, D. 2006. The temporal program of DNA replication: new insights into old questions. *Chromosoma.* 115:273-87.
- Zink, D., M.D. Amaral, A. Englmann, S. Lang, L.A. Clarke, C. Rudolph, F. Alt, K. Luther, C. Braz, N. Sadoni, J. Rosenecker, and D. Schindelhauer. 2004. Transcription-dependent spatial arrangements of CFTR and adjacent genes in human cell nuclei. *J Cell Biol.* 166:815-25.
- Zink, D., and R. Paro. 1995. Drosophila Polycomb-group regulated chromatin inhibits the accessibility of a trans-activator to its target DNA. *Embo J.* 14:5660-71.

Supplementary material

presented on a CD:

Figure S1. Organization of trimH3K4 / RNA pol II-enriched sites in malpighian tubule nuclei of FLW-1 transgenic 3rd instar larvae. trimH3K4 (green) and the active form of RNA pol II (phosphorylated at Ser 2) (red) were visualized with specific antibodies. Images in (A-E) and (F-J) are subsequent light optical sections from two different nuclei, respectively. Asterisks mark the nucleolus in each nucleus. Note enrichment of active sites at nuclear and nucleolar peripheries (arrowheads in A, B, D, H, I). Scale bars: 10 μ m.

Figure S2. Association of Pc-binding sites with heterochromatin in nuclei from salivary glands. Single light optical sections of nuclei from different Pc-GFP transgenic 3rd instar larvae are shown. Pc-GFP-binding sites are shown in green, while the dimH3K9-enriched domain is shown in red. Arrowheads mark Pc-GFP binding sites in close contact with heterochromatin. Scale bar: 10 μ m.

Movie 1. 3D Amira reconstruction of Pc-binding sites in a malpighian tubule nucleus from a Pc-GFP transgenic larva. Pc-binding sites are shown in green and the heterochromatin domain is shown in red.

Movie 2. A projection of the multiview reconstruction of a section of a nerve from a Pc-GFP transgenic larva. Imaging of the specimen was performed with the SPIM microscope.

Movie 3. A projection of the multiview reconstruction of a section of a salivary gland from a Pc-GFP transgenic larva. Imaging of the specimen was performed with the SPIM microscope.

Curriculum Vitae

Name: Elena Rybakina (Andreeva)
Date of birth: 06.03.1979
Place of birth: St.Petersburg, Russia
Citizenship: Russian

School education:

September 1986 – June 1994 ground school № 314, St.Petersburg
September 1994 – June 1996 advanced school № 314, St.Petersburg

University education:

September 1996 – June 2000 Bachelors degree student, St. Petersburg State University, Faculty of Biology and Soil Sciences, Dept. of Genetics and Selection. Bachelors work entitled „Morphometric Analysis of Pericentromeric Q-segments of Chromosomes 1, 9, 16 in Human Embryos“ defended in 2000 with mark „Excellent“. The work was done at the laboratory of Antenatal Diagnostics in the Institute of Obstetrics and Gynecology, Russ. Acad. Med. Sci., under scientific supervision of Dr. Tatjana V. Kuznetsova. Honors degree.

September 2000 – July 2002 Masters degree student, St. Petersburg State University, Faculty of Biology and Soil Sciences, Dept. of Genetics and Selection. Masters thesis entitled „Comparative analysis of cytogenetic reactions of peripheral blood lymphocytes from cancer patients to gamma- irradiation *in vitro* and *in vivo*“. The work was done at the laboratory of Radiation Genetics, Central Research institute Radiology and Roentgenology, under supervision of Prof. Dr. Irena E. Vorobtsova. Honors degree.

August 2002 – December 2006 PhD student at the Department Biology II, LMU Munich, Germany, research group of Privat-Dozent Dr. Daniele Zink.

Publications

Rybakina E., Paro R., Dahlsveen I., Becker P., Zink D. 2004. Analysis of the relationships between functional states of the *Drosophila melanogaster* Fab-7 element and its nuclear position. *European Journal of Cell Biology*. 83 (Supplement 54).

Elena Rybakina, Donna Arndt-Jovin, Ina K. Dahlsveen, Peter B. Becker, Elisabeth Kremmer, Dirk Eick, Renato Paro, and Daniele Zink. The nuclear organization of PREs in larval tissues of *Drosophila melanogaster*. Manuscript in preparation.

Andreas Englmann, Elena Rybakina, Luka A. Clarke, Margarida D. Amaral, Nicolas Sadoni, Volker C. Cordes, and Daniele Zink. The influence of peripheral proteins on positioning and transcriptional activity of the human CFTR gene. Manuscript in preparation.

Presentations

Rybakina E., Becker P., Ringrose L., Paro R., Zink D. 2005. Is nuclear architecture involved in the functional regulation of Polycomb response elements? *Transregio 5 Annual Symposium*.

Rybakina E. 2006. The role of nuclear architecture in the functional regulation of the PRE Fab-7. *Transregio 5 Annual Symposium*.

Also poster presentations on following meetings:

DGZ meeting (September 2003, Jena)

DGZ meeting (March 2004, Berlin)

Transregio meeting (October 2004, Heidelberg)

Workshop on Nuclear Organization meeting (October 2004, Elmau)

Transregio meeting (November 2004, Munich)

Abcam meeting (March 2005, York)